Aston University

Some pages of this thesis may have been removed for copyright restrictions.

If you have discovered material in AURA which is unlawful e.g. breaches copyright, (either yours or that of a third party) or any other law, including but not limited to those relating to patent, trademark, confidentiality, data protection, obscenity, defamation, libel, then please read our Takedown Policy and contact the service immediately

DEFORMATION MICROSTRUCTURES AND RECRYSTALLIZATION IN HEAVILY WORKED COPPER.

ADIL ALI RIDHA

A thesis submitted in supplication for the degree of Doctor of Philosophy.

Department of Metallurgy and Materials Engineering
University of Aston in Birmingham.

DECEMBER 1981.

SUMMARY.

The University of Aston in Birmingham.

Title :- Deformation Microstructures and Recrystallization in Heavily Worked Copper.

Author :- Adil Ali Ridha.

Degree :- Ph.D. 1981.

Deformation microstructures in two batches of commercially pure copper (A and B) of almost similar composition have been studied after rolling reductions from 5 % to 95 %. X-ray diffraction, optical metallography, scanning electron microscopy in the back-scattered mode, transmission and scanning electron microscopy have been used to examine the deformation microstructure. At low strains ($\sim$10 %) the deformation is accommodated by uniform octahedral slip. Microbands that occur as sheet like features usually on the {111} slip planes are formed after 10 % reduction. The misorientations between microbands and the matrix are usually small (1 - 2°) and the dislocations within the bands suggest that a single slip system has been operative. The number of microbands increases with strain, they start to cluster and rotate after 60 % reduction and, after 90 %, they become almost perfectly aligned with the rolling direction. There were no detectable differences in deformation microstructure between the two materials up to a deformation level of 60 % but subsequently, copper B started to develop shear bands which became very profuse by 90 % reduction. By contrast, copper A at this stage of deformation developed a smooth laminated structure. This difference in the deformation microstructures has been attributed to traces of unknown impurity in B which inhibit recovery of work hardening. The preferred orientations of both were typical of deformed copper although the presence of shear bands was associated with a slightly weaker texture. The effects of rolling temperature and grain size on deformation microstructure were also investigated. It was concluded that lowering the rolling temperature or increasing the initial grain size encourages the material to develop shear bands after heavy deformation.

Recovery and recrystallization have been studied in both materials during annealing. During recrystallization the growth of new grains showed quite different characteristics in the two cases. Where shear bands were present these acted as nucleation sites and produced a wide spread of recrystallized grain orientations. The resulting annealing textures were very weak. In the absence of shear bands, nucleation occurs by a remarkably long range bulging process which creates the cube orientation and an intensely sharp annealing texture. Cube oriented regions occur in long bands of highly elongated and well recovered cells which contain long range cumulative micorientations. They are transition bands with structural characteristics ideally suited for nucleation of recrystallization. Shear banding inhibits the cube texture both by creating alternative nuclei and by destroying the microstructural features necessary for cube nucleation.

Key Words : Microband, shear band, cube texture.

CONTENTS.

LIST OF TABLES

LIST OF FIGURES.

CHAPTER ONE.

INTRODUCTION.

Deformation microstructures of cold worked materials have been investigated many times especially in copper and copper based alloys. Early studies were concerned with metallographically polished and etched specimens deformed to low or medium strain levels ($\varepsilon < 1$). Polished surfaces were studied by optical microscopy and electron microscopy of replicas, but these studies were restricted to low strain levels. When transmission electron microscopy was first employed to study the deformed structure in thin foils it was also confined to small strain levels, but had the further limitation that specimens were prepared parallel to the sheet plane in rolled materials. Significant advances in understanding the structure of heavily deformed materials were made when examining foils prepared from other sections. Information about the cold worked state has also been deduced from studies of x-ray line broadening, and indirectly from deformation textures. Despite all this effort, many details of the substructure in copper remain uncertain. Only recently has electron microscopy been concerned with heavily deformed metals and with the systematic development of substructure with increasing strain. No serious attempt has been made to correlate the optical microstructures with those observed in the electron microscope.

Primary recrystallization is normally considered as nucleation of new strain free grains and the gradual consumption of the cold worked matrix by the growth of these

grains. There have been numerous studies of these phenomena and considerable understanding has been gained about the growth process, whereas the nucleation mechanism remains a subject of controversy. Similarly there has been much discussion for many decades about the origin of recrystallization textures, especially the cube texture which develops in many FCC metals and alloys. Extensive studies have been carried out in order to determine how cube nuclei form and how these nuclei develop into the sharp annealing texture. Despite all this the origin of this texture has remained uncertain.

In the course of the present work a wide range of techniques have been used to study the development and nature of the deformation microstructure in two commercial purity coppers deformed to different strain levels. Initially, the aim was to have more information about the origin and nature of the microbands which have been previously reported. Secondly, the aim was to obtain more data about the deformed structure, especially the orientation topography of the elongated cells in the cube oriented regions. The progress of recrystallization and annealing texture development in heavily deformed (90 %) copper has also been investigated. Special attention was paid to the nature and geometry of the cube nuclei, their subsequent growth upon annealing, and the variables effecting them.

CHAPTER TWO

STRUCTURES IN COLD WORKED METALS.

2.1. Introduction :-

The history of deformation microstructure studies goes back to 1900 when Ewing and Rosenhain (1) stated that "with the onset of plastic deformation the surface of a polished and etched specimen shows fine black lines, and they increase in number as the strain increases".

Before 1960 optical microscopy was used extensively in the examination of metallographically etched specimens. Most of these studies were concerned with copper and copper based alloys deformed to small or medium strain levels eg. (0-60 % reduction by rolling or compression). A few studies have been made of surface relief on pre-polished deformed specimens using optical microscopy and replica techniques, but again these were restricted to small strain levels only.

After 1960 with the development of transmission electron microscopy, the thin foil technique has been applied to deformation microstructure studies, and the use of optical microscopy has decreased. Very recently, the interest in optical metallography has renewed and many workers now believe there is a clear association between the type and nature of the deformation markings observed optically and the deformation microstructure observed in the transmission electron microscope.

2.2. Optical microscopy :-

When copper and copper based alloys are deformed plastically to a small strain level (~0.03 % reduction in thickness) (2), manifestations of deformation can be observed on a pre-polished surface as fine dark lines parallel to the operative slip planes. These dark lines are called slip lines; their density increases very rapidly as the strain increases, and after only 0.7 % reduction (true strain ε = 0.007) they are observed on several systems. Transmission electron microscopy of replicas has shown that the slip line spacing in copper is approximately 0.03μm and that the associated slip step is 0.001-0.005μm in height(3-4). As the strain increases further slip occurs preferentially in clustered bands or slip bands, and it has been found that the step heights associated with the slip bands vary between 0.02-0.04μm and the spacing between the slip lines within the bands is unaltered.

In 1916 Mathewson and Phillips (5) revealed indications on polished and etched cold rolled 70 : 30 brass which they named lines of deformation. Since then the same indications have been variously termed in the literature strain markings, etch bands and slip bands, and it has been found that these indications are associated with {111} planes (6-8). In 1954 Samuels (9) made thorough and systematic studies of the deformation indications in copper and copper based alloys, and on the basis of his observations he classified them into four distinct types of indications which he termed types I, II, III, IV.

Type I indications :-

These features were described by Samuels as systems of parallel grooves or lines of etch pits extended across the individual grains as shown in figs. (1(a), 2(a)), oriented parallel to the slip plane. They developed in copper and its alloys after small amounts of deformation (approximately 2.5 % compression). As the deformation increases their frequency increases rapidly. The first type I indications developed as short dark lines which were confined largely to areas adjacent to twin and grain boundaries. These indications were called slip lines.

Type II indications :-

These are revealed after low to medium strain levels (5-10 %) in compression, and they developed only in copper alloys. Type II indications have similar orientations to type I, and also they are restricted within individual grains but they are relatively wider as shown in Fig 2 (b). Their frequency increases as the deformation increases, and they reach their maximum density at 20 % compression, but decrease rapidly in both number and extent with further deformation. Samuels identified them as slip band indications, and he suggested that they are related to and developed from type I indications.

Factors affecting type II indications

a - strain level :- As the strain level increases their frequency increases up to a certain level (9-10).

b - Deformation mode :- It has been found (11) that both the strain at which the indications started to form and their frequency were deformation mode dependent. The frequency in compression was more than in tension, and in multiple impact more than in single blow.

c - Deformation temperature :- As deformation temperature increases the indications become wider, shorter, and more widely spaced. The threshold deformation for the development of the indications is also affected by deformation temperature. (12). Type II indications do not develop in copper at room temperature, but occur readily if the deformation is performed at 77K (12).

d - Composition :- It has been shown (9, 12) that increasing the zinc content, i.e. lowering the stacking fault energy, had the same effect as decreasing the deformation temperature.

The nature of type II indications :-

Samans (13) studied two deformed single crystals of alpha brass in the $(111)[\bar{1}01]$ and $(001)[\bar{1}00]$ orientations and obtained results which suggested that type II indications are mechanical twins. This was supported by Mathewson (14). However after examination of 80 : 20 brass single crystals Burke and Barrett (8) concluded that the volume of twinned material is less than 0.1 %, and the possibility that the indications were twins was eliminated. Barrett (15) proposed that the indications are associated with stacking faults, and this view was strongly supported by Warren (16) and Wagner (17) who studied alpha brass by x-ray line broadening and found that

the stacking fault probability in cold worked alpha brass increased as zinc content was raised.

In the last few years and with the aid of transmission electron microscopy a number of reports (18-23) have related the features observed in cold worked copper-based alloys by optical microscopy to those observed in transmission electron microscopy. It is now well established that when copper alloys are cold worked to a small strain level ($\sim\varepsilon = 0.2$) the deformation is accommodated by stacking faults, and at higher strains ($\varepsilon = 0.3$-0.7) by twinning. Most workers in this field now agree to give the name strain markings to type II indication.

Type III indications :-

These features are developed in copper and low zinc alpha brass after low to medium amounts of strain($\varepsilon = 0.2$-0.7). They form as two sets of parallel lines oriented at 70°-75° to the direction of compression as shown in fig. 1(b). Very little is known about the nature of these markings which have received almost no attention in the literature. Recently Malin and Hatherly (24) proposed that these indications and type I indications (slip lines) were associated with microbands observed in transmission electron microscopy of thin foils. Microbands and slip lines both form on $\{111\}$ slip planes and it was claimed that both have the same angular relationship to the macroscopic stress.

Type IV indications :-

These indications are described by Samuels(9) as two

Fig.(1) - Deformation structure in cold-worked tough pitch copper.

a - Type I indications after 2.5 % compression.

b - Type III indications after 40 % compression.

c - Type IV indications after 70 % compression.

Ref (9)

-a-

-b-

-c-

-a-

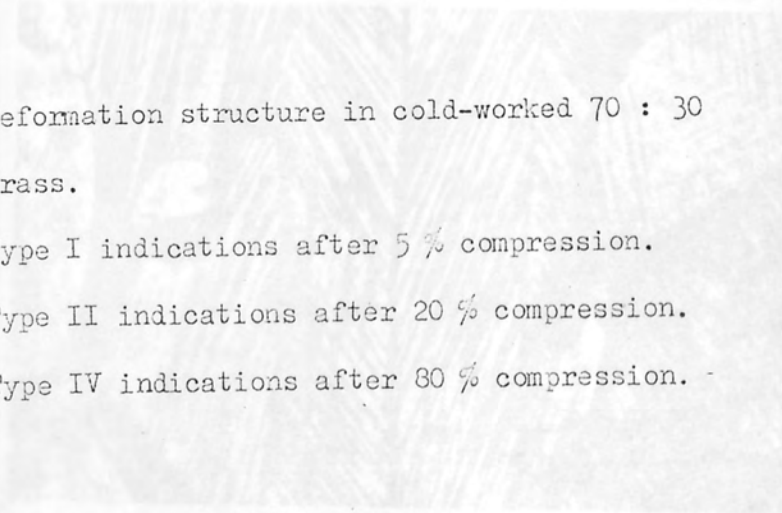

-b-

-c-

Fig.(2) - Defomation structure in cold-worked 70 : 30 brass.

a - Type I indications after 5 % compression.

b - Type II indications after 20 % compression.

c - Type IV indications after 80 % compression.

Ref.(9).

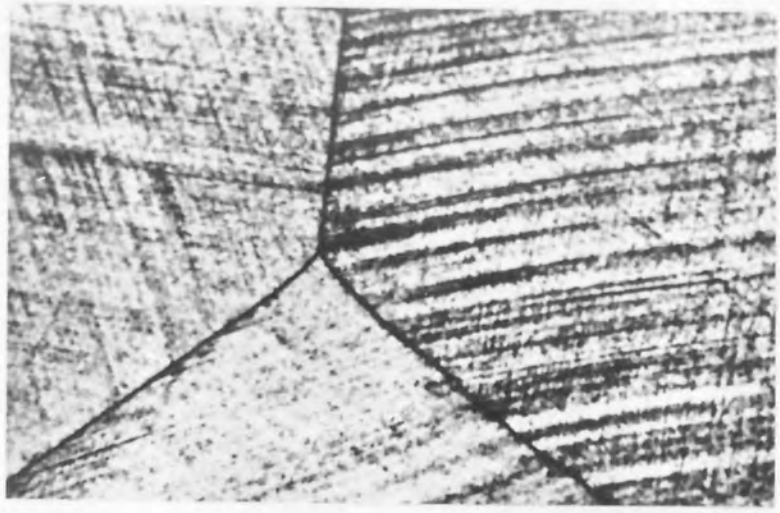

-a-

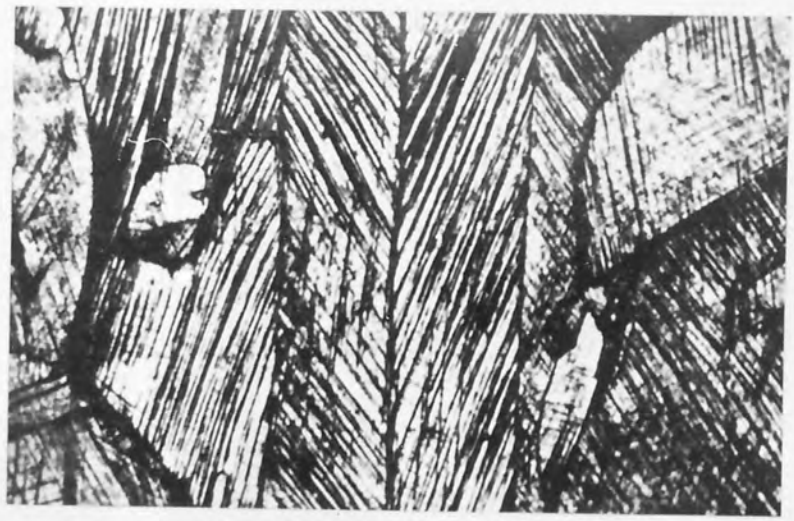

-b-

-c-

sets of parallel undulations uniformly oriented throughout the specimen at 55°-60° to the compressiom direction as shown in figs. 1(c) and 2(c). They developed in copper after heavy deformation (70 % compression) and in alpha brass after 50 % compression. Samuels suggested that they be termed deformation-band indications. It is apparent that these are the same structures as observed by Adcock (25), in cold rolled Cupro-Nickel (Cu - 20wt % Ni alloy). They were oriented at 25°-40° to the rolling direction, and parallel to the transverse direction. Recent studies (18-23) have shown that these features are associated with extensive macroscopic shearing and they have been referred to as shear bands.

2.3. Transmission electron microscopy :-

The early transmission electron microscopy investigations of deformed metals were confined to the rolling or compression plane which hampered interpretations of the structures especially in heavily deformed metals. Understanding of the structure of heavily deformed metals advanced significantly when foils were prepared in other sections for electron microscopy examination (22, 26-27). These sections are typically the longitudinal section (normal to the transverse direction) and the transverse section (normal to the rolling direction). The early investigations were concerned with dislocations and their interaction in the various stages of work hardening. Single crystal specimens deformed in tension were generally studied and the work has been reviewed several times (28-30). Most of these investigations concerned copper

and its low stacking fault energy alloys. Nevertheless copper has not been studied systematically to any great extent. According to transmission electron microscopy observations the deformation microstructure of F.C.C. metals and alloys can be classified as follows :-

a - Deformation microstructures of medium or high stacking fault energy metals which involves the formation of equiaxed dislocation cells, microbands, clustering of microbands and shear bands.

b - Deformation microstructures of low stacking fault energy metals. In such metals the difficulty of cross-slip makes the dislocations remain in planar arrays and the deformation process involves the formation of stacking faults, mechanical twins and shear bands.

2.3.1 Deformation microstructures of medium or high S.F.E. metals :-

a - Dislocation cell structures :-

Heidenreich (31) was first to show this structure in deformed high purity aluminium by using electron microscopy. Gay et al (32-33), using a micro-beam Laue method, found that after small amounts of deformation the grains break up into a number of small particles which are slightly misoriented relative to each other, and the size of these particles decreases as the strain increases until, after sufficient deformation, the particle size reached a constant minimum value of $\sim 0.3\mu m$ at a strain level of $\sim \varepsilon = 1$. Embury (26) attributed this to a high rate of dynamic recovery. Many

workers studied this structure by transmission electron microscopy in different deformed metals and it has been established that, at very low amounts of deformation ($\varepsilon < 0.05$) the dislocations are distributed on random {111} planes, but as the deformation increases large numbers of dislocations are produced and an equiaxed cell structure is formed, see figs. 3(a) and (b). The average cell diameter is usually of the order of 0.5-3μm, the interior of the cells relatively free from dislocations and those that do exist form arrays that divide the cells into a small number of domains. The misorientation between cells is small and usually less than 2 . The main features of this cell structure in F.C.C. metals have been summarised by Swann(28) as follows :-

a - The cell size is independent of the initial grain size and decreases to a limiting value after a certain strain.

b - This limiting value of the cell size increases with the softness of the metal.

c - The width of the cell walls increases with the hardness of the metals.

d - The cell size is reduced by increasing the impurity content.

e - The cell interiors are relatively free from dislocations, whereas the cell walls are regions of high dislocation density.

f - The cell walls tend to lie parallel to low index planes such as {100}, {110} and {111}, often in the form of twist boundaries.

Gay et al (33)found that the cell size is similar to the minimum spacing between slip bands, which led them to suggest that the cells are regions between slip bands. Weissmann et al

Fig.(3) - Equiaxed dislocation cell structure.

a - The initial stage of cell formations in lightly deformed aluminium, {111} planes traces indicated by arrows.

b - Dislocation cells structure in copper deformed 5 %.

Ref.(28).

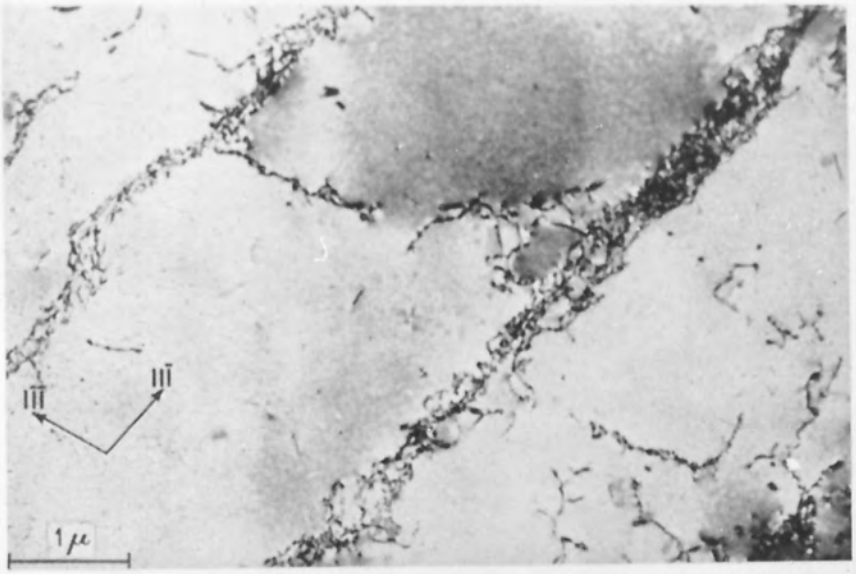

-a-

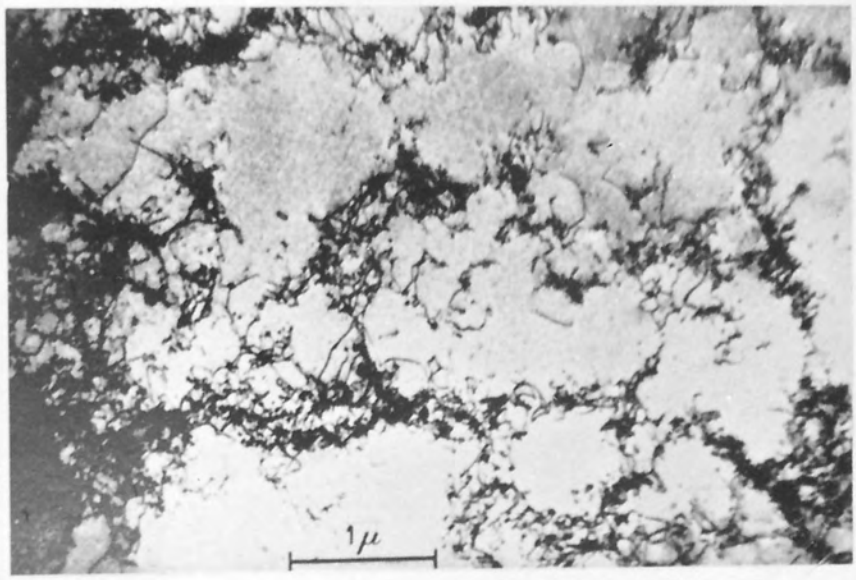

-b-

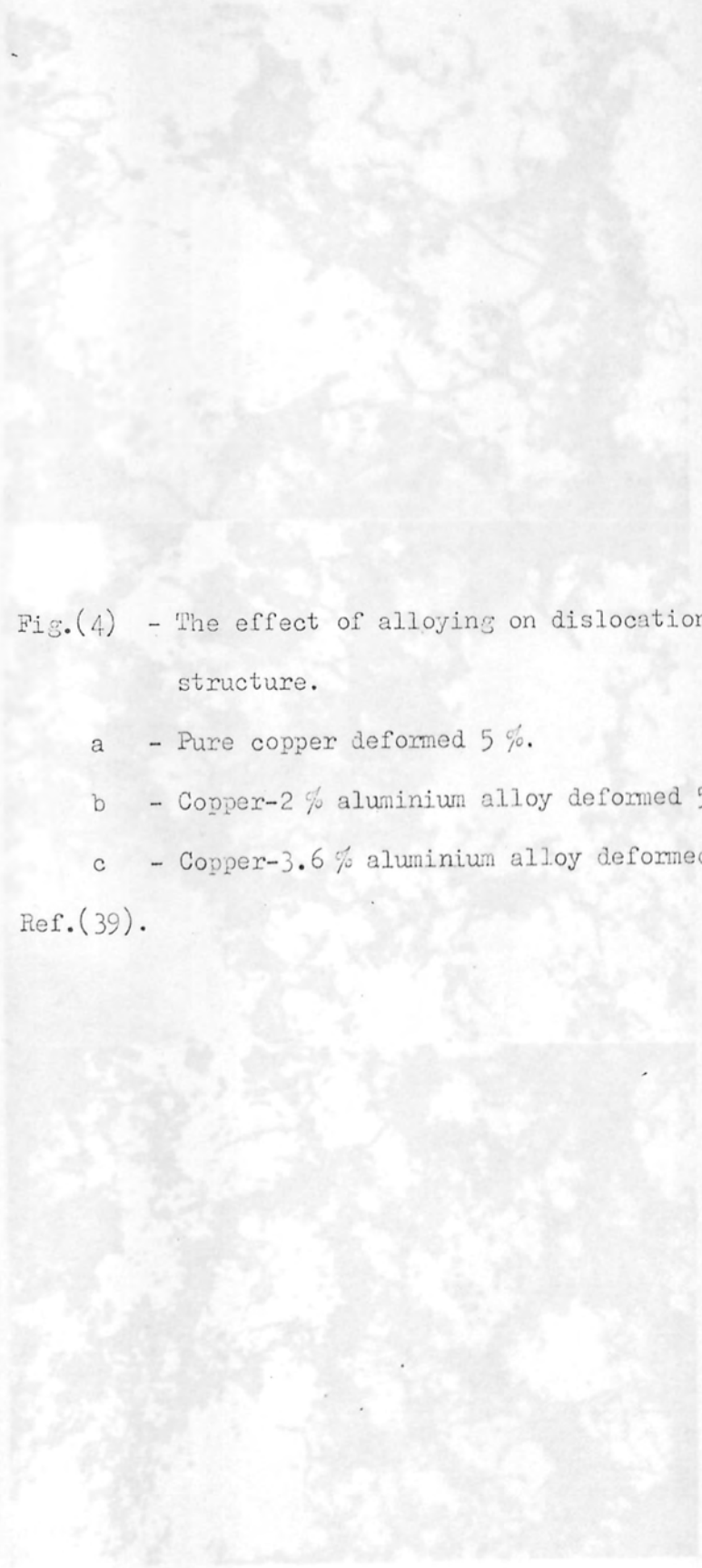

Fig.(4) - The effect of alloying on dislocations cell structure.

a - Pure copper deformed 5 %.

b - Copper-2 % aluminium alloy deformed 5 %.

c - Copper-3.6 % aluminium alloy deformed 5 %.

Ref.(39).

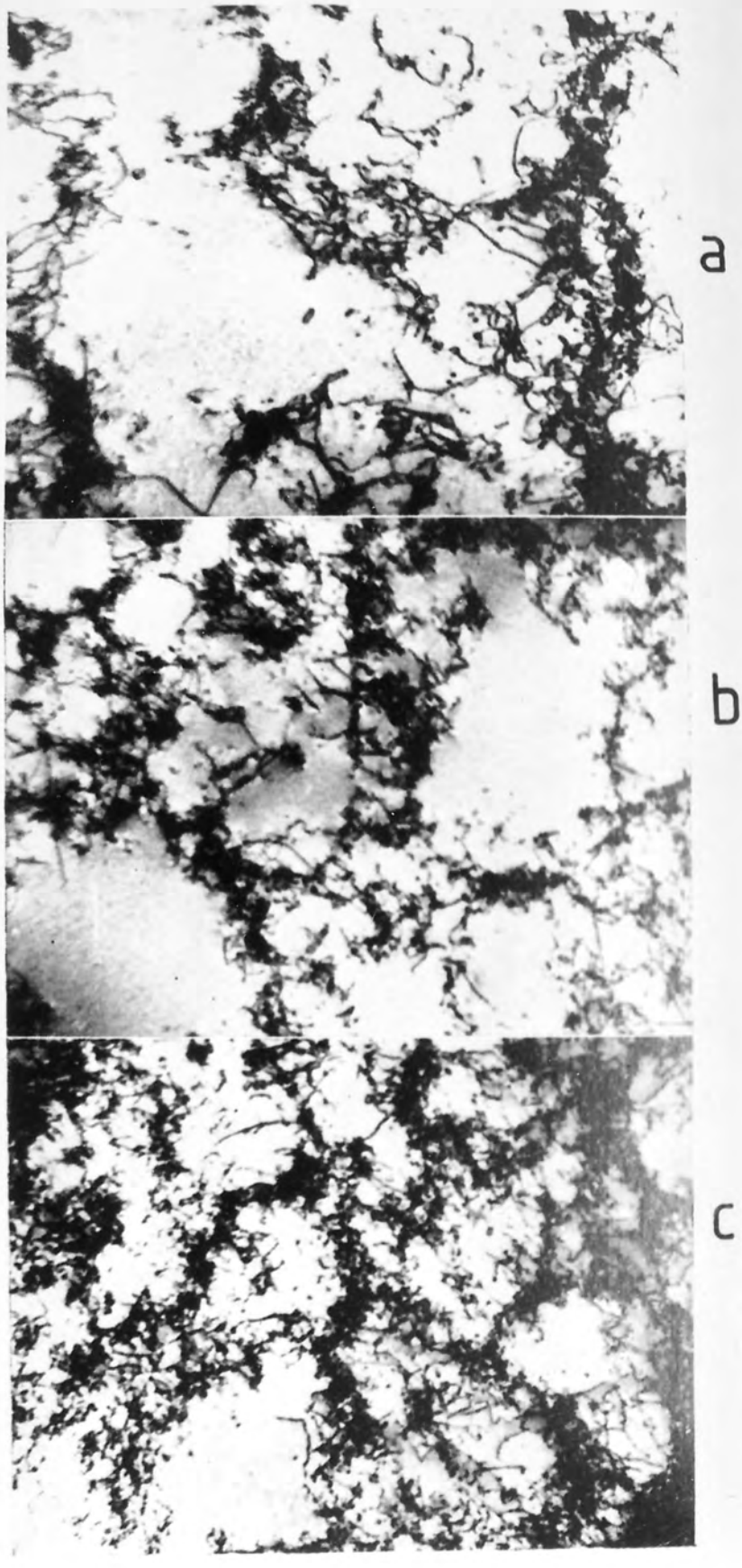
a
b
c

(35) identified the dislocation network (which he considered as the initial stage of cell formation) in 5 % cold rolled high purity aluminium specimens as screw dislocations derived from different {111} slip planes. However, Seeger (36) proposed that the tilt boundaries of the cell structure formed by cross-slip of screw dislocations pile-up behind Lomer-Cottrell barriers. Whelan (37) and Hirsch (38) observed that Lomer Cottrell barriers and pile-ups are not present in thin foil of medium to high stacking fault energy metals, and Hirsch found screw dislocation networks, which led him to postulate that the cell structure is formed by screw dislocations cross-slipping from their original slip planes to form relatively strain-free walls. It is very well established (33, 38-39) that stacking fault energy is the major factor in determining the dislocation distribution and cell morphology. As shown in figs. 4(a),(b), (c) with increasing amounts of alloy element (ie. decreasing S.F.E.) the dislocation density increases and the cell size decreases. Malin (24) and Wakefield (40) support the view that such dislocation cell structures are not manifestations of the deformation process itself but are formed by relaxation processes after the deformation.

Microband formation :-

Although the majority of transmission electron microscopy observations of deformation microstructure have been reported during and towards the end of the present investigation, all the literature concerning deformation microstructures developed in copper at different strain levels will be reviewed here.

Microbands were first observed by Essman (41) in copper single crystals deformed by tension at different temperatures and referred to "schichtstruktur". The term microband had been used earlier by Hu (42) to describe the long parallel, narrow segments between two deformation bands in rolled (001) [100] Si-Fe single crystals. Hu found that the large misorientation between deformation bands was accommodated by narrow zones 2-3μm in width, which are composed of a number of parallel segments only 0.1-0.3μm in width, the maximum misorientation between two neighbouring segments being $< 4^{\circ}$. These have a similar appearance but different origin to the features discussed here . Ahlborn et al (43) investigated deformation microstructures in drawn copper single crystal and found that after low strains (ε =0.01) another feature developed besides the equiaxed cell structure. These were long sheet-like bands (microbands) 0.25μm in thickness separated from the matrix by low angle boundaries. Their frequency increased with strain and by 90 % deformation the microbands clustered and became parallel to the drawing direction. It was assumed that they had developed from the equiaxed cells by elongation and amalgamation. However, a similar investigation by Horiuchi et al (44) on copper $\langle 111 \rangle$ and $\langle 100 \rangle$ single crystals deformed 80 % by drawing revealed clusters of microbands and an equiaxed dislocation cell structure on sections perpendicular to the drawing axis. The cells size was $\sim 0.5\mu$m and the microbands' thickness was 0.1-0.2μm with a mean misorientation of $\sim 1^{\circ}$ across the microband boundaries. In sections parallel to the drawing direction they found microbands with sharper boundaries, their thickness was 0.15μm,

they were misoriented about 2° relative to the matrix and were not parallel to the drawing direction. From selected area diffraction patterns and trace analysis they found that the microband boundaries were parallel to {111} slip planes, although some exceptions to this orientation were also found. Horiuchi et al concluded that microbands did not develop from the equiaxed cell structure but they gave no account of their origin. Wakefield et al (20) investigated deformation microstructures in copper and copper-6.4 wt % aluminium alloys deformed by cold rolling. They observed that after 17 % reduction, longitudinal sections of copper showed an equiaxed cell structure, 0.5-1.0μm in diameter, with occasional very long sheet-like features at angles of ~35° to the rolling plane, as shown in fig.5(a), These features are similar to those reported in (43, 44). The microbands were about 0.2μm thick and up to 10μm long with a high dislocation density along their boundaries. With further strain the microband frequency increased and at high strain levels they clustered and bacame aligned parallel to the rolling plane, but their thickness remained constant. At 94 % reduction equiaxed cell structures were still observed with ~0.5μm diameter, but their boundaries and the microbands' boundaries became sharper indicating that recovery processes had occurred. At all strain levels irregular dislocation arrays with a spacing of 100-300Å were observed. In transverse sections at low strain levels the microband traces were nearly parallel to the rolling plane. Malin and Malin et al (45, 24) carried out similar investigations using a wider range of techniques. They found that the microbands formed in deformed copper after only 5 % reduction by rolling; they did

not cross into adjacent grains, but did displace the grain boundaries. With increasing strain two sets of microbands developed, each making ~35° with the rolling direction. The incidence increased with strain, and the microbands clustered together while their thickness remained constant at ~ 0.2μm. Individual microbands were misoriented with respect to the matrix by 1-2° and the matrix orientation on either side of the microband was the same. Optical metallography showed thin parallel lines developed in many grains at similar strain levels (< 39 % reduction). These were 20-40μm long and inclined in longitudinal sections at about ~35° to the rolling direction. Similarity between the geometry of the microbands and these thin lines observed optically in the etched specimen and the type III indications reported by Samuels (9) led Malin and Malin et al (45, 24) to conclude that all these features are microbands. Replicas of pre-polished and scratched specimens showed that by about 43 % reduction most of the grains contain two sets of slip lines as shown in fig. 5(c). Spacings between slip lines varied irregularly between 1 to 5μm. The slip line produced abrupt and marked displacement of the scratch as shown in fig. 5(d). The displacement across the width of the band indicated a large and almost homogeneous shear, while analysis of diffraction patterns from thin foils showed that microbands developed on {111} slip planes. It was concluded that microbands form on the (111) plane most nearly parallel to the transverse direction and close to 35° to the rolling direction as shown in figs. 5(a) and (b).

At high strain levels the microbands rotated into

the rolling plane and their boundaries were sharp indicating that recovery process had taken place. Occasional areas of equiaxed cell were still present even at strain levels of ε = 2.9-3.6 and these areas were traversed by fresh microbands at $\sim 35^{\circ}$ to the rolling direction. Also it was concluded that the deformation was accommodated almost entirely by microbands in the strain range ε =0.2 to 2. Almost the same observation has been reported by Hatherly et al (22) and Grewen et al (46). As mentioned before, when copper was heavily deformed (> 65 % reduction) the microbands clustered and their boundaries became very sharp due to the dynamic recovery. Cairns et al (47) observed that polygonization took place only after 70 % reduction in phosphorus-deoxidized drawn copper tubes, and recrystallization occured after 95 % reduction. Nutting (48) observed that recrystallization started in OFHC copper after 98 % reduction by rolling. In contrast, Malin and Hatherly (49) found no evidence of recrystallization even after 98 % reduction and they argued (22) that the differences in these observations are probably due to chemical purity, strain rate and deformation temperature. Hu (27) investigated electrolytic copper of 99.92 % purity cold rolled with an initial grain size of 0.06mm. Longitudinal sections of copper rolled 90 % revealed a very thin elongated structure in the form of ribbons mostly parallel to the rolling plane as shown in figs. 6(a) and (b). The cell thickness decreased gradually with strain to a limiting value of $\sim 500\text{Å}$ at 99 % reduction (ε =5) and was somewhat finer at comparable strain than that reported by Embury et al (26) for cold drawn copper wires. In rolled OFHC copper, Wingrove (34) reported a limiting thickness of $\sim 3000\text{Å}$,

and observed similar elongated cells in both longitudinal and transverse sections indicating that the cells were pancake-shaped.

There has been considerable interest in the cell dimensions and a number of measurements have been made on different materials (26, 34) to show that the cell width decreases to a limiting value at strain level $\varepsilon > 2$ and that this corresponds to a sharpening of the cell boundaries. However, recent work (22) cast doubt on the idea that elongated cells are produced by deformation of an earlier substructure. The cells in heavily deformed copper are too thick to have developed from the equiaxed cell structure which was observed at low strain level. Furthermore, equiaxed cells are still retained in the microstructure even after heavy deformation (47). Finally, the development of microbands at intermediate to high strain level (45, 49) has to be taken into account.

Shear band formation :-

It has been suggested (45) that once the microbands rotate and become parallel to the rolling plane they are no longer able to contribute to the deformation process, and the need for new deformation to accommodate any further deformation is necessary to maintain continuity of the material. Grewen et al (50) have observed macroscopic shear bands in copper and copper 0.6 % chromium alloy deformed by rolling to a strain level of $\varepsilon = 3$. They were described as coarse bands about 2μm wide, making an angle 20-35° to the rolling direction, parallel to the transverse direction, and they consist of

elongated cells parallel to the shearband as shown in fig. 7. Diffraction pattern analysis showed that the shear bands were not associated with a particular crystallographic plane like the microbands, but that the shear bands are intensive inhomogeneous deformations producing local shear textures {111} <112>, {001} <110> and {112} <011>.

In cold rolled aluminium and aluminium -0.8 % magnesium alloy Brown (51) reported that after 80 % reduction, occasional severe shear bands began to propagate from grain to grain, causing marked displacement of grain boundaries by about 1-5μm. Only one set of bands was present under each surface making an angle of $\sim 35^\circ$ or $\sim 110^\circ$. At high strain levels, $\sim$90 % reduction, Malin (45) observed that the elongated cell structure and the equiaxed cells were crossed by long thin bands $\sim$0.5-1μm thick, they were inclined at $\sim 35^\circ$ to the rolling direction and had no simple crystallographic relationship with the specimen. Electron microscopy of replicas of a copper specimen deformed by a 94 % reduction showed that the amount of shear associated with the bands is very large and localised as shown in fig. 8. In copper (112) $[\bar{1}11]$ single crystals deformed 75 % by rolling Karduck et al (52) reported that very fine deformation twins were seen inside shear bands running parallel to the elongated cells of the shear band. They claimed that it was very difficult to resolve the twins by bright field imaging but that they were evidenced in dark field and diffraction modes. Deformation twinning has also been reported by Slakhorst et al (53), in heavily deformed (91 % reduction) copper deformed by plane strain. However there are

very few TEM observations of shear bands in medium-high SFE materials in the literature, and most of the observations which have been reported showed the same picture. Probably this is due to the difficulty of obtaining a thin foil containing shear bands because shear bands either tend to polish faster than other deformation micro structures or the frequency of the bands is not high. However shear band detection is much easier by optical metallography. The similarity between the geometry of the shear bands and deformation indication type IV reported first by Samuels (9) has led many investigators to conclude that they are the same.

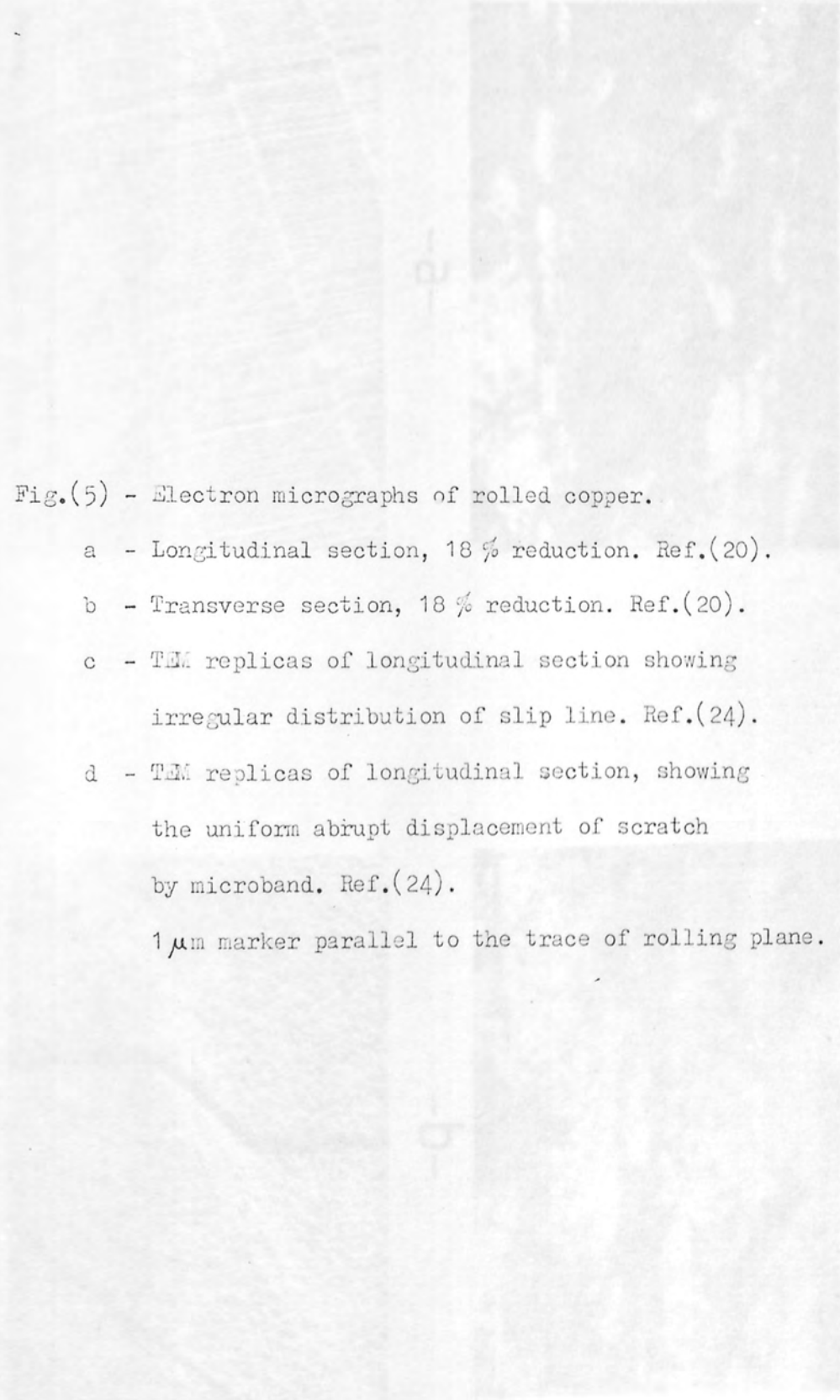

Fig.(5) - Electron micrographs of rolled copper.

a - Longitudinal section, 18 % reduction. Ref.(20).

b - Transverse section, 18 % reduction. Ref.(20).

c - TEM replicas of longitudinal section showing irregular distribution of slip line. Ref.(24).

d - TEM replicas of longitudinal section, showing the uniform abrupt displacement of scratch by microband. Ref.(24).

1 μm marker parallel to the trace of rolling plane.

-a-

-b-

-c-

-d-

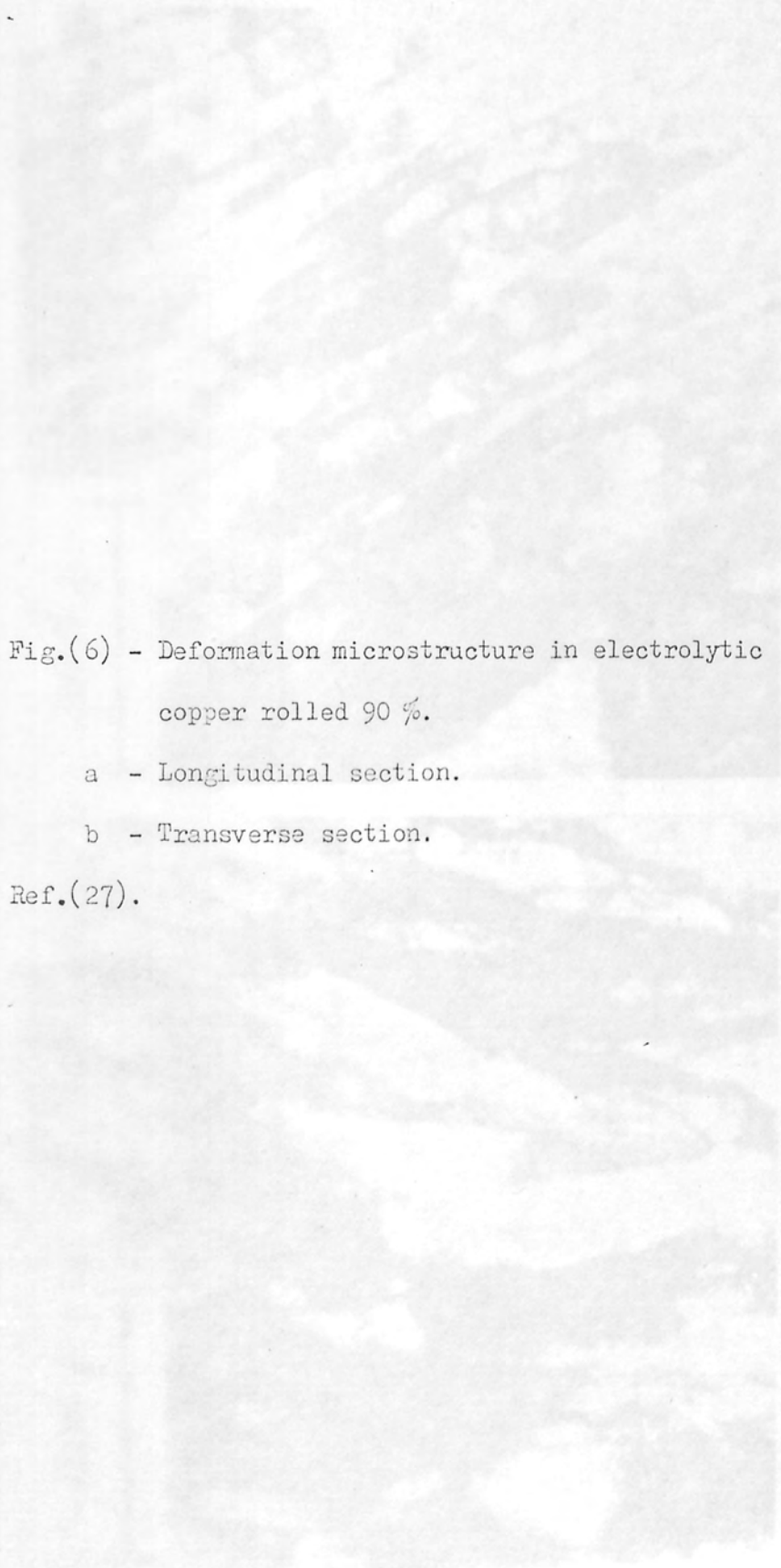

Fig.(6) - Deformation microstructure in electrolytic copper rolled 90 %.

a - Longitudinal section.

b - Transverse section.

Ref.(27).

a
1 μm
RD
b
1 μm

Fig.(7) - TEM micrograph of cold-rolled copper-0.6(wt)Cr showing shear band developed on longitudinal section after heavy deformation. Ref.(50).

Fig.(8) - Heavily deformed copper.

a - TEM replicas of longitudinal section showing shear band.

b - Optical metallography of a longitudinal section rolled 86 % showing shear band.

Ref.(24).

-a-

-b-

2.3.2 Deformation microstructure in low SFE metals :-

In general there is not much confusion about the nature and morphology of deformation microstructures in these metals. Many investigators have studied the deformation microstructure of low SFE metals and alloys, especially copper-based alloys with different alloying contents, at different deformation levels. It is generally accepted that the deformation in these alloys is accommodated by the movement of partial dislocation, twinning and shear bands.

Stacking faults and twinning :-

Manifestations of plastic deformation which develop in low SFE metals and alloys after low-medium deformation are described by Samuels (9) as systems of parallel grooves and lines of etch pits. Hu et al (54) studied the deformation microstructure in a (112) $[11\bar{1}]$ single crystal of Cu-4 % Al deformed by rolling. They observed that after 10 % reduction the microstructure consisted of dislocations, closely spaced stacking faults and micro-twins. The micro-twins thickness varied from 50 to a few thousand angstroms; within these thin twins were finely spaced stacking faults. As deformation increased the frequency of stacking faults increased and the spacing between the twins decreased. Later many investigators (18-20, 55-57) made similar studies on Cu-Al alloys and they reported that neither dislocation cells nor microbands were observed in any Cu-Al alloys containing more than 4 % Al. Instead, stacking faults were visible at low strain level ($\varepsilon > 0.1$). With increasing strain level, twins developed on

two systems and after 85 % strain the microstructure consisted of long twin bands parallel to the rolling direction. The twinned bands are $\sim$ 300Å thick and contain a very fine dislocations array with spacing $\sim$ 50Å. Twin frequency decreases rapidly after 80 % reduction. Alloys containing less than 3.5 % Al showed mixed deformation microstructure (microbands and twins). Leffers et al (58) examined the rolling plane of 85/15 brass deformed by rolling. They did not find any twins before 25 % deformation, and the twins became very extensive after 65 % reduction, being present in almost all grains. Examinations of thin foils of deformed 70/30 brass (59) showed that after 20 % reduction the microstructure consisted of dislocations on {111} planes in more than one system, stacking faults, and heavily faulted regions often associated with grain boundaries. After 20 % reduction the structures were similar to that reported by Leffers (58). The most detailed and systematic studies of deformation microstructures in low SFE alloys have been reported by Duggan et al (21) and Hutchinson et al (23). In these studies 70:30 brass was cold rolled to different deformation levels (17 % - 98 % reduction). Longitudinal sections have been examined by optical and electron metallography. The only manifestation of deformation revealed by optical metallography in specimens rolled up to 40 % were strain markings as shown in fig.9(a), while electron microscopy showed many grains containing bands of fine twins that were distributed in faulted structures of high dislocation density, see fig.9(b). Then after a strain level of ($\varepsilon = 0.7$) the density of microtwins became very prolific but uneven as shown in fig.9(c). As the

strain increased the twins rotated towards the rolling plane, and by 90 % the alignment was nearly perfect.

Baker et al (60) and Liu et al (61) examined the deformation microstructure in rolling plane sections of Cu-Sn alloys cold rolled to low strain levels. They found that deformation twins form only in alloys containing more than 2 % Sn. The twin density increases with Sn content and it is dependent on the initial grain size, twins being fewer and narrower in fine grained material. Alloys containing less than 2 % Sn showed a diffuse cell structure similar to that found in copper.

It is now generally believed that deformation twins observed by TEM in low SFE materials and alloys after low-medium deformation correspond to strain markings (type II indication reported by Samuels (9)) observed by optical microscopy in the same alloys deformed to the same strain level.

Shear bands :-

TEM and optical metallography showed that when f.c.c. alloys of low SFE are deformed to moderate levels they develop two sets of bands oriented $\sim 35^{\circ}$ to the rolling direction which are associated with intense macroscopic shear strain. Wakefield et al (20) detected shear bands in rolled Cu-6.4 % wt Al alloy in longitudinal sections after $\sim$ 60 % reduction; they were $\sim 35^{\circ}$ with the rolling direction, and parallel to the rolling plane in transverse section.

Examinations of TEM replicas from etched longitudinal sections indicated that shear bands and type IV indications are identical. Analysis of electron diffraction patterns suggested that the crystallites within the shear bands had no preferred orientation. The bands cut and sheared the aligned twins and grain boundaries and, as the deformation increased, their number increased. Duggan et al (21) and Hutchinson (23) found that one set of shear bands started to form first in 70:30 brass deformed 50 % by rolling and by 70 % two sets of shear bands were present in most of the grains. With further deformation their frequency increased and by 90 % they became very dense, subdividing the material into a series of rhomboidal prisms, see fig.10(a-d). In pre-polished and scratched longitudinal sections large displacements were observed where the shear bands intersected the scratches, and it was found that the shear strain associated with the bands was about 3-4. It was concluded that once the shear bands had formed they did not subsequently operate during restraining. TEM observations showed that shear bands started to form after 50 % reduction, they were inclined $\sim 35^{\circ}$ to the rolling direction and parallel to the transverse direction, their thickness varied from 0.1-1μm, and they were composed of slightly elongated crystallites of 0.02-0.1μm in diameter. It has been suggested that these crystallites formed by the rotation of the aligned twin structure into the bands by large localised shears.

STEM micro diffraction has been used to determine the orientation of crystallites within shear bands. The

results shown in fig.11(b) indicate that there is a wide scatter in the orientation, but with a distinct tendency for orientations near {110} [001]. Misorientations between neighbouring crystallites were large, and there was little tendency for the orientation change across the shear band to be cumulative. Similar shear band morphology has been reported by Blicharski et al (62) in austenitic stainless steel deformed by rolling.

The investigation discussed above demonstrated clearly that there are many overlapping modes of deformation in low SFE materials and alloys. The strain levels at which each mode starts and ends is alloying content dependent. However, Duggan et al (21) listed the following strain levels at which each mode started and ended in 70:30 brass deformed by rolling :-

a - 0-50 % deformation by octahedral slip with some stacking fault formation.

b - 40-60 % the deformation proceeds by deformation twins.

c - 50-80 % the difficulty of slip on other than the slip planes parallel to the twin boundaries leads to overshooting and rotation of the twin plane towards the rolling plane.

d - 60-95% shear bands play the major role in the deformation process. Shear bands are believed to form due to the inability of the aligned twins to accommodate any further deformation. Shear band density increases with strain at the expense of the twinned region and by 95 % reduction the twinned material is

almost eliminated.

e - At high reductions (> 90 %), where the twinned structures have been largely destroyed, the shear bands become less frequent and the deformation becomes more homogeneous. At this strain level the microstructures consist of thin elongated cells with very occasional twinned areas. (78).

Recently Dillamore et al (64) have presented a theory to explain shear band formation on a mechanistic basis. Before reviewing the details of this theory we shall review some of the formulae used in it.

The stress-strain curves often fits the relation

$$\tau = k(\gamma)^n$$

Where τ is the resolved shear stress, γ is the total shear strain in all active slip systems, k is the strength coefficient and n is the work hardening coefficient.

The relation between the stress and the velocity of the mobile dislocation can be written

$$\tau = \tau_o \left(\frac{V}{V_o} \right)^m$$

Where τ_o is the shear stress, V is dislocation velocity, which is equal to Vo when $\tau = \tau_o$, and m is the strain rate sensitivity.

The shear strain rate can be written

$$\dot{\gamma} = NbV$$

Where $\dot{\gamma}$ shear strain rate, N the number of mobile dislocations, and b is the Burgers vector.

The normal strain rate $\dot{\varepsilon} = \frac{\dot{\gamma}}{M}$

Where M is tha Taylor factor. Likewise the normal strain

$\varepsilon = \frac{\gamma}{M}$ and $\sigma = M\tau$

Where σ is the normal stress. Collecting all these together

$$\sigma = \frac{k}{(bVo)^m} M^{(1+n+m)} \varepsilon^n . \dot{\varepsilon}^m . N^{-m}$$

Then

$$\frac{1}{\sigma}\frac{d\sigma}{d\varepsilon} = \frac{n}{\varepsilon} + \frac{m}{\dot{\varepsilon}}\frac{d\dot{\varepsilon}}{d\varepsilon} + \frac{1+n+m}{M}\frac{dM}{d\varepsilon} - \frac{m}{N}\frac{dN}{d\varepsilon} \quad \text{---------} \quad 1$$

Shear bands form as a result of load instability; the condition for instability is $\frac{d\sigma}{d\varepsilon} < 0$ (ie the rate of hardening being negative) and this is caused by geometeric softening.

In equation (1) the first and the second terms are generally positive. Dillamore et al (64) used the contribution from $\frac{dM}{d\varepsilon}$ (the third term) to explain shear band formation due to geometric softening. They have calculated the strength of the crystals as a function of the angle of the shear band and considered in their calculation only the following orientations $(\bar{1}10)\ [001]$, $(\bar{4}\bar{4}11)\ [11\bar{1}\bar{1}8]$, $(4\bar{4}11)\ [11\bar{1}\bar{1}8]$, $(\bar{1}10)\ [\bar{1}\bar{1}2]$, and $(\bar{1}01)\ [1\bar{2}1]$, because these orientations are found to be the stable orientations, after 40-50 % deformation. Experimental observations showed that at this deformation level shear bands start to form in low SFE metals and alloys. However, the calculations showed that the M value rises steeply when the angle θ goes outside the range $\pm 9°44'$, where $\theta = (45-\beta)$ and β is the angle between the shear band and the rolling direction. This will limit the shear band forming at any angle between $35°16'$ and $54°44'$ to the rolling direction. A strong

texture is a pre-requisite for shear banding to occur on a plane that is not the plane of maximum shear stress (normally 45° to the rolling direction).

The geometric softening factor ($\frac{1}{M}\frac{dM}{d\varepsilon}$) has been calculated for the five orientations mentioned previously, and the result is shown in fig.12(a) in which the geometric softening factor is plotted as a function of shear band angle. The curve for the aggregate passes through a minimum value for the geometric softening factor of -0.11 at a shear band angle close to 35°16′, and since M is nearly constant over the range ($-9°44' \leqslant \theta \leqslant 9°44'$) this was considered to explain the observed shear band angle. Dillamore et al also explained why some grains develop one set of shear bands, while other grains develop two sets. Their explanation was that some orientations like (110) [001] and (110) (112) are symmetrical in their behaviour and would form shear bands equally readily on planes at both positive and negative value of β. Whereas the orientation (4,4,11) [11,11,$\bar{8}$] does not have this characteristic. They calculated the geometric softening factor for this orientation and the results are plotted as a function of β in fig.12(b). It can be seen clearly that the geometric softening factor is greater for the negative shear than for the positive shear. This makes the shear band which is associated with the negative shear sharper and more evident than the shear band associated with positive shear.

2.4. Variables affecting the deformation microstructure :-

It has been shown in the previous sections that

Fig.(9) - Longitudinal section of deformed 70 : 30 brass, trace of the rolling direction horizontal.

a - Optical microstructure after rolling 30 %, showing strain marking. X500. Ref.(21)

b - Electron micrograph showing deformation microstructure after 30 % reduction. Ref.(23).

c - Electron micrograph showing deformation microstructure after 51 % reduction. Ref.(23).

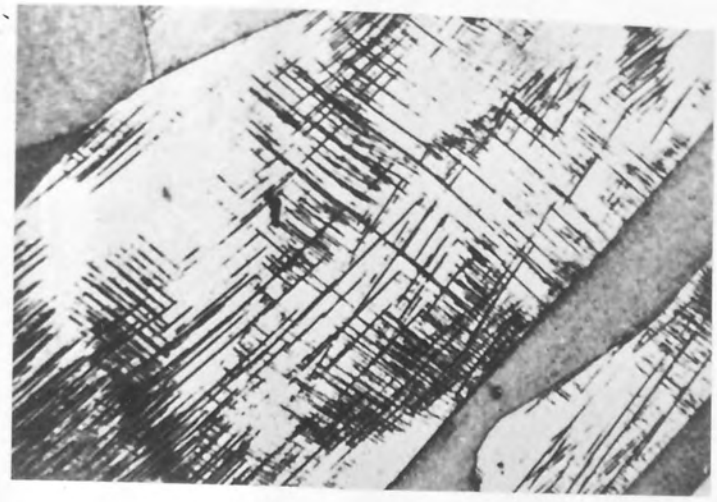

-a-

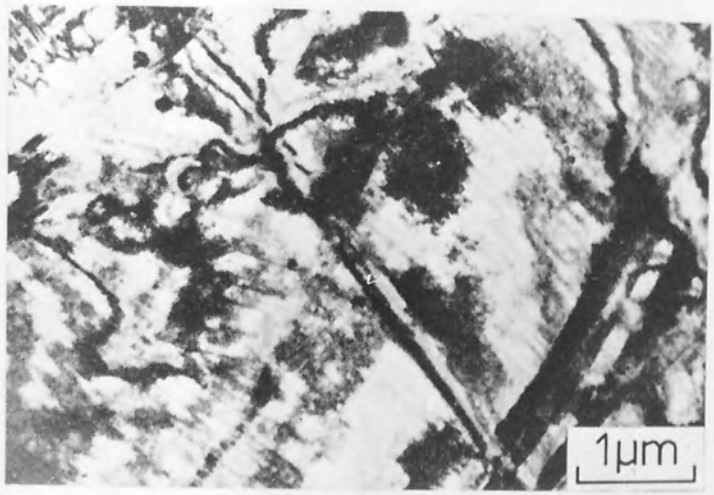

-b-

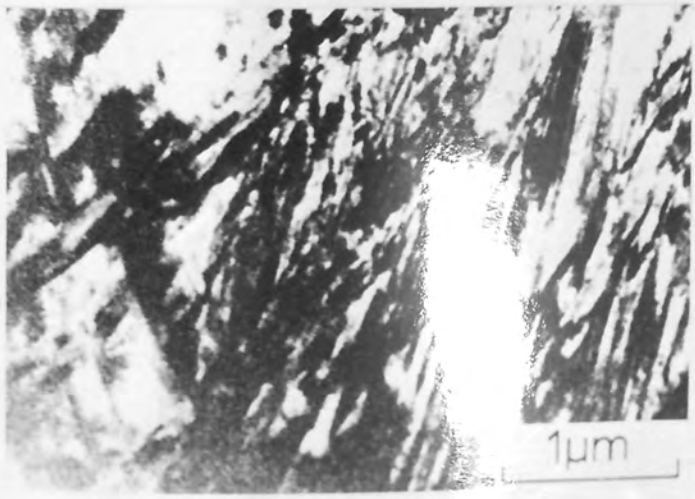

-c-

Fig.(10) - Longitudinal sections showing deformation microstructure in rolled 70 : 30 brass, trace of the rolling direction horizontal.

a - Optical micrograph showing shear bands after 60 % reduction X550. Ref.(21)

b - Optical micrograph showing shear bands after 90 % reduction X500 Ref.(23)

c - Electron micrograph showing shear bands after 60 % reduction. Ref.(23)

d - Electron micrograph showing shear bands after 90 % reduction. Ref.(23).

-c-

-a-

-b-

-d-

Fig.(11) - Analysis of orientation in shear bands.

a - Single shear band showing location of STEM diffraction patterns.

b - Orientations from location in (a) and other shear band sites.

Ref.(21)

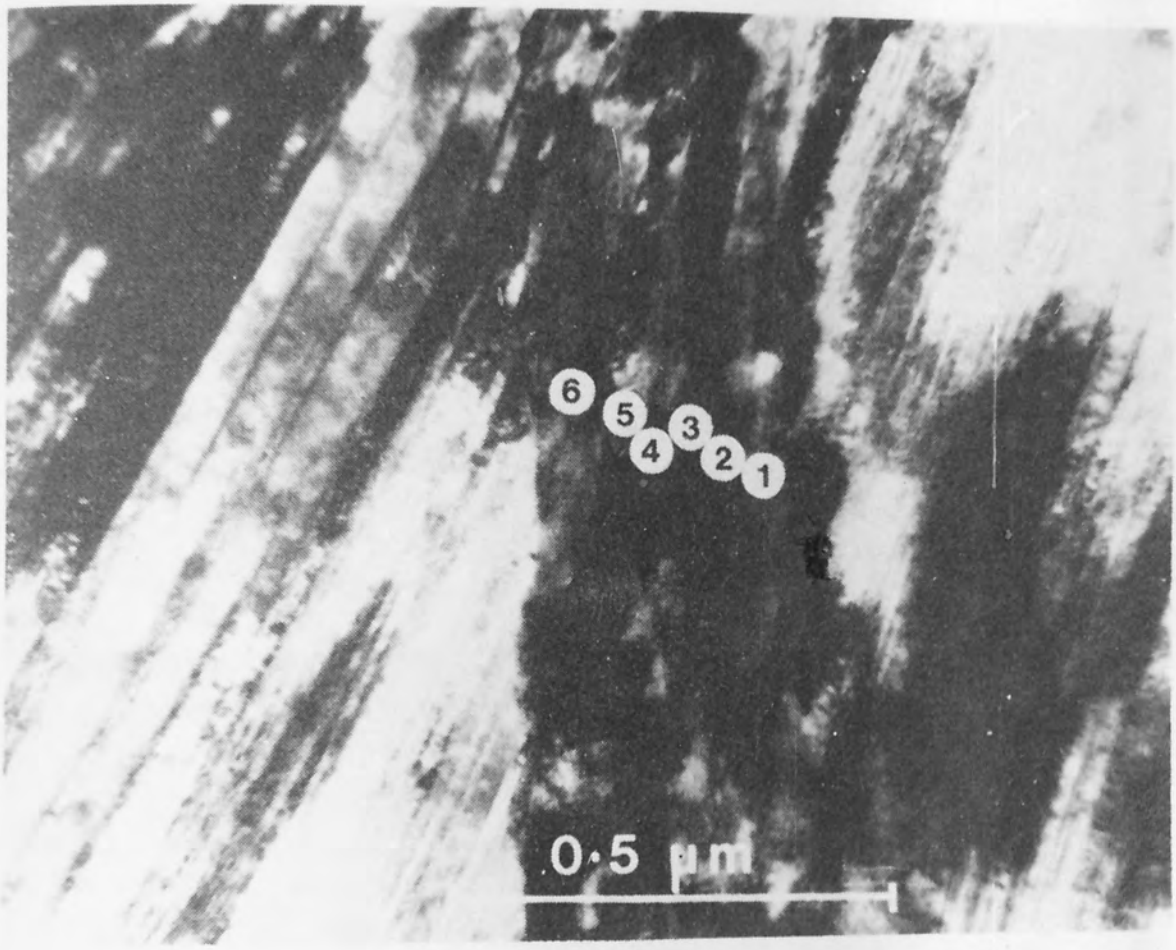

(*a*)

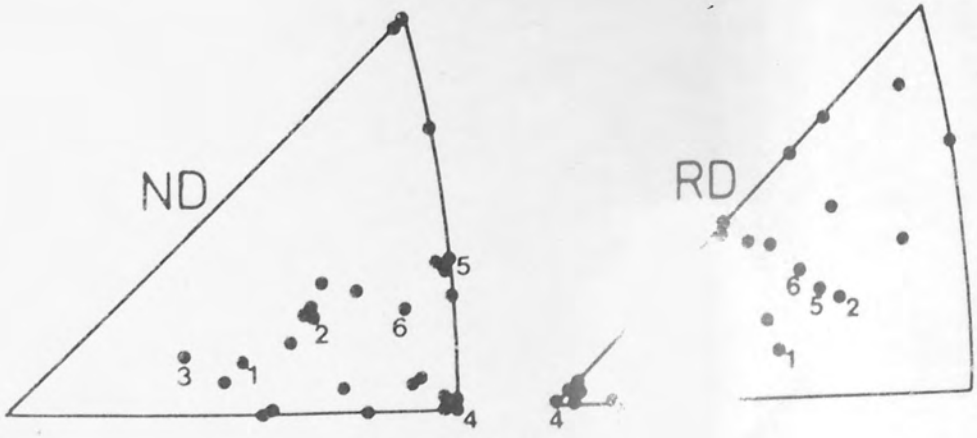

(*b*)

Fig.(12) -

a - Geometric softening factor $(\frac{1}{M} \cdot \frac{dM}{d}) \cos 2\Theta$ as a function of shear angle β. Curve b for $\{44\ 11\}\ \langle 11\ 11\ 8\rangle$ and curve c for $\{110\}\ \langle 112\rangle$ are averages for two symetrical variants of these orientations. Curve a is for $\{110\}\ \langle 001\rangle$. Weighted average for these curves has minimum at $\beta \sim 35^{\circ}$.

b - Geometrical softening factor for positive and negative shear bands in the $\{441\}\ \langle 11\ 11\ 8\rangle$ component.

Ref.(64)

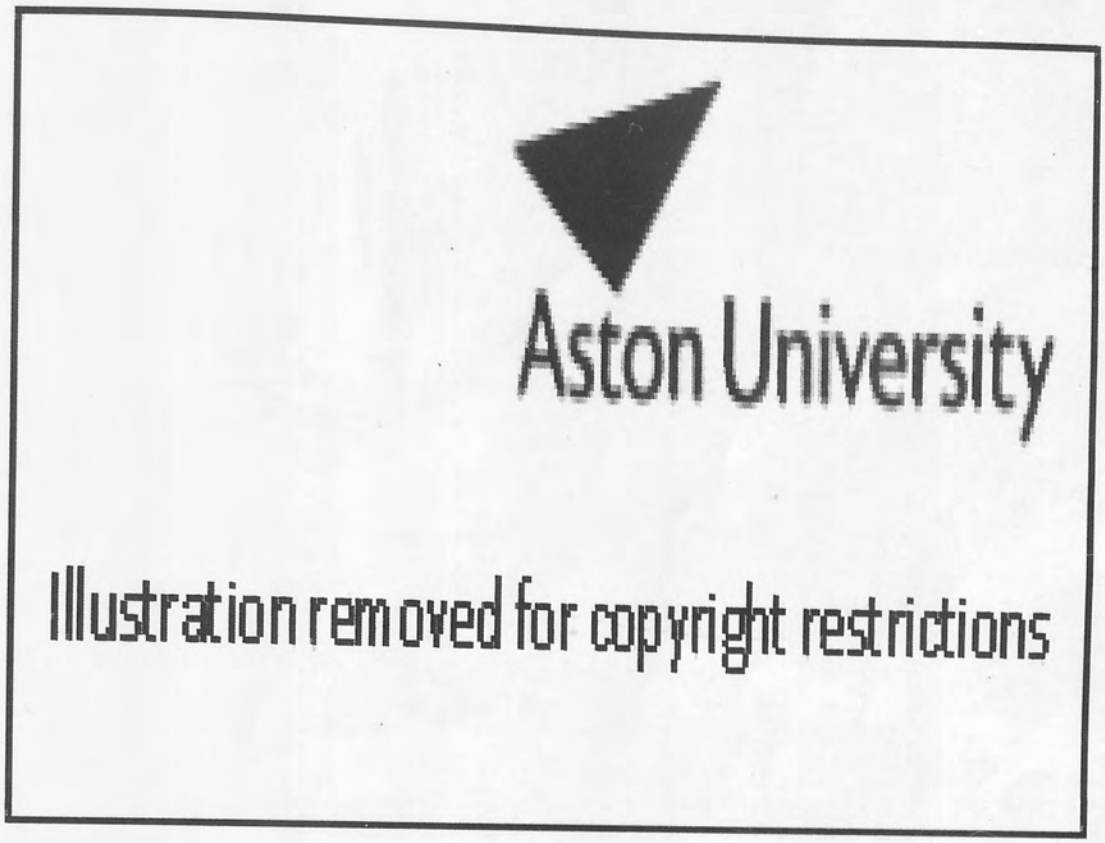
Aston University
Illustration removed for copyright restrictions

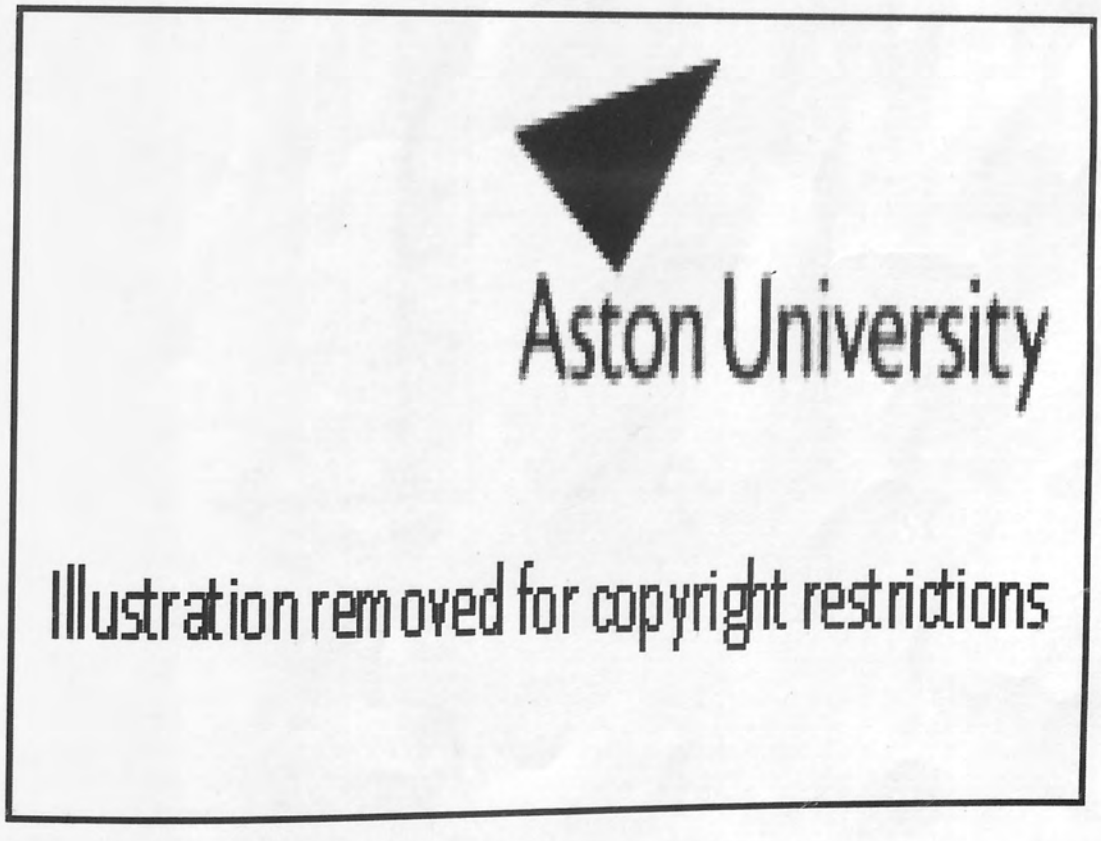
Aston University
Illustration removed for copyright restrictions

the microstructure developed in deformed F.C.C. metals appears to be determined by SFE. The other factors which may also affect the microstructure are strain rate, deformation temperature, grain size, and the orientation in the case of single crystals. Most studies have been concerned with the effect of these variables on the development of texture, annealing characteristics and flow stress of the materials.

Strain rate :-

Increasing strain rate causes an increase in the number of moving dislocations and thus an increase in the frequency of tangle formation and decrease in the cell size. Many investigators (65-68) have reported that increasing strain rate decreases the size of the equiaxed cell structure. Johari et al (65) studied the microstructure of explosive shock-loaded copper and reported a limiting cell size of $\sim 0.15\mu m$, and as the pressure was increased fine mechanical twins developed, their thickness was $\sim 0.05\mu m$, and the equiaxed cells that were formed were slightly elongated. Similar results have been reported in shock-loaded nickel (67-68). Roberts (69) has shown that the effect of explosive shock on Hadfield manganese steel is to produce multiple twinning on all $\{111\}$ planes in each grain, whereas at low strain rate they only develop on one or two systems. Most studies of the effect of strain rate on deformation characteristics of F.C.C. metals have not involved detailed investigations of the development of microstructure, however it appears that increasing the strain rate has a similar effect to that of decreasing the SFE.

Grain size :-

The influence of grain size on the deformation microstructure has received very little attention. However, in copper deformed to a strain level of $\varepsilon=0.2$ Johari et al (65) reported that the dislocation density in single crystals was less than in polycrystalline materials. At high strain levels differences in the limiting cell size in deformed copper observed by Hu (27) and Embury et al (26) were attributed by Hu to differences in the initial grain size or impurity content. In an examination of Cu-Sn alloys, Baker et al (60) have shown that the extent and morphology of twins was dependent on the initial grain size. twins were fewer and narrower in fine grained material: Liu et al (61) made a texture analysis of Cu-Sn alloys in which they found that fine grained alloys developed copper type textures, whereas coarse grained alloys formed brass-type textures. It appears that increasing initial grain size has the same effect as decreasing SFE, but to a less marked extent.

Deformation temperature :-

A number of investigators (28, 65, 68) have shown that the dislocation density and distribution in F.C.C. metals deformed to low strains is influenced greatly by the deformation temperature. With decreasing temperature, the equiaxed cell size decreases and the dislocation density within the cells and cell walls increases in aluminium (28), copper (65), and nickel (68). Keh et al (70) observed that the dislocation distribution becomes more uniform for a given strain as the deformation temperature is lowered. Furthermore, the tendency

for cell formation becomes less pronounced and the formation of a distinct cell structure requires more deformation. Increasing the deformation temperature causes a sharp increase in cell size and dynamic recovery is believed to occur. Malin (45) has shown that polycrystalline and (100)[001] single crystals of copper, which do not form twins when rolled at room temperature, developed a mixed structure containing equiaxed cells, microbands and twins when rolled at 77 k. Similar results were obtained by Leffers et al (58) in copper deformed at 77 k. Morii et al (71) studied the effect of orientation and temperature on the deformation characteristics in Cu 8 % Al single crystal, and found that twinning was more extensive at 77 k than at 273 k. It is generally accepted that the effect of lowering deformation temperature is similar to decreasing the SFE.

Orientation :-

Hu et al (42) have shown that the recrystallization behaviour of rolled (001) [110] Si-Fe is quite different from rolled (001) [100] and they attributed this to differences in the deformation microstructure. Transmission microscopy showed that the substructure was quite uniform in the first crystal, whereas in the second the microstructure consisted of deformation bands and elongated cells parallel to the rolling plane. Dillamore et al (72-73) found that the subgrains in deformed polycrystalline iron rolled 70 % were 0.5-1μm in diameter and had average misorientations from 2° to 6°. The variation came with different orientations of the grains in which the substructure had formed (Fig.13). Blicharski et al (62)

reported that in deformed austenitic stainless steel, the grains having orientation close to {110} <001> were stable on rolling, and that deformation was accommodated only by dislocation glide. These grains did not form deformation twins unlike most other orientations.

In the case of low SFE materials, investigations of Cu-6 at % Al by Sekine et al (55) showed that both (123) $[\bar{2}\bar{1}1]$ and (111) $[0\bar{1}1]$ single crystals rolled to 50-80 % reduction developed a large number of fine deformation twins. Hu et al (54) observed significant differences in the substructure of rolled (112) $[11\bar{1}]$ and (110) $[1\bar{1}2]$ crystals of Cu-8.94 at % Al. The (112) $[11\bar{1}]$ crystal exhibited profuse clusters of faults and fine twins at a low strain level ($\varepsilon < 0.2$), whereas, the incidence of twins was much lower in the (110) $[1\bar{1}2]$ crystal and remained relatively constant to high strain levels.

Investigations of copper (medium SFE) on (110) $[1\bar{1}2]$, (111) $[0\bar{1}1]$ and (100) [001] crystals deformed by rolling (45) showed that at high strains the structures are basically similar. At low deformations ($\varepsilon < 0.2$) the effect of orientation is not clear. Johari et al (65) were unable to correlate orientation with the structure developed in deformed copper because of the widely varying dislocation density and cell morphology. These observations suggest that the effect of orientation on the deformation microstructure developed in F.C.C. metals is most pronounced for low SFE materials.

2.5. Work hardening :-

It is well known that when a metal is deformed

Fig.(13) - The variation of substructure in iron with orientation and degree of deformation.

Ref.(73).

Fig.(14) - Relationships between true stress and true strain (●); hardness and true strain (○); subgrain size and true strain (▲) (from transverse sections).

Ref.(34).

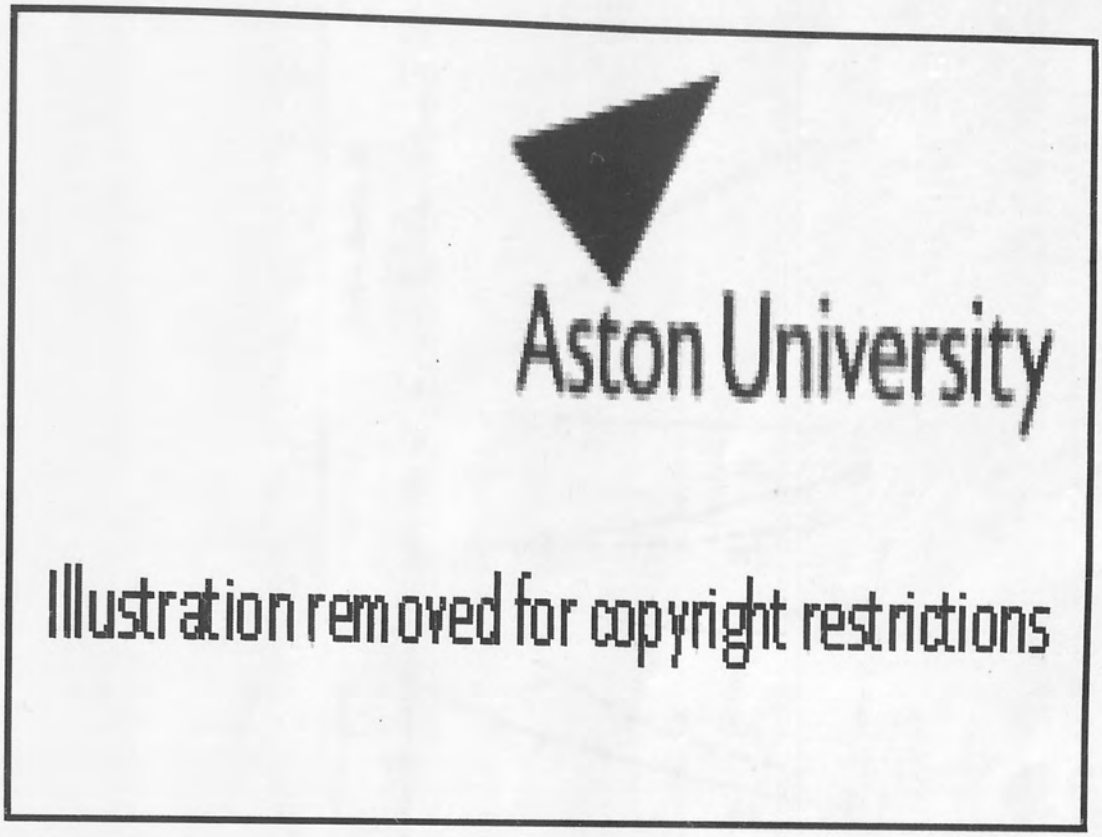
Aston University
Illustration removed for copyright restrictions

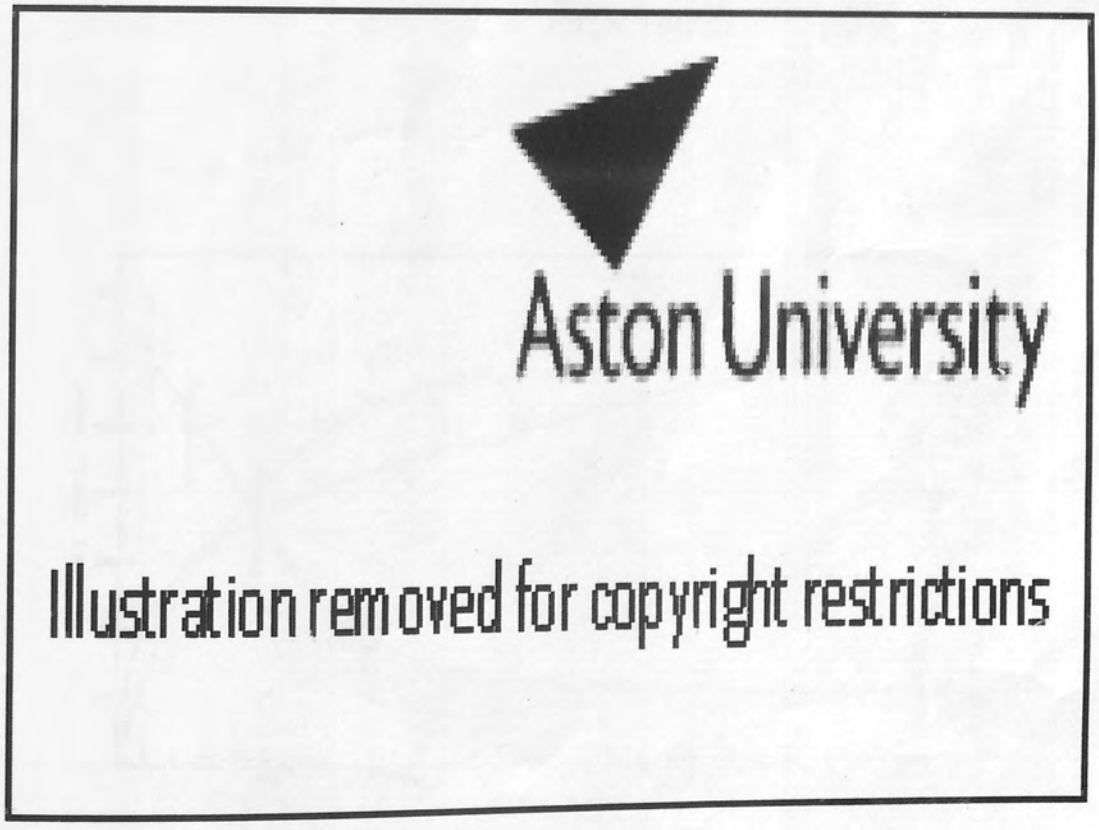
Aston University
Illustration removed for copyright restrictions

plastically it becomes harder and a continual rise in stress is required to continue deformation. The changes in mechanical properties of materials due to plastic deformation have been extensively investigated by many workers. The majority of these investigations have been concerned with the development of a description of the plastic behaviour of single crystals in terms of dislocation theory. This discussion, however, will be restricted to the less frequently investigated area of high strain work hardening in polycrystals.

Embury et al (26) examined the changes in mechanical properties and their relation to the deformation microstructure in copper and a variety of ferrous alloys deformed by drawing and rolling. TEM revealed that during the first 15 % deformation there was a large increase in dislocation density. The distribution of dislocations was not uniform but consisted predominantly of dense tangles which eventually formed into well defined cell walls. The cells' size decreased with strain until they reached a limiting value, which was attributed to dynamic recovery. In most cases the correlation observed between the cells size (d) and the flow stress (σ_f) was of the form $\sigma_f \propto d^{-\frac{1}{2}}$. This relationship is analogous to the Hall-Petch equation for grain size strengthening of annealed metals which is written :-

$$\sigma_f = \sigma_o + K(d^{-\frac{1}{2}})$$

Where σ_o is the friction stress resisting dislocation motion, and K is a constant. In a similar kind of study Langford et al (74) reported a hyperbolic dependence of flow stress $\sigma_f \propto d^{-1}$. In phosphorous-deoxidized copper deformed by drawing,

polygonization after 70 % deformation and even recrystallization after 95 % deformation has been reported by Cairns et al (47). It was believed that the flow stress at low strain levels is controlled by the grain boundaries which provide the most effective barriers to dislocation movement. With further deformation the subgrain size decreases far more rapidly than the grain size; consequently flow stress becomes subgrain size dependent. Recently, Wakefield et al (20) showed that the attainment of a limiting cell size in Cu-Al alloys was associated with the appearance of shear bands in the substructure, while in the case of deformed copper it corresponded to a general sharpening of sub-boundaries and the alignment of microbands with the rolling direction.

Many workers (20,26, 34, 74, 75) have shown that the work hardening rate increases rapidly in the early stages of plastic deformation and it becomes virtually constant after certain strain level. In the case of copper this happens after a true strain of about unity as shown in Fig.(14). Hardness measurements for OFHC deformed by compression (34) showed that the hardness reached a maximum after a true strain of $\varepsilon = 1$, which corresponded to the stage where the cell size reached a constant value with the occurrence of dynamic recovery, see Fig. (14). Aghan et al (76) studied the changes in deformation microstructure with strain and their contribution to the work hardening in deformed low carbon steel. TEM showed that the initial high work hardening rate was associated with high dislocation density, large jogs in dislocations, dipoles, small loops, and the tangling of dislocations into the

beginning of cell walls. After 5 % deformation dislocation, cells were developed, their size was 1-2μm, which was strain independent. This observation led Aghan et al to conclude that after initial cell formation no further work hardening contribution would be expected from this source. They observed that once the initial equiaxed cell structure formed, the dominant structural change was the formation of microbands which became the dominant factor contributing to work hardening. They also suggested that the linear portion of the stress-strain curve is associated with microband formation, and that the increase in strength is related to the proportion of the total volume occupied by microbands. At very high strain levels the ribbon like cells occupied almost the total volume; they were approximately constant in size, apparently due to a balance between cell reduction and dynamic recovery.

2.6. Stored energy :-

When metals and alloys are deformed plastically some of the energy expended (usually from 1 % to 10 %, the fraction decreasing at large strains) is not released as heat but is stored in the metal causing an increase in the internal energy. This is normally in the form of elastic strain energy, dislocations, point defects and energy associated with stacking faults and twins.

The elastic strain energy contribution to the total stored energy is usually very small. Averbach et al (77) found that the elastic strain energy was about 3 % of the total stored energy in filed 75 % gold - 25 % silver alloys,

whereas in ground nickel it was about 12 % (78-79). This minor contribution to the stored energy indicated that the major portion is due to the energy associated with lattice imperfections.

The increase in the internal energy of the cold worked metal and alloys makes them thermodynamically unstable, consequently when they are annealed the stored energy will be released. The release of the stored energy is associated with the reduction and rearrangement of the lattice defects. Haessner (80) has made a systematic classification of the multitude of phenomena that may occur on annealing cold worked materials at temperatures below the melting point. These are essentially the following :-

1 - Reactions of point defects and point defect agglomerates; in particular the annihilation of these defects.

2 - The annihilation of dislocations of opposite signs and the shrinking of dislocation loops.

3 - The rearrangement of dislocations to form energetically favourable configurations.

4 - The absorption of point defects and dislocations by grain boundaries migrating through the metal.

5 - The reduction in total grain boundary area.

Haessner (80) termed processes (1) and (2) recovery, processes (4) and (5) recrystallization and process (3) polygonization.

It has been found that the value of the stored energy of cold worked metals varies with the metal purity, deformation mode, deformation temperature, grain size, and material. Additions of foreign atoms to a metal invariably allow larger amounts of stored energy of cold work. Bohnenkamp et al (81) found that in copper specimens of 99.96 % and 99.88 % purity after similar amounts of wire drawing the stored energies were about 19 and 95 cal/gm - atom respectively.

The temperature at which the deformation is carried out is a very important variable affecting the amount of stored energy. Greenfield (82) found that the stored energy in drilled gold was about 20 cal/gm - atom when the deformation took place at room temperature but increased to about 90 cal/gm atom when deformed at -195°C . This could be explained on the basis that the work hardening rate generally increases at lower deformation temperatures because thermal activation becomes less helpful to dynamical recovery processes.

The stored energy is also found to be a sensitive function of the grain size particularly at low strain levels. Clarebrough et al (83) compared the stored energy in polycrystalline copper in fine grained ($\sim 30\mu m$) and coarse grained ($\sim 150\mu m$) conditions. For strain levels below 50 % the fine grain sized copper had larger values of stored energy, but after 50 % deformation the values were the same for both materials. These findings are consistent with the view that dislocations density is dependent on grain size particularly at low strain levels.

The amount of stored energy released in each relaxation process (recovery and recrystallization) during annealing is based on the definiton of each process. Recovery includes all annealing phenomena which occur before the appearance of recrystallized grains, whether these are detected by optical or electron microscopy, and recrystallization is the nucleation and growth of these new strain free grains and the gradual consumption of the cold worked matrix by the movement of large angle grain boundaries. Clarebrough et al (84) found significant differences in the behaviour of stored energy release for two grades of copper of 99.967 % and 99.988 % purity, which had been deformed to the same strain level. As shown in Fig.(15), in the case of purer copper the fraction of stored energy released during recovery was 5 %. whereas for the less pure copper it was about 30 %; the corresponding recrystallization temperatures were 170°C and 290°C respectively.

Alloying can significantly change the energy release characteristics of deformed materials on heating. Clarebrough et al (85) investigated the release of stored energy in 99.8 % copper deformed to 40 % by elongation. They found that for the pure copper there was one sharp (Δ Power) peak at about 300°C whereas in the case of arsenical copper a smaller (Δ Power) peak is found at about 440°C. As shown in Fig.(16) this latter peak is superimposed on a low energy release plateau which begins at about 70°C.

It has also been found that the initial grain size

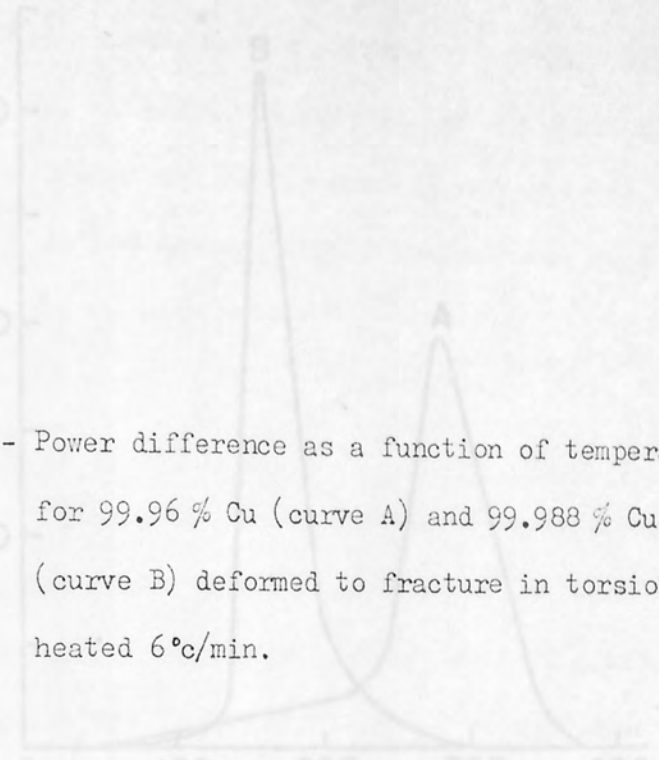

Fig.(15) - Power difference as a function of temperature for 99.96 % Cu (curve A) and 99.988 % Cu (curve B) deformed to fracture in torsion and heated 6 °c/min.

Ref.(84).

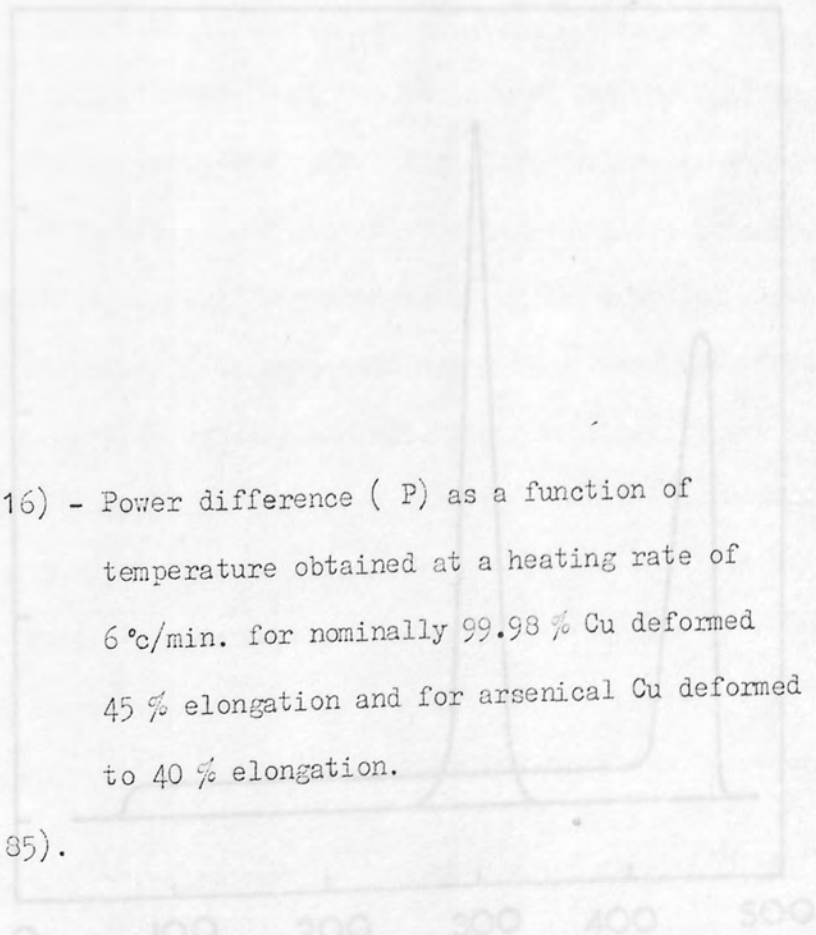

Fig.(16) - Power difference (P) as a function of temperature obtained at a heating rate of 6 °c/min. for nominally 99.98 % Cu deformed 45 % elongation and for arsenical Cu deformed to 40 % elongation.

Ref.(85).

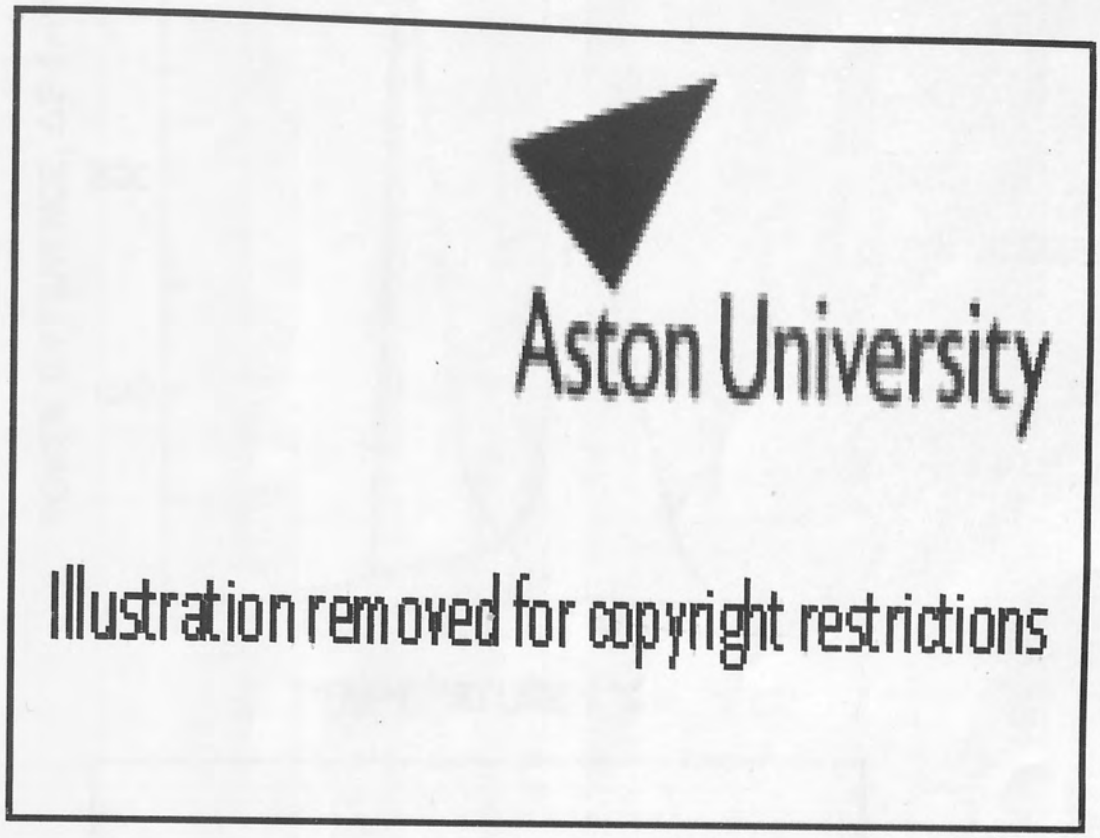
Aston University
Illustration removed for copyright restrictions

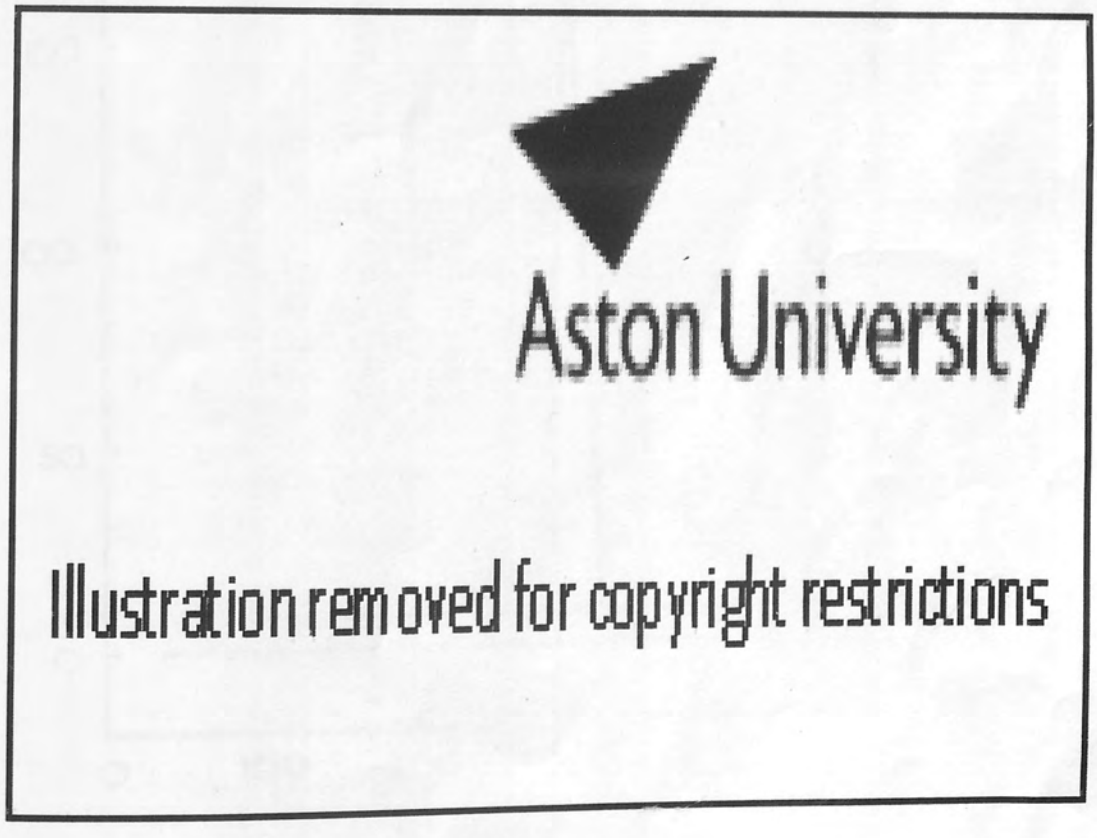
Aston University
Illustration removed for copyright restrictions

has an effect on the manner in which the stored energy is released. The fine grained material releases its stored energy more rapidly than the coarse grained material and the recrystallization temperature is always found to be lower in the fine grained material.

2.7. Recovery :-

Recovery can be considered to be any modification of properties during annealing, which occurs before the appearence of new strain free recrystallized grains. Properties change occurs due to the migration of vacancies and of dislocations, leading to annihilation or rearrangement of a certain portion of them. During recovery there will be no change in the orientation of the deformed matrix. It is usual to find that during recovery both the mechanical and physical properties of materials show some change from their values in the deformed state. Normally, the restoration of a mechanical property such as hardness or yield strength to its fully annealed value is only about one fifth completed during recovery (87). Physical properties like density and electrical resistivity are also found to undergo detectable change from their cold worked values during subsequent annealing. Likewise particle size and residual stress measured by x-ray diffraction show some change from their values in the cold worked state. Fig.(17) demonstrates how these properties may change during recovery.

Following the work of Drouard et al (88) a parameter R may be defined which gives a measure of the fraction of the particular property recovered.

$$R = \frac{Xm-X}{Xm-Xo} \qquad \text{- - - - - - - - - - - - - - - (1)}$$

Where Xo is the value of the property in the fully annealed material, Xm is the strain hardened value, and X is the value after the recovery anneal.

Equation (1) can be written in the following form :-

$$1-R = \frac{X-Xo}{Xm\ Xo}$$

TEM evidence indicated in general that the deformed metal has a cell structure. The cell walls consist of dislocation tangles, and some additional dislocations are found to exist in the cell interiors. As annealing starts, the tangled dislocations in the cell walls rearrange themselves while the dislocations within the cells are attracted to the cell walls which makes these more clearly defined and eventually they form subgrains of about the same size as the initial cells. This process is normally called polygonization. Keh (89) found direct experimental evidence that the dislocation density decreases during the initial stage of recovery Fig.(18). It has also been found (90) that elongated dislocation loops, which formed during plastic deformation, gradually become circular and finally vanish during recovery.

2.8. Primary recrystallization :-

Recrystallization is the process in which deformed crystal structures are completely replaced by new unstrained ones. It is well known that recrystallization of deformed metals involves the formation of strain-free regions (nuclei) and the growth of these into the surrounding cold worked matrix by high angle grain boundary migration.

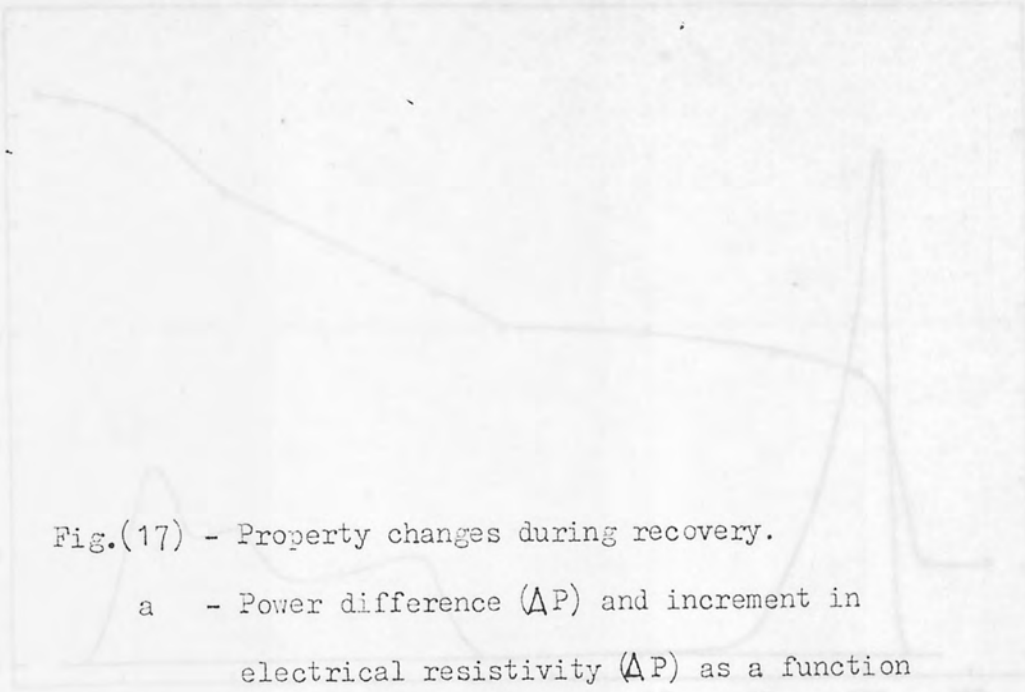

Fig.(17) - Property changes during recovery.

a - Power difference (ΔP) and increment in electrical resistivity (ΔP) as a function of temperature for Cu wire (99.98 %) drawn 54 % at -195°C. Heating rate 2°C/min.

Ref.(83).

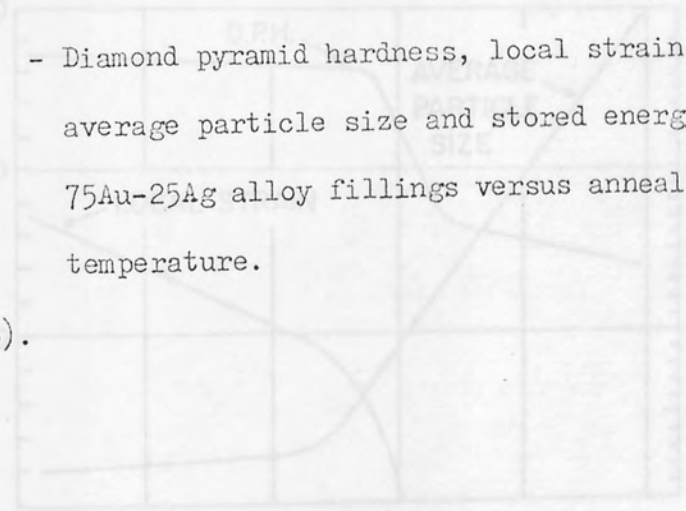

b - Diamond pyramid hardness, local strain, average particle size and stored energy of 75Au-25Ag alloy fillings versus annealing temperature.

Ref.(86).

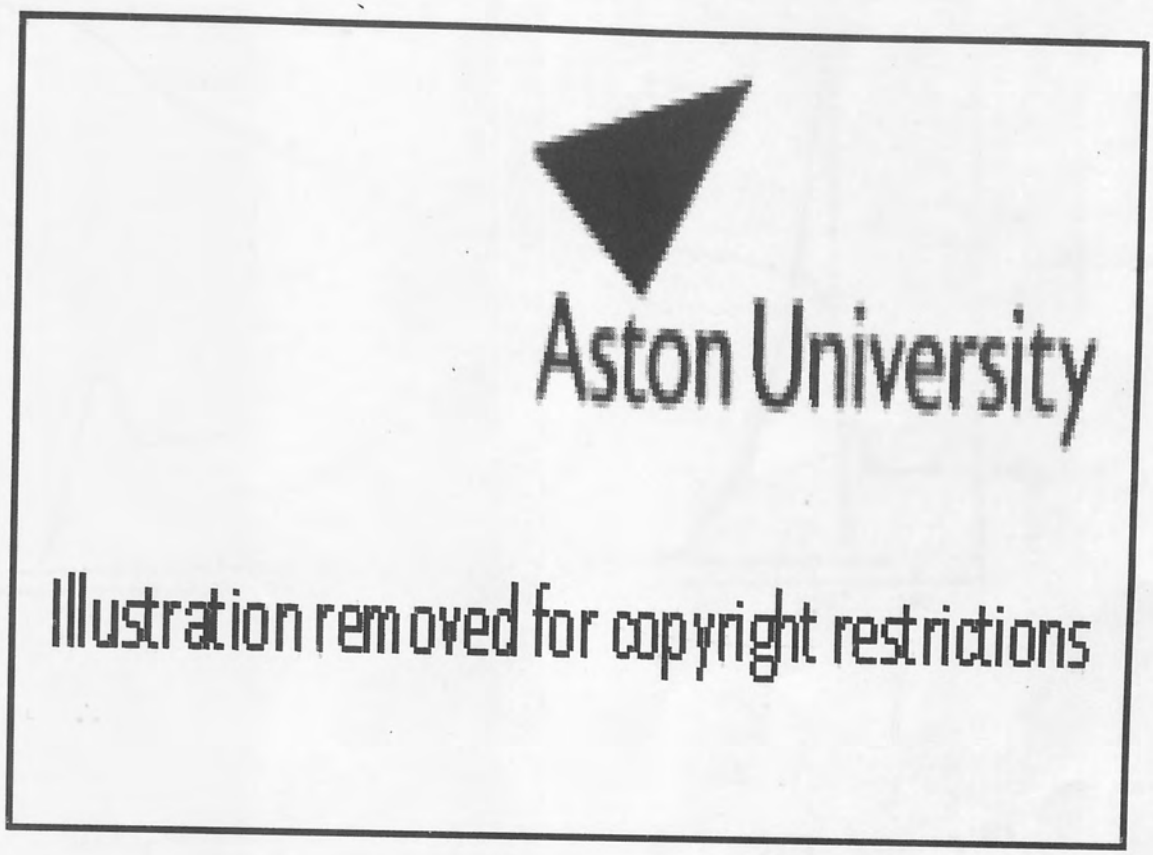
Aston University
Illustration removed for copyright restrictions

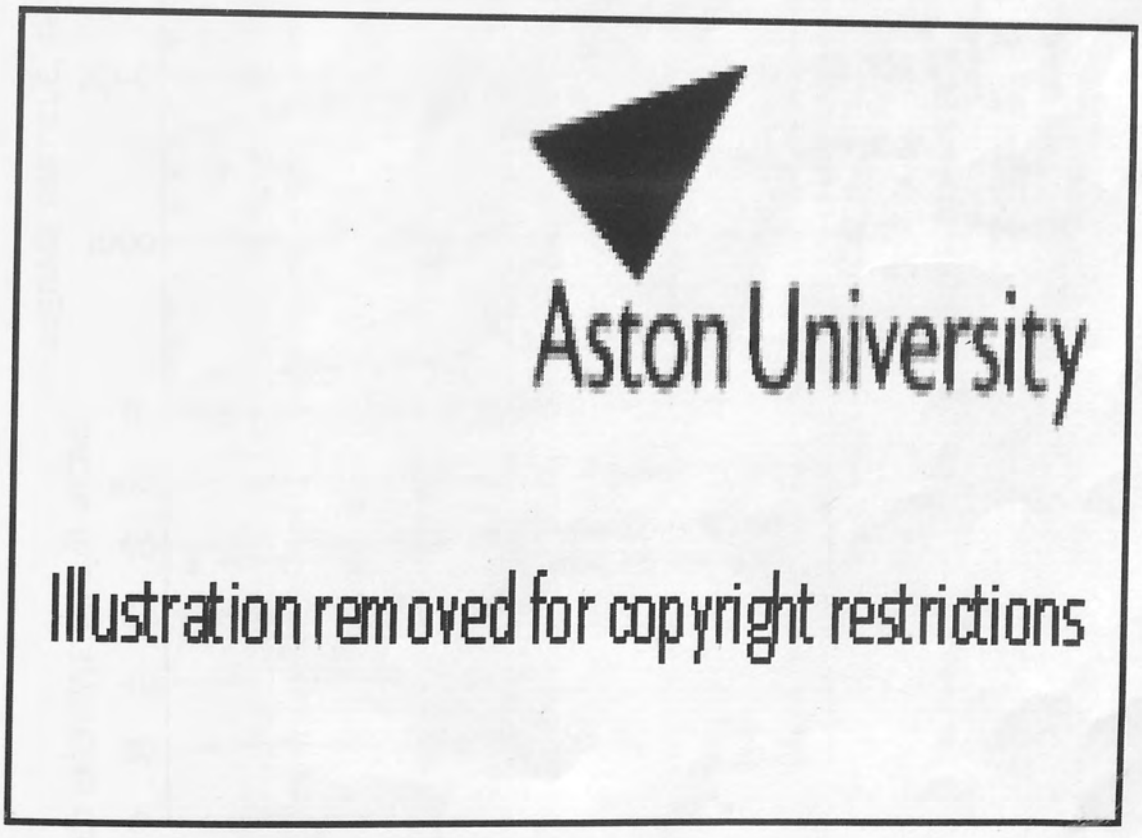
Aston University
Illustration removed for copyright restrictions

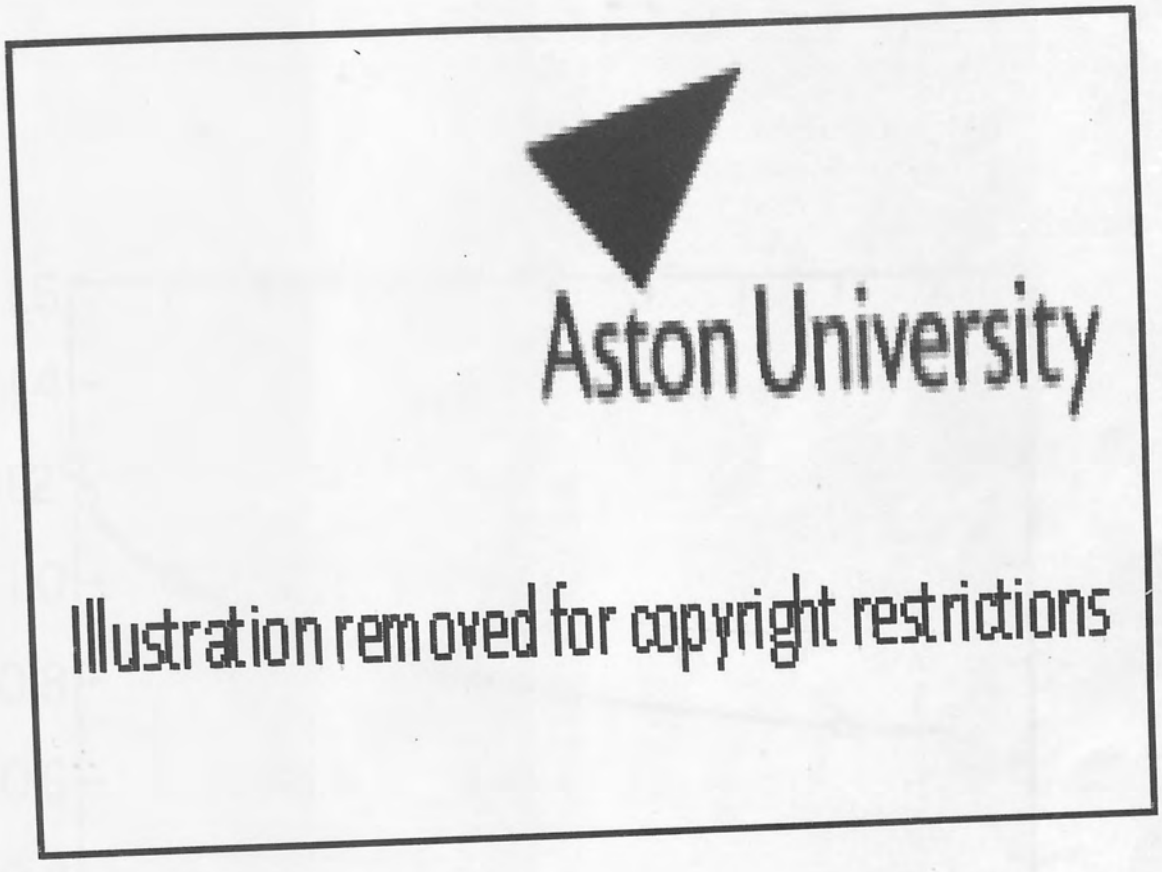
Aston University
Illustration removed for copyright restrictions

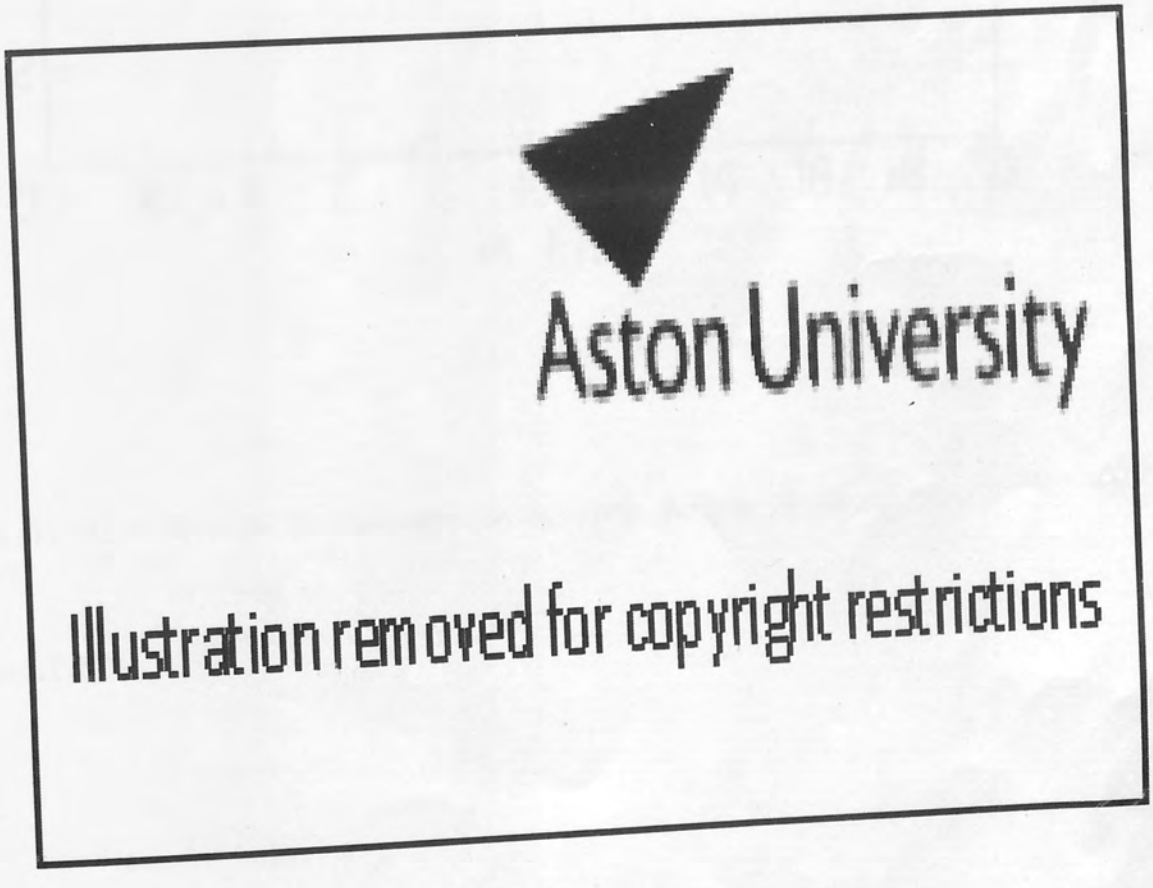
Aston University
Illustration removed for copyright restrictions

Nucleation processes :-

Despite a considerable amount of research in this subject it is still not clear what is the important mechanism (or mechanisms) during nucleation. This is quite understandable since nuclei, by nature, are small and so extremely difficult to observe before they start growing. Nucleation processes have been reviewed and discussed by many workers (90-95). According to Doherty (95) there are four suggested nucleation models.

a - The classical fluctuation theory :- The classical Volmer-Becker theory of nucleation, as ordinarily applied to the formation of solid nuclei in super cooled liquids, has been extended by Burke and Turnbull (96) to the nucleation problem during primary recrystallization.

b - The martensitic model (reverse Rowland Transformation). This model was proposed by Burgers and Verbraak (97-98).

c - The growth of polygonized subgrains as suggested by (99) and Beck (100) and further discussed by Cottrell (101).

d - The model of strain-induced boundary migration (SIBM). This model was proposed by Beck and Sperry (102).

Only models (c) and (d) will be considered in this section, because there are experimental results supporting them. In these two models nucleation does not require formation of new orientation in the cold worked material, but rather the development of subgrains already present after deformation. Ray et al (103-105) have made direct observations by HVEM of

nucleation in heavily rolled copper. They found that nuclei came from identified subgrains previously seen in the as rolled material. Hu and Hu et al (42, 106) and Walter et al (107) have found that the formation and growth of nuclei normally takes place in transition bands, and the nuclei have the same orientation as the orientation of the sub-band from which they originate. Noda et al (108) observed cube oriented regions in deformed copper and aluminium alloy; with subsequent annealing these regions polygonized faster than the other orientation in the deformed state and started to grow at the expense of the deformed matrix. Doherty et al (109-111) observed that nucleation occurs by growth of regions in transition bands. TEM and TK (Transmission Kossel diffraction) showed that the developing nuclei were very close in orientation to one part of the adjacent cold worked material.

Subgrain growth model :-

This model was suggested independently by (99) and Beck (100). It was based on the idea that the cold worked structure polygonized during annealing, i.e. the uniformly distributed edge dislocations in the deformed material rearrange themselves into arrays normal to their Burgers vector, which creates strain-free cells capable of growth into the differently oriented surrounding matrix. The process of subgrain formation usually takes place either by the end of the deformation process or in the early stages of the annealing treatment.

It is well known that the factors which make any

nucleus viable are the stored energy of the matrix and its lattice curvature. In order for a nucleus to be formed and be capable of rapid growth it is necessary that the matrix is of high stored energy (72) and that the nucleus is surrounded by a boundary of high mobility (101). A number of workers have also indicated the importance of a potential nucleus acquiring a single advantage over its neighbours (73, 92, 94, 106, 112). These factors may be drawn together in the following expression (94)

$$\frac{dR}{dt} = M\left[\Delta F - \frac{2\sigma}{R}\right]$$

Where R is the radius of the nucleus, M its interface mobility, ΔF the free energy per unit volume for growth, and σ the specific free energy of the interface. This equation predicts that with increasing R the over driving force for growth increases. However, also with increasing R the misorientation of the boundary increases. This has two effects, one is to increase the mobility of the boundary, and secondly to increase the specific boundary energy. The former accelerates the growth rate, while the latter retards it. As a result, some equilibrium between the two factors will be set up dependent upon stored energy and lattice curvature. At equilibrium $\frac{dR}{dt} = 0$, so that $R = \frac{2\sigma}{\Delta F}$. It follows that growth will occur if $R > \frac{2\sigma}{\Delta F}$

The way in which the potential nucleus in a locally misoriented region acquires the necessary size advantage for growth has been the subject of much discussion. Hu (113-114) argued that coalescence of several subgrains into one large subgrain was the vital step, while Walter et al (107,115)

and Dillamore et al (112) believed that subgrain boundary migration was the important mechanism.

According to the coalescence model the increase in size of subgrains during annealing occurs by adjoining subgrains with slightly different orientation merging into the same orientation and so giving rise to a bigger subgrain. The process of coalescence is shown schematically in Fig.(19). The boundary CH between two adjoining subgrains in (a) is shown being eliminated by the rotation of the right hand side subgrain in (b). Clearly, if this is to be accomplished it is necessary to have some atom diffusion along the boundary from the shaded areas to the corresponding open area (b). The subgrain structure just after coalescence is shown in (c), where a geometrical adjustment of the connecting boundaries (CB, CD, HI and HG, originally connecting with the common sub boundary CH) is necessary. The final structure after straightening out of the connecting boundaries by boundary migration is shown in (d). Thus the whole process requires co-operative climb of dislocations along the disappearing subgrain boundary and also some atom movement by vacancy diffusion around subgrain. The kinetics and thermodynamics of the coalescence process have been examined in detail by Li (116). Many TEM observations in support of this mechanism have been reported in deformed aluminium by Doherty and co-workers (109,111), and by Fujta (117), in tungsten single crystals by Koo et al (118), and in silicon-iron single crystals by Hu (42,114, 119).

Walter et al (107, 115) observed nucleation in transition bands in deformed silicon-iron crystals as used by

Hu but did not observe the coalescence that Hu had reported. They argued that the faint subgrain boundaries which Hu had observed were not due to coalescence but due to electron diffraction contrast (115). Furthermore they have suggested that the subgrains acquire the necessary size to become potential nuclei by subgrain boundary migration. Evidence in support of this proposed mechanism has been reported by Michels et al (120) and by Marsden (121).

Smith et al (112) measured the rate of subgrain growth in deformed high purity iron, and they found that subgrain growth occurred much faster than predicted on the basis of coalescence by Li (116). The most satisfactory model for subgrain growth is that developed by Dillamore et al (72). This model has been proposed for nucleation in transition bands by sub-boundary migration. The model is shown schematically in Fig.(20). It is assumed that prior to annealing a large subgrain of length D_r exists in a matrix of subgrains of average length d_r and width d_t. On annealing the structure relaxes to form triple point angles of ϕ given by

$$\text{Cos}\,\phi = \frac{\sigma_r}{2\sigma_t}$$

Where σ_r is the horizontal boundary specific energy (such as bc and de), and σ_t is the vertical boundary specific energy (such as ab and df). If the points b and c come into contact before this equilibrium angle is achieved, then the subgrain ahgfdb will grow. This should occur if

$$D_r > \frac{4}{3}\left(d_r + d_t\left[\frac{4\sigma_t^2}{\sigma_r^2} - 1\right]^{\frac{1}{2}}\right).$$

This equation predicts that if a particular subgrain is

sufficiently long compared with the average transition band subgrain d_r, that subgrain is capable of growth. By this mechanism the growing subgrain will acquire the size advantage and the misorientation to become a viable nucleus. Observations by Ray et al (103-105) and Grewen et al (122) support the conclusions of this analysis.

Strain induced boundary migration (SIBM) or bulge model :-

In lightly rolled aluminium Beck et al (100) found that sometimes recrystallization does not involve any nucleation but only growth of strain free regions brought about by grain boundary migration. This is shown schematically in Fig. (21). It has also been observed in silver, nickel, and copper (123-124). It was proposed that circular regions of diameter 2L of the boundary bulge out due to a difference ΔE in stored energy across the boundary. If growth is to occur then :-

$$L > \frac{2\gamma}{\Delta E}$$

Where γ is the specific energy of the grain boundary (124). Thus the operation of this mechanism depends on the stored energy difference across the boundary. Dillamore et al (72-73) found that in deformed iron different orientations had different subgrain sizes and misorientation between neighbouring subgrains and, accordingly, different value of stored energy as shown in Fig.(13). For a [110] rolling direction the stored energy rises as the rolling plane alters from (001) through $(1\bar{1}2)$ and $(1\bar{1}1)$ to $(1\bar{1}0)$. Frequently it is observed that the "victim" grain is the one which is more severely work-hardened, the stored energy of this grain providing the

driving force for the entire process. The grain with the larger cell size will normally have the lower energy, so that recrystallization occurs by the movement of a portion of the boundary into the high energy grain having a smaller cell size. It has been reported (111, 125) that this mechanism is the predominant one in recrystallization when materials are deformed to low-medium strains (up to 60 % deformation).

Nucleation sites :-

As mentioned in sections (2.2, 2.3) deformation creates regions of high local strain and sharp lattice curvature in cold worked metals. In high SFE materials the nuclei must form from the equiaxed cells, clusters of micro-bands, shear bands, or pre-existing grain boundaries. In low SFE materials deformation twins, shear bands, or pre-existing grain boundaries are expected sites. At very low strain levels (< 10 % reduction by rolling)there is little inhomogeneity suitable for nucleation. Recrystallization should not occur and it is well known that in such cases recovery or polygonization processes dominate. At higher strain levels (10-50 %) strain induced boundary migration (SIBM) at existing high angle grain boundaries is a common process for recrystallization (111-125). At strain levels $>$ 50 % reduction by rolling, the nucleations sites are transition bands, clusters of microbands, and shear bands.

The high dislocation density and sharp lattice curvature in shear bands make them highly favourable sites for nucleation in heavily deformed metals. In 1922 Adcock (25),

who was the first to report shear bands in heavily deformed cupro-nickel, showed also that, recrystallization on annealing occurred in the shear bands. Recently similar observations have been reported by Grewen et al (46) in Cu-0.6wt % Cr, by Duggan et al (126)in 70 : 30 brass, and Blicharski (127) in austenitic stainless steel. Duggan et al (126) reported that after 40 % reduction by rolling deformation the structure contained no shear bands and nucleation occurred preferentially but sparsely at the grain boundaries resulting in a relatively coarse grained product. Shear bands form in 70 : 30 brass after 50 % deformation by rolling. On annealing, HVEM examinations showed that numerous recrystallized grains formed along the shear bands and especially at the intersection of two shear bands. The new grains were restricted to the shear bands and showed little tendency to intrude into the twinned volumes. Duggan et al made direct observations of recrystallization in thin foils by heating inside the microscope. They found that recrystallization always commenced in the shear bands but there was no preference for edge or central regions as shown in Fig.(22). Lateral growth of the recrystallized grains stopped as soon as the boundaries reached the edge of the shear bands and impinged on the twinned region. The orientation distribution for the first recrystallized grains formed within the shear bands was determined and the results shown in Fig.(23). This shows clearly that there is a large spread in orientation, in agreement with the texture determined from x-ray pole figures. The role of shear band nucleation has not been investigated in high SFE materials. The density of shear bands in heavily deformed high SFE materials is usually

not sufficiently large to provide all the nuclei needed for recrystallization, and so transition bands and microband clusters remain favoured sites for nucleation.

2.9. Preferred orientation :-

Rolling textures in FCC metals :-

When a randomly oriented polycrystalline aggregate is subjected to continuous plastic deformation the individual grains are not only distorted and broken down into smaller subgrains, they also tend to turn progressively into certain specific orientations. The non-random orientation distribution is normally called texture or preferred orientation. The nature of deformation texture depends on the crystal structure, deformation mode, and state of strain. Rolling textures of polycrystalline FCC metals and alloys can be classified into two types. First, the "pure metal" or "copper-type" rolling texture, which consists of a range of orientations from near $\{112\}\langle 111\rangle$ through $\{123\}\langle 412\rangle$ to $\{110\}\langle 112\rangle$. In general, FCC metals and alloys with medium or high SFE exhibit such a texture when heavily deformed by rolling at room temperature. The second type is the "alloy" or "brass-type" which, after heavy reductions, is mainly $\{110\}\langle 112\rangle$ with a minor $\{110\}\langle 001\rangle$ component. FCC metals and alloys with low SFE normally develop such a texture when they are heavily deformed at room temperature. Figs.(24 and 25c) show typical (111) pole figures for these two types of rolling texture.

Transitions from the "copper" texture to the "brass" texture can be accomplished by increasing alloy content or

Fig.(19) - Schematic representation of subgrain coalescence by subgrain rotation.

Ref.(116).

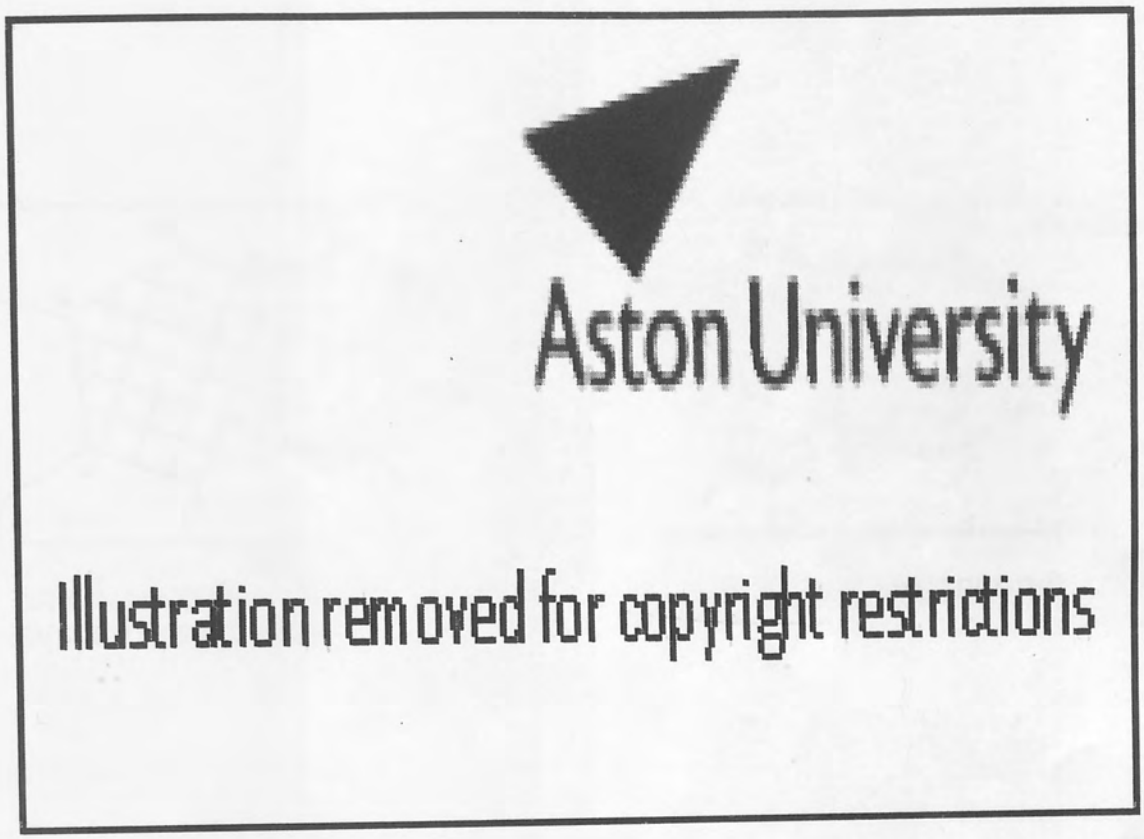
Aston University
Illustration removed for copyright restrictions

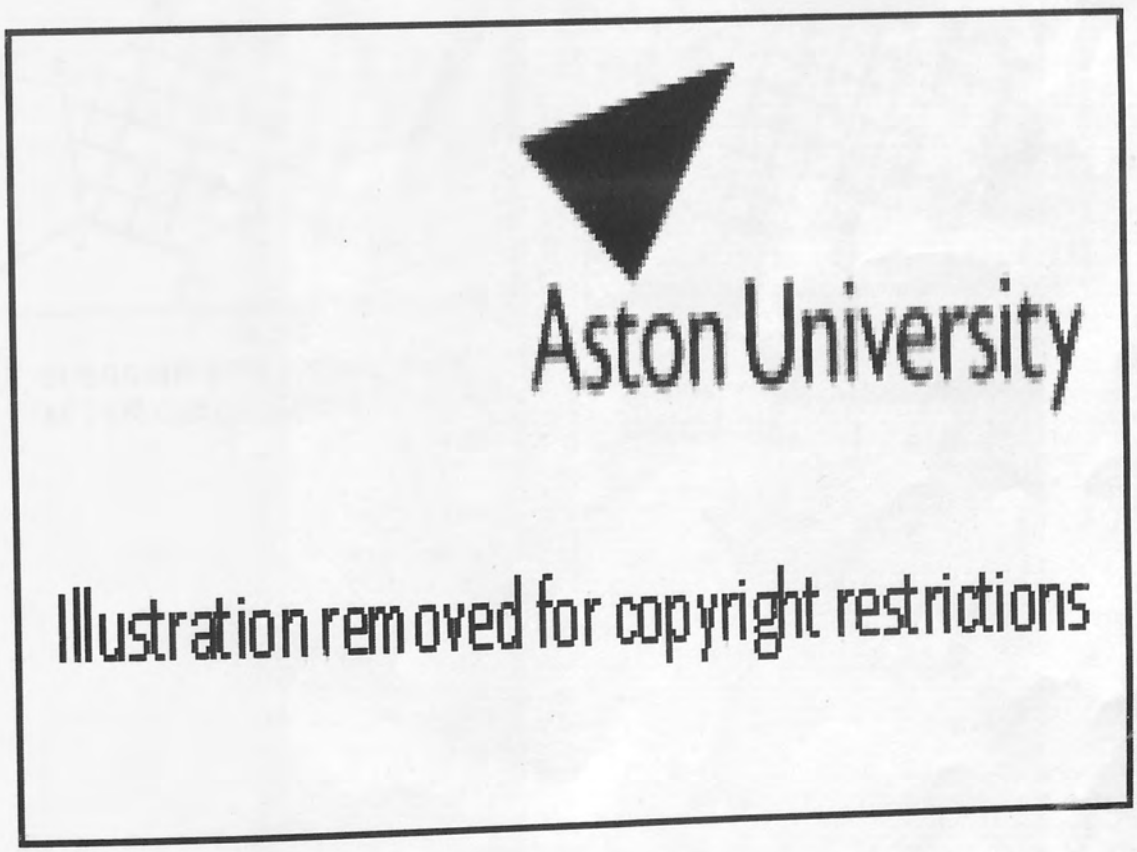
Aston University
Illustration removed for copyright restrictions

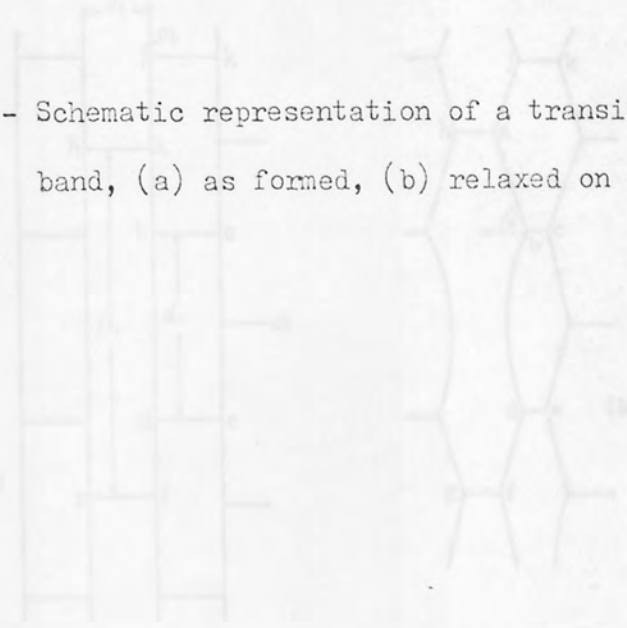

Fig.(20) - Schematic representation of a transition band, (a) as formed, (b) relaxed on annealing.

Ref.(73).

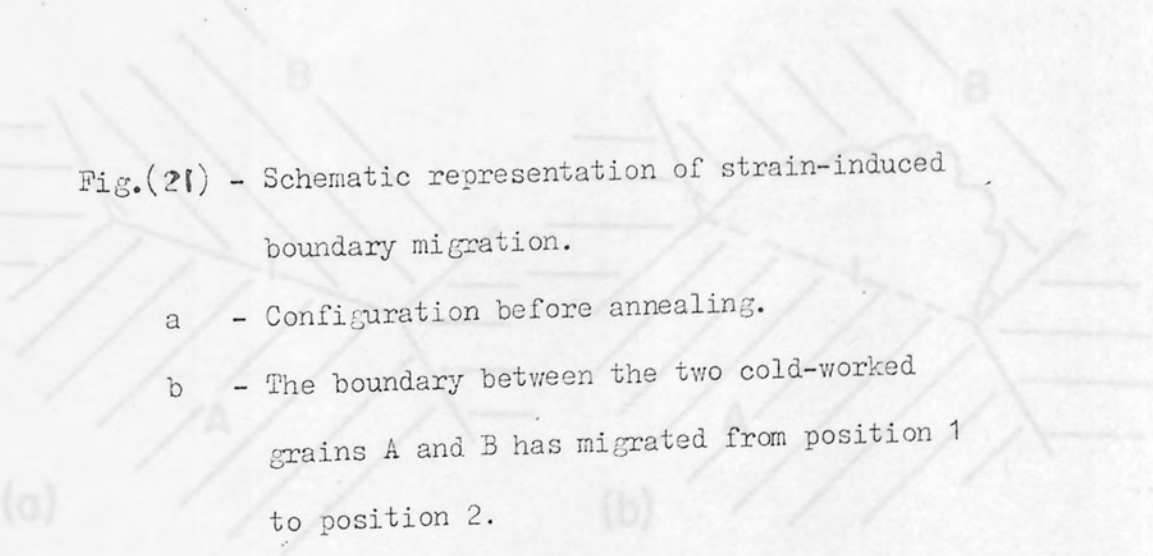

Fig.(21) - Schematic representation of strain-induced boundary migration.

a - Configuration before annealing.

b - The boundary between the two cold-worked grains A and B has migrated from position 1 to position 2.

Ref.(87).

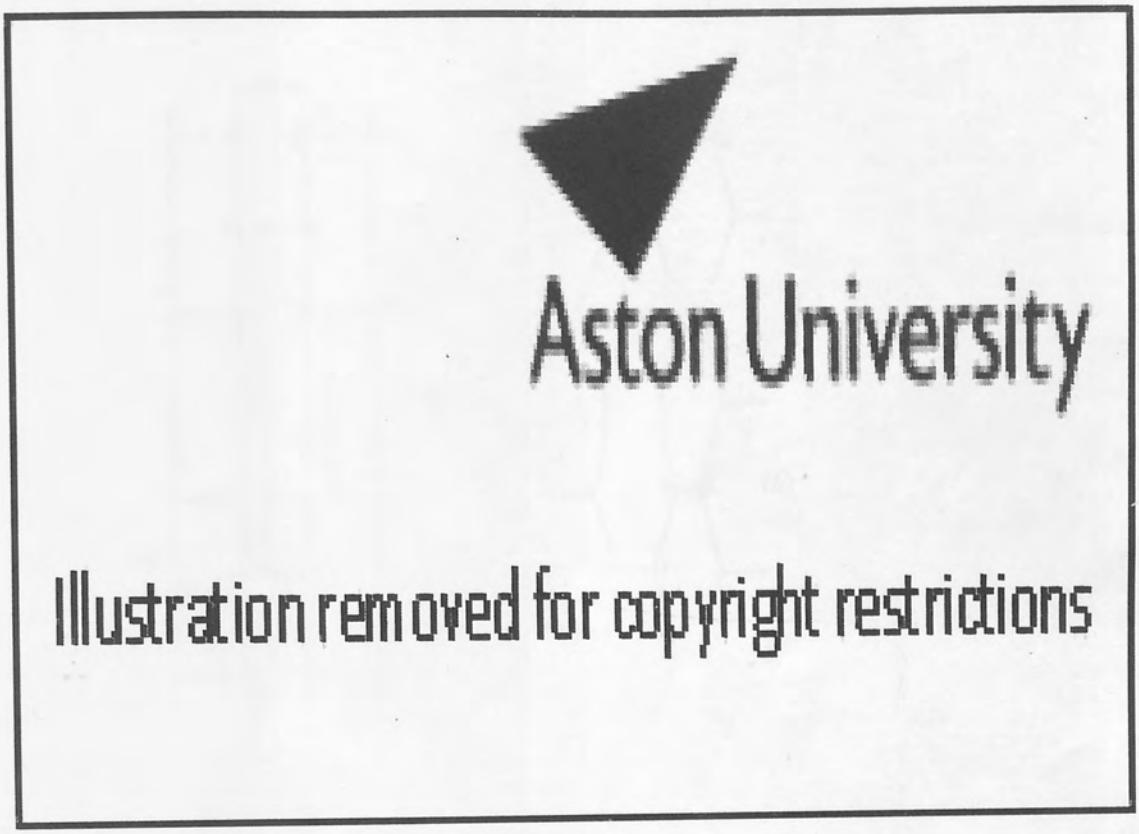
Aston University
Illustration removed for copyright restrictions

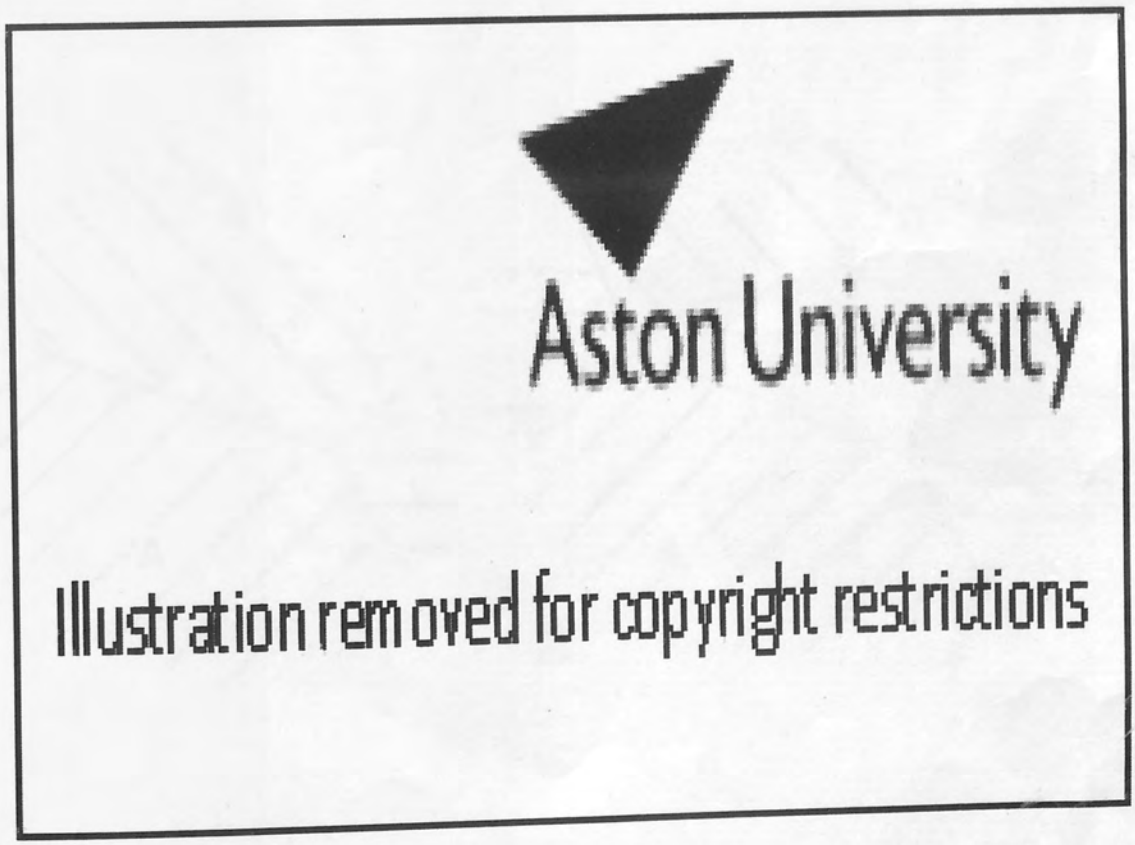
Aston University
Illustration removed for copyright restrictions

Fig.(22) - Longitudinal section rolled 60 % and annealed 3 minutes at 300° C.

Ref.(126)

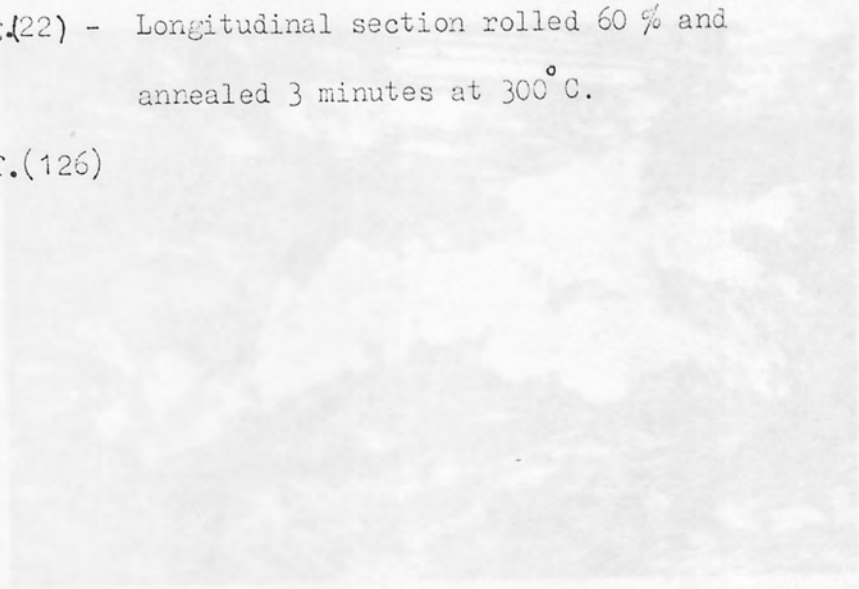

Fig.(23) - Orientaion of recrystallized grain in shear bands; 60 % reduction, annealed 3 minutes at 300° C.

Ref.(126).

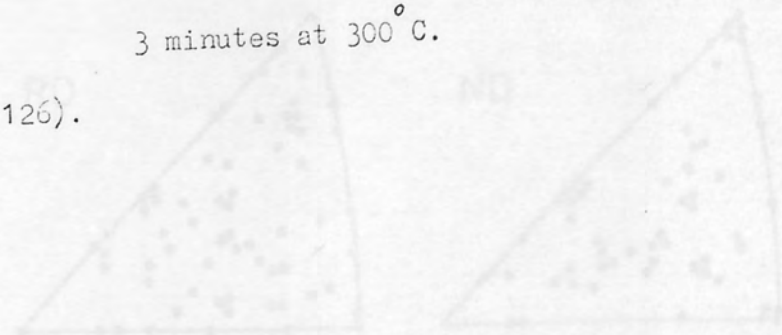

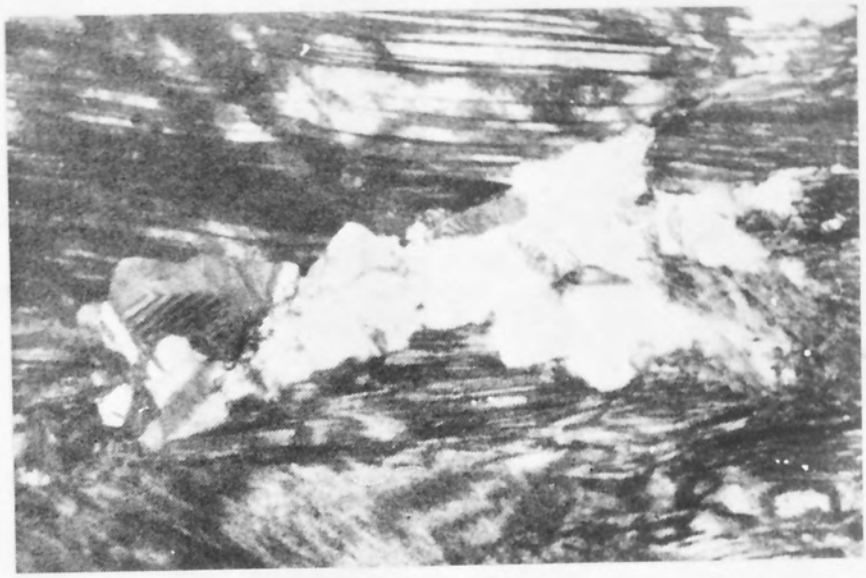

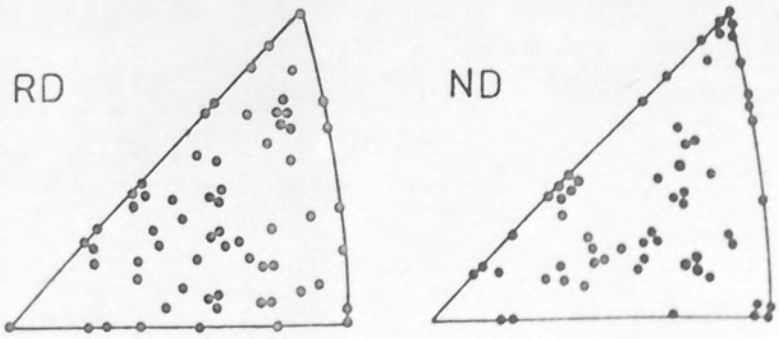
RD
ND

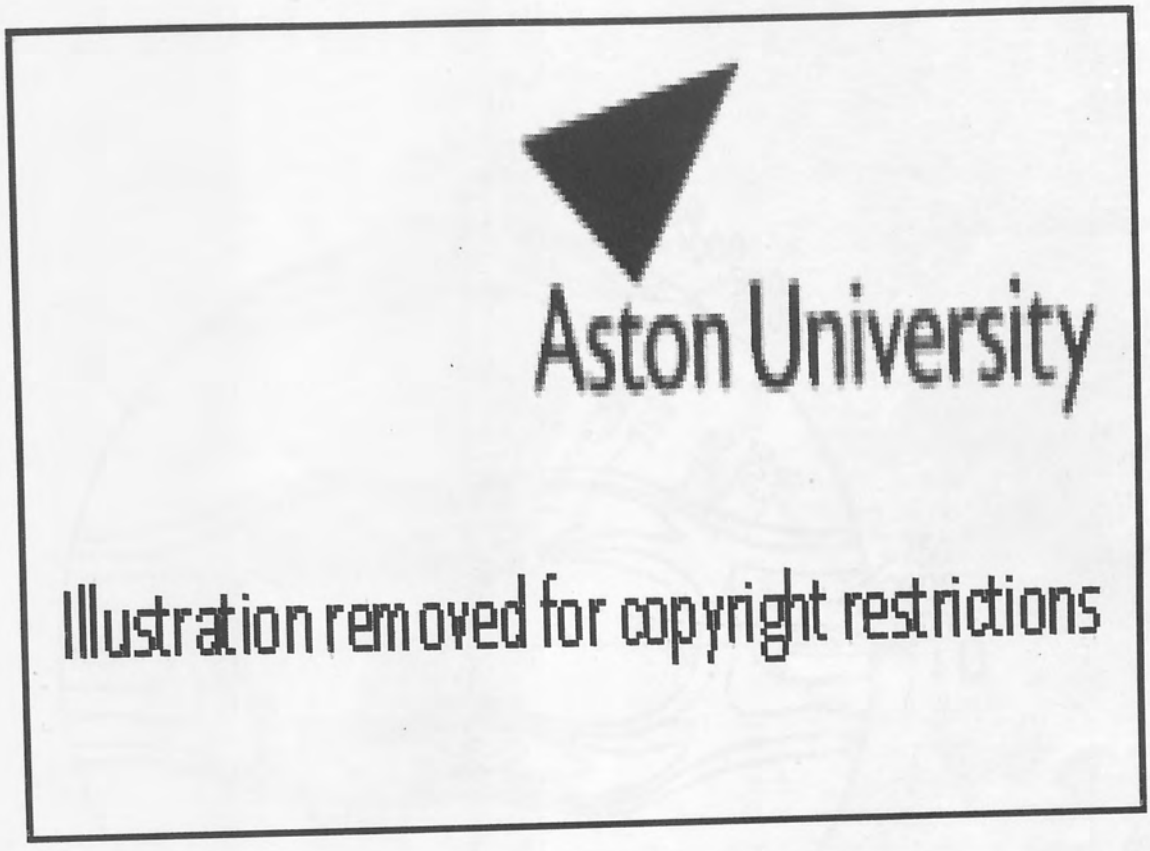
Aston University
Illustration removed for copyright restrictions

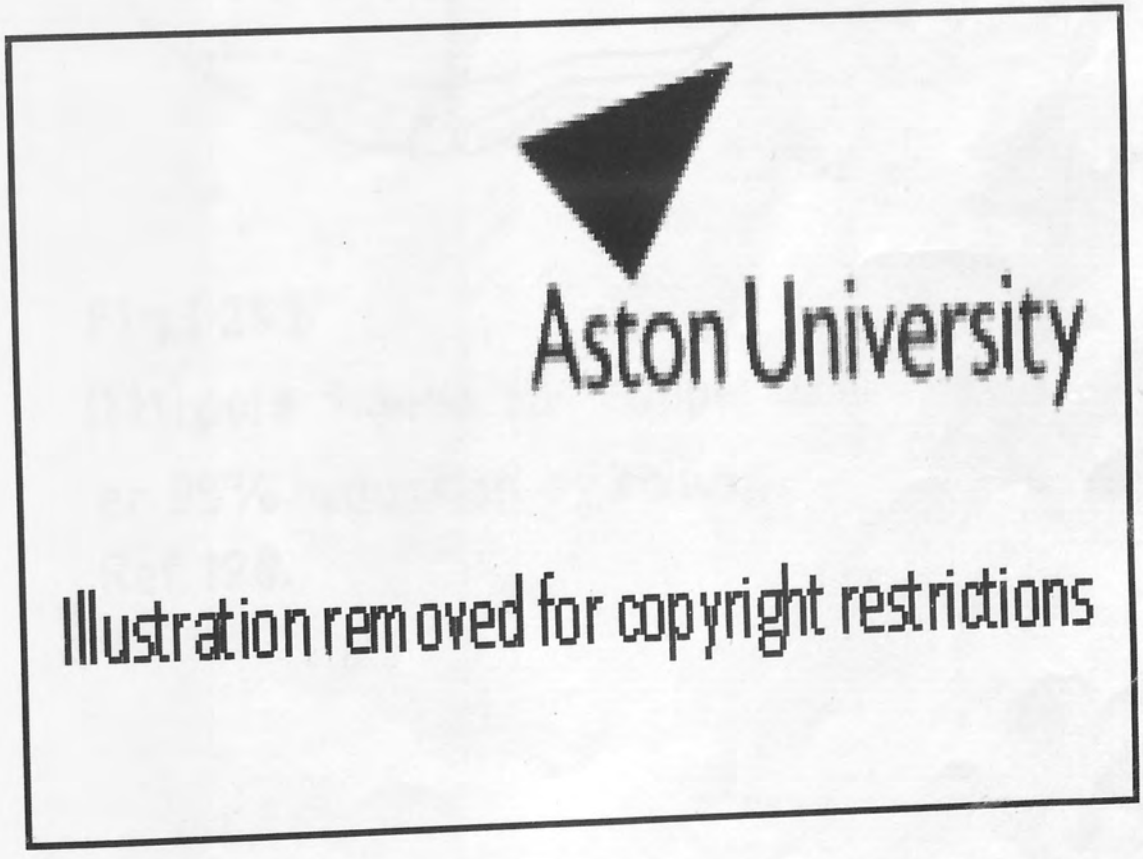
Aston University
Illustration removed for copyright restrictions

decreasing the deformation temperature (ie.decreasing the effective SFE). The effect of solutes on the development of rolling texture in various FCC alloys have been extensively investigated by many workers. Merlini et al (129) found that the change in the rolling texture of copper into brass-type was gradual and progressive as the concentration of zinc increased in copper-zinc alloy, and the transition from "copper" texture to "brass" texture was completed as the zinc content reached 10 %. A typical example of texture transition in copper is shown in Fig.(25). In the case of copper aluminium alloys Wakefield et al (20) found that the complete texture transition was obtained after adding 6.4 % (wt) Al to copper. Similar observations for copper texture transition have been reported (103, 130-133) by adding aluminium, zinc, germanium, tin, phosphorus, arsenic and antimony to copper. In general, for a given solute, a minimum amount is required to initiate the transition and the degree of transition increases with increasing solute concentration. For complete transition, a characteristic amount of the solute is required, which varies from solute to solute and further addition does not change the rolling texture.

Transition of texture in FCC metals and alloys can also be effected by changing the deformation temperature. Examination of the texture in brass containing 5 % zinc deformed to 95 % by rolling at different temperatures(130) showed that rolling at room temperature produced 40 % transition, whereas the specimen rolled at liquid air temperature had almost a complete "brass" type texture.

ASTON UNI LIBRA

Rolling at 200°C, resulted in complete "copper" texture.

Hu et al (134-137) conducted a series of investigations on the temperature dependence of rolling temperature transition in high-purity silver, copper, and austenitic 18-8 stainless steel. They found in all these cases that the transition can be effected by varying deformation temperature. At elevated rolling temperature the texture changed gradually from the "brass" to the "copper" texture, and with decreasing rolling temperature transition in the opposite direction occurred. Similar observations have been reported (45, 58) in copper rolled at -196°C. Fig.(26) shows the gradual transition in copper due to decreasing deformation temperature.

Numerous theories have been proposed to explain the texture transition. Most of these fall into one or other of two broad groups. Hutchinson et al (23) have recently summarised the alternative mechanisms that have been proposed in each group of theories.

Group (A) :- In these it is assumed that normal octahedral slip generates the brass texture. Texture transition to the copper type is than attributed to a variety of causes.
a - Non crystallographic shear proposed by Richards (138) was based on the observation of new type of shear, which become operative after 50 % reduction by rolling. Richards et al (139) studied the structural and textural changes in rolled 99.99 % pure aluminium. They concluded that deformation in the initial stages occurs by $\{111\}\langle 110\rangle$ slip, which leads to the brass rolling texture $\{110\}\langle 112\rangle$, while in the later stage

Fig.(25) - Texture transition in brass as a function of zinc content. (a) 3 %, (b) 6 %, (c) 10 % Zn.
Rolling reduction 96 %

Ref.(129).

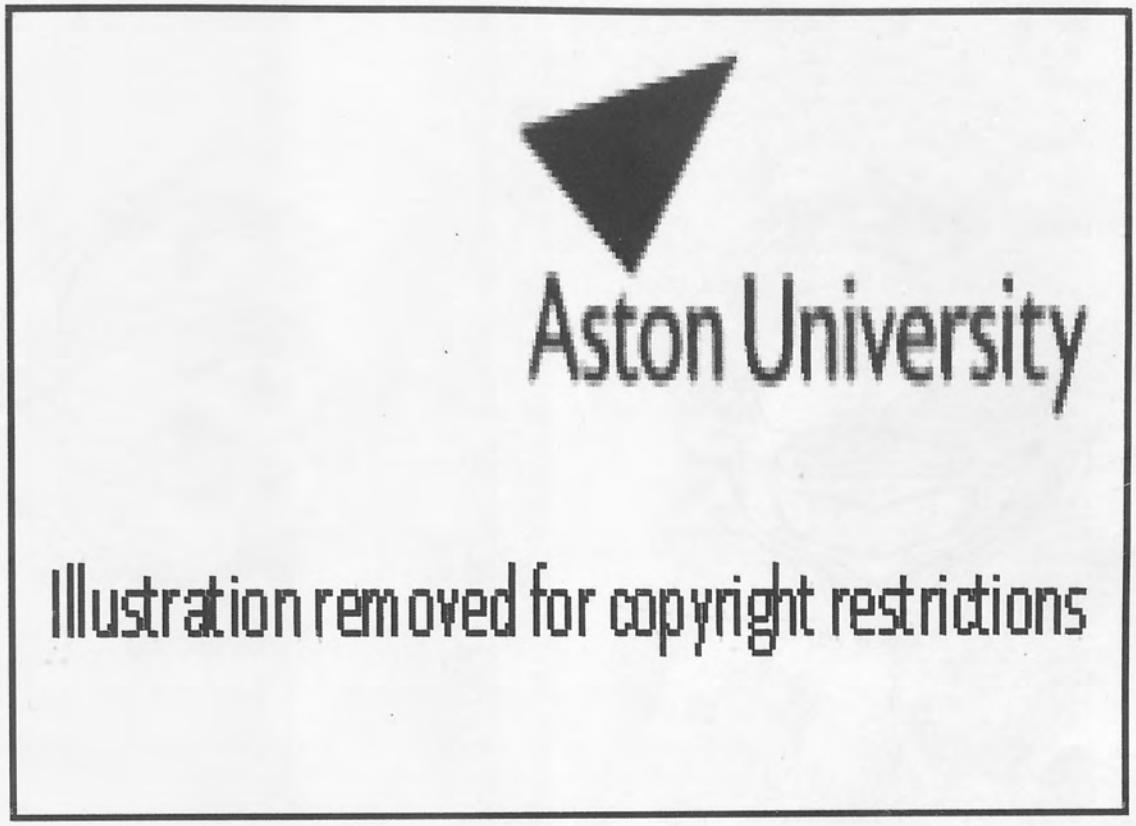
Aston University
Illustration removed for copyright restrictions

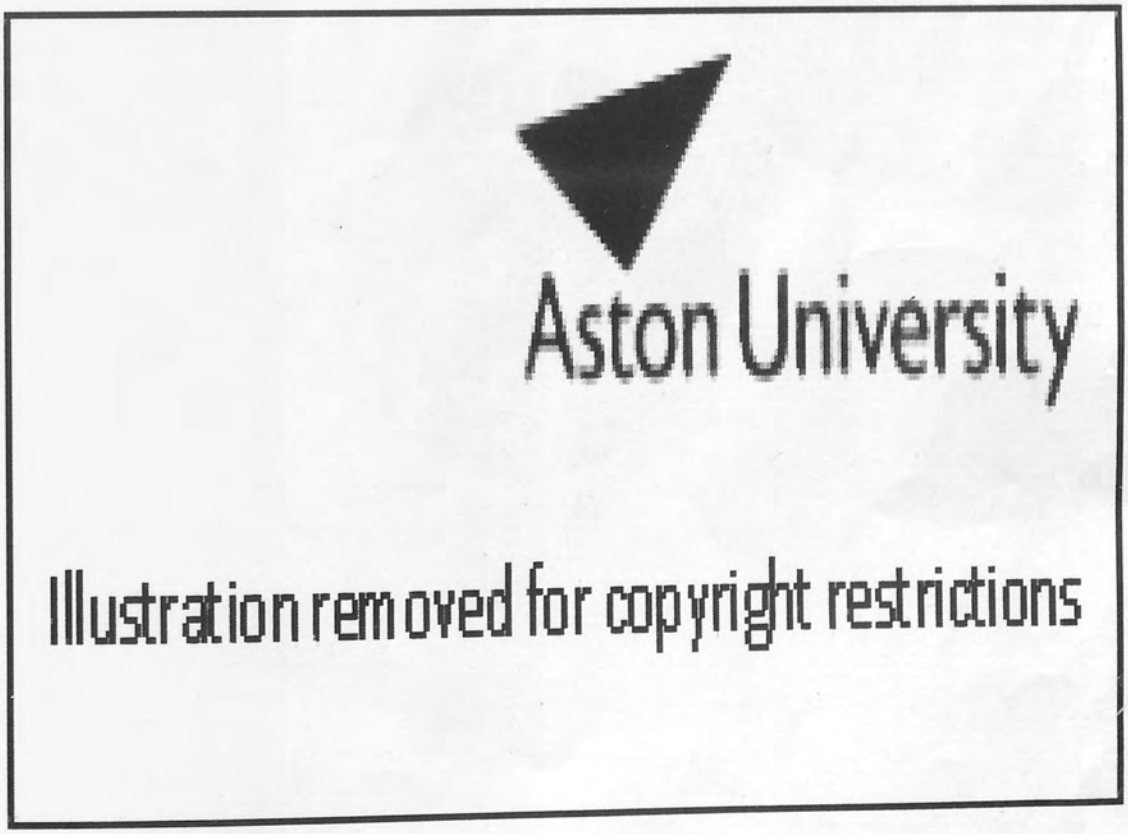
Aston University
Illustration removed for copyright restrictions

Fig.(26) - Texture transition in copper as a function of deformation temperature.
(a) -80 C, (b) -140 C, and (c) -196 C.
Rolling reduction 96.6 %

Ref.(136).

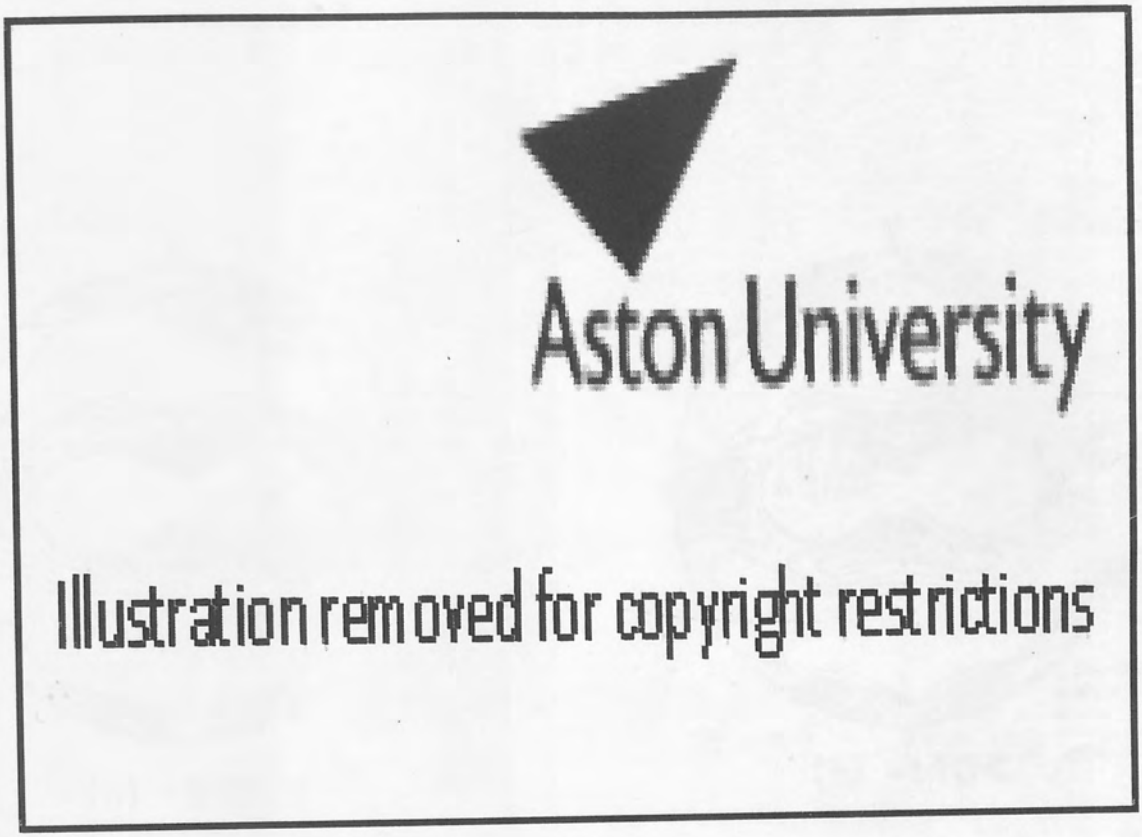
Aston University
Illustration removed for copyright restrictions

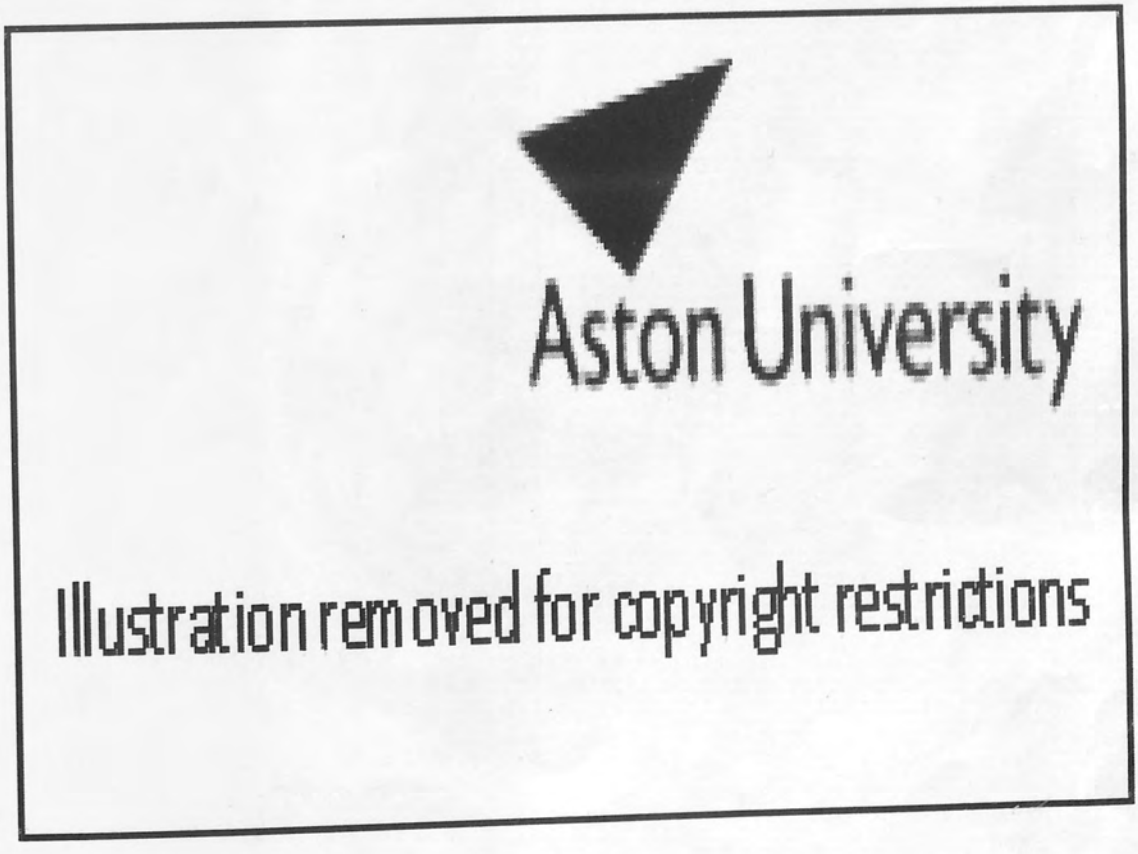
Aston University
Illustration removed for copyright restrictions

(after 50 % reduction) secondary shear {100} <110> become operative producing a typical copper-type texture {112} <111> . A similar theory has been proposed by Haessner (140).

b - Cross-slip theory due to Dillamore et al (141) and Smallman et al (142). It has been suggested that the transition in brass texture occurs when in addition to {111} slip on the primary and secondary systems, large amounts of cross-slip also take place on other planes. For metals and alloys of low SFE, cross-slip is difficult and plastic deformation occurs largely by normal slip. Hence the final texture remains as {110} <112>. For metals and alloys of high SFE, cross-slip is easier and the texture undergoes further re-orientation to give the copper type texture. Since the SFE of metals decreases with increasing alloying addition, and since cross-slip can be activated thermally, the cross-slip hypothesis seems to be consistent with both the composition and temperature dependence of the texture transition in FCC metals and alloys.

c - Dislocation interaction, Liu (143) considered that during deformation the slip systems which operate are determined by the ability of dislocations on these slip systems to interact producing a net reduction of energy. He predicted that for metals of low SFE the ideal end orientations were $\{110\}\langle\bar{1}12\rangle$ plus an orientation spread with (110) in the rolling plane. The ideal orientation for metals of relatively high SFE was shown to be close to $(358)\ [52\bar{3}]$.

Group (B) :- In this category, it is assumed that normal octahedral slip operates to generate the "copper" type texture.

Transition to the brass texture is caused by:-

a - Latent hardening (over shooting). Bishop (144) and Calnan (145) have proposed this theory which is based on the idea that over shooting occurs due to unequal hardening of primary and latent slip systems and this influences the texture formation. A difficulty here was that silver, a pure metal not known to exhibit over shoot was found to have the brass texture. Calnan (146) later rejected the theory of over shooting.

b - Twinning, Wassermann (147) assumed that, during deformation all metals tend to develop the "copper" type texture by means of slip on {111} planes. For the development of the "brass" texture, mechanical twinning as an additional deformation mode, is essential. If mechanical twinning on the systems $\{111\}\langle 211\rangle$ is considered as a possible deformation mode additional to normal slip, then the material in the $\{112\}\langle 111\rangle$ orientation may be transformed by twinning to the $\{552\}\langle 115\rangle$ orientation which rotates into the $\{110\}\langle 001\rangle$ orientation by subsequent slip.

c - Slip by partial s : Hu et al (54) proposed this theory to explain the development of the rolling texture in Cerium (a metal with very low SFE).

On the basis of orientation distribution function analyses, it is now generally accepted that a theory of group (B) is correct or nearly so for "copper" type texture, and Kallend et al (148) have incorporated a twinning mechanism of the type postulated by Wassermann (147) to obtain fair agreement with the observed "brass" texture. Hutchinson et al (23)

pointed out that all existing theories were deficient in that they were based on purely crystallographic arguments and made little or no attempt to rationalise texture changes with deformation microstructural changes in the material. Hutchinson et al (23) went on to show that there is a close relationship between the texture changes occuring during the rolling of 70 : 30 brass and the microstructure generated. As shown in Fig.(27) an increase in the (111) ND intensity at intermediate reduction is associated with the alignment of fine mechanical twins parallel to the rolling plane and the subsequent development at high reduction of the $\{110\}\langle 112\rangle$ "brass" type texture is associated with formation of shear bands in the microstructure. Kenji et al (149) studied the development of texture and deformation microstructure in rolled $(211)\ [\bar{1}11]$ single crystal of α - brass (Cu-13wt % Zn). They showed that substantial mechanical twinning developed after about 40 % reduction by rolling and the $(211)\ [\bar{1}11] + (255)\ [5\bar{1}\bar{1}]$ orientation changed gradually into the $\{111\}\langle 211\rangle$ duplex orientation with further deformation (about 75 % reduction), corresponding to the stage of twins aligned parallel to the rolling plane. The occurrence of the $\{011\}\langle 100\rangle$ and $\{011\}\langle 211\rangle$ orientations was ascribed to the development of texture within the regions of shear bands during rolling to high reduction, and to the presence of untwinned grains with these orientations.

Recrystallization cube texture in FCC metals :-

When heavily deformed FCC metals of medium-high SFE are annealed they develop the most remarkable recrystallization texture known as the cube texture $\{100\}\langle 001\rangle$. It is an

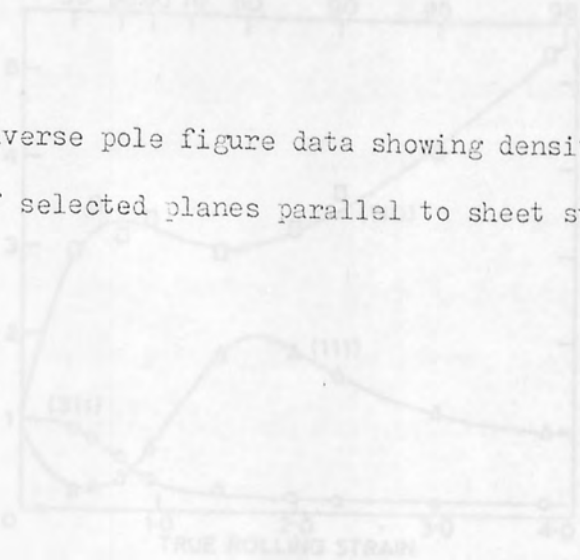

Fig.(27) - Inverse pole figure data showing densities of selected planes parallel to sheet surface.

Ref.(23)

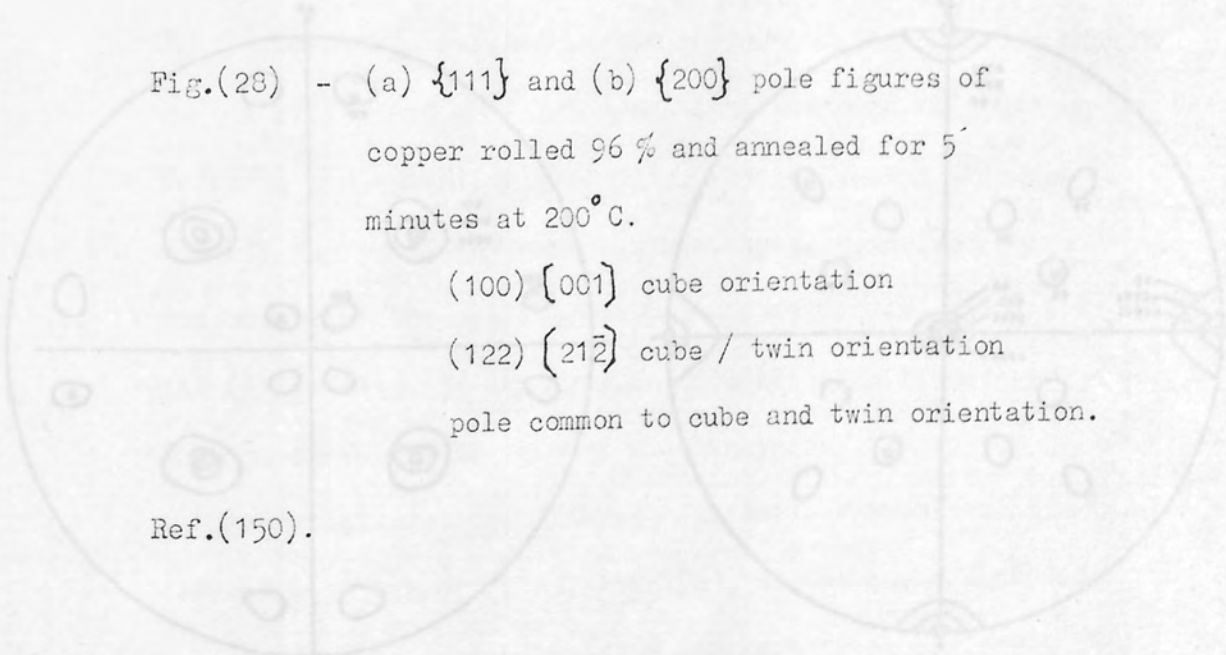

Fig.(28) - (a) {111} and (b) {200} pole figures of copper rolled 96 % and annealed for 5 minutes at 200° C.

(100) [001] cube orientation

(122) [21$\bar{2}$] cube / twin orientation

pole common to cube and twin orientation.

Ref.(150).

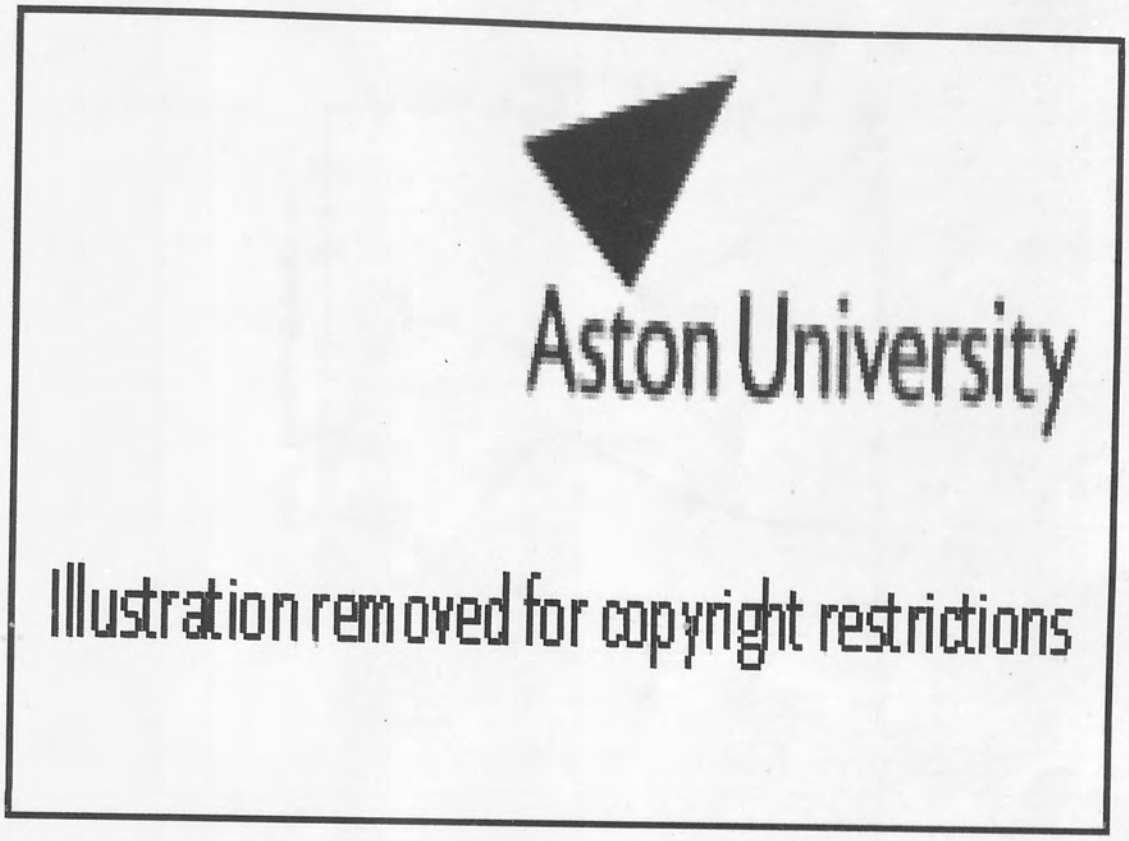
Aston University
Illustration removed for copyright restrictions

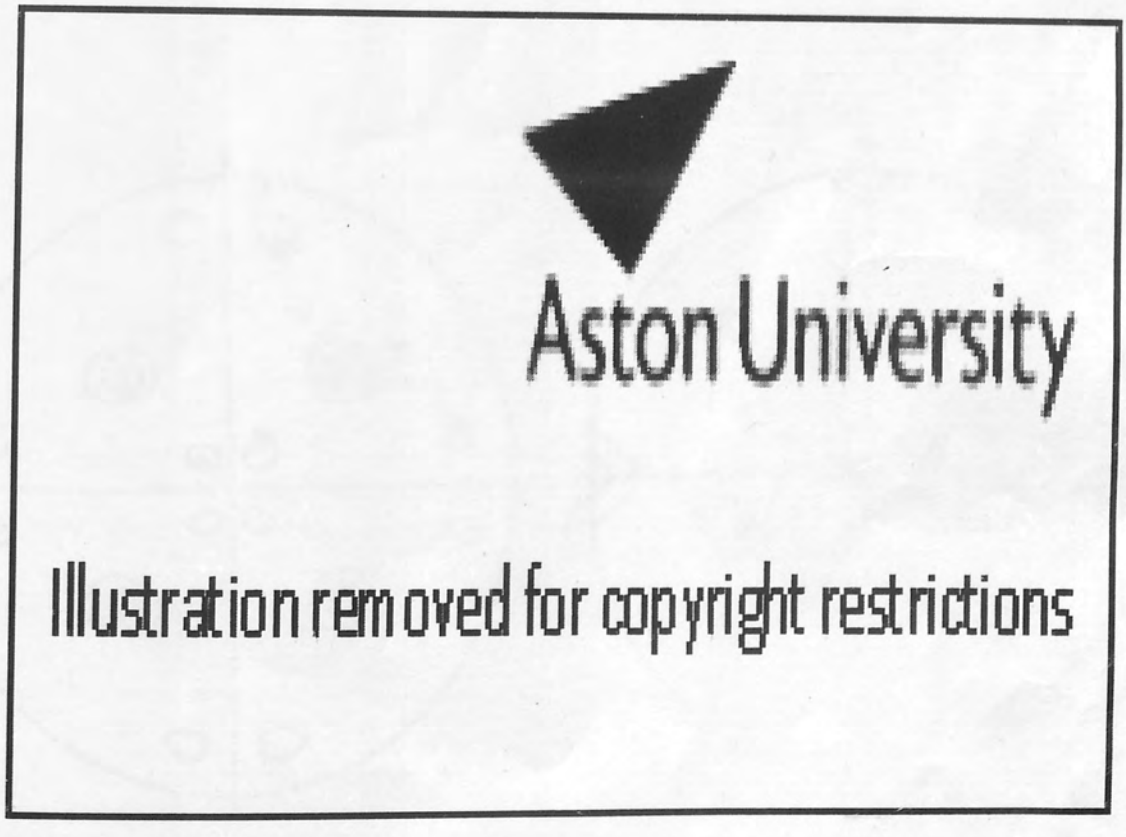
Aston University
Illustration removed for copyright restrictions

extremely sharp texture when fully developed, see Fig.(28), resembling a single crystal, although sometimes containing a minor component of material in twin relationship $\{122\}\langle 212\rangle$ to the principal orientation. A well developed deformation texture must be obtained before recrystallization will give a strong cube texture. Usually 80-95 % cold reduction is required. Schmid et al (151) found that the cube texture became sharper in the deformation range between 95-99.9 %, but decreased with higher deformation. In polycrystalline copper a large number of workers (98, 131-132, 152-153) have confirmed that the cube texture is more perfect and the twin density lower for fine-grained starting material and high annealing temperatures.

The effect of adding solute elements to copper varies from solute to solute and on their concentration. Ray (105) examined the kinetics and mechanism of recrystallization as well as the texture in copper and copper-phosphorus alloys. Fig.(29), taken from this work, shows how the addition of only 0.1 % phosphorus influences the texture of 95 % reduced sheet in the rolled and annealed condition. Although the rolling textures are essentially similar, the phosphorus addition totally supresses the cube texture, leaving instead certain components of the rolling texture approximately $\{110\}\langle 112\rangle$ and $\{112\}\langle 111\rangle$. As the phosphorus content in copper was further increased there were great changes in both the rolling and recrystallization textures. Similar observations have been made by many workers (133, 154-155). It has been concluded that phosphorus is an element which segregates profusely to crystal defects in copper. When segregated to high angle

boundaries it should give rise to strong solute drag which impedes their migration. The effect of adding phosphorus to copper (as a dilute solid solution) is to increase the ratio of nucleation rate to growth rate. This reduces the sharpness of the recrystallization texture and causes it to approach more closely to the cold rolled texture.

Similar effects to that of phosphorus in copper have been reported for arsenic and antimony. (155). Merlini et al (129) and Schmidt et al (133) made detailed studies of the effect of zinc on copper annealing textures. They found that the rolling texture for low-zinc alloys (up to 5 % Zn) were essentially similar to that in pure copper. As zinc alloying increased gradual changes in the rolling texture to the brass type texture were observed, and complete transition occurred at about 10 % Zn. Along with this change in the deformation texture the fraction of the cube component in the recrystallization texture gradually decreased and almost completely vanished as the alloying content reached about 10 %. The (111) pole figures of the recrystallization texture with 3, 6 and 10 % Zn are shown in Fig.(30). Alloys of copper with aluminium (156), and tin (152) show annealing texture transitions essentially similar to the Cu-Zn alloys. Increasing the alloy content in each case causes the volume fraction of the cube texture component to decrease.

As has already been mentioned, the various solute elements that have been added to pure copper are not equally effective in supressing the cube texture in recrystallized copper. Table (1) shows the minimum alloying additions to

copper necessary for complete supression of the cube texture when metals are deformed at room temperature.

Meixner et al (156) and Schmidt et al (133) studied the effect of rolling temperature on textures in copper. They found a complete transition in both rolling and recrystallization textures from copper type to brass type after rolling at -196°C.

Recrystallization textures in aluminium are rather more complex than those of copper. Normally on annealing heavily deformed aluminium the recrystallization texture consists of a cube component plus a component described as "retained rolling texture" (139, 159) or "S" texture (158), which is similar to the main rolling texture component for aluminium, Fig.(31). The annealing behaviour of aluminium depends very much upon the purity, prior to heat treatment, and the deformation history of the material. In high purity aluminium of 99.99 % and better, the recrystallization textures are similar to those of copper, with the exception that it is rather more difficult here to produce 100 % cube texture. The amount of the cube component in the annealing texture of pure aluminium can be increased by prolonged annealing or by raising the annealing temperature (157, 160). For prior deformation, less than 90 % reduction, the annealing texture is mainly S-texture, but at 90 % and above the cube component is introduced in addition.

The origin of recrystallization textures :-

Recrystallization has been described as a nucleation

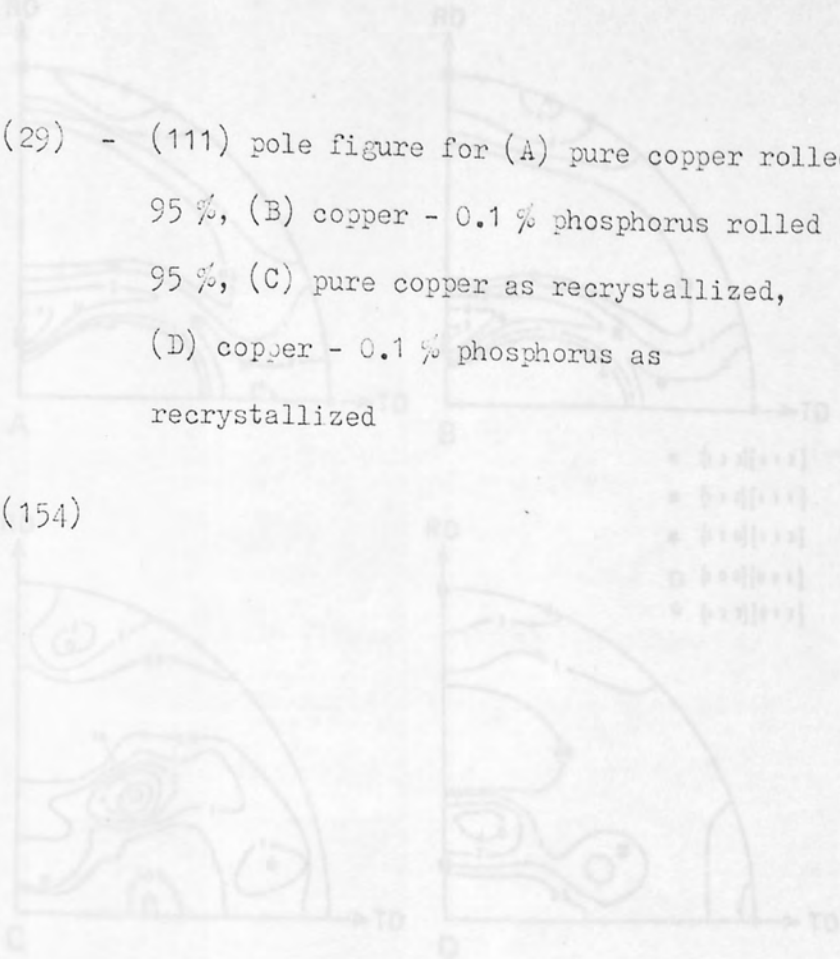

Fig.(29) - (111) pole figure for (A) pure copper rolled 95 %, (B) copper - 0.1 % phosphorus rolled 95 %, (C) pure copper as recrystallized, (D) copper - 0.1 % phosphorus as recrystallized

Ref.(154)

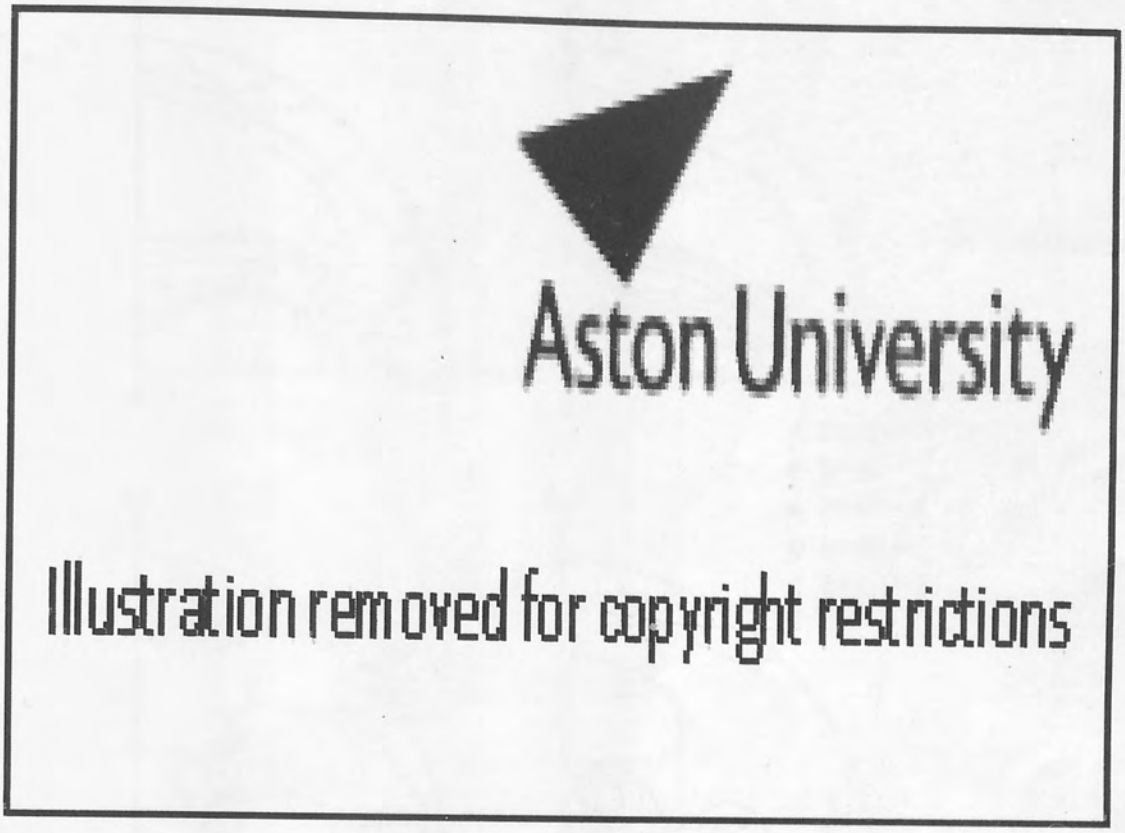
Aston University
Illustration removed for copyright restrictions

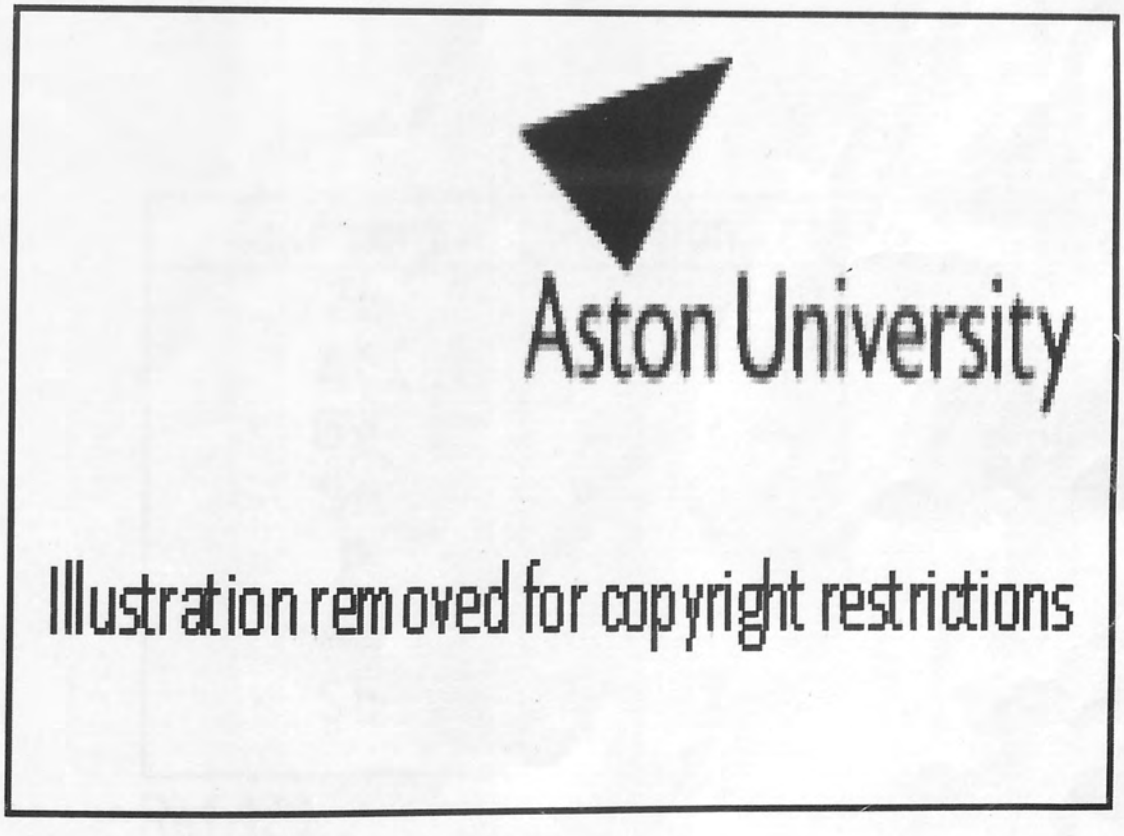
Aston University
Illustration removed for copyright restrictions

Fig.30 - (111) pole figures showing the annealing texture transition in copper - zinc alloy containing (a) 3 %, (b) 6 %, (c) 10 %.

Ref.(129).

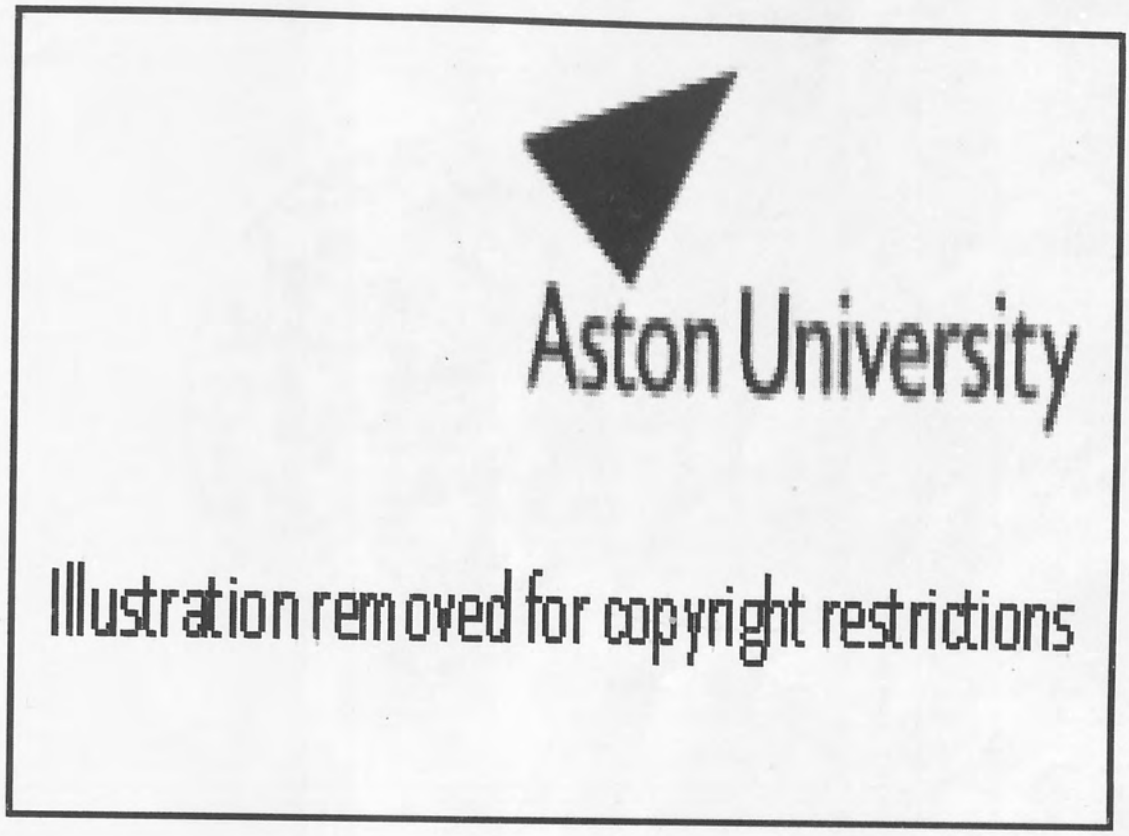
Aston University
Illustration removed for copyright restrictions

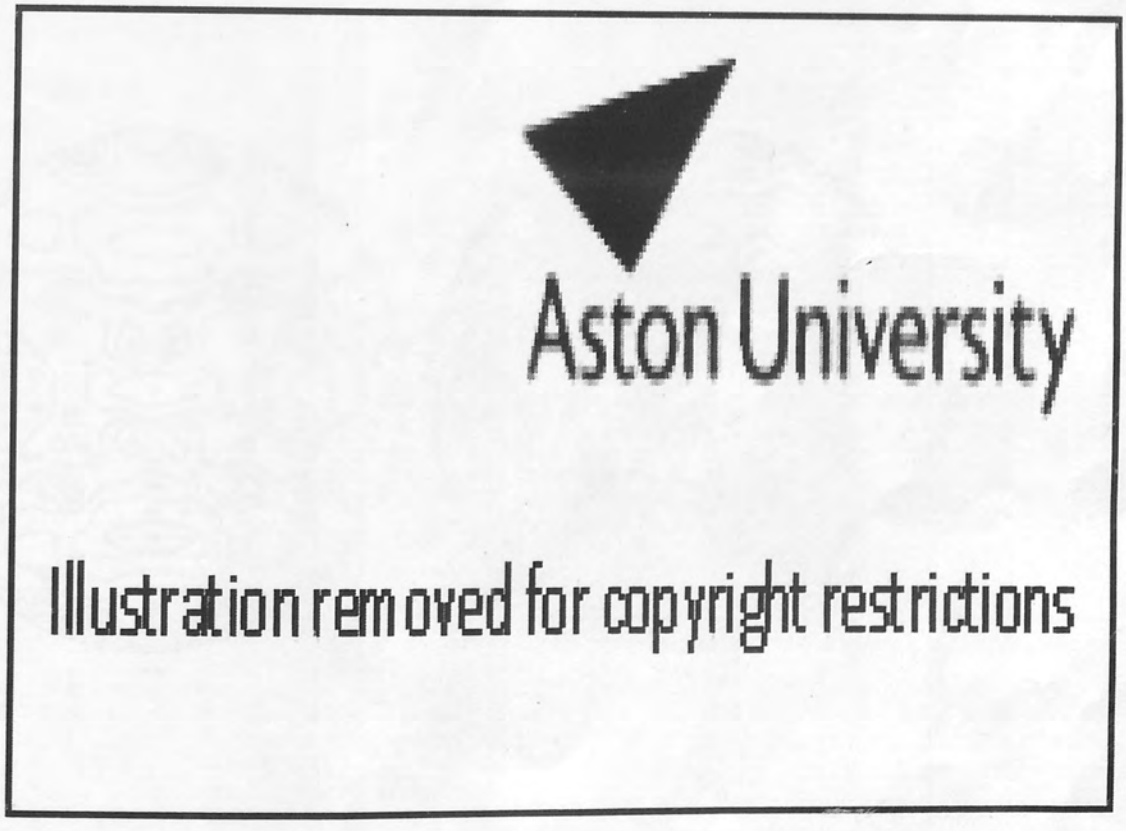
Aston University
Illustration removed for copyright restrictions

Fig.(31) - (111) pole figure showing annealing texture for commercial purity aluminium rolled to 95 % reduction and annealed 5 min. at 300 C.

Ref.(159)

Fig.(32 - (111) pole figures for (110) [1$\bar{1}$2] copper single crystal cold rolled and recrystallized at 400 C (left), and streographic projection of 30 rotation around <111> poles for crystal in (110) [1$\bar{1}$2] orientation.

Ref.(166).

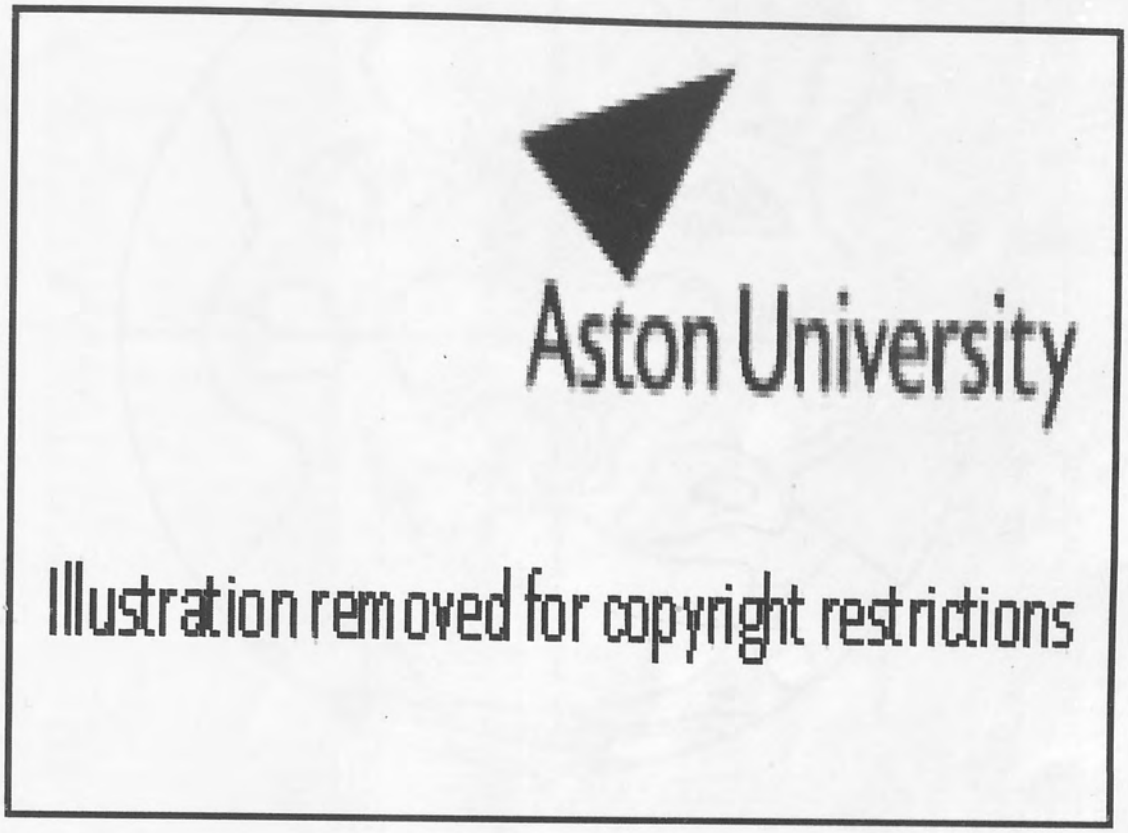
Aston University
Illustration removed for copyright restrictions

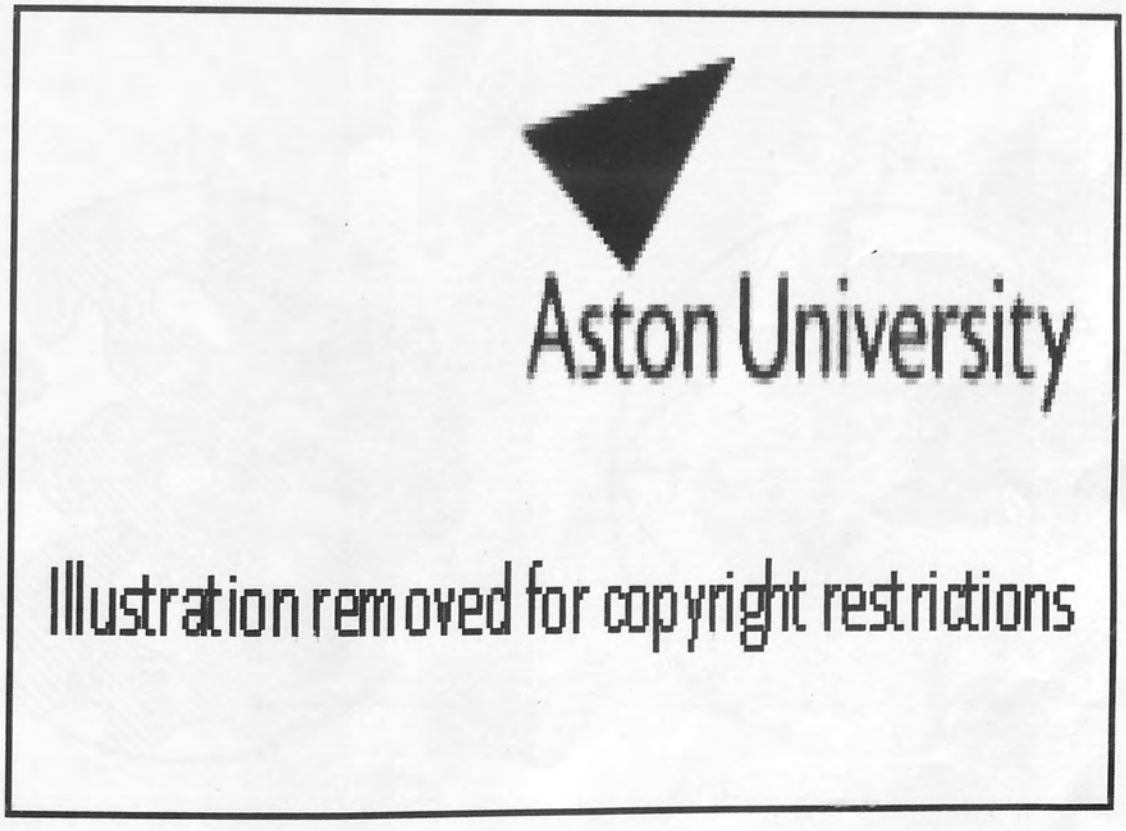
Aston University
Illustration removed for copyright restrictions

and growth process. It is now generally accepted that all the orientation components present in the recrystallization texture derived from the growth of nuclei having the same orientations. There has been much discussion for many decades about the origin of recrystallization texture. One of the principal questions to be decided is whether the orientations absent from (or only weakly represented) in the recrystallization texture are suppressed because of the unavailability of nuclei to grow to an appreciable volume in competition with nuclei of other orientations (oriented - growth). These two ideas form the basis of two theories that have been put forward to explain the development of primary recrystallization textures. In the oriented-nucleation theory the nucleation process is supposed to be of primary importance in determining the range of available nuclei which can contribute to the recrystallization temperature. In oriented-growth theory on the other hand, the recrystallization texture is considered to result from growth selection due to the orientation dependence of the rate of grain boundary migration.

Following the concept that recrystallization textures are determined by the orientation of the available nuclei, Burgers et al (162) tried to relate the nucleus orientations in turn to a model of the structure of his compressed aluminium single crystal specimens. They assumed that on annealing the nuclei of the recrystallized grains developed from the most heavily deformed fragments which were located in the vicinity of active glide planes. Burgers considered that these fragments were rotated with respect to

the main body of the crystal around ⟨112⟩ axes parallel to the active slip planes and normal to the corresponding active slip direction. Later Barrett (163) made orientation determinations on 50 recrystallized grains in compressed aluminium single crystals. He found the orientations to correspond to approximately 45° rotations around ⟨111⟩ axes. The contradiction between the Burgers mechanism and Barrett's observation led the latter to suggest the oriented-growth mechanism. The ⟨111⟩ rotational relationship in aluminium has been confirmed by other workers (164, 165). In rolled copper single crystal of the (110) $[1\bar{1}2]$ orientation, Liu et al (166) found, after annealing, a recrystallization texture where the individual components were related to the deformation orientation by 30° rotations clockwise and anticlockwise, about common ⟨111⟩ poles as shown in Fig.(32). Maddin et al (167) reported that the recrystallized grains formed on annealing of α-brass single crystals deformed in tension were related to the respective matrix crystals by rotations around approximately common ⟨111⟩ axes. Further experimental evidence in support of oriented growth was provided by Beck and co-workers (168, 169). They studied the annealing texture of some aluminium single crystals which were rolled 80 % and whose surface was abraded prior to annealing in order to induce random nucleation. They found that for both (110) $[1\bar{1}2]$ and (123) $[41\bar{2}]$ orientations, the relationship between deformation and recrystallization orientations could be described by rotations of about $\pm$ 40° around common ⟨111⟩ poles. Furthermore Lücke et al (170) studied the growth rate in commercial purity aluminium deformed by tension, and found a very pronounced orientation

dependence of the growth rate with a maximum at 40° rotation around ⟨111⟩ axes. They also found a corresponding growth selectivity among the recrystallized grains nucleated randomly by severe local deformation at one end of their long cylindrical single crystal specimen deformed 15 % by tension.

The cube texture found in medium-high SFE-FCC metals and alloys has excited much curiosity because of its high degree of sharpness. To explain the formation of the cube texture in cold-rolled polycrystalline copper after annealing, an oriented-nucleation mechanism has been proposed by some workers (171, 172). They assumed that in rolled polycrystalline copper, there are present, small local regions in the deformed structure that posses the cube orientation. These regions would then serve as nuclei for recrystallization on annealing. Dillamore et al (173) have given another explanation for the cube texture. They showed in a model that cube regions can be developed during deformation in transition bands, and that these fulfil all the necessary conditions for nuclei.

The proponents of the oriented-growth theory objected to this mechanism, and their objection is based on some reported experimental data (98, 174-176). Haessner et al (174) and Lücke et al (175) have determined, with the aid of electron microscopy and electron diffraction, the orientation of a large number of individual crystallites (600 and 234 respectively) in heavily deformed rolled copper. In both investigations not one of these grains in the rolling texture had the cube orientation. Merlini et al (176) observed that cross-rolled copper, which has about twice as much cube

oriented material present as in straight-rolled copper, does not recrystallise to the cube orientation. Furthermore Verbraak (98) has reported that in a heavily rolled copper single crystal of the (100) [001] orientation has a deformation texture very similar to that of highly rolled polycrystalline copper, except that a relatively large volume fraction of the metal retains the cube orientation. In spite of this, the recrystallization texture comprises only a very weak cube texture component.

Recently, detailed electron microscopy studies in heavily deformed copper and aluminium (103, 108, 177) have supported the views of Burgers et al (171) and Decker et al (172), and also cast doubt on growth selection as the cause of cube texture development. Ray (103) and Noda et al (108) found that the deformation microstructure in longitudinal sections of heavily deformed copper consists of elongated cells parallel to the rolling plane; some of these elongated cells have cube orientation. In these cubic oriented regions, recovery processes leading to nucleation were extremely rapid. These observations led to the conclusion that rapid nucleation and growth may be the reason for the development of the cube texture. On the other hand, it was often observed that the surrounding deformed matrix does not have an orientation corresponding to a rotation of 30°-40° about a common $\langle 111 \rangle$ direction

It is now generally accepted that the rolling texture of copper consists of a string of orientations from $\{110\}\langle 112 \rangle$ near $\{123\}\langle 412 \rangle$ near $\{112\}\langle 111 \rangle$. Hutchinson

(178) has derived the recrystallization orientation from all orientations of the orientation string of the copper type texture (ODF) by 35° clockwise and anticlockwise rotation around the four <111> poles of each orientation of the deformed matrix. The cube texture was not among the orientations predicted and furthermore the closest it comes to one of the predicted orientations was 15°.

Several investigators (e.g. 98) have pointed to experimental evidence indicating that identical rolling textures can give rise on annealing to quite different recrystallization textures. It has been suggested by them that these observations are incompatible with the oriented-growth mechanism of the formation of annealing texture.

CHAPTER THREE.

3.1. Materials and initial treatments.

Two batches of commercial purity tough pitch copper (A and B) supplied by I.M.I. have been used for the present investigation. The two batches were of similar composition. Mass spectroscopic chemical analyses are given in Table (2)., where the only substantial difference is seen to be the higher oxygen content of copper A. The starting materials were annealed in a muffle furnace for one hour at 500°C, which yielded an initial grain size of $\sim$ 85μm in both batches. Some samples of copper A were also further annealed at 600°C for 4 hours to obtain a grain size of about 300μm.

Slabs of 1.6cm (copper A) and 1cm (copper B) thickness, 5cm wide and 20cm long were cold rolled to different reductions from 10 - 95 % as shown in Table (3) on a laboratory mill with 150cm diameter rolls operating at a rolling speed of 3.5cm/sec. Oil lubrication was used with water cooling between passes to ensure that no temperature build-up occurred with increasing reduction. Samples from copper A of 85μm grain size were also rolled to 90 % reduction after cooling to a temperature of -100°C in acetone cooled with liquid nitrogen. Specimens were generally examined in the freshly rolled condition to minimise recovery and recrystallization effects which were sometimes found to take place at room temperature in copper A rolled between 90 % and 95 % reduction. Whenever specimens required storage after rolling they were maintained at -20°C.

Table (2)

Chemical Analyses of the Two Batches of Copper (ppm)

	Zn	Sn	Pb	Fe	Ni	Mn	Al	Cd	Ag	Sp	Bi	As	Si	P	O
Copper A	<5	<5	<5	5	<5	<5	<5	<5	<5	<5	<5	<5	<5	<5	390
Copper B	<5	<5	5	5	<5	<5	<5	<5	<5	<5	<5	<5	<5	<5	240

Table (3)

Rolling Reduction	True Strain
10 %	0·1
20%	0·22
40%	0·51
60%	0·91
80%	1·6
90%	2·3
95%	3

Recrystallization studies were carried out only on copper A and B cold rolled to 90 % reduction and annealed in boiling water for different periods of time.

3.2. Experimental techniques :-

A wide range of experimental techniques were used to examine the deformation microstructure, texture and recrystallization behaviour during annealing. These techniques were as follows :

a - Optical metallography :-

Longitudinal sections from different rolling reductions were removed for optical examination, using a diamond wheel at low cutting speed to minimise surface damage. The small amount of damage produced was removed during subsequent preparation. After sectioning, the samples were mechanically ground using the finest grade of emery paper (grade 1200) and polished using 6μ and 1μ diamond paste. To obtain damage free surfaces the samples were electropolished for 3 minutes in a commercially available solution based on orthophosphoric acid. Polishing was carried out at room temperature at 1.8 - 2.5 volts in a stainless steel beaker as cathode. For optical examination the specimens were etched in aqueous ferric chloride ($100FeCl_3$ + 40Hcl + 920Alcohol), or in a dilute electrolytic thiosulphate solution (0.5 % $Na_2S_2O_3$, at a voltage varying from 7 - 20 volts, normally the voltage increases as the deformation level increases) with a copper sheet as cathode. Very often the latter solution was used, because the first reveals only grain boundaries.

b - Scanning electron microscopy :-

A Cambridge S2A scanning electron microscope was used in the back-scattered mode to examine the deformation microstructure and the grains in fully and partially recrystallized bulk specimens. This technique employs electron channelling contrast and has a number of advantages over optical and transmission microscopy which may be summarised as :-

1 - Specimen preparation is relatively easy, allowing statistical studies to be made.

2 - It is a powerful technique allowing a 5K magnified image with reasonable resolution and forms a bridge between optical microscopy and transmission electron microscopy.

3 - The orientation of grains or subgrains $> 3\mu m$ could be accurately determined by selected area channelling patterns.

All the principal sections (rolling plane, transverse section, and longitudinal section) at different rolling reductions were examined. The specimens were mechanically and electro polished as described in the previous section.

Grain orientations in partially recrystallized specimens were determined by selected area channelling patterns.

c - Transmission electron microscopy :-

Most specimens were examined in a Jeol 100B electron microscope operating at 100kv, equipped with a single

tilt and rotate specimen stage. The microscope also had a scanning transmission (STEM) attachment. When orientation determinations of fine substructures (< 0.25 m) were required, the Jeol 100B STEM attachment and/or Phillips EM 400 STEM operating at 100kv were used. The Jeol 100B TEM was calibrated for magnification using latex spheres of known radius, and for rotations relative to the diffraction patterns by using molybdenum trioxide (Mo_2O_3) single crystals. The latter calibration was checked many times using twins in a thin foil of copper.

Grain and substructure orientations were determined by conventional selected area diffraction (SAD) patterns. In most cases, microbeam diffraction was used to produce Kikuchi patterns which gave accurate crystallite orientations. For fast and accurate analysis, standard Kikuchi diffraction patterns covering the whole unit triangle were made for copper using the Phillips EM400 equipped with a double tilt specimen stage. The rolling direction of every foil was identified in the electron micrographs and diffraction patterns from images of the edge of the specimen cut parallel to or perpendicular to the rolling direction.

The method which has been followed to identify the microband habit plane was to rotate the specimen inside the microscope until the microband boundary became parallel to the microscope tilting axis. Then the specimen was tilted until the microband width became minimum, and the boundary became relatively sharp (i.e. parallel to the electron beam). The diffraction pattern was then solved to determine the plane

which corresponded to the habit plane trace. The accuracy of this method was found to be better than 5° by defining the known habit plane for twins in copper foils.

In addition to bright-field imaging in TEM, high resolution dark-field mode was used to study the dislocations within the micro bands and their boundaries.

Longitudinal sections from all reductions (5 - 90 %) were usually used, although other sections were examined for some specimens. Initially, twin, parallel-sided sections about 0.4mm thick were removed by the diamond cutting wheel. The thickness was reduced to about 0.1mm by abrading both sides on water lubricated 400 and 1200 grade abrasive paper. Great care has been taken, especially at the final stage of mechanical polishing. Then further thinning was done chemically by immersion in 50 % HNO_3 + 50 % water. This yielded parallel sided sections of $<$ 0.075mm thick and free from artefacts. Final foil preparation was carried out by a modified window method. The electropolishing solution and polishing conditions have already been described in section (3-2a).

Some copper B specimens rolled to large strain levels (90 % reduction), were electroplated before sectioning. This process was carried out as follows :

1 - Cathodic surface cleaning in hot alkaline solution for a few minutes at a current density of $4A/dm^2$, followed by washing in running water.

2 - Dipping for 30 seconds in 50 % Hcl, and then washing with water.

3 - Cathodic cleaning in cold cyanide solution, $4A/dm^2$, followèd by washing in running water.

4 - Electroplating in pyrophosphate copper solution PH 8.6 at $4A/dm^2$, with air agitation and a plating temperature of $40^{\circ}C$.

The thickness was built up to about 1.7mm before sectioning. Thereafter, the foil preparation was identical to that described above.

d - Texture determination :-

Quantitative {111} pole figures were determined for the rolling specimens (60-93 % reduction). Square specimens ($\sim$ 2cm square) were cut from the rolled materials. All the texture specimens were lacquered on one face, and half of the thickness was removed in a solution of 50 % HNO_3 + 50 % H_2O.

Pole figures were measured using Siemens texture goniometer (Schulz reflection method) (179) with copper Kα radiation and a nickel filter. The diffracted intensity was measured with a proportional counter and displayed on a chart recorder via a pulse height discrimination circuit. Intensity obtained by using a random copper sample.

CHAPTER FOUR.

EXPERIMENTAL RESULTS AND DISCUSSION.

4.1. Optical metallography :-

These examinations have been carried out for a wide range of deformations (20 % - 90 %), in both materials (coppers A and B). The examinations showed that aqueous ferric chloride etch is of limited value for revealing deformation inhomogeneities. Longitudinal sections of deformed copper at different strain levels etched in aqueous ferric chloride are shown in Fig.(33). As deformation increased the grains gradually elongated in a direction parallel to the rolling direction, and by strain levels > 2 the microstructure consisted of fine striations parallel to the rolling direction.

Deformation inhomogeneities that are not seen by etching with aqueous ferric chloride can be revealed by electrolytic etching with thiosulphate solution. At a low strain level $\sim$ 0.22 Fig.(34a) many grains demonstrate one or two sets of thin parallel etch pit lines (20-40μm long) confined within the grains (i.e. they did not cross the grain boundaries). The two sets of etch pit lines were usually observed near to the grain or annealing twin boundaries, where stress concentrations favour multiple slip conditions. These features are similar to type III indications observed by Samuels (9) in compressed copper (ε = 0.2-0.7) etched under similar conditions. The angle between etch pit lines and the rolling direction were measured in 150 grains and the results are plotted in Fig.(35a). About 77 % of the observed lines lay

in the angular range 20° to 50° to the rolling direction, although angles as big as 70° and as small as 3° were occasionally observed. As deformation increased the number of the grains containing etch pit lines and the number of these lines within the grains increased Fig.(34a and b). At 40 % reduction the angle between the lines and the rolling direction were again measured and the results plotted in Fig. (35b). This shows that the range of angles are in general decreased, with 50 % of the grains containing lines in the range 20°-30°, and 21 % 10°-20°. With continued deformation these angles decrease further, and by 90 % reduction almost all the lines become parallel to the rolling direction Fig.(35c and d). It seems that after the formation of these lines, they rotate and become parallel to the rolling plane after heavy deformation (> 90 %) see Fig.(37).

After small or medium deformations (20 % - 40 %) the etch pit lines were often observed parallel to annealing twins. In Fig.(34b) the large grain in the middle of the photograph contains two parallel sets of etch pit lines, each parallel to an annealing twin boundary, suggesting that the lines are parallel to the traces of the {111} slip planes.

Usually etch pit lines produce a notable displacement in grain and twin boundaries, when they meet each other, Fig.(36a), a longitudinal section of 40 % deformed copper shows two parallel lines of etch pits, one of them parallel to a twin, and the other crossing the twin. It can be seen clearly that there are displacements in the twin and the grain boundaries at the intersection areas. This indicates that

the formation of these lines is associated with considerable shear strain.

Both materials (A and B) developed similar deformation microstructure up to 60 % reduction. After this level copper B started to develop a new type of deformation inhomogeneity, coarser striations consisting of a bundle of very fine etch lines making 25°-40° with the rolling direction. These cross the grain and twin boundaries producing an abrupt displacement in them. The shear strain associated with their formation appears to be much larger than that associated with the etch pit lines. Fig.(36 b) shows an example of this effect. From the displacements, the estimated shear strain associated with these striations vary from 1 to 2. These coarser striations are similar to type IV indications reported by Samuels (9). This new type of inhomogeneity will be referred to as shear bands in the following. The number of shear bands increases rapidly with deformation, and by 90 % they were present in more than half of the deformed grains. At high deformations the microstructure in material B consisted of banded regions parallel to the rolling plane, crossed by only one set of shear bands. In adjacent banded regions the shear bands are frequently in the opposite sense, so that their structure appears to zig-zag across the width of the rolled sheet Fig. (37 c). In copper A, by contrast, shear bands were only occasionally observed and the deformed structure, after heavy deformation, generally had a smooth laminar appearance. Fig. (37) shows a comparison between the two materials after 80 % and 90 % reduction.

Remarkable changes in shear band density in copper A were found to take place when the deformation was performed at low temperature (below zero Celsius). Fig.(38a) shows a longitudinal section of copper A rolled to 90 % after cooling to -100° C between the passes (the rolls were at room temperature). No deformation twins were observed but instead, banded regions parallel to the rolling plane and shear bands were developed similar to those in copper B.

Shear band density was also found to increase in copper A when the initial grain structure was larger. A piece of copper A annealed to produce a larger grain size of $\sim 300\mu m$ and then rolled to 90 % at room temperature showed a dramatic change in the deformation structure pattern. Instead of the smooth laminar appearance, very dense coarse shear bands were developed Fig.(38b).

4.2. Scanning electron microscopy :-

All the three principal sections (ND, RD, and TD), for all deformations (20 % - 95 % reduction) in the case of copper A, and only 90 % reduction for copper B, were investigated. 20 % reduction longitudinal sections show one and two parallel sets of banded regions confined within the grains. Each band was 9-20μm long, 0.2-0.3μm thick, making 20-60° with the rolling direction Fig.(39a). In order to find the statistical distribution of the angles between the bands and the rolling direction, measurements were carried out in 50 fields at 1K magnification and the results are plotted in Fig.(35a). The angle distribution of these bands are in a good agreement with

Fig.(33) - Optical microstructures of longitudinal sections of cold rolled copper, etched in aqueous ferric chloride. a - rolled 20 %, b - rolled 60 %, and c - rolled 90 %.

Trace of rolling plane horizontal.

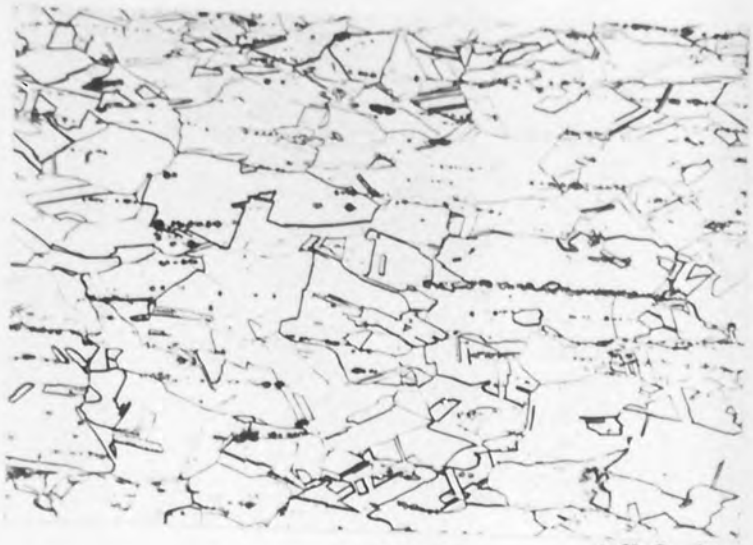

-a- 150 µ

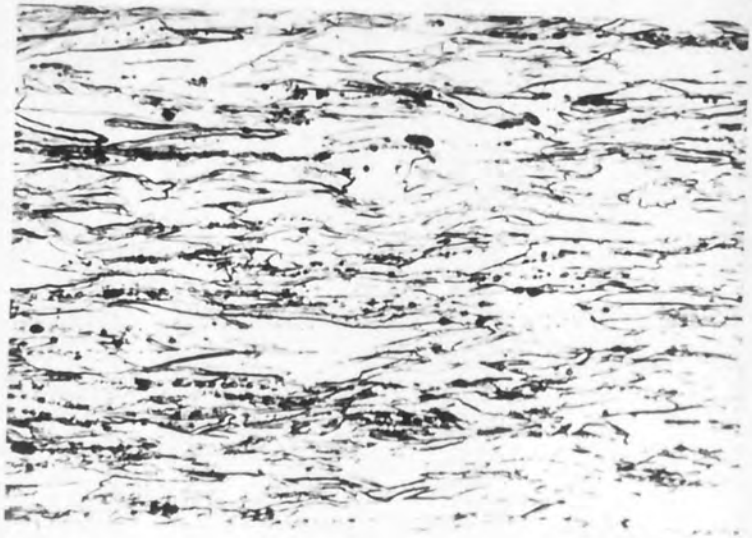

-b- 150 µ

-c- 150 µ

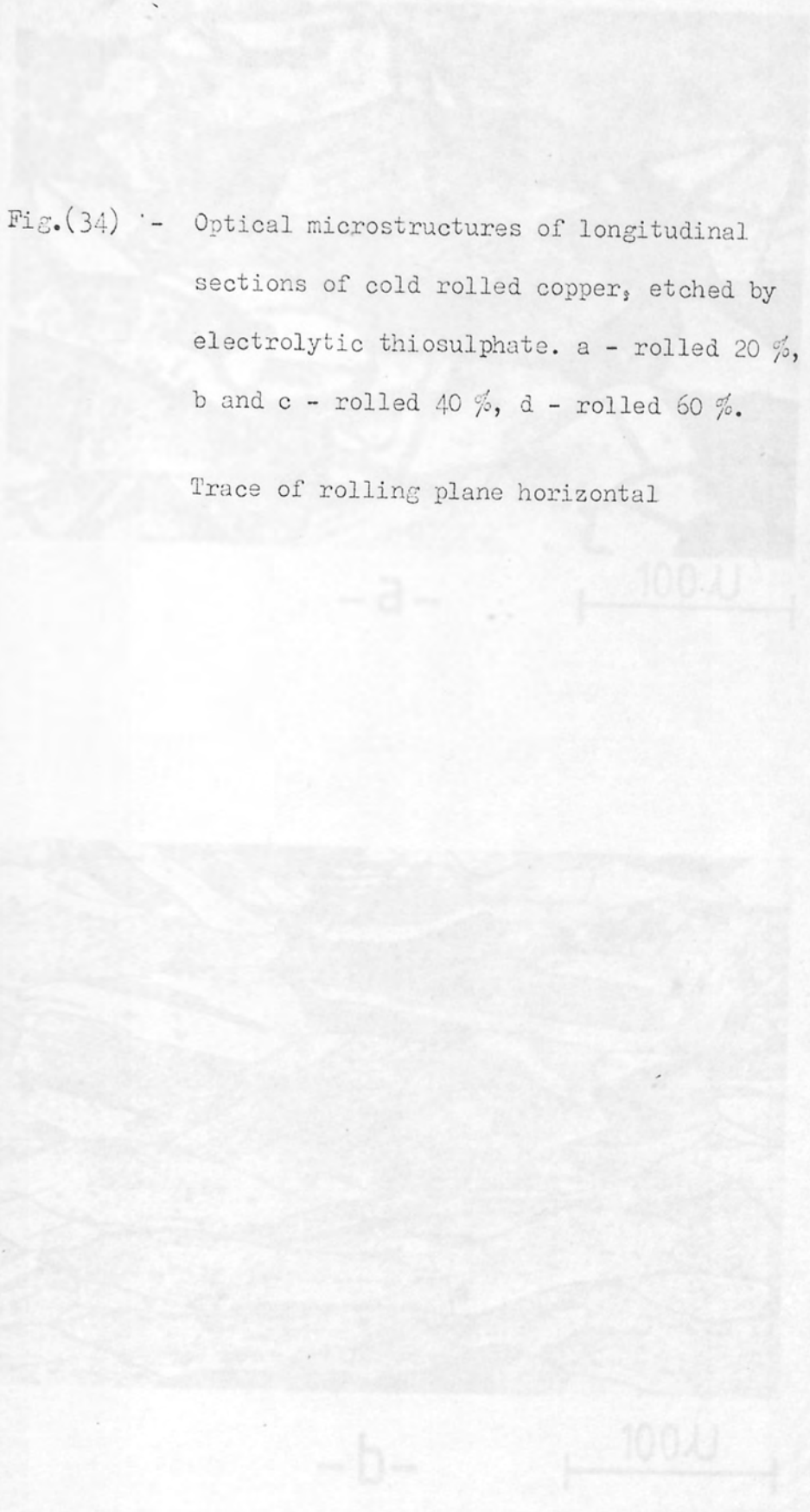

Fig.(34) :- Optical microstructures of longitudinal sections of cold rolled copper, etched by electrolytic thiosulphate. a - rolled 20 %, b and c - rolled 40 %, d - rolled 60 %.

Trace of rolling plane horizontal

-a- 100 µ

-b- 100 µ

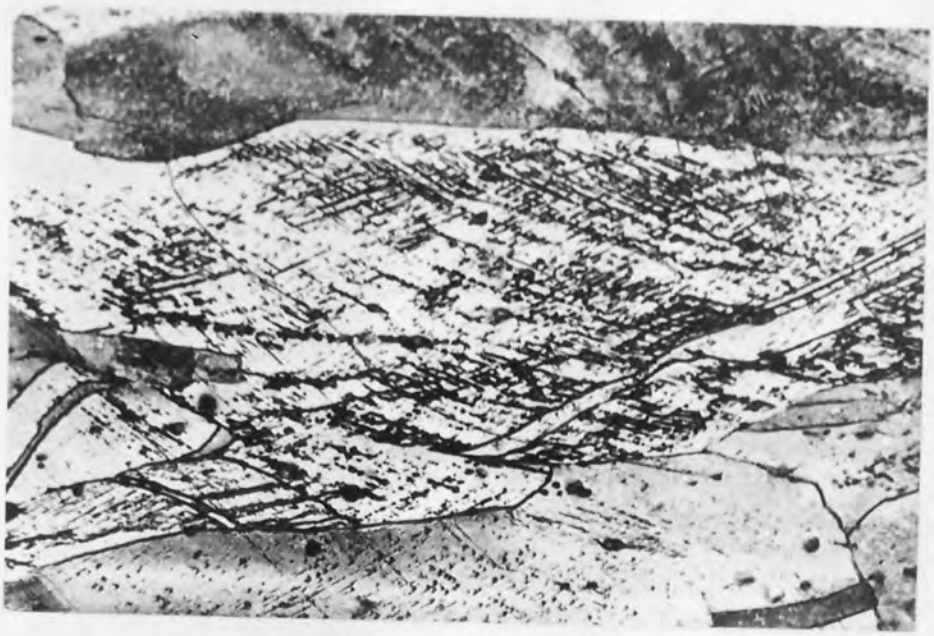

-c- 50 μ

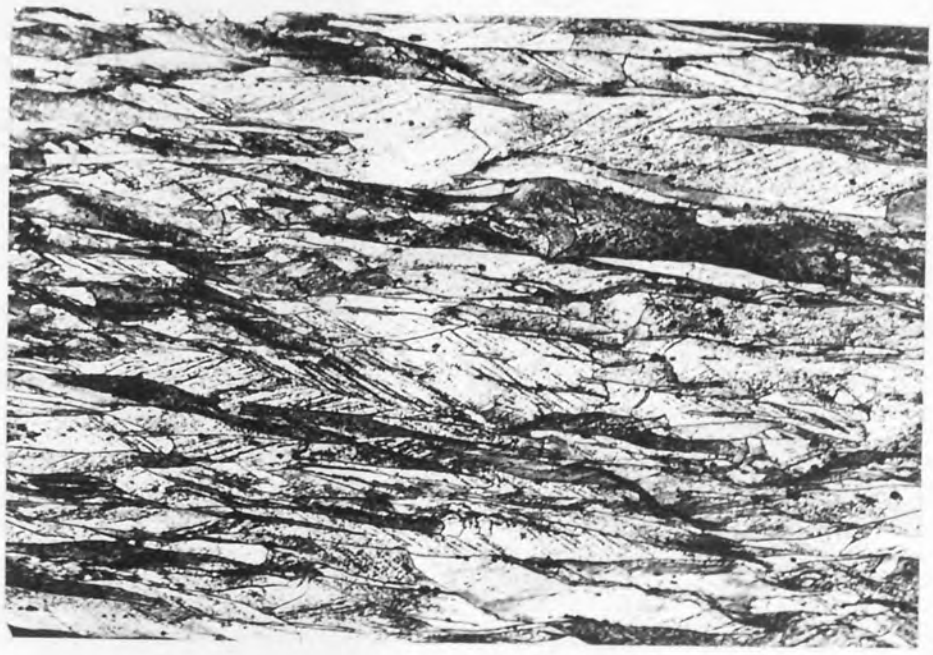

-d- 100 μ

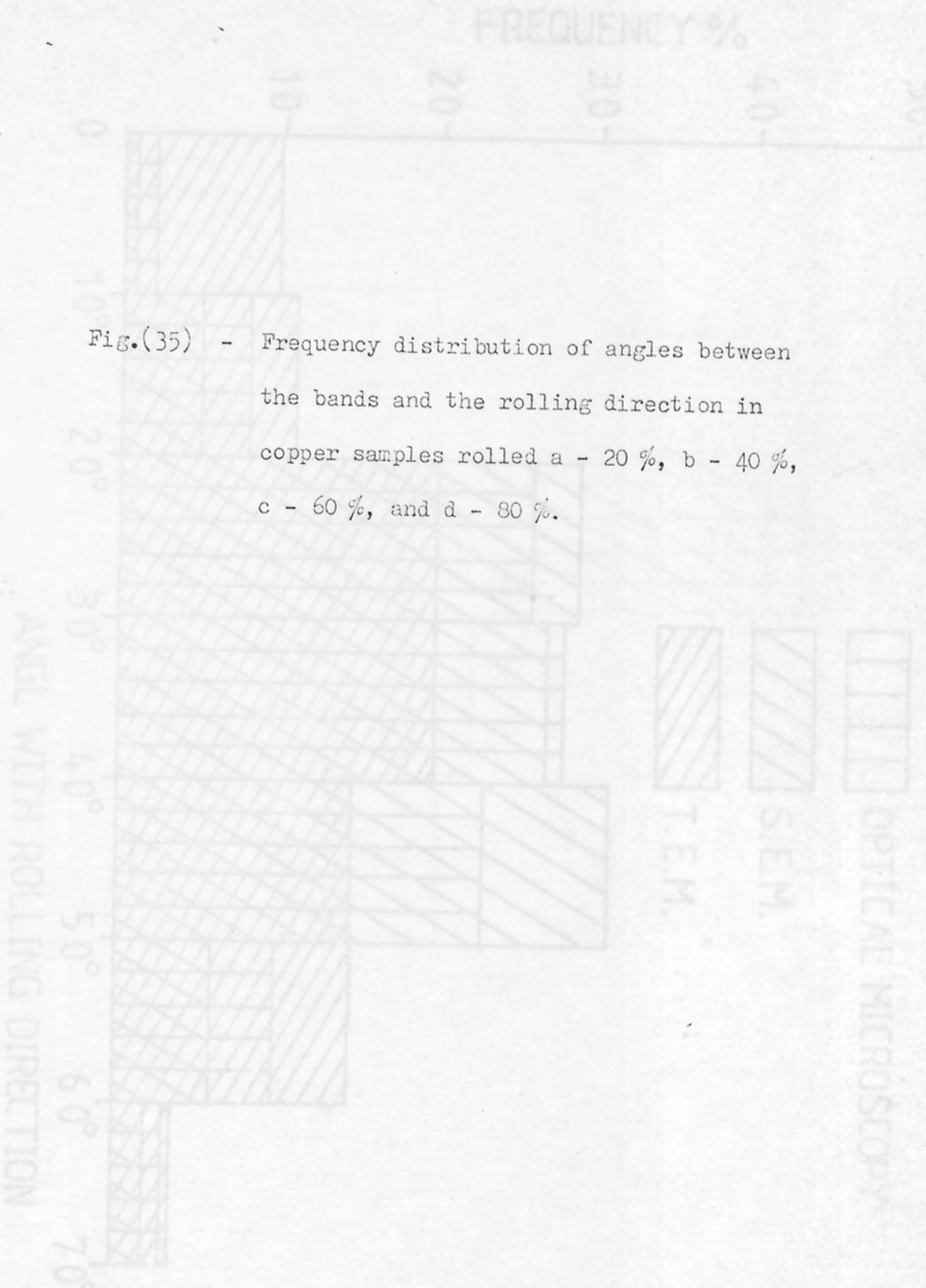

Fig.(35) - Frequency distribution of angles between the bands and the rolling direction in copper samples rolled a - 20 %, b - 40 %, c - 60 %, and d - 80 %.

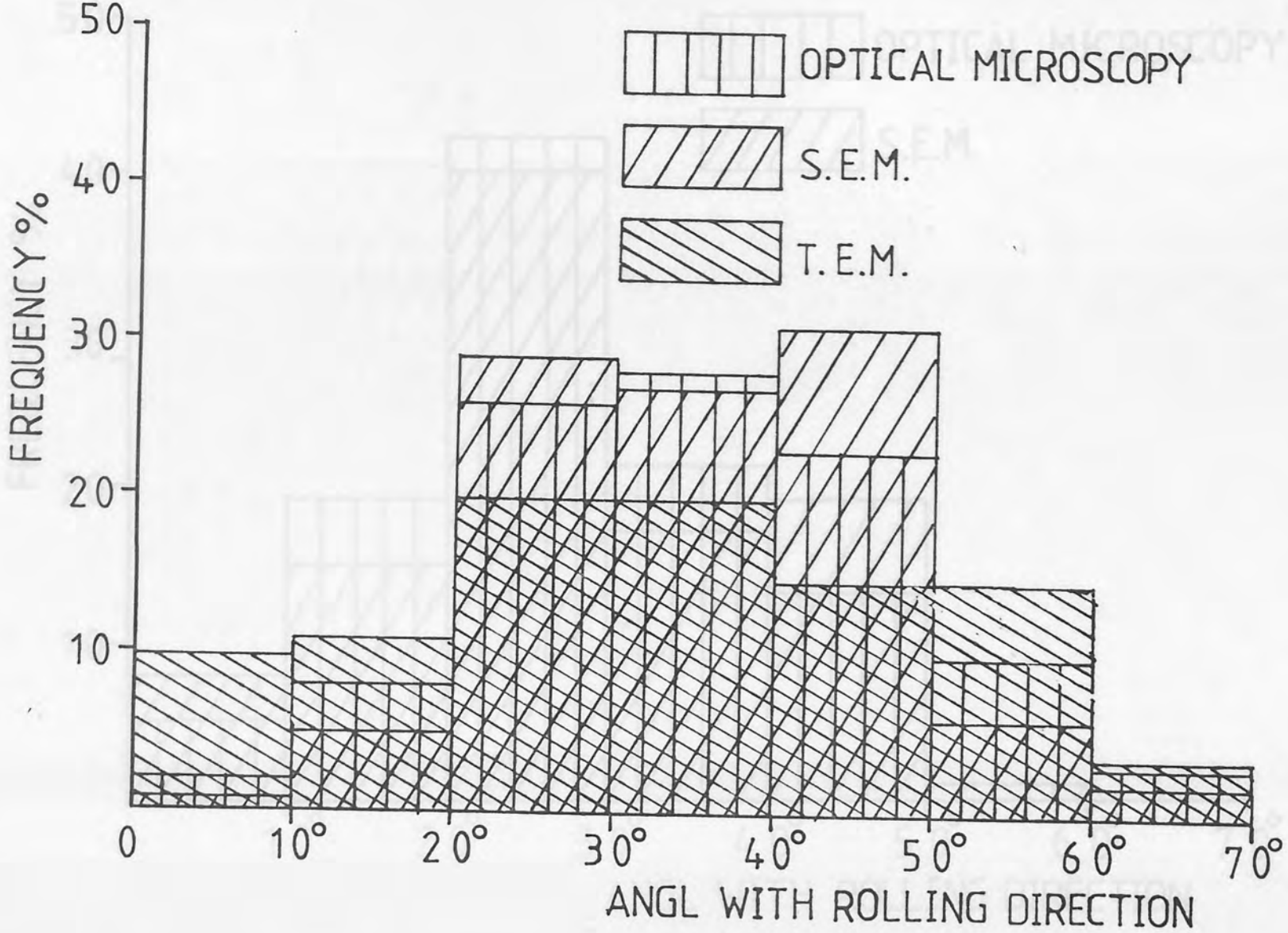
OPTICAL MICROSCOPY
S.E.M.
T.E.M.
FREQUENCY %
50
40
30
20
10
0
10°
20°
30°
40°
50°
60°
70°
ANGL WITH ROLLING DIRECTION

-a-

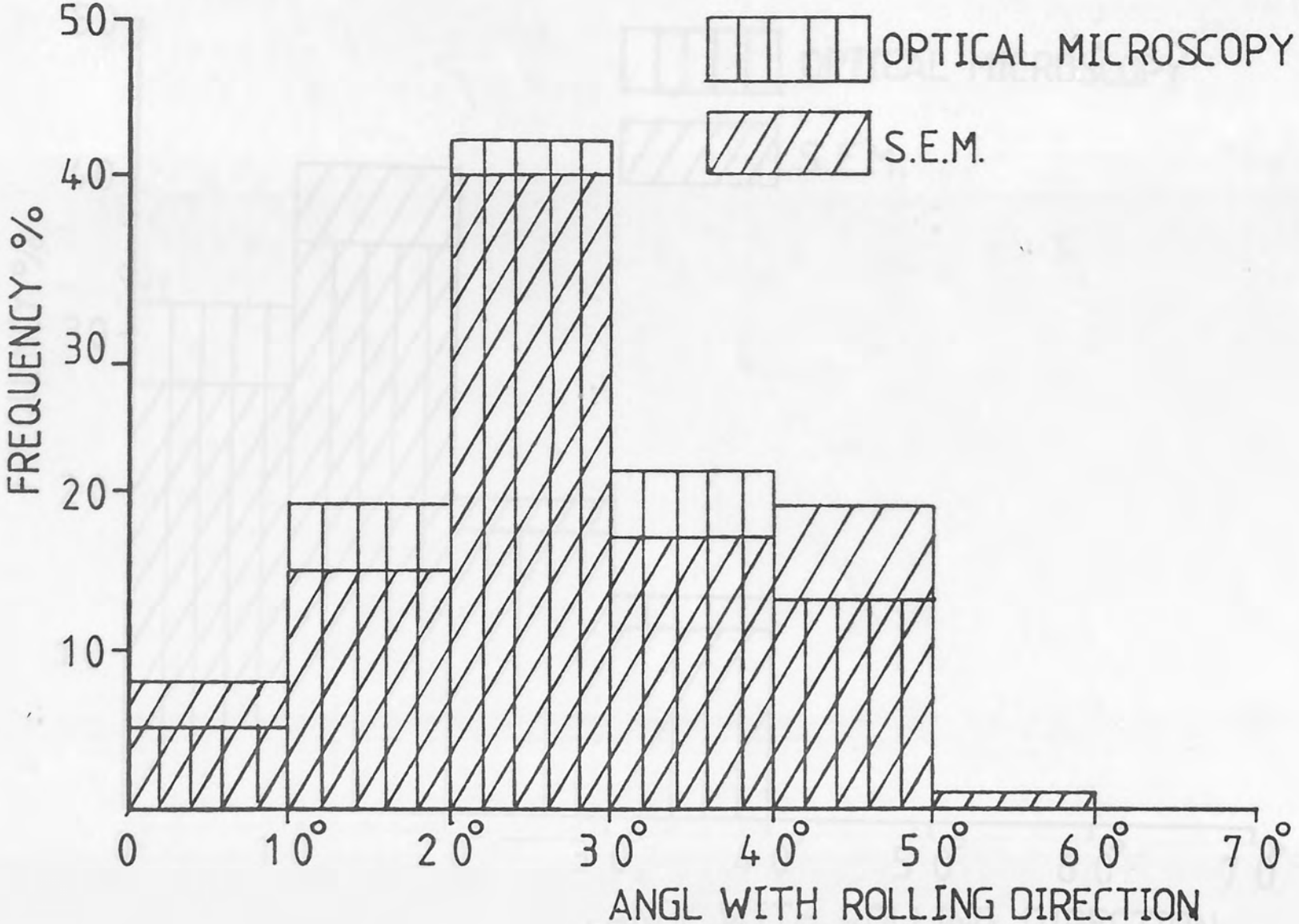
50
40
30
20
10
FREQUENCY %
OPTICAL MICROSCOPY
S.E.M.
0
10°
20°
30°
40°
50°
60°
70°
ANGL WITH ROLLING DIRECTION

-b-

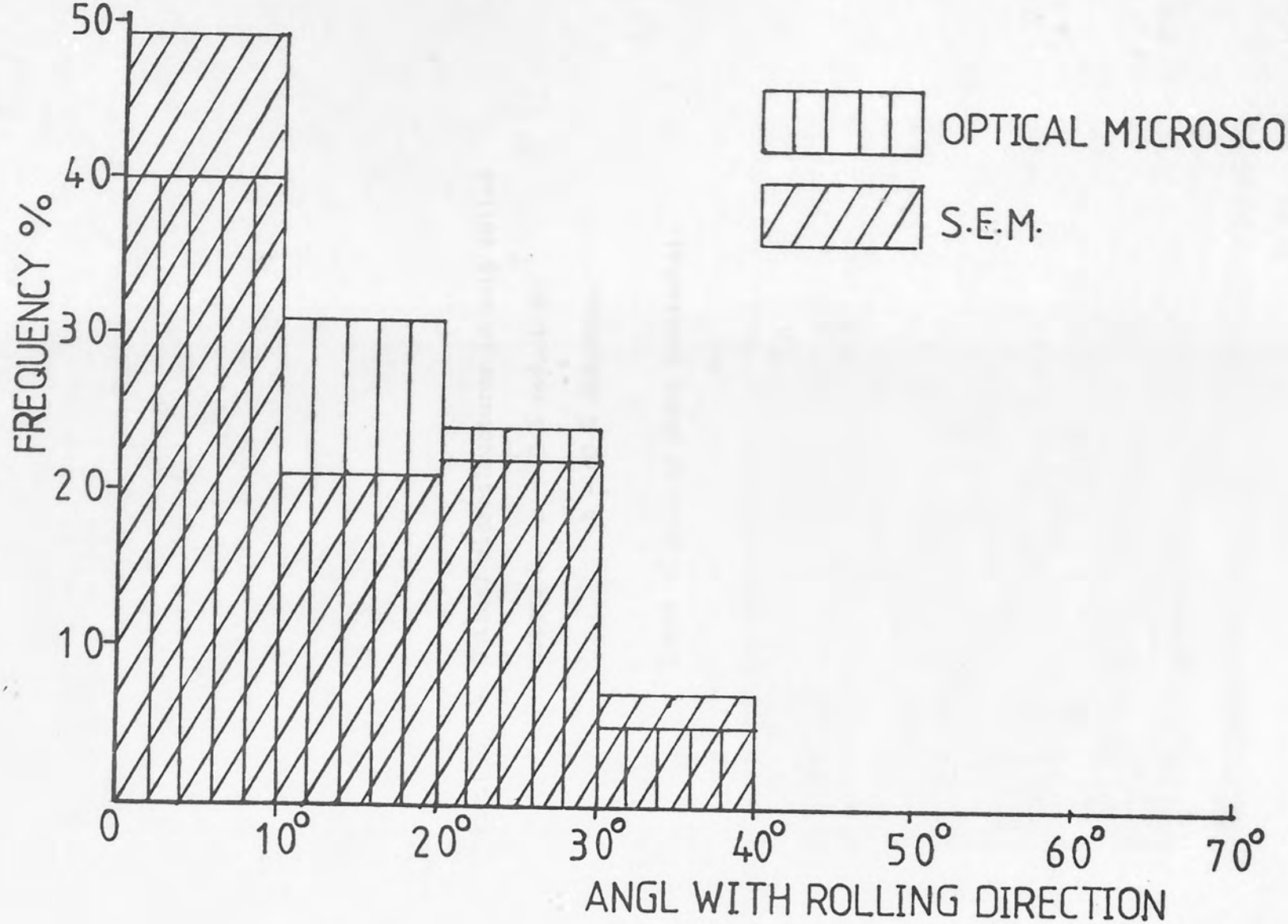
50
40
30
20
10
FREQUENCY %
OPTICAL MICROSCOPY
S.E.M.
0
10°
20°
30°
40°
50°
60°
70°
ANGL WITH ROLLING DIRECTION

-d-

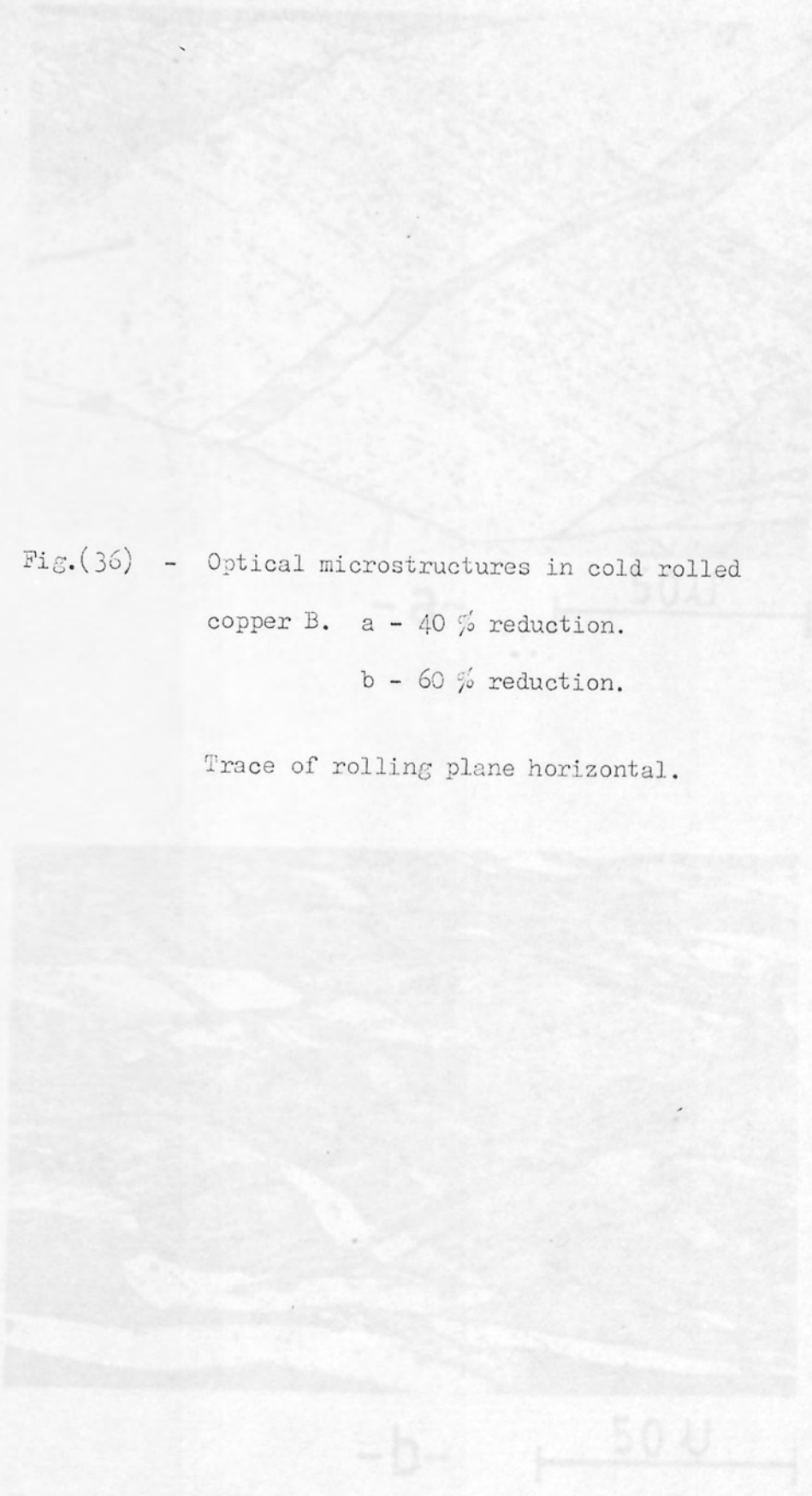

Fig.(36) - Optical microstructures in cold rolled copper B. a - 40 % reduction.
b - 60 % reduction.

Trace of rolling plane horizontal.

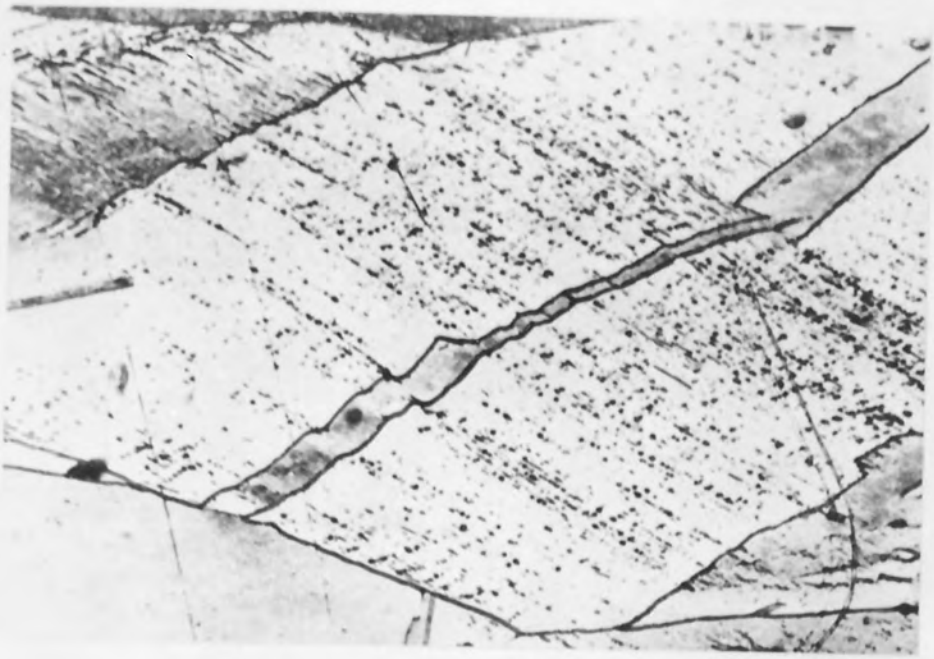

-a- 50 μ

-b- 50 μ

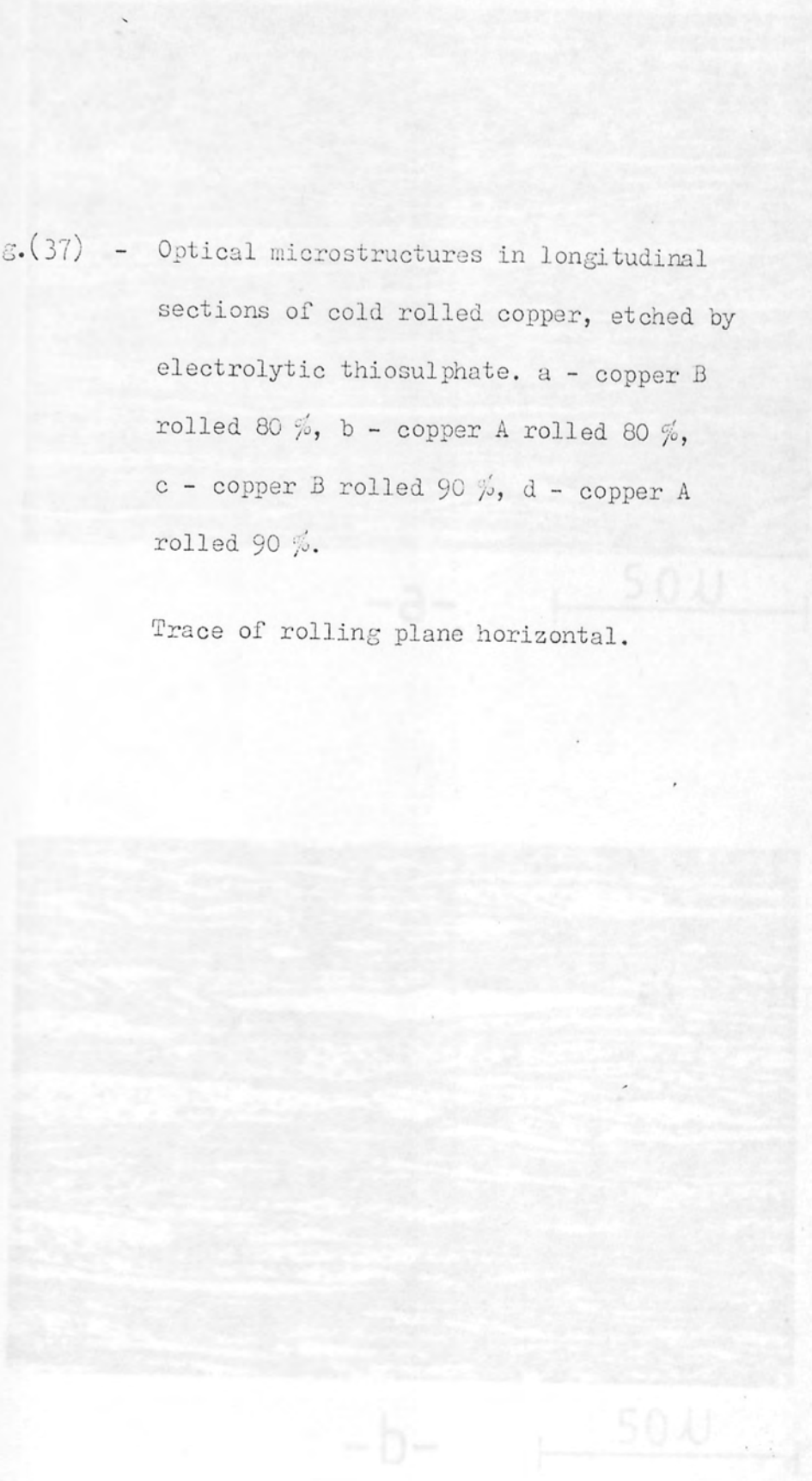

Fig.(37) - Optical microstructures in longitudinal sections of cold rolled copper, etched by electrolytic thiosulphate. a - copper B rolled 80 %, b - copper A rolled 80 %, c - copper B rolled 90 %, d - copper A rolled 90 %.

Trace of rolling plane horizontal.

-a- 50 μ

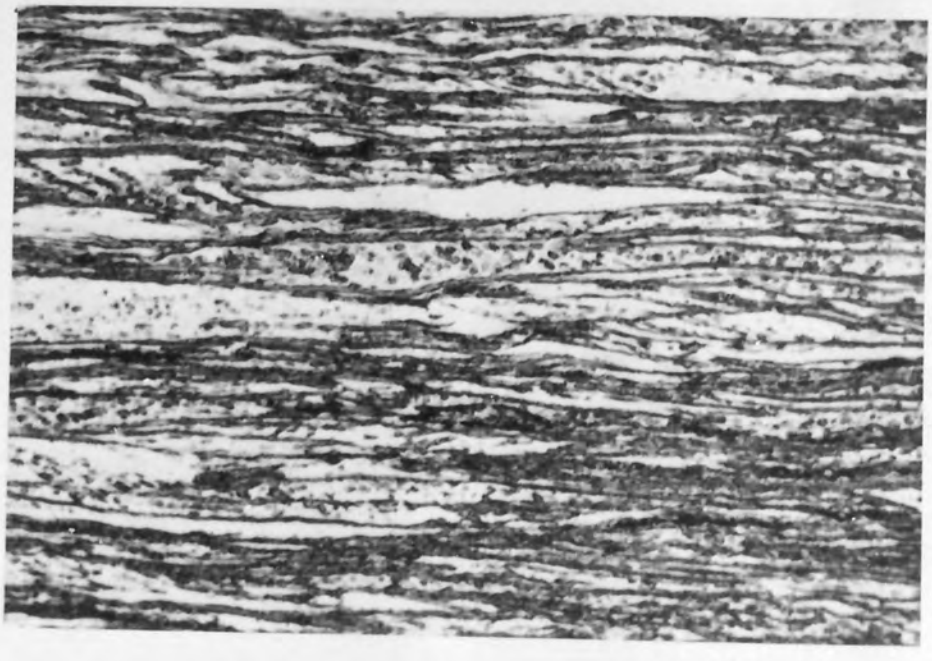

-b- 50 μ

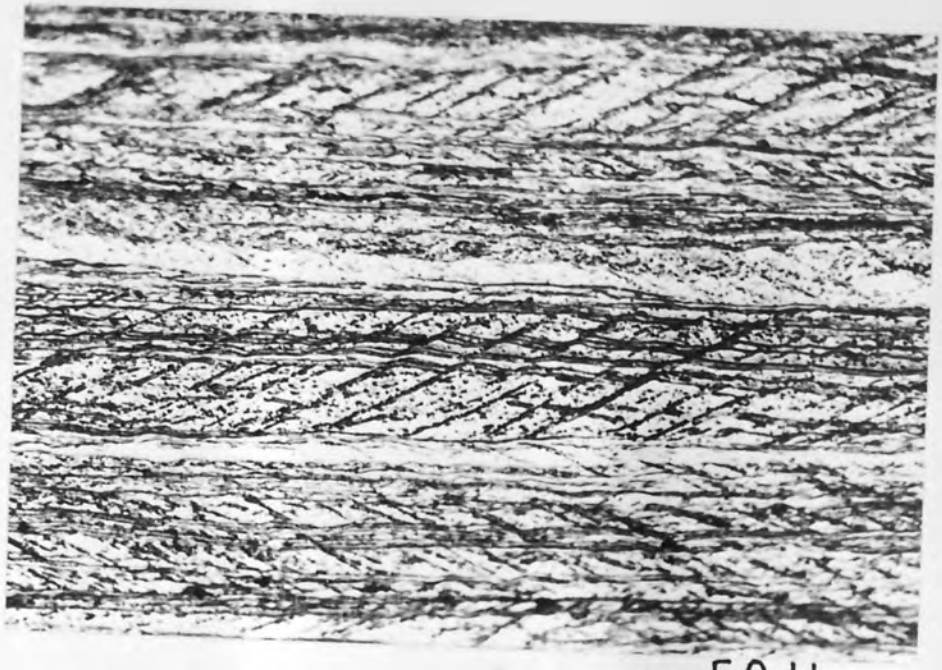

-c- 50μ

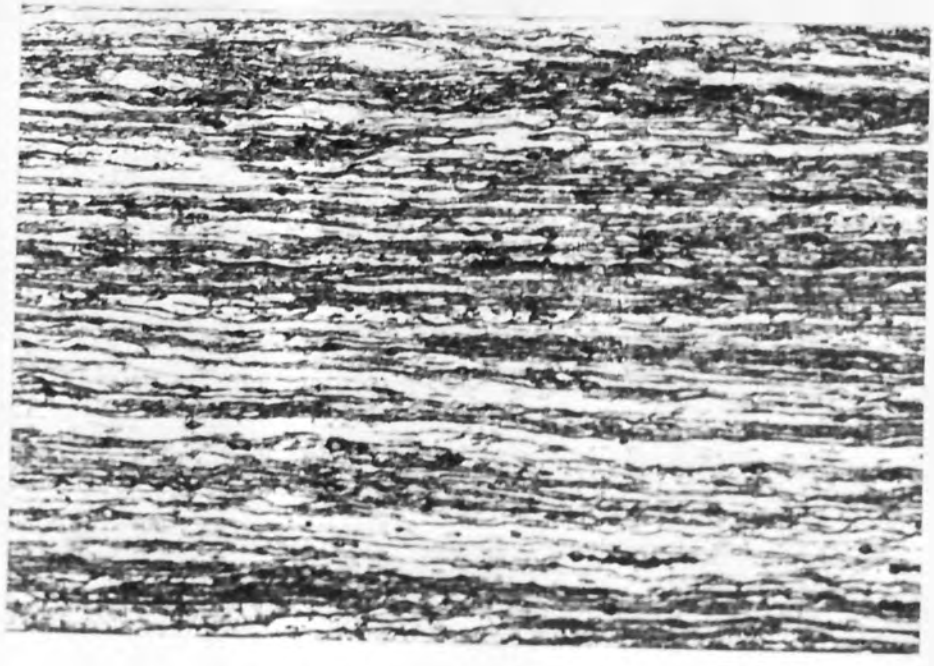

-d- 50μ

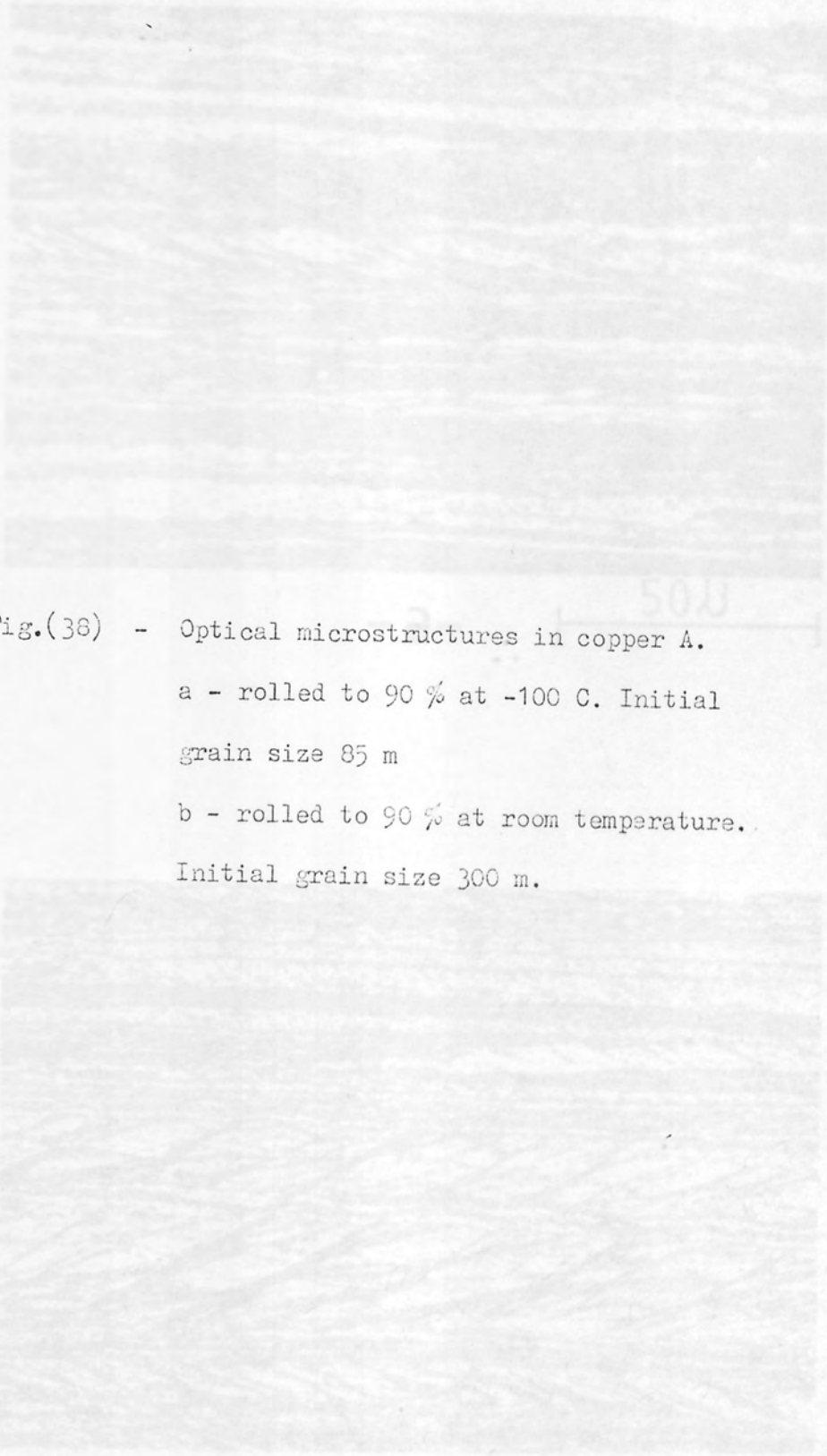

Fig.(38) - Optical microstructures in copper A.

a - rolled to 90 % at -100 C. Initial grain size 85 m

b - rolled to 90 % at room temperature. Initial grain size 300 m.

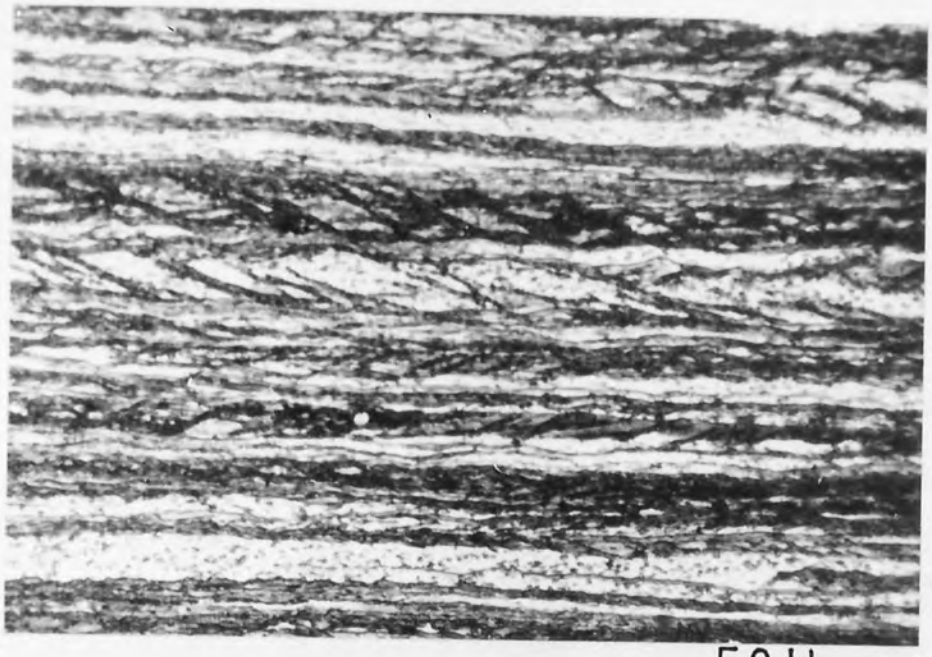

-a- 50μ

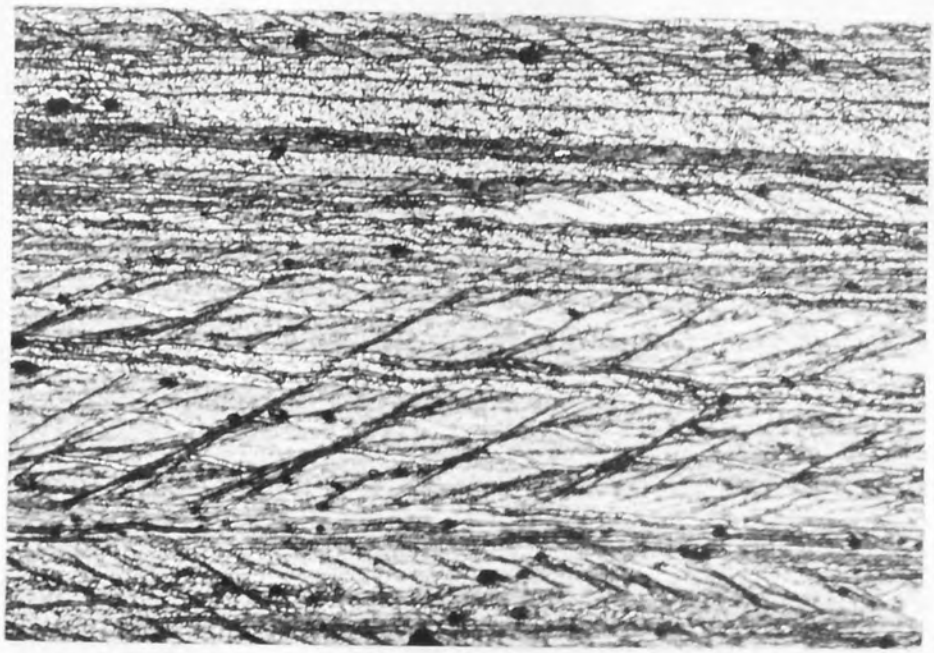

-b- 50μ

the angle distribution of etch pit lines observed in optical metallography. The two parallel sets of bands normally developed near to the grain or annealing twin boundaries Fig. (39a). Annealing twins were commonly parallel to these bands, which indicated that the bands were traces of {111} slip planes on the specimen surface. The geometry and morphology of these banded regions are similar to etch pit lines observed in optical metallography at the same strain level (compare Figs.34a and 39a). In transverse sections only one parallel set of bands was observed, 0.2-0.3μm thick, 7-15μm long and making 0°-10° with the trace of the rolling plane Fig.(39a). In rolling plane sections the examinations revealed only one parallel set of rather diffuse bands, usually making an angle of 90° with the rolling direction, Fig.(39a). It seems that the banded regions observed in all three sections are the intersection of a thin sheet like band within these sections. The sheet like bands are 9-20μm long, 0.2-0.3μm thick, 7-15μm wide, making an angle 20°-60° with the rolling direction, and approximately parallel to the transverse direction. It will be shown in the following sections that these bands correspond to the microbands observed in thin foils by transmission electron microscopy and they will be referred to as microbands in the following.

As the deformation increased the number of microbands increased, especially the two parallel sets of microbands. Furthermore, the number of grains containing microbands also increased, but the microband thickness seemed to remain unchanged. A comparison between the transverse and longitudinal sections in Figs.(39a and b) shows the difference between the

band densities at 20 % and 40 % reduction. The angles between the bands and the rolling direction were measured for 40 % reduction in 55 fields at 1K magnification and the results are plotted in Fig.(35c). It shows that the percentage in the angle range has decreased compared to 20 % reduction. At 60 % the individual bands in the longitudinal section become less distinct, Fig.(39 c). The average angle between the microbands and the rolling direction becomes smaller, and as the deformation increased further the angles became still smaller, Figs. (39d and e). By 90 % reduction the alignment of the bands with the rolling direction was almost perfect, Fig.(39e). These measurements indicate that after formation, the bands do rotate with further deformation to become parallel to the rolling plane after heavy deformation.

Scanning electron microscopy examination showed some differences in the deformed structures of copper A and B. The most obvious difference was the frequency of shear bands, these were evident in material B after 90 % reduction. Fig. (40) shows longitudinal sections of the two materials deformed 90 %. In copper B the deformation structure consists of elongated cells (microbands) parallel to the rolling direction and shear bands. When the elongated cells are crossed by shear bands, they rotate toward the shearing direction. Material A at this strain level develops a smooth laminar structure, and shear bands are very rarely observed. The boundaries of the elongated cells are relatively sharper, which is probably due to dynamic recovery. In this material dynamic recrystallization was often observed in specimens deformed 95 %, and even static

recrystallization was found to take place when the material was left for a few weeks at room temperature, Fig.(41).

Experiments were carried out involving small rolling passes on specimens of cold rolled copper B with polished and scratched longitudinal sections. The specimens were examined by scanning electron microscopy in the secondary electron mode. Fig.(42a) shows a longitudinal section of specimen deformed 40 % which was then polished and scratched normal to the rolling direction, and re-rolled to 46 % total deformation. It shows two parallel sets of slip lines making 45° (the dark slip lines), and 27° (the white slip line) with the rolling direction, the spacings of these slip lines are irregular (1-5μm). The dark lines sheared the white lines but not vice-versa suggesting that the amounts of shear are very different on the two systems or, more probably, that the white lines were formed first. The similarity between the slip lines and the microbands observed by optical metallography and SEM/BSE at the same deformation level, encourages one to believe that these lines are microbands with localised shear confined to individual grains.

Edge section specimen deformed 90 %, polished, scratched normal to the rolling direction, and re-rolled to 91 % developed a parallel set of coarser striations, Fig.(42b), oriented at 30°-40° relative to the rolling direction. They corresponded to regions of macroscopic localised shear. Evident displacement of scratches occurred, where the bands intersected them, and the shear strains were estimated to be in the range 100 % to 300 %.

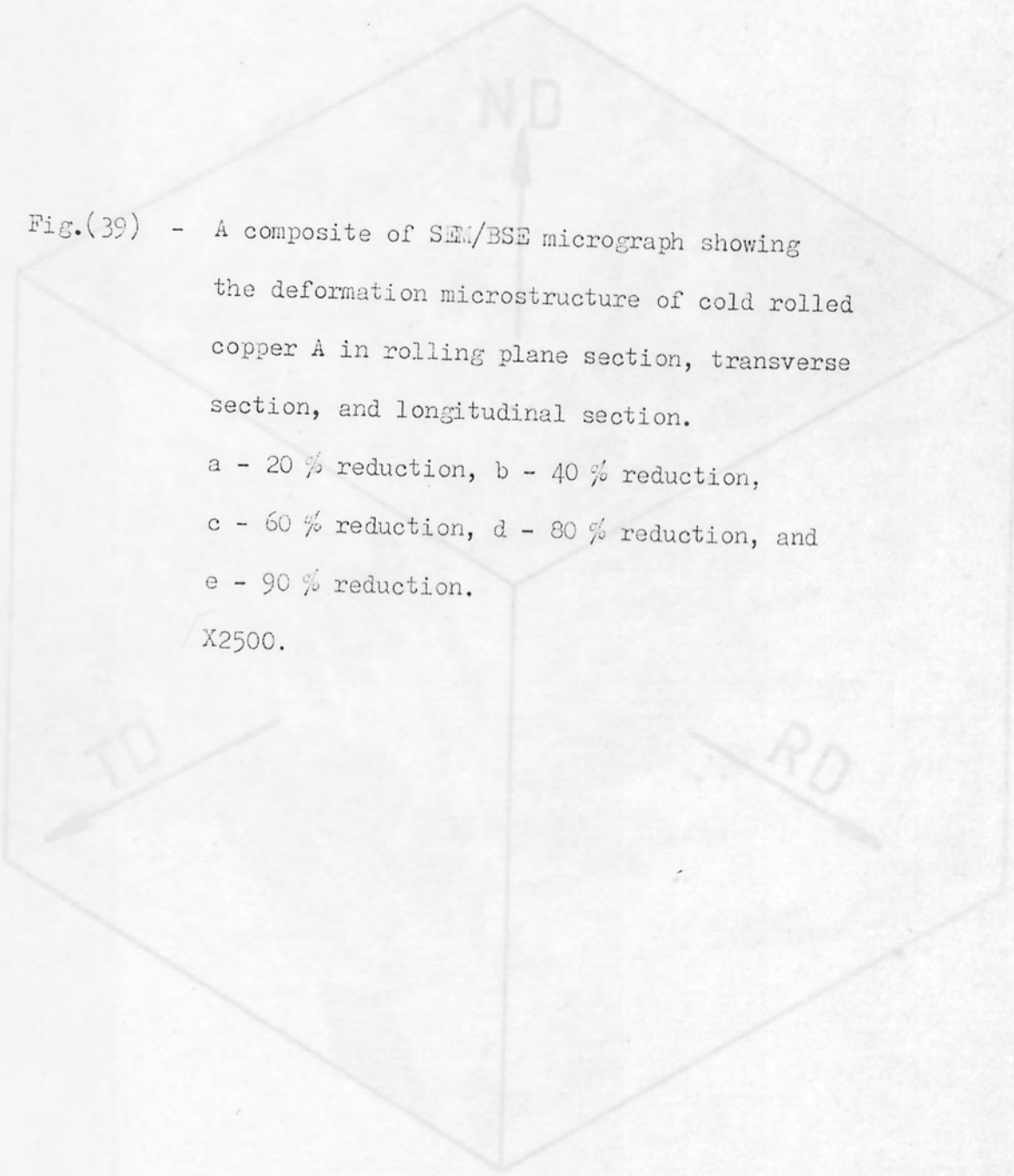

Fig.(39) - A composite of SEM/BSE micrograph showing the deformation microstructure of cold rolled copper A in rolling plane section, transverse section, and longitudinal section.
a - 20 % reduction, b - 40 % reduction,
c - 60 % reduction, d - 80 % reduction, and
e - 90 % reduction.
X2500.

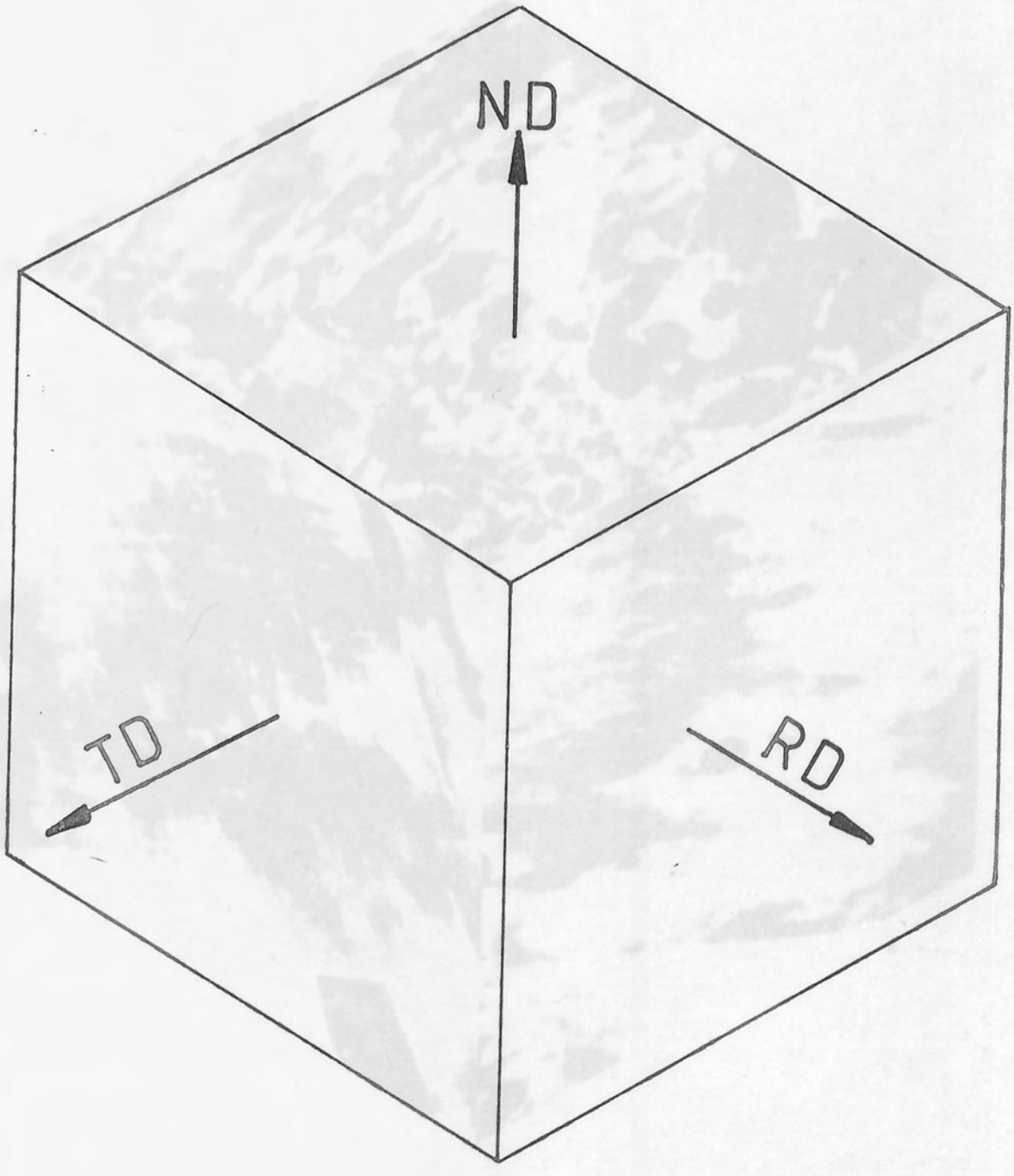
ND
TD
RD

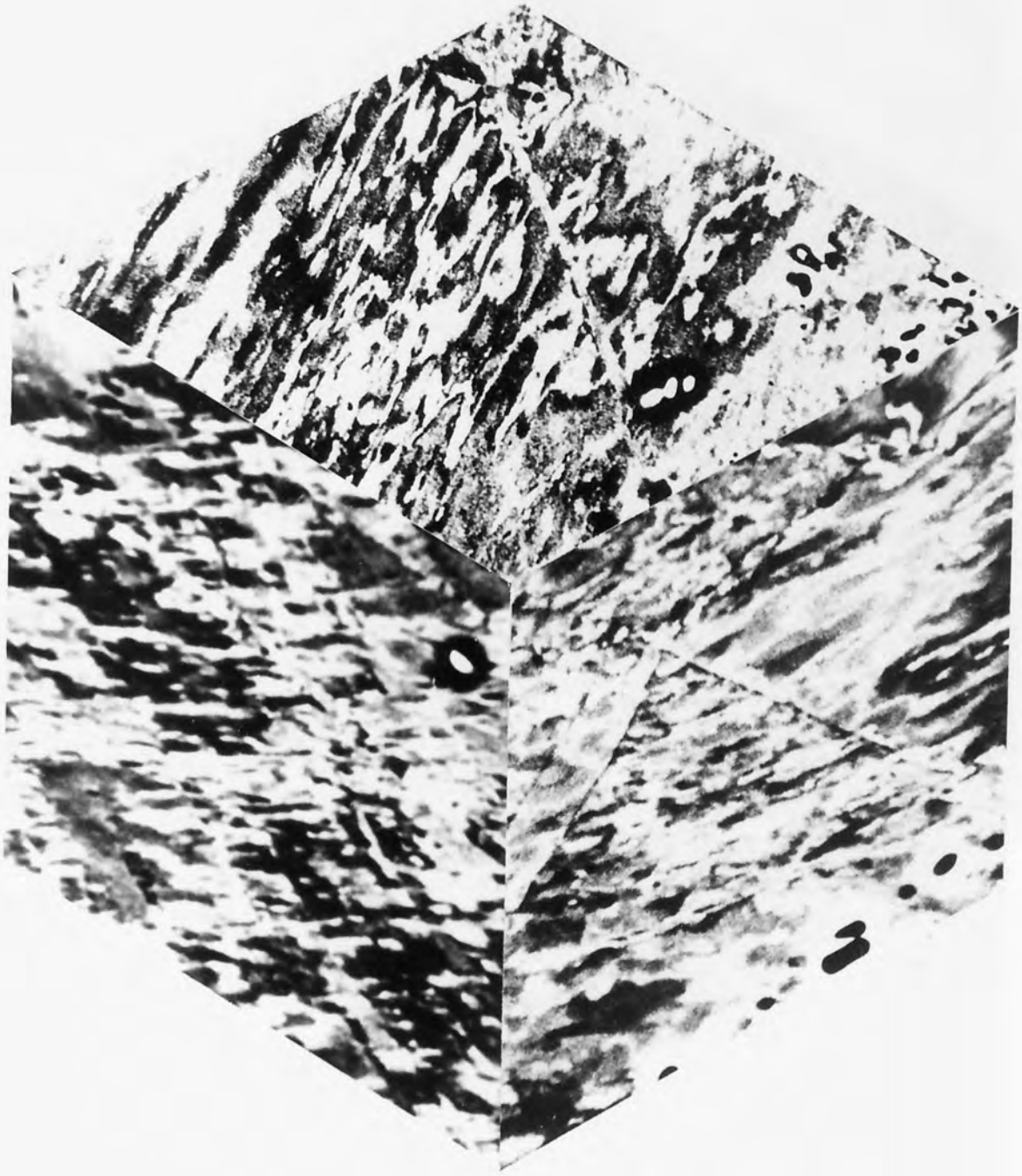

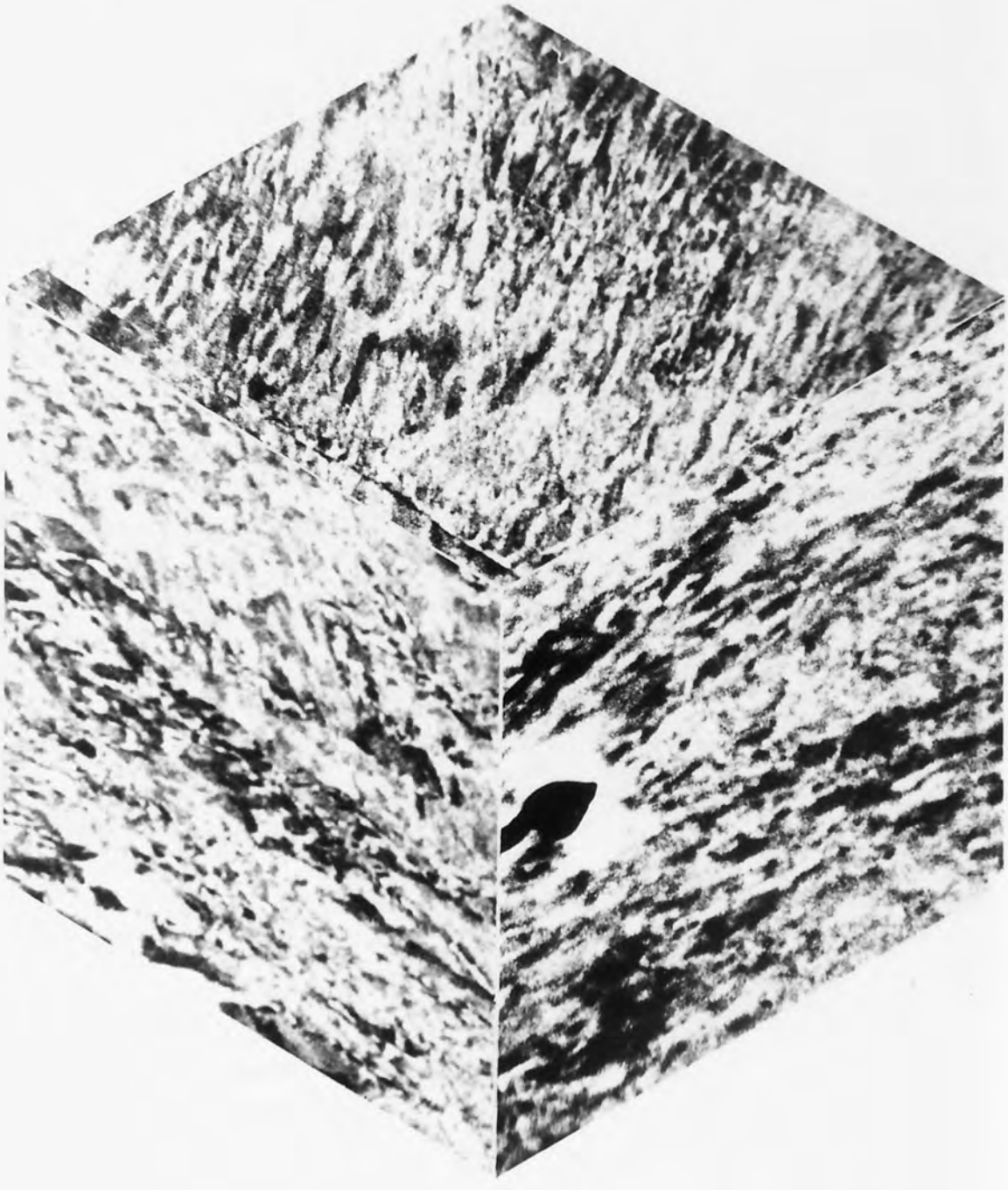

d

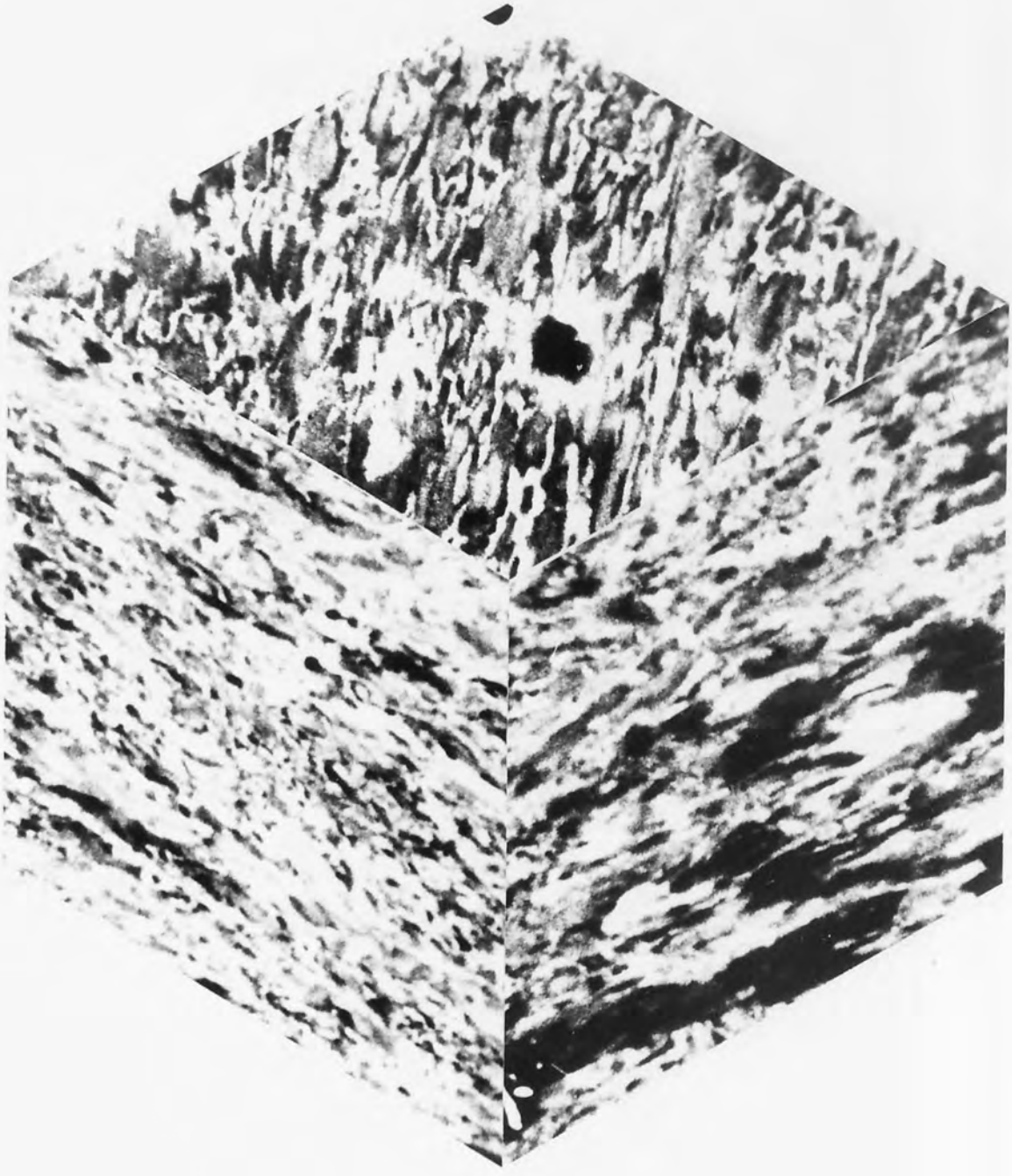

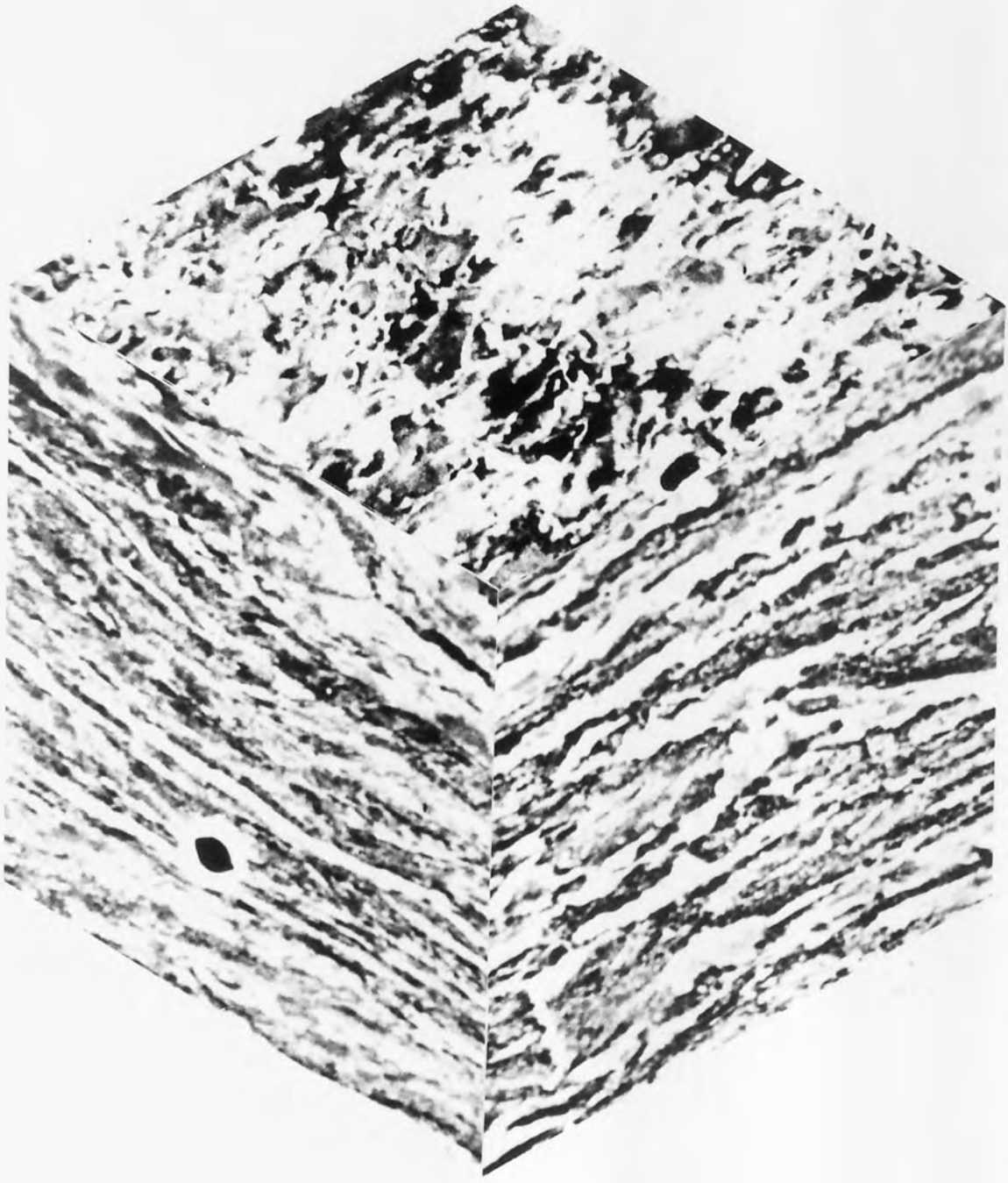

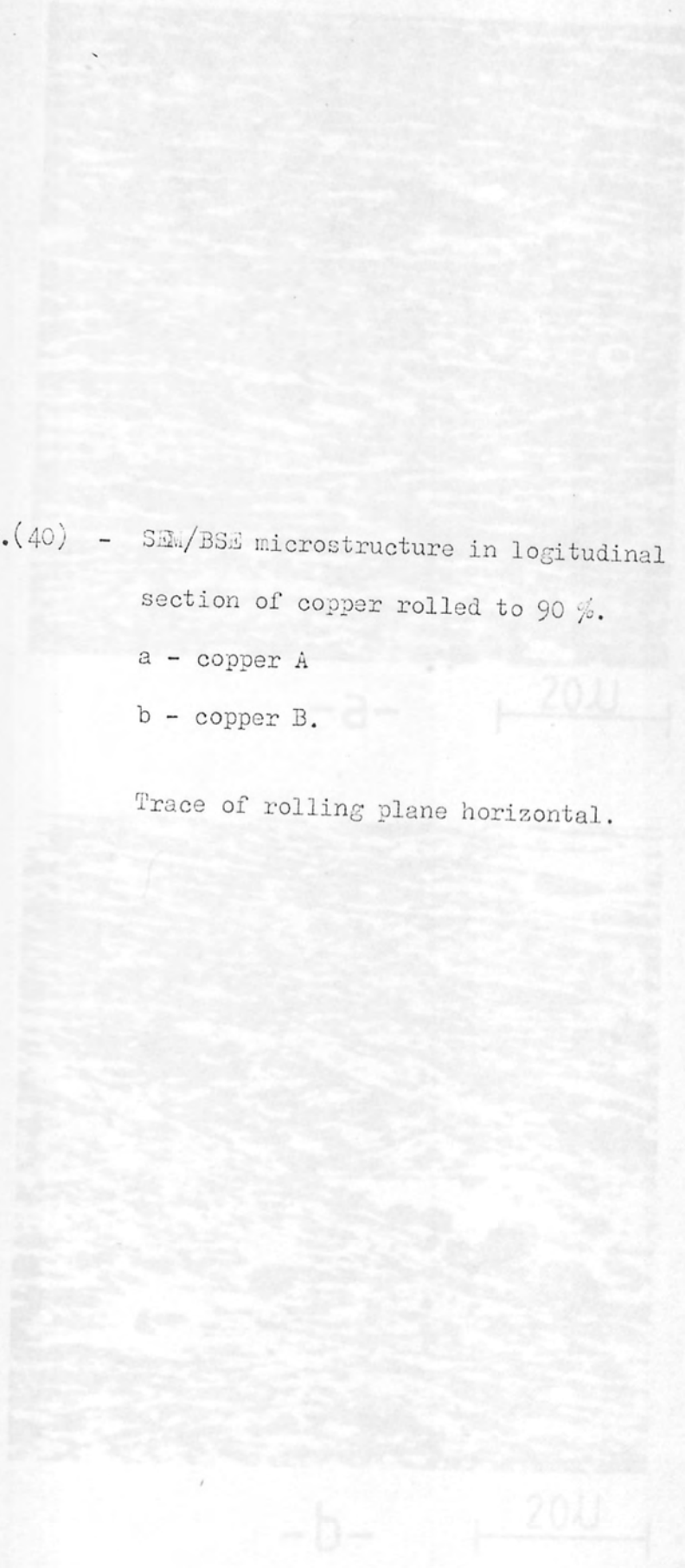

Fig.(40) - SEM/BSE microstructure in logitudinal section of copper rolled to 90 %.

a - copper A

b - copper B.

Trace of rolling plane horizontal.

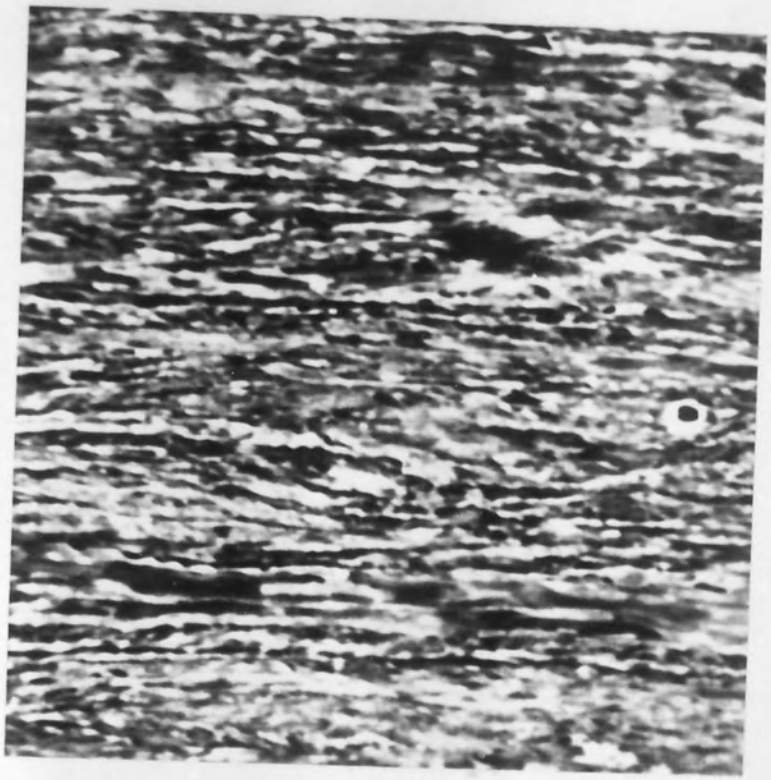

-a- 20μ

-b- 20μ

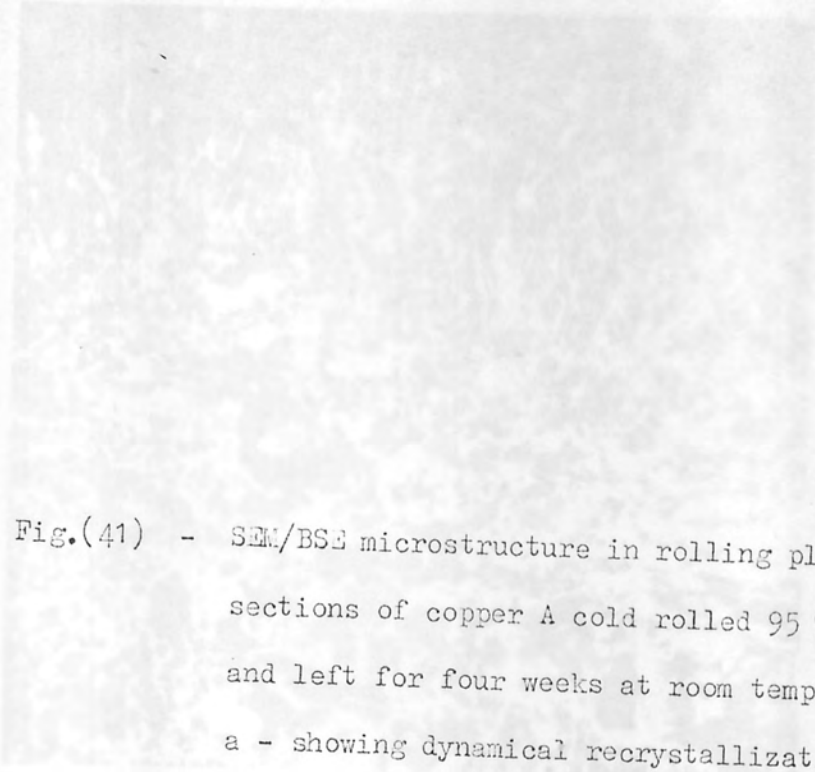

Fig.(41) - SEM/BSE microstructure in rolling plane sections of copper A cold rolled 95 % and left for four weeks at room temperature :

a - showing dynamical recrystallization

b - showing static recrystallization.

Rolling direction horizontal.

20 μ

95% COLD ROLLED COPPER

Fig.(42) - SEM micrographs of polished and scratched longitudinal sections.

a - Specimen rolled 40 %, polished, scratched, and rerolled to 46 % total deformation.

b - Specimen rolled 90 %, polished, scratched, and rerolled to 91 % total deformation.

Rolling plane trace horizontal.

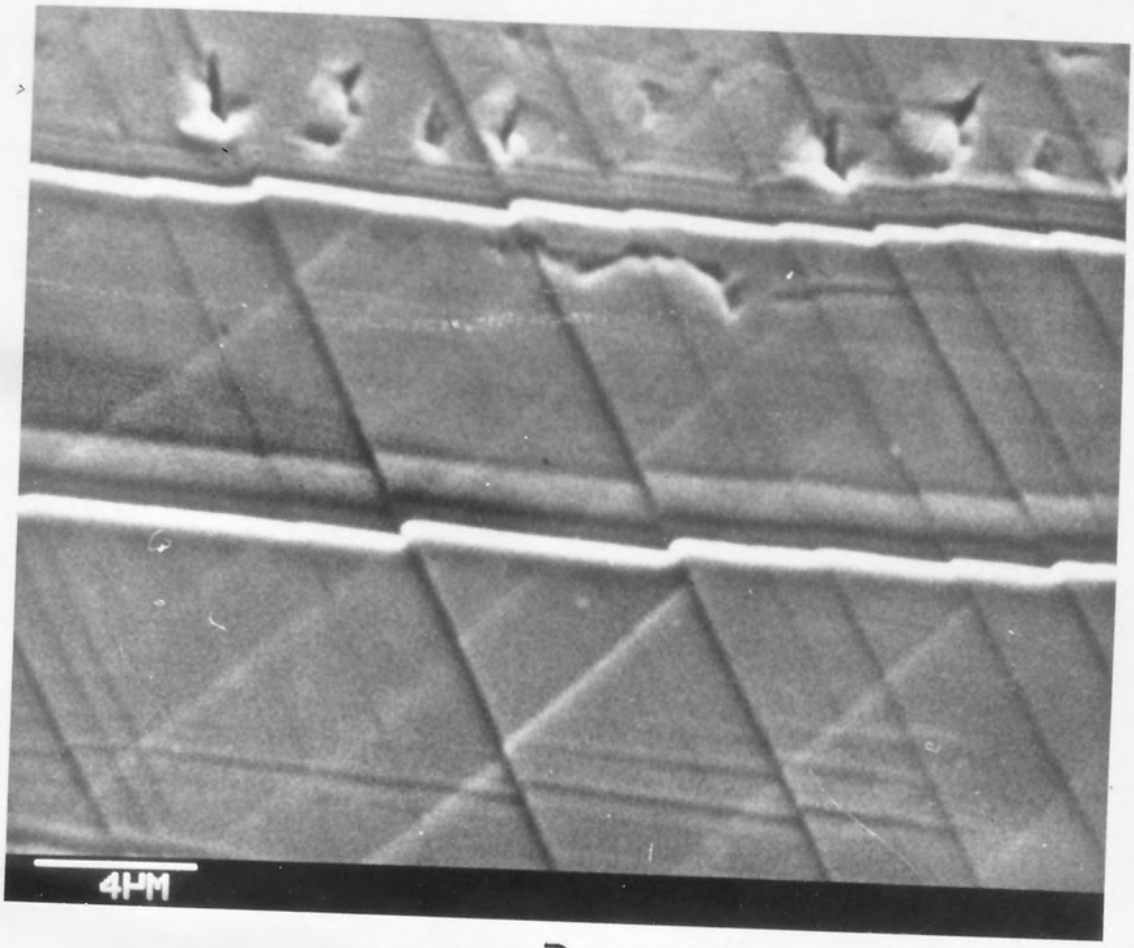

-a-

-b-

4.3. Transmission electron microscopy :-

Examinations in the TEM revealed that the deformed materials developed three distinct substructural features. These were equiaxed dislocation cells, microbands, and shear bands. Each of them usually started to form at a certain deformation level. No differences were detected in the deformed structures of the two materials up to a strain level of 1.6.

Equiaxed dislocation cell structures :

At low strain levels ($\varepsilon < 0.1$) the only feature observed was an irregular equiaxed cell structure with cells 0.5 - 1μm in diameter (Fig.43 a). Their interiors were relatively free of dislocations, while the boundaries were rather diffuse regions of high dislocation density. By 20 % reduction the cell boundaries become relatively sharper due to an increase in the dislocation density, Figs.(44,46,47). Selected area diffraction pattern analysis indicated that the misorientation across the cell boundaries was usually small ($\sim 2^{\circ}$). This was confirmed by using the microdiffraction technique. Clear Kikuchi line patterns were obtained from which accurate orientations were derived for the individual cells. The study was carried out on a number of thin foils prepared from edge sections of copper deformed 20 %. Fig.(44) shows a typical example of one of these studies, where microdiffraction patterns were obtained from eight cells, the cells were numbered from 1 to 8 and the associated patterns are shown in the same figure. This analysis indicated that the transverse directions of the cells are scattered

around $[\bar{1}14]$ by 1° - 1.5°, and that the boundaries between them are not pure tilt type. The cells were rotated around TD and around an axis perpendicular to TD, but the latter rotation was usually smaller than the former. In general, the misorientations between neighbouring cells were found to be varying from 1° to 2.5°. The misorientation measurements between cell number 1 and the other cells (2 - 8) are plotted in Fig.(45), it is apparent that the senses of rotation between adjacent cells relative to cell (1) are opposite to each other. This indicates that the equiaxed cell structure does not create any long range lattice curvature.

In order to obtain more information about this structure experiments for defining the dislocation type within and in the boundaries of the cells were carried out. The dislocation Burgers vector is usually determined by finding the reflections in which the dislocation becomes invisible. This happens when $g.b = 0$, where g is the reflection plane normal, and b the Burgers vector. It can be done by tilting and rotating the specimens to obtain a series of images of the same view with a number of specific reflecting planes operating separately (two beam condition). However, many unsuccessful attempts were carried out to obtain such conditions. This was attributed to the misorientations between the cells and the high dislocation density, which cause the diffraction conditions to vary markedly from region to region. Another technique has been employed for this study, which is based on dark field imaging. When the crystal is oriented close to a prominent pole the conditions for diffraction persist over

relatively large angles and so are insensitive to small misorientations from cell to cell in the deformed material. Two beam conditions obviously cannot be obtained at the pole but individual diffracted beams can be deflected through the objective aperture to give dark field images which contain information related to the selected diffracting vector. The normal visibility conditions apply but the dislocations appear bright when in contrast. Fig.(46a) is a bright field micrograph of copper deformed 20 %, the orientation of the area is $[\bar{1}12]$. In Table (4) all the reflections associated with this zone are given and the type of dislocation which will be visible or invisible for each reflection.

Table (4).

b / g.b	$1\bar{1}1$	$\bar{2}20$	$\bar{1}\bar{3}1$	$\bar{3}1\bar{1}$
$\frac{1}{2}(110)$	invisible	invisible	visible	visible
$\frac{1}{2}(101)$	V	V	I	V
$\frac{1}{2}(011)$	I	V	V	V
$\frac{1}{2}(1\bar{1}0)$	V	V	V	V
$\frac{1}{2}(10\bar{1})$	I	V	V	V
$\frac{1}{2}(0\bar{1}1)$	V	V	V	I

Comparison between the bright field and the dark field images, Fig.(46) and this table indicates that there is no tendency for any specific type of dislocation inside the cells or in the walls of the equiaxed dislocation cell structure. This structure was observed at all deformation levels, but with increasing strain the volume fraction

associated with them decreased while the range of the cell dimension was unchanged and the misorientation across the cell boundaries remained small ($\sim 2^{\circ}$), suggested that they are strain independent. This may indicate that the cells are a relaxation structure which forms after straining has stopped, a view put forward by Kochs and other workers. However, after heavy deformation the cells usually have sharper walls and their interiors are almost free from dislocations, especially in copper A.

Microbands:-

After cold rolling 10 % the materials started to develop a new type of deformation microstructure besides the cell structure. They were parallel sets of thin sheet-like ribbons, or occasionally isolated bands traversing the equi-axed cell structure. These features are normally about 0.25μm thick, but some as thick as 0.5μm were found. The length of the bands was difficult to determine; several were traced in the microscope for more than 15μm before they disappeared into thicker regions of the foil. The bands are similar to the microbands observed by other workers (40-41, 43-45), and they will be referred to as such in the following. The microband boundaries are regions of high dislocation density. There are also numerous dislocations within each microband, although careful tilting in the electron microscope is required to reveal them in regions which at first sight appear to be dislocation free . A typical isolated microband traversing an equiaxed cell structure in copper deformed 20 % is shown in Fig.(47). The angles between the freshly formed

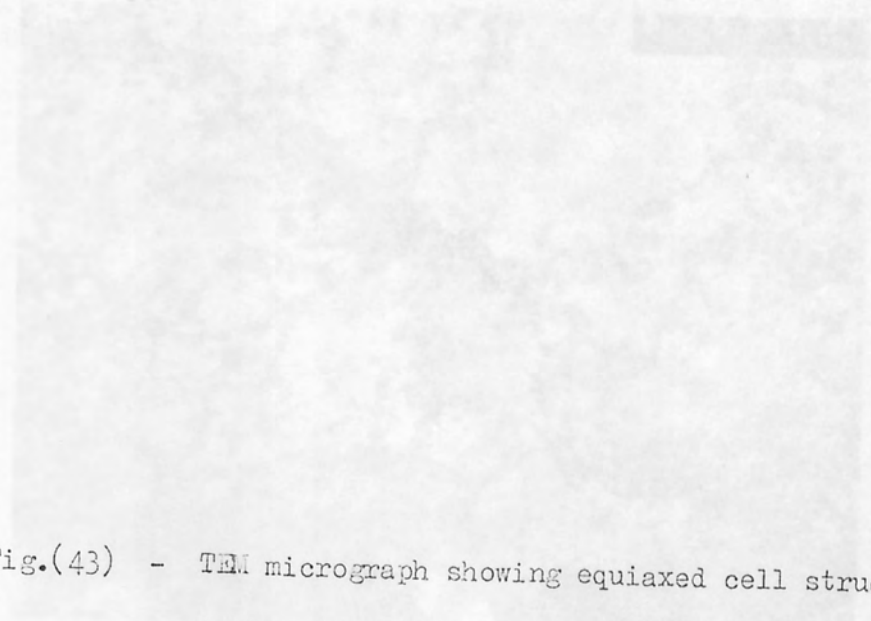

Fig.(43) - TEM micrograph showing equiaxed cell structure in longitudinal sections of rolled copper.

a - 10 % reduction.

b - 20 % reduction.

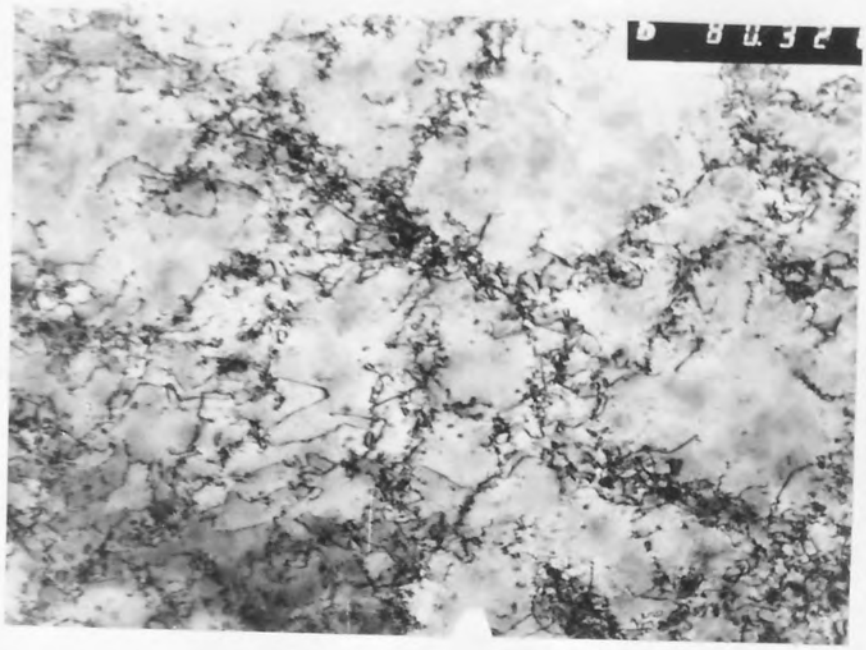

-a- 0·5 μ

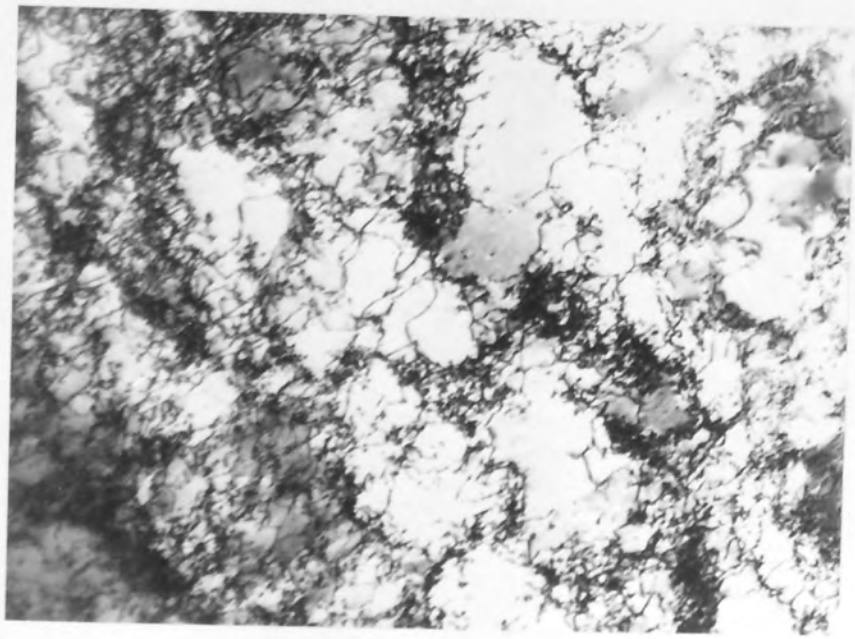

-b- 1 μ

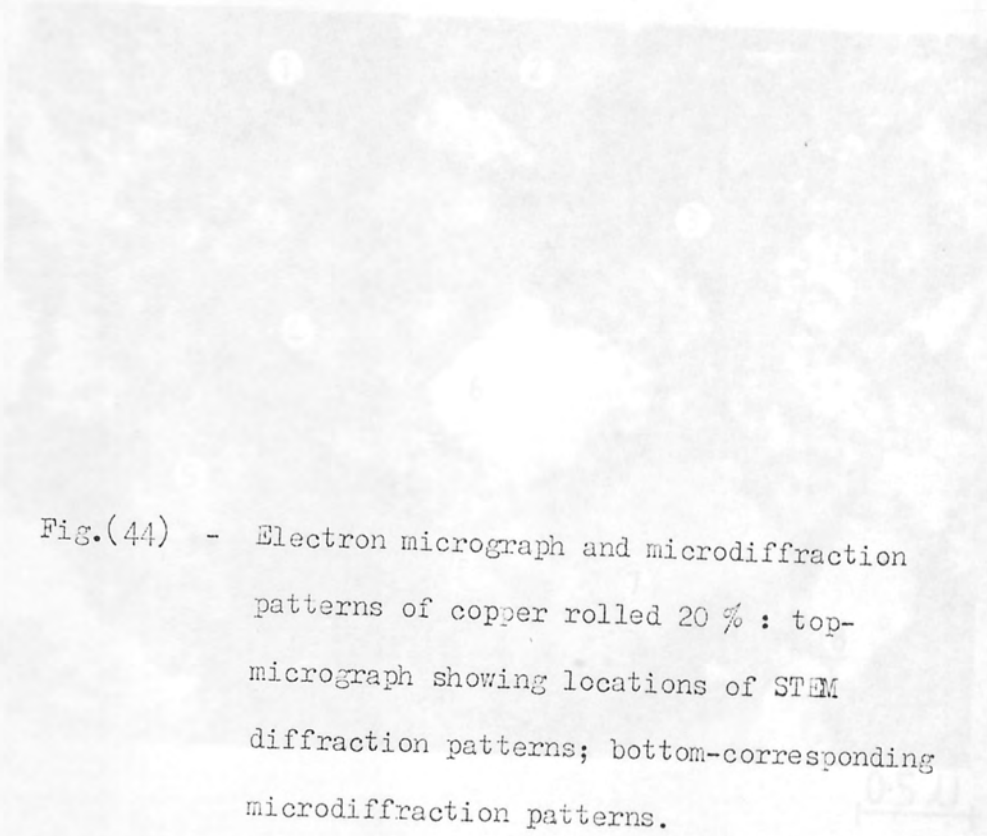

Fig.(44) - Electron micrograph and microdiffraction patterns of copper rolled 20 % : top-micrograph showing locations of STEM diffraction patterns; bottom-corresponding microdiffraction patterns.

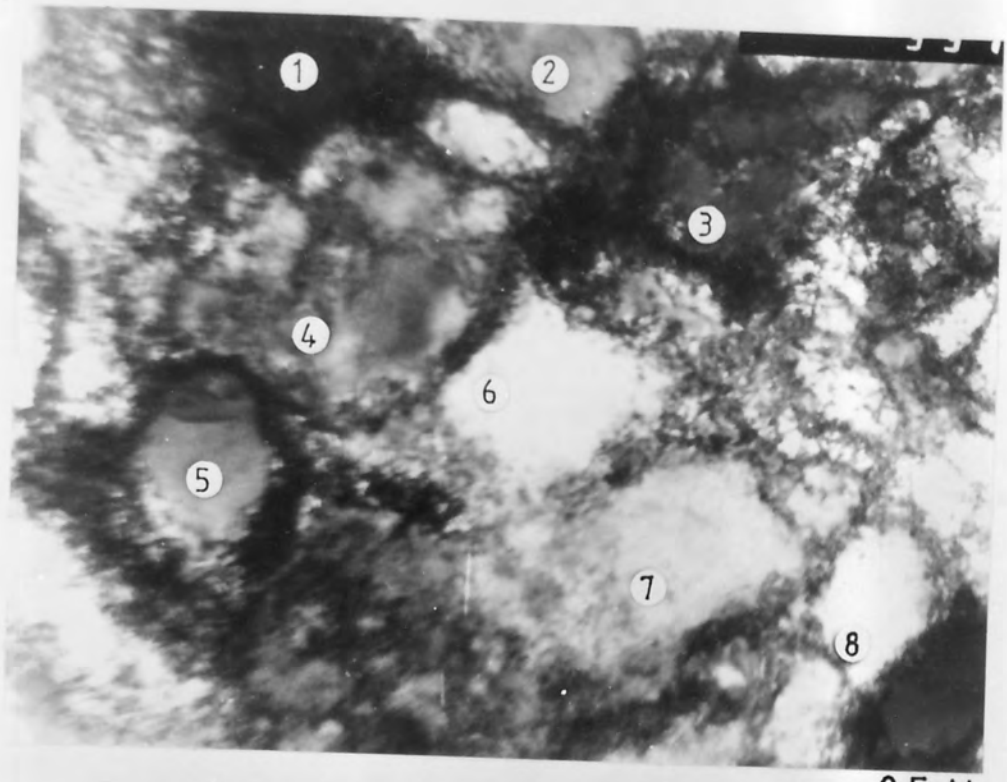

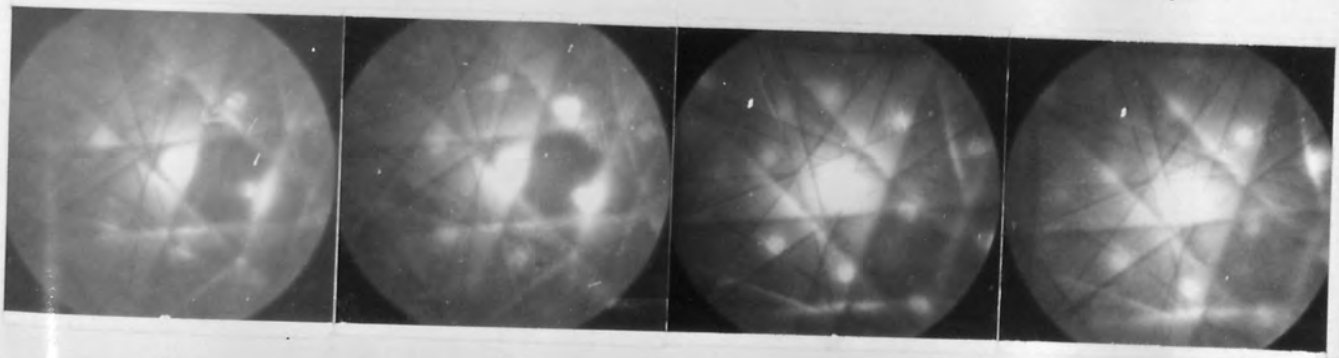

-1- -2- -3- -4-

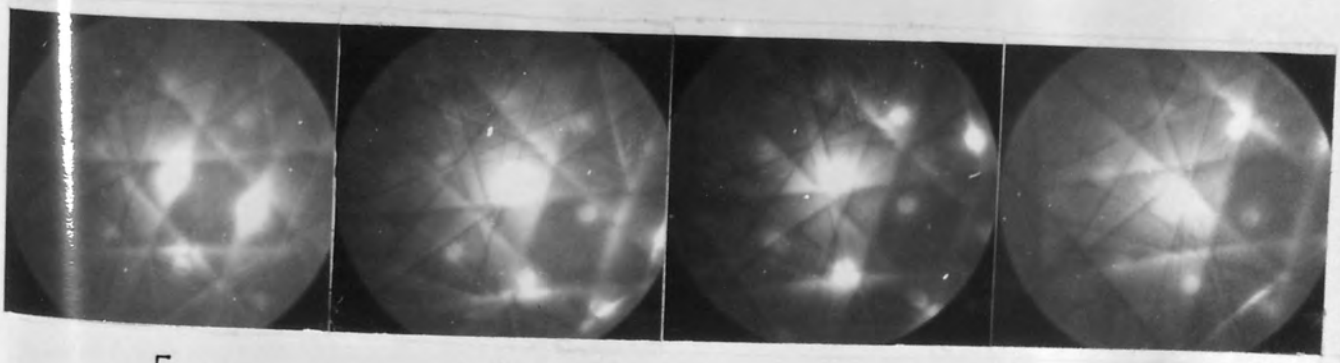

-5- -6- -7- -8-

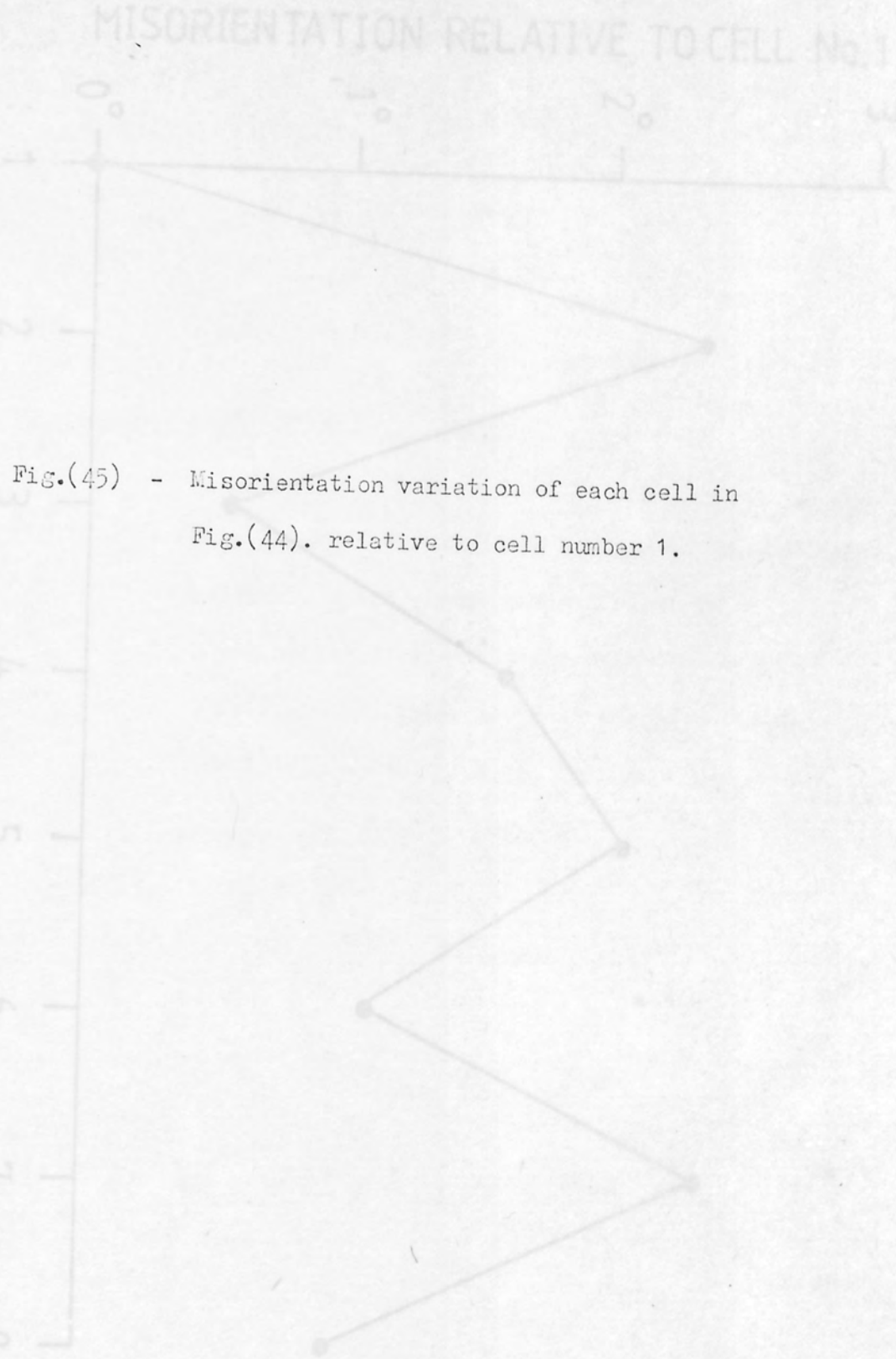

Fig.(45) - Misorientation variation of each cell in Fig.(44). relative to cell number 1.

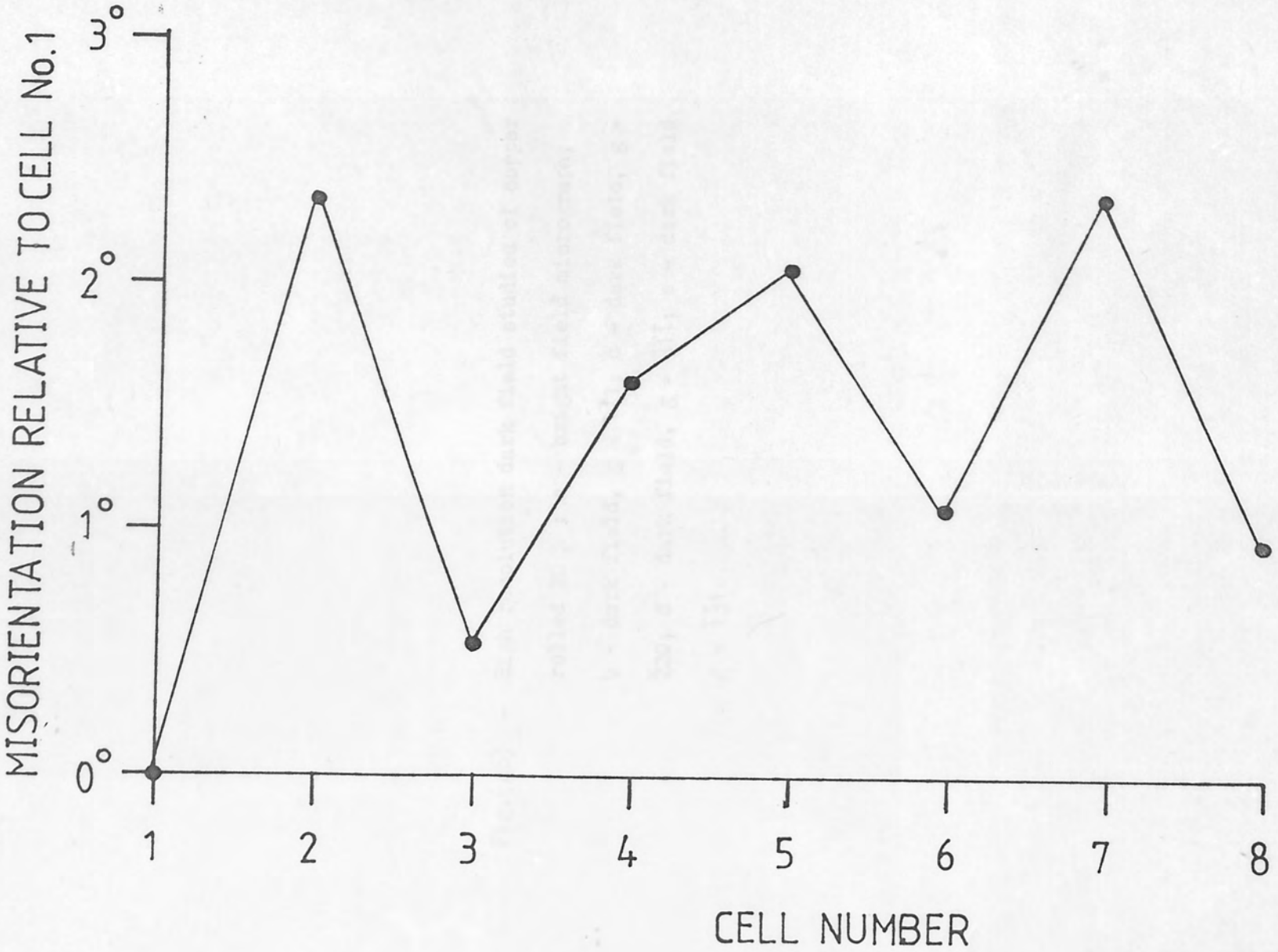
MISORIENTATION RELATIVE TO CELL No.1
3°
2°
1°
0°
1
2
3
4
5
6
7
8
CELL NUMBER

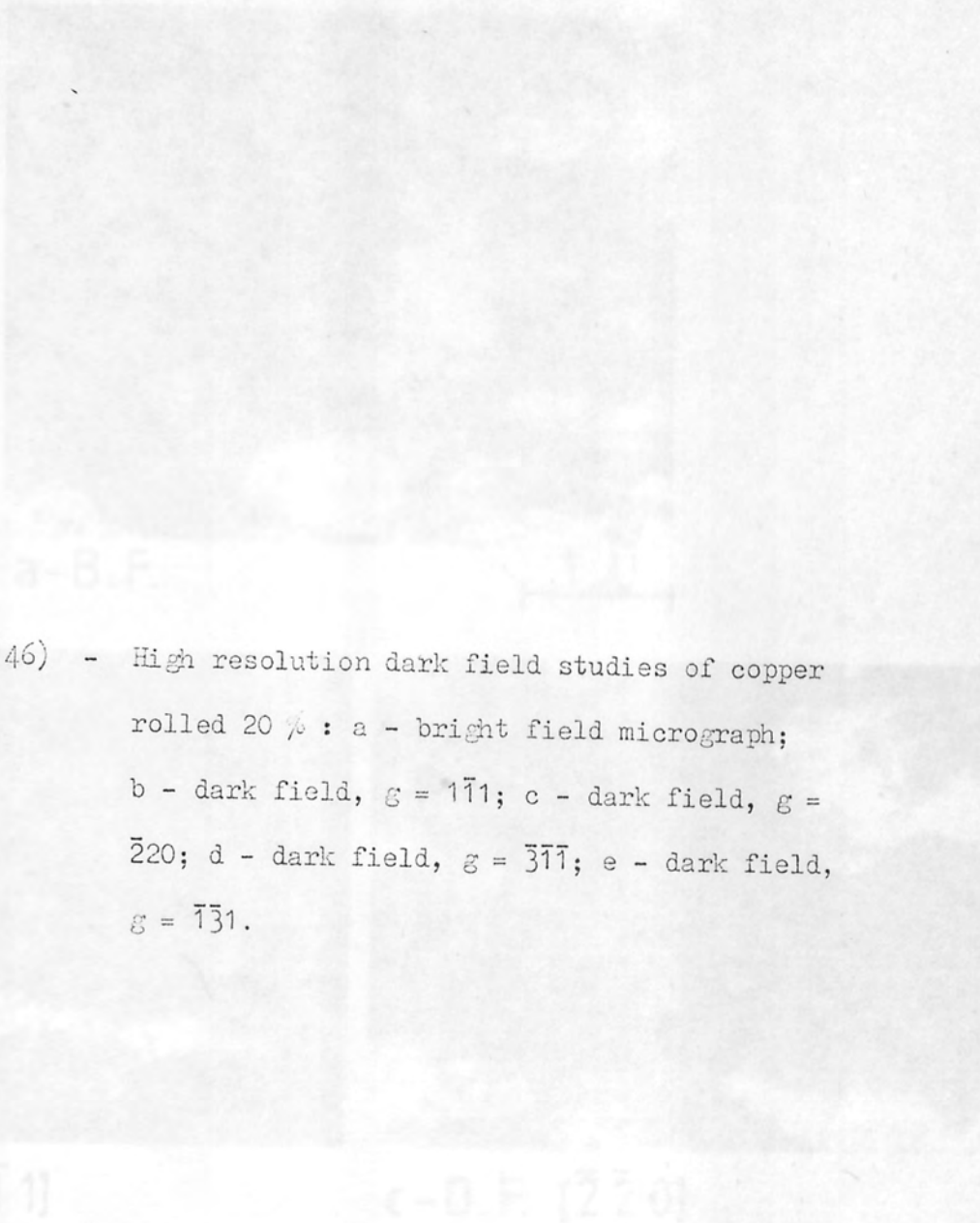

Fig.(46) - High resolution dark field studies of copper rolled 20 % : a - bright field micrograph; b - dark field, $g = 1\bar{1}1$; c - dark field, $g = \bar{2}20$; d - dark field, $g = \bar{3}1\bar{1}$; e - dark field, $g = \bar{1}\bar{3}1$.

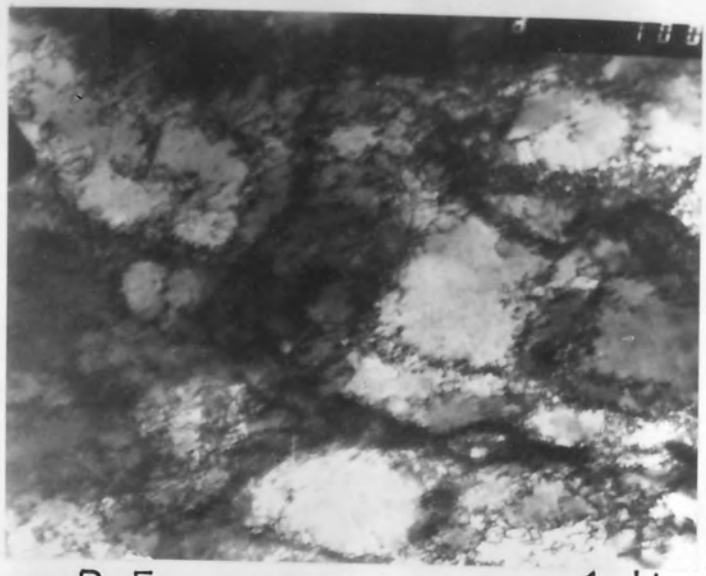

a-B.F. 1 μ

b-D. F. [1 $\bar{1}$ 1]

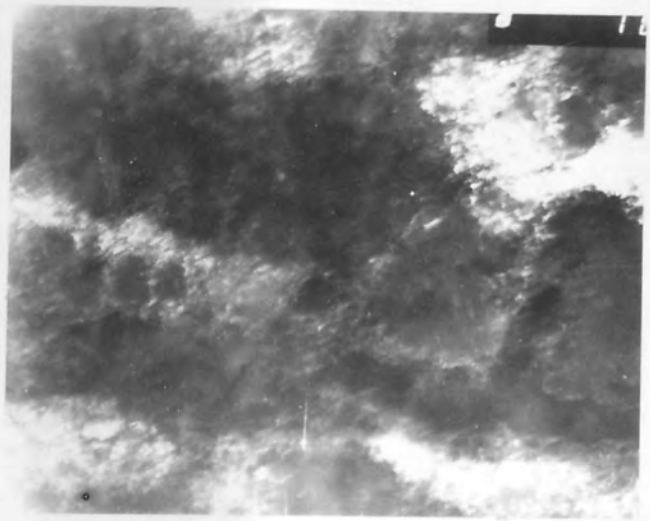

c-D.F. [$\bar{2}$ $\bar{2}$ 0]

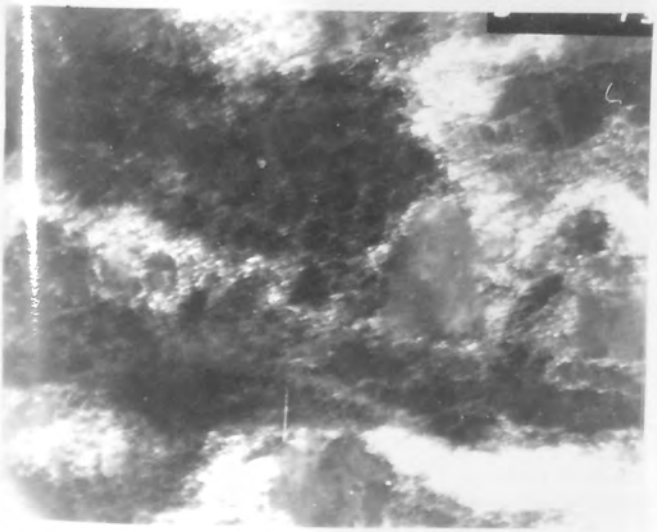

d-D.F [$\bar{3}$ $\bar{1}$ $\bar{1}$]

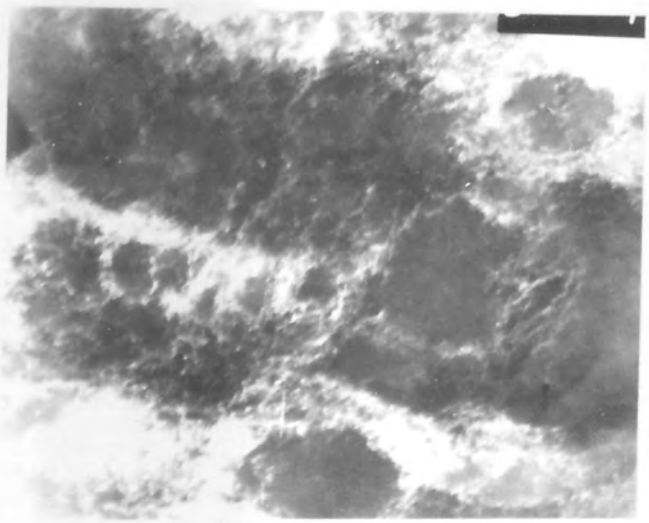

e-D.F. [$\bar{1}$ $\bar{3}$ 1]

microbands and the rolling direction varied from 0° to 60°. Statistical studies on specimens deformed 20 % were carried out on 75 microbands, and the results are plotted in Fig.(35a). It seems that they are in a reasonable agreement with those of optical and scanning microscopy. However, these results are in disagreement with those reported by Malin (45), who reported that microbands consistently form at ~35° to the rolling direction. Microbands do not appear to cross the grain boundaries, but they are associated with large shears and produce marked grain boundary displacements.

At the same strain level (0.2) many grains were found to develop two parallel sets of microbands, frequently near to grain boundaries, Fig.(48). This montage shows three different grains (A,B,C). The deformed structure in grain A consists of two sets of microbands with equiaxed cell structure, grain B contains a dislocation cell structure with boundaries tending to align parallel to the two sets of microbands in grain A, whereas, grain C contains a diffuse cell structure. The size of the cells' structure in grain C is larger than those in grains A and B. The grain boundaries between these grains have a wavy appearance, which is due to intersection of the boundaries by microbands. In general, the incidence of microbands increases with strain and, by a strain level of 0.5, most of the observed grains contain two sets of microbands, Fig.(49). It was usually observed that only one set of the microbands sheared the other which lead to the formation of parallelogram shaped blocks. The similarity between these observations and those on the scratched specimens and optical

microscopy at the same strain level is very obvious.(Compare Figs.34b,42a,49). At a strain level of 70 % the microbands seem to be developed in almost all the grains and frequently there was one dominant set of long microbands making a small angle with the rolling direction ($< 15^{\circ}$), while the other set seems to have been cut into smaller segments, Fig.(50). Examinations of heavily deformed material (90 % reduction) showed that the structure consists of clusters of thin long microbands aligned parallel to the rolling direction together with small areas of nearly equiaxed cells, Figs.(51 and 52). The boundaries of the aligned microbands (or elongated cells) and the equiaxed cell structure appeared very sharp especially in material A, indicative of dynamic recovery. The microband thickness throughout the whole deformation range (10 % - 90 %) was 0.1 to 2.5μm.

Attempts were made to determine the origin and the nature of the microbands by detailed study of their crystallography at low strains (ε =0.2). The orientation changes across isolated and parallel sets of microbands were carefully determined. Two experiments were conducted. First, the misorientation between the bands and the matrix were examined from selected area diffraction patterns. Rotations about TD relative to the matrix were determined. The results indicated that the microband rotation was usually small ($1 - 2^{\circ}$). Secondly, STEM micro diffraction was used to determine the misorientation between the microbands and the matrix. The examinations showed that the matrix orientation on either side of the microbands differ by less than 1°. The orientation

Fig.(47) - TEM micrograph showing isolated microband in longitudinal section of copper rolled 20 %

0.5 marker parallel to trace of rolling plane.

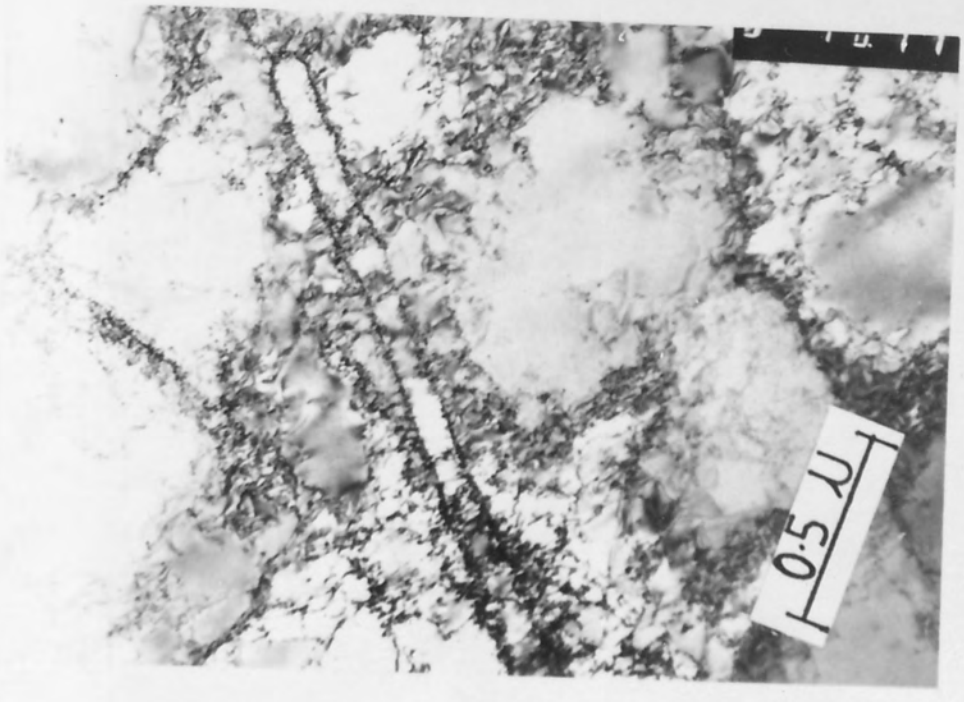
0·5 μ

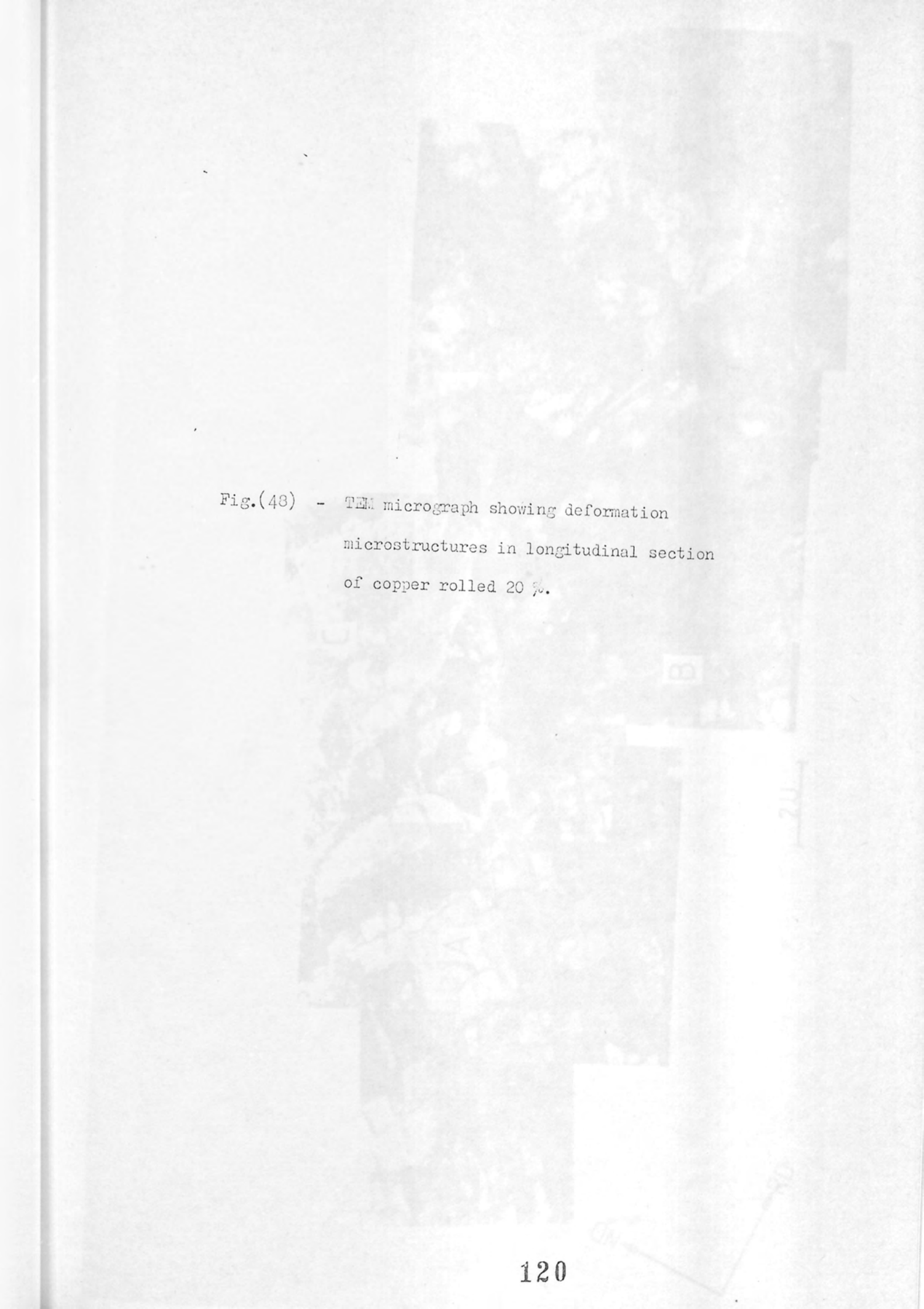

Fig.(48) - TEM micrograph showing deformation microstructures in longitudinal section of copper rolled 20 %.


A
B
C
ND
RD
2μ

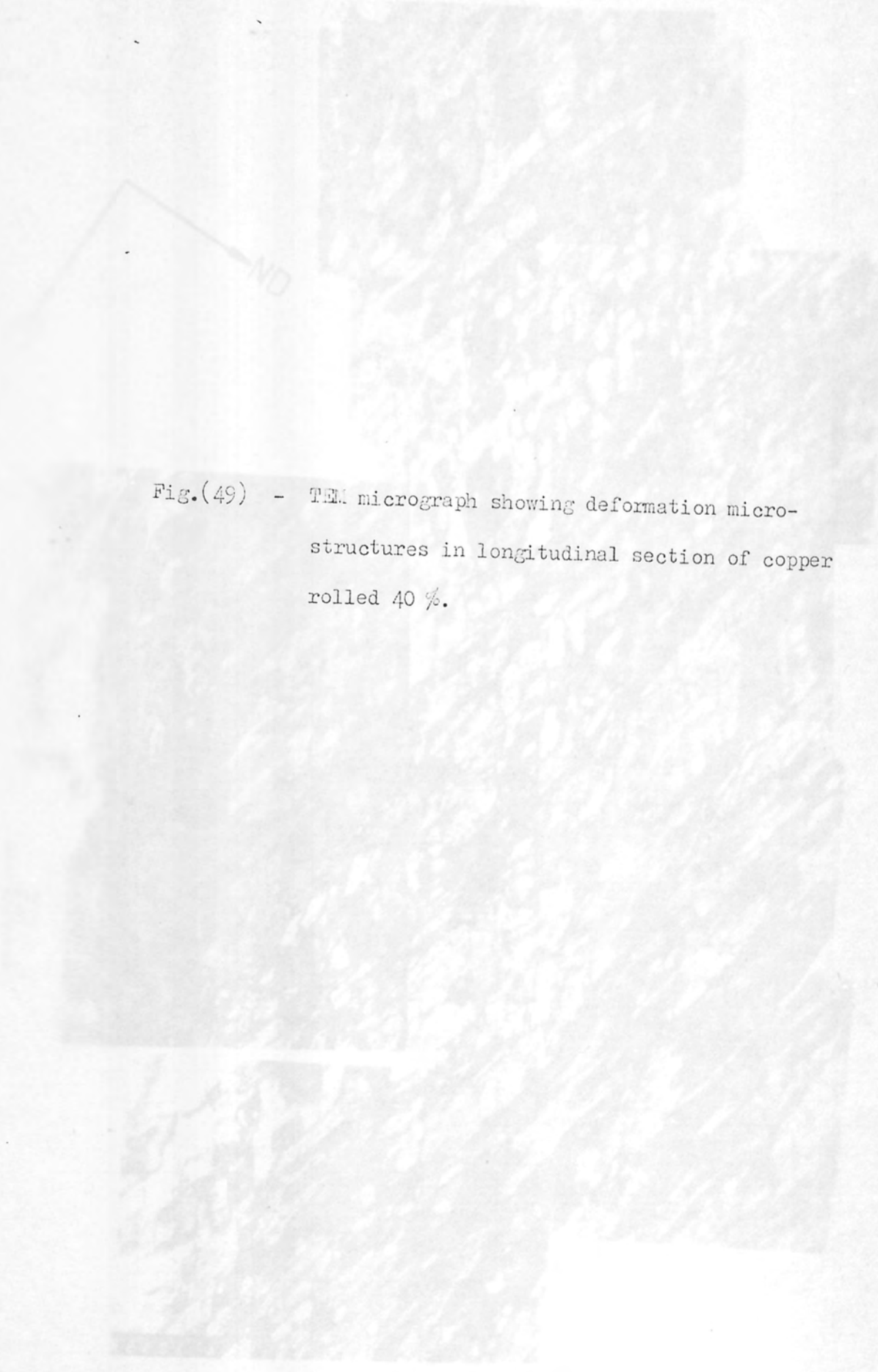

Fig.(49) - TEM micrograph showing deformation micro-structures in longitudinal section of copper rolled 40 %.

ND
RD
2U

Fig.(50) - TEM micrograph showing deformation micro-structures in longitudinal section of copper rolled 60 %.

ND
RD
2U

Fig.(51) - TEM micrograph showing deformation microstructures in longitudinal section of copper A rolled 90 %.

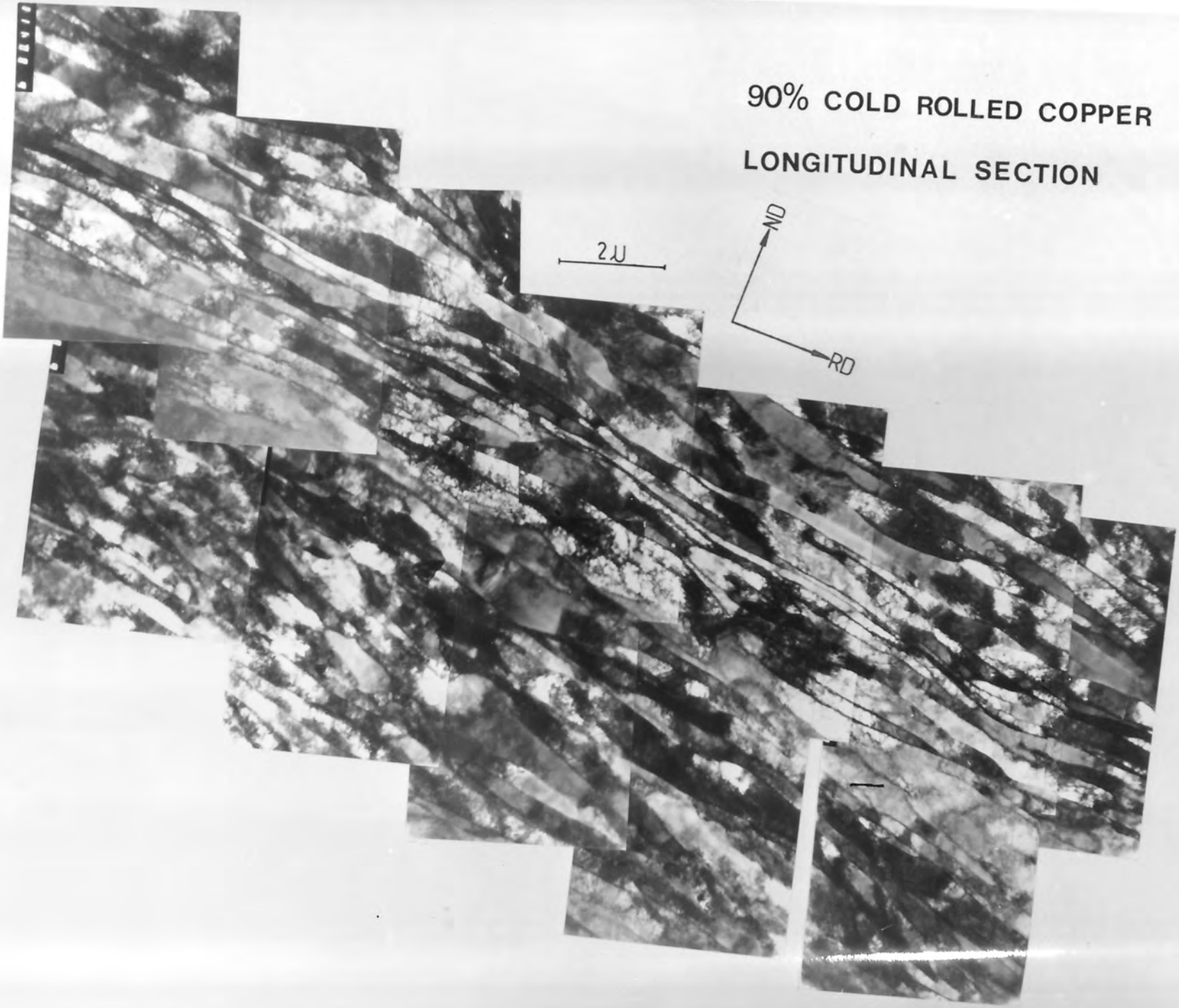
90% COLD ROLLED COPPER
LONGITUDINAL SECTION
2μ
ND
RD

Fig.(52) - TEM micrograph showing deformation microstructures in longitudinal section of copper B rolled 90 %.

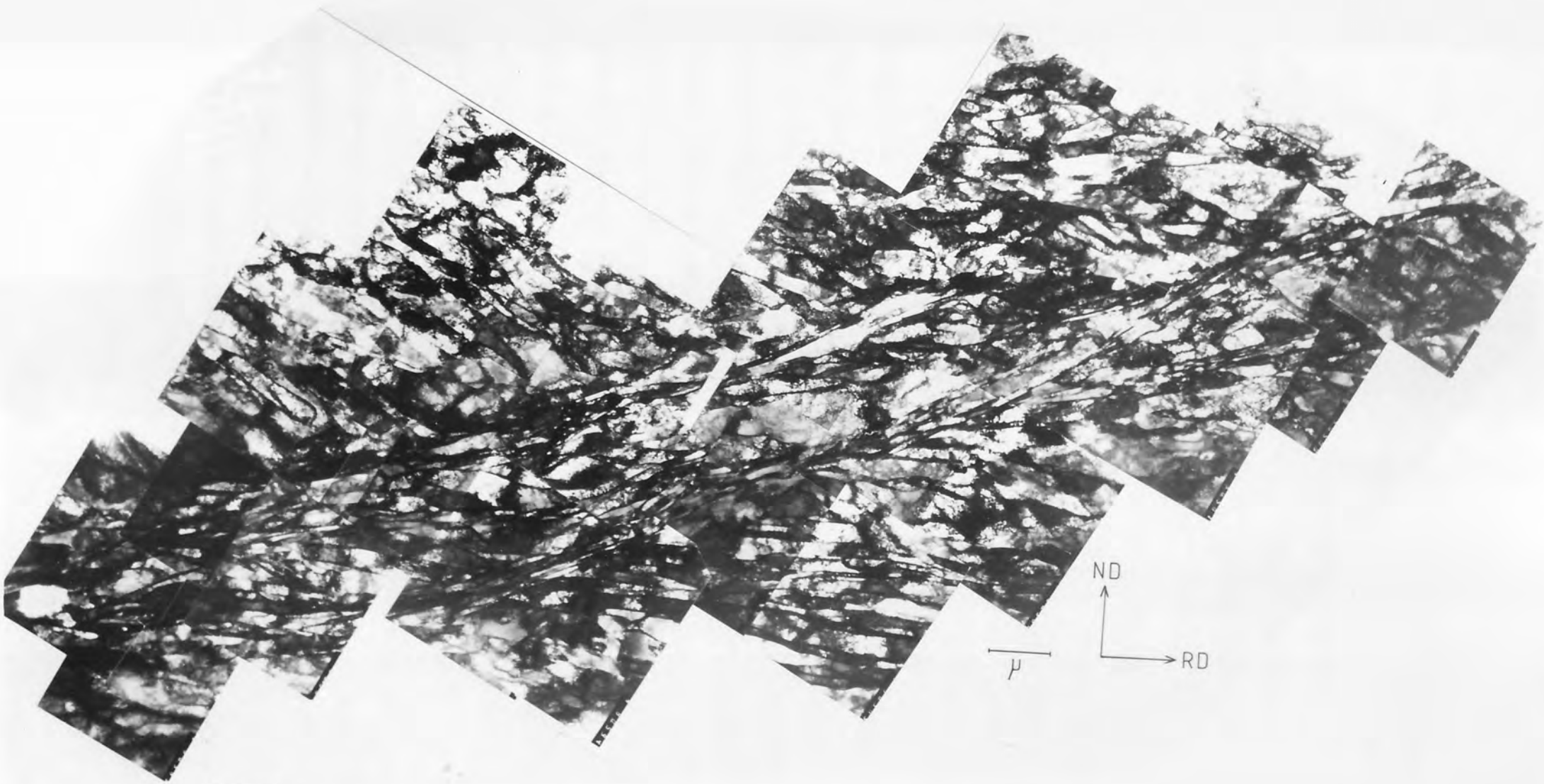
ND
RD
μ

within the microbands differs from that of the matrix by only $1^{\circ} - 2^{\circ}$. Fig.(53) shows a typical example of one of these studies. The misorientation between the microband in position (1) and the matrix in position (2) is 1.4°. The largest component of misorientation is rotation around an axis perpendicular to TD but there is also a very small rotation about TD. The misorientation between the matrix in position (3) and the microband in position (4) is 2.1°, and position (5) and (6) is 1.1°. The components of rotation in the last two cases are similar to those between (1) and (2).

The crystallography of the microband habit planes has been stated by most previous workers (44, 45) to be $\{111\}$. They drew their conclusions after examining only a few microbands which may lead to misleading results. The habit plane was, therefore, redetermined by using the method outlined in Chapter (3) for 70 microbands in specimens deformed 20 %. The results are plotted in a unit triangle, Fig.(56). The examination shows that in 49 microbands out of the 70 (i.e. 70 %) the habit plane was found to be $\{111\}$ within 5°, and in 21 cases (30 %) it had different orientations scattered without any preference. No difference was detected in morphology or geometry between the microbands with $\{111\}$ habit planes and the others. Previous workers have not attempted to determine whether microbands tend to form in particular grain orientation or not. Therefore, the orientations of 43 grains containing microbands in specimens deformed 20 % were determined. The results are plotted in two unit triangles Fig.(57), one for the rolling plane orientation and the other for the rolling

direction. The open squares represent grains containing microbands with $\{111\}$ habit planes while the open circles are for those with microbands on different habit planes. The results indicate clearly that both types of microband could form almost at any grain orientation.

In order to see whether there was any tendency for specific dislocations within the microbands or their boundaries, high resolution dark field experiments were conducted on specimens deformed 20 %. Seven separate isolated microbands were examined. A typical example is shown in Fig.(54) where the orientation (TD) of the area under examination is $[\bar{1}12]$. Possible Burgers vectors and visibility conditions are listed in Table (4). Comparison between the bright field and dark field micrographs, and Table (4) indicated that the dislocation in the equiaxed cell boundaries and the microband boundaries showed similar contrast and contained several different types of Burgers vector. Thus there is no significant difference in dislocation terms between the cell and microband boundaries. The interiors of the microbands are different in that with some diffracting conditions all the dislocations are out of contrast. This suggests that the microbands involve only a single system. In other contrast conditions the dislocation density is uniformly high across the microbands. Fig.(55) demonstrates this clearly in the difference between the $(1\bar{1}1)$ and $(11\bar{1})$ reflections. The same general characteristics were found whether the boundaries lay along $\{111\}$ or irrational planes.

Returning to the heavy deformation level, the most

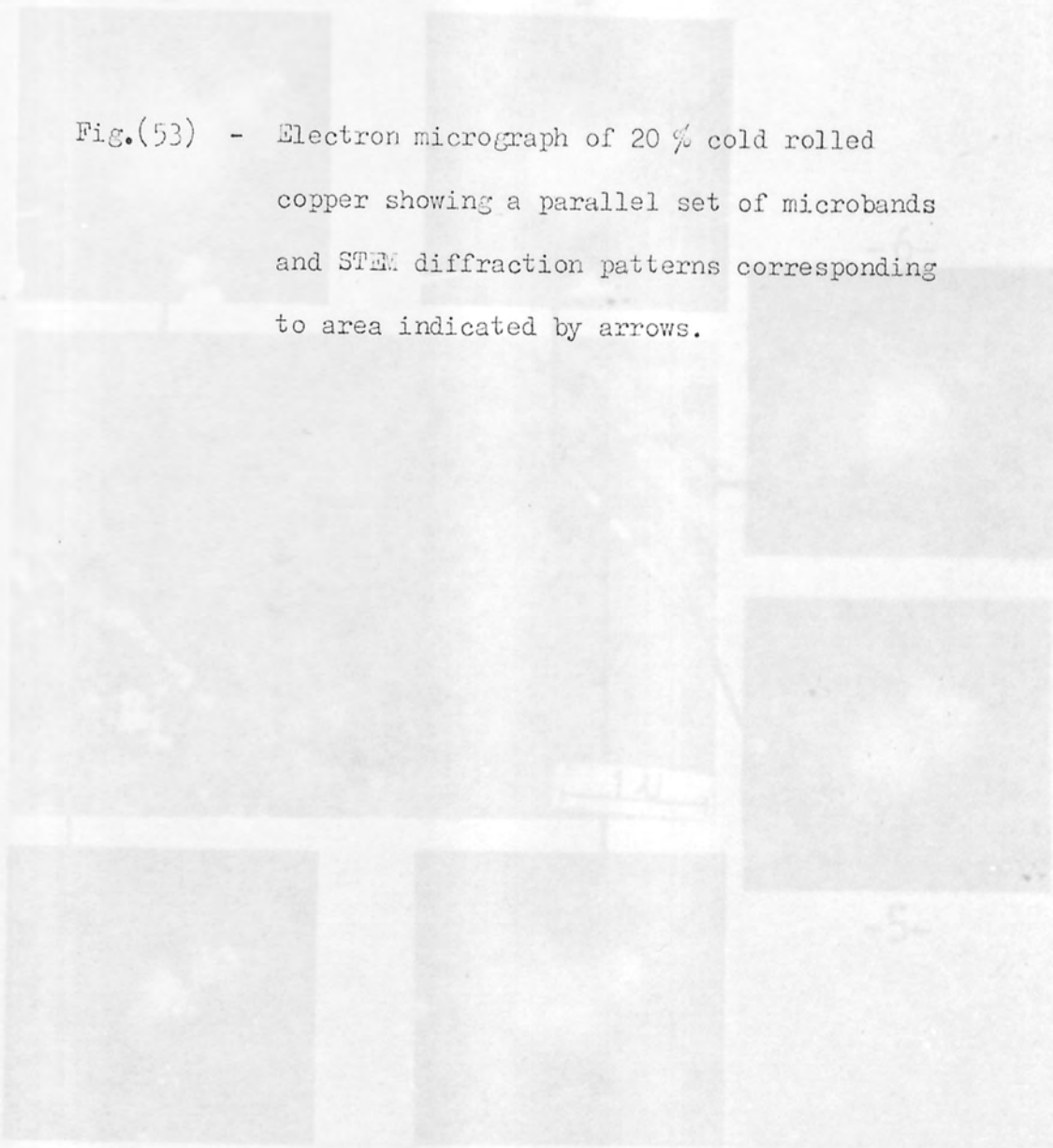

Fig.(53) - Electron micrograph of 20 % cold rolled copper showing a parallel set of microbands and STEM diffraction patterns corresponding to area indicated by arrows.

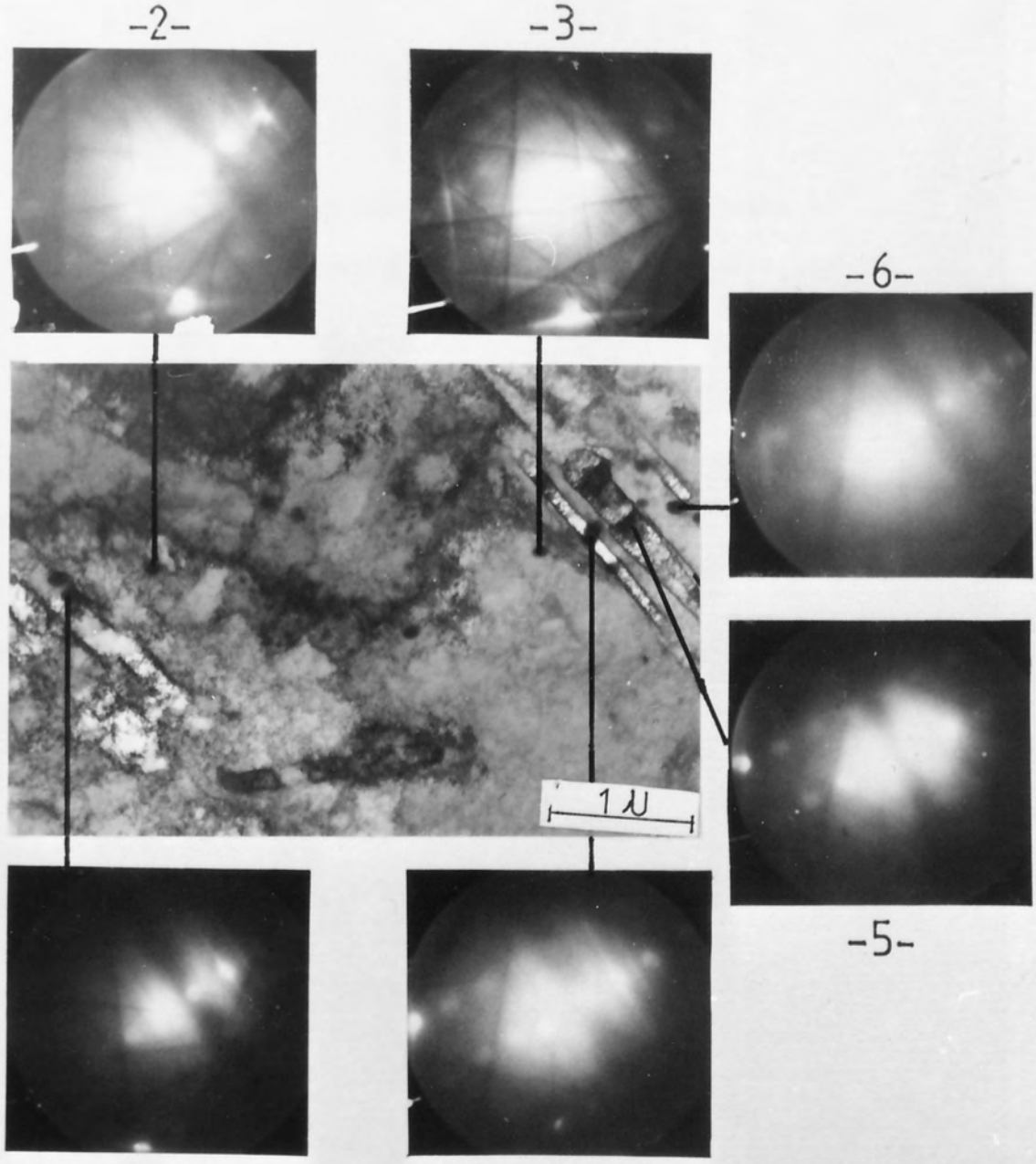
-2-
-3-
-6-
1 µ
-5-
-1-
-4-

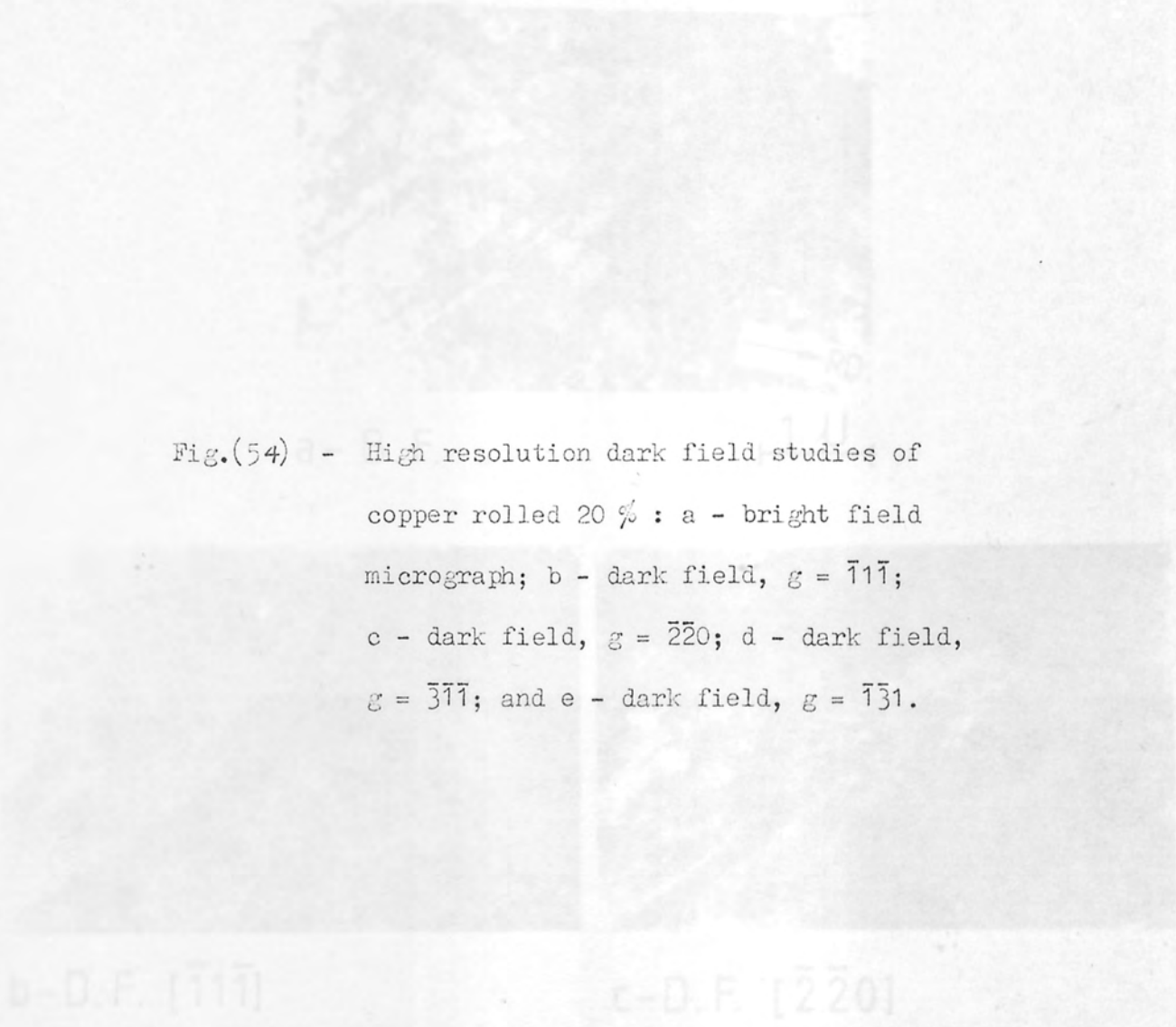

Fig.(54) - High resolution dark field studies of copper rolled 20 % : a - bright field micrograph; b - dark field, $g = \bar{1}1\bar{1}$; c - dark field, $g = \bar{2}\bar{2}0$; d - dark field, $g = \bar{3}\bar{1}\bar{1}$; and e - dark field, $g = \bar{1}\bar{3}1$.

a- B. F.

1 μ

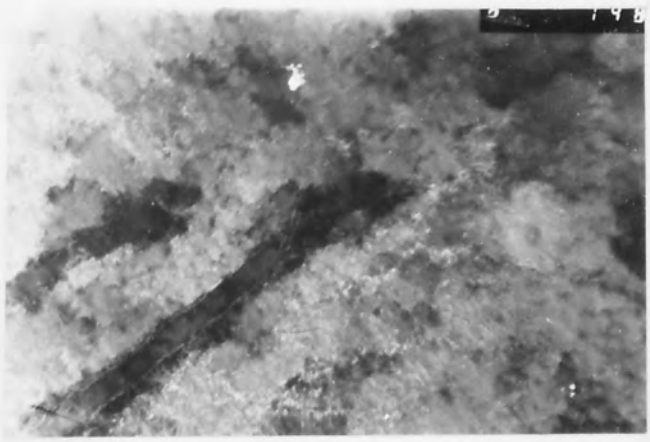

b- D. F. [$\bar{1}1\bar{1}$]

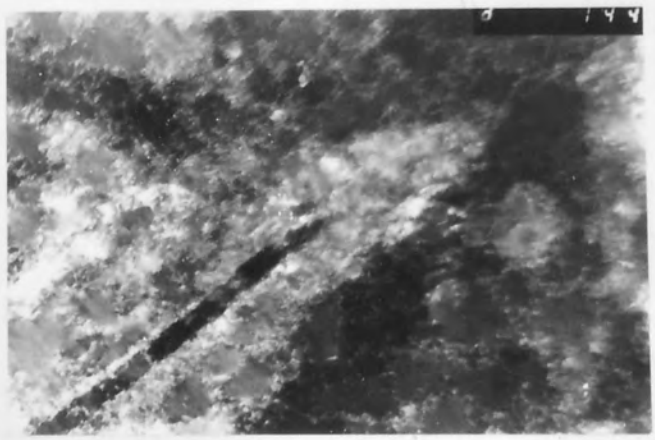

c- D. F. [$\bar{2}\bar{2}0$]

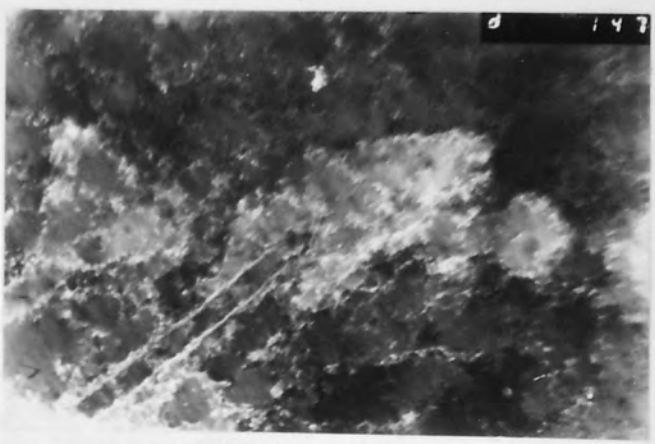

d- D. F. [$\bar{3}\bar{1}\bar{1}$]

e- D. F. [$\bar{1}\bar{3}1$]

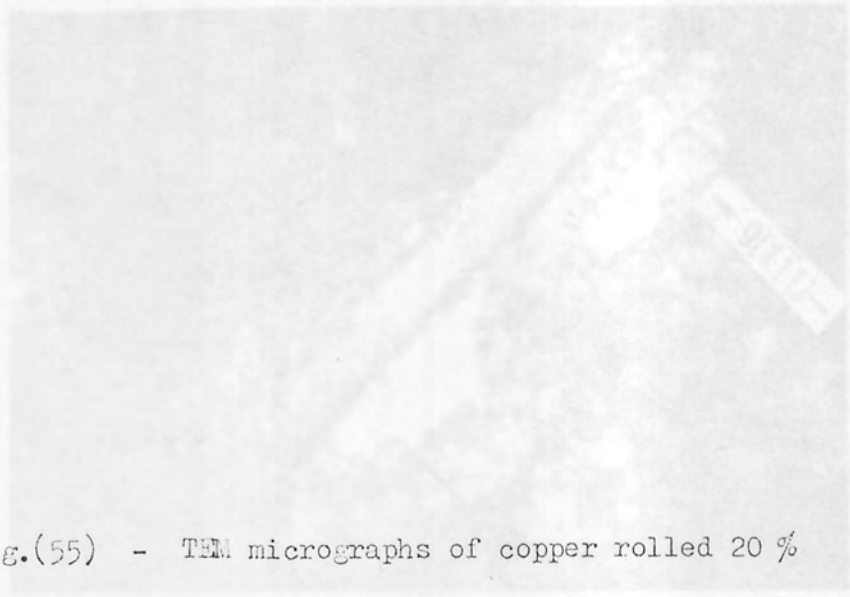

Fig.(55) - TEM micrographs of copper rolled 20 % showing a microband in two different contrast conditions :

a - transmitted beam plus $g = 1\bar{1}1$;

b - transmitted beam plus $g = 11\bar{1}$.

-a-

-b-

Fig.(56) - Microbands habit plane orientations.

Fig.(57) - Orientations of grains containing microbands.

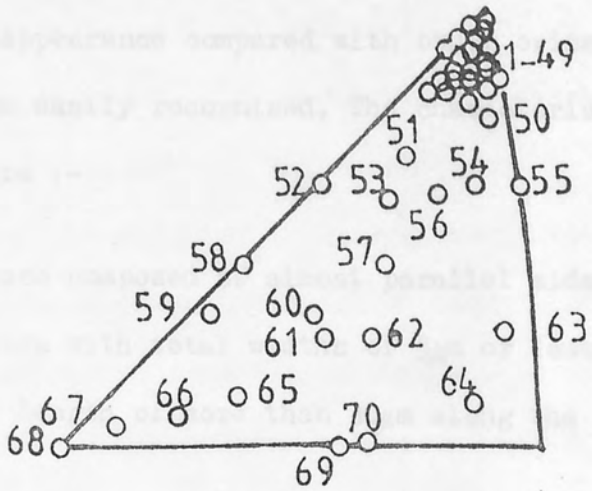

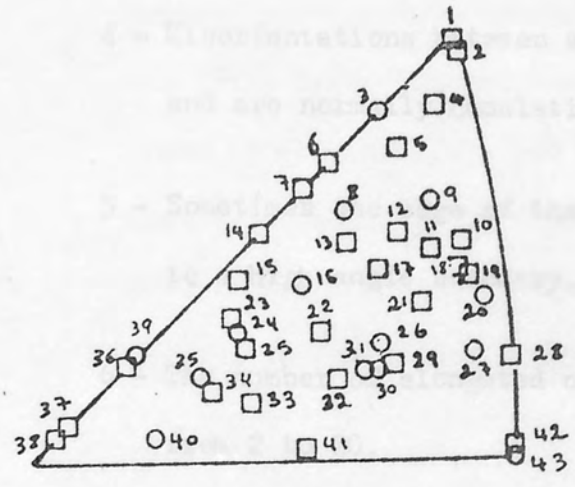

ND

-a-

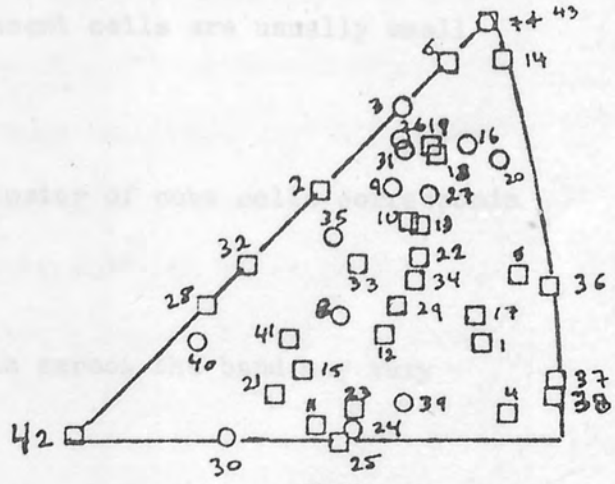

RD

-b-

interesting finding in the present work is the observation of several cubic oriented regions (100) [001] within the structure (90 % reduction), especially in copper A. Fig.(58) shows a typical example of these cubic regions. They have a very distinct appearance compared with other orientations which makes them easily recognised. The characteristics of these regions are :-

1 - They are composed of almost parallel sided cells clustered in bands with total widths of 3μm or less which extend for a length of more than 30μm along the rolling direction.

2 - The individual elongated cells are also very long compared with those in other orientations.

3 - The cell boundaries are very sharp and their interiors rather free of dislocations indicating that these areas are more recovered than other regions.

4 - Misorientations between adjacent cells are usually small and are normally cumulative.

5 - Sometimes the edge of the cluster of cube cells corresponds to a high angle boundary.

6 - The number of elongated cells across the band may vary from 2 to 20.

7 - In the thin foil they are usually rather thick compared with other oriented regions suggesting a slower rate of electropolishing.

In view of the importance of cube oriented regions in the recrystallization process, more than twenty such oriented areas were examined, six of them in detail using STEM microdiffraction to find the orientations of the individual elongated cells within the bands. Examples of these analyses are given in Figs(59 and 60). Fig.(59) shows a cluster of 17 elongated cells with thicknesses varying from 0.1 to 0.2μm with total thickness of about 2μm. The orientations of individual elongated cells are plotted in Fig.(59b). It is clear that the orientation changes gradually across the band. The misorientation between position A and J is about 37°, however, this is divided into smaller steps by 9 cell boundaries, each one of them accommodating an average misorientation of 4°. This change in the orientation has been brought by progressive lattice rotation around the rolling direction [001]. The misorientation between positions J and O is about 33° subdivided by 8 elongated cells and, again, the adjacent cells is about 4°. The gradual orientation change between average misorientation between J and O is a rotation around the [1$\bar{1}$1] axis. Another example of a cube oriented region is shown in Fig.(60), it can be seen that there are high angle boundaries adjacent to the cube region. The misorientation between A and B is ~54° and between M and L is ~20°, but in general the misorientations between adjacent cells are small.

Shear bands :-

With heavy rolling reductions (90 % reduction) some differences between copper A and B have been detected. The most obvious one is the development of shear bands in copper B, whereas, almost no snear bands were found in A. In material B

after the elongated cells have become well established, bands of intense shear are observed in longitudinal sections. Fig. (52) is a montage showing a typical deformation structure of copper B deformed 90 %. In this there are three shear bands about 20μm long, and about 0.5μm wide, each band consisting of a number of very fine cells (0.04μm) elongated in the shear direction. It was frequently observed that the elongated cells are rotated away from the rolling direction towards the shear direction, suggesting that the fine elongated units form from pre-existing elongated cells by the shear process. By considering that the average thickness of the original cells is about 0.2 μm and the average thickness of the thin elongated units within the shear bands is about 0.04μm, then the estimated shear strain associated with the shear band is ~ 8.7.

4.4. Texture studies :-

$\{111\}$ pole figures for three rolling reductions (60, 80 and 90 %) of both materials were determined. The results in Fig.(61), show the various stages in the development of the final copper texture. This type of texture is somewhat recognisable at 60 %, and both materials developed essentially similar textures in all cases. The only detectable difference was that the texture in B after 90 % reduction was more diffuse and a little weaker. Copper B had maxima of 4, 6, and 7 random, after 60, 80, and 90 % respectively, whereas, A at some deformations reached 3, 6,10 random. The final texture can be described as a spread of orientations from $\{112\}\langle 111\rangle$ to $\{110\}\langle 112\rangle$.

The {111} pole figures for copper A rolled 90 % at -100° C is shown in Fig.(62a). The rolling texture also determined for copper A with an initial large grain size (~ 300μm) rolled to 90 % at room temperature, is shown in Fig.(62b). In both of these cases the textures closely resembled that of copper B rolled to the same deformation levels at room temperature.

4.5. Hardness measurements :-

Microhardness values were measured on the edge sections for all deformations in both materials using 300g load. The results plotted in Fig.(63) show that both materials have more or less the same hardness and this increases very rapidly with deformation up to a strain of approximately unity. After this the work hardening rate decreases and at high strains there is a small but consistent trend for lower values in material A.

4.6. Discussion :-

At small strains the predominant sub structure was equiaxed dislocation cells approximately 0.5 - 1μm in diameter with boundaries of high dislocation density. It seems that these boundaries consist of all types of dislocations. The misorientation across the boundaries is usually small, about 2.5°, and they are not associated with long range lattice rotations. The rotation between adjacent cells is a combination of a rotation around TD with a lesser rotation around an axis perpendicular to TD. It seems that the misorientation between the cells and their size is strain independent.

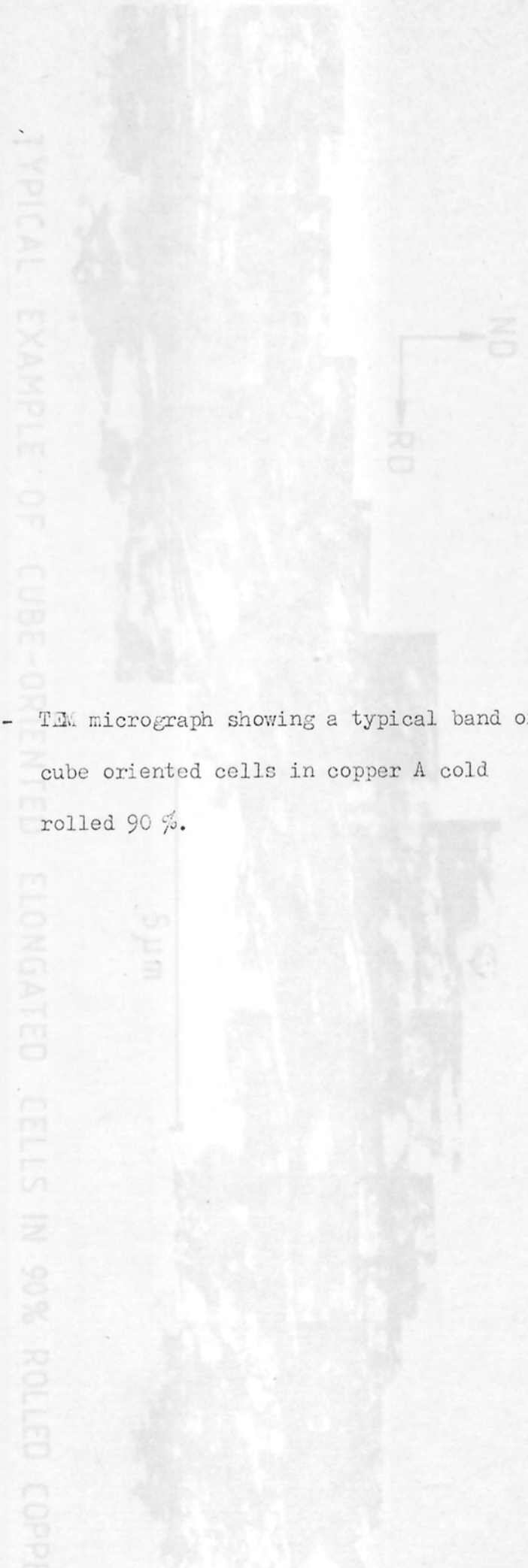

Fig.(58) - TEM micrograph showing a typical band of cube oriented cells in copper A cold rolled 90 %.

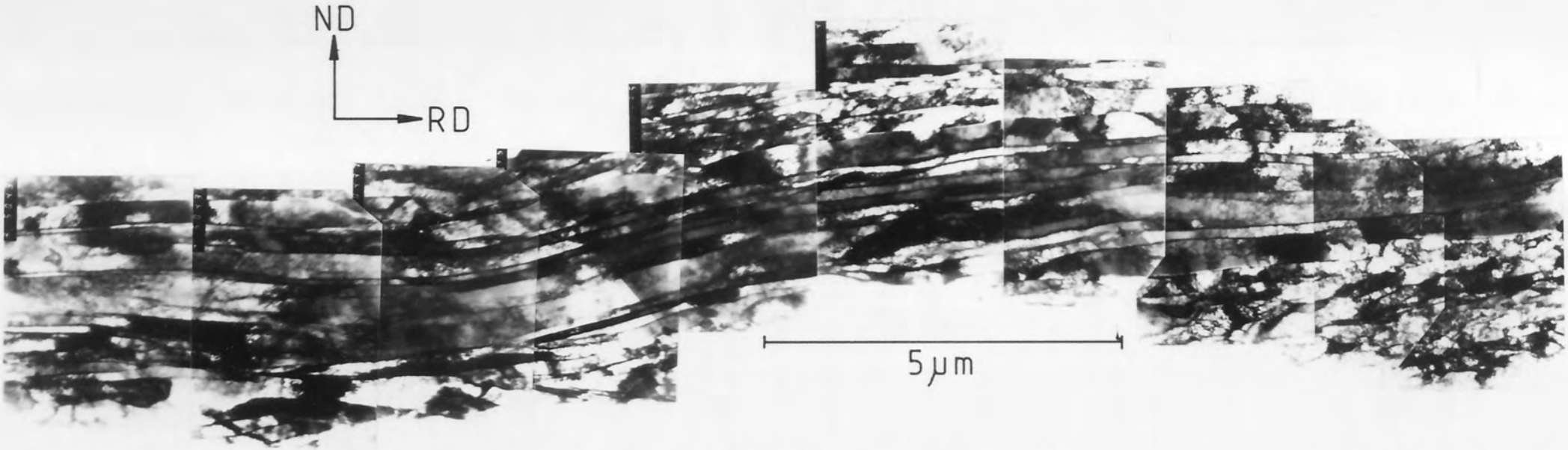

TYPICAL EXAMPLE OF CUBE-ORIENTED ELONGATED CELLS IN 90% ROLLED COPPER

Fig.(59) - (a) Micrograph of a region containing the cube orientation in copper A cold rolled 90 %. Locations of selected area Kikuchi patterns are indicated.

(b) Orientations of the cells shown in (a).

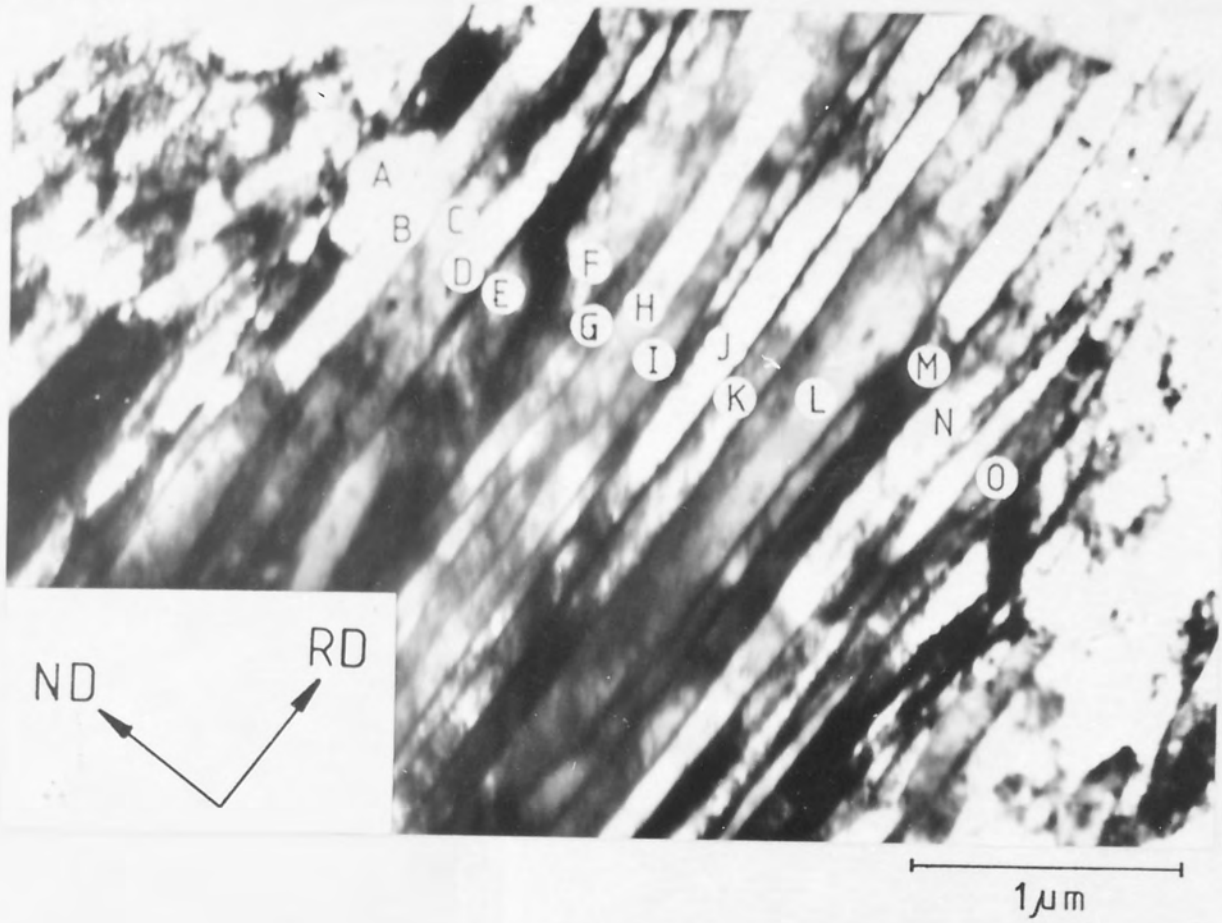
A
B
C
D
E
F
G
H
I
J
K
L
M
N
O
ND
RD
1 µm

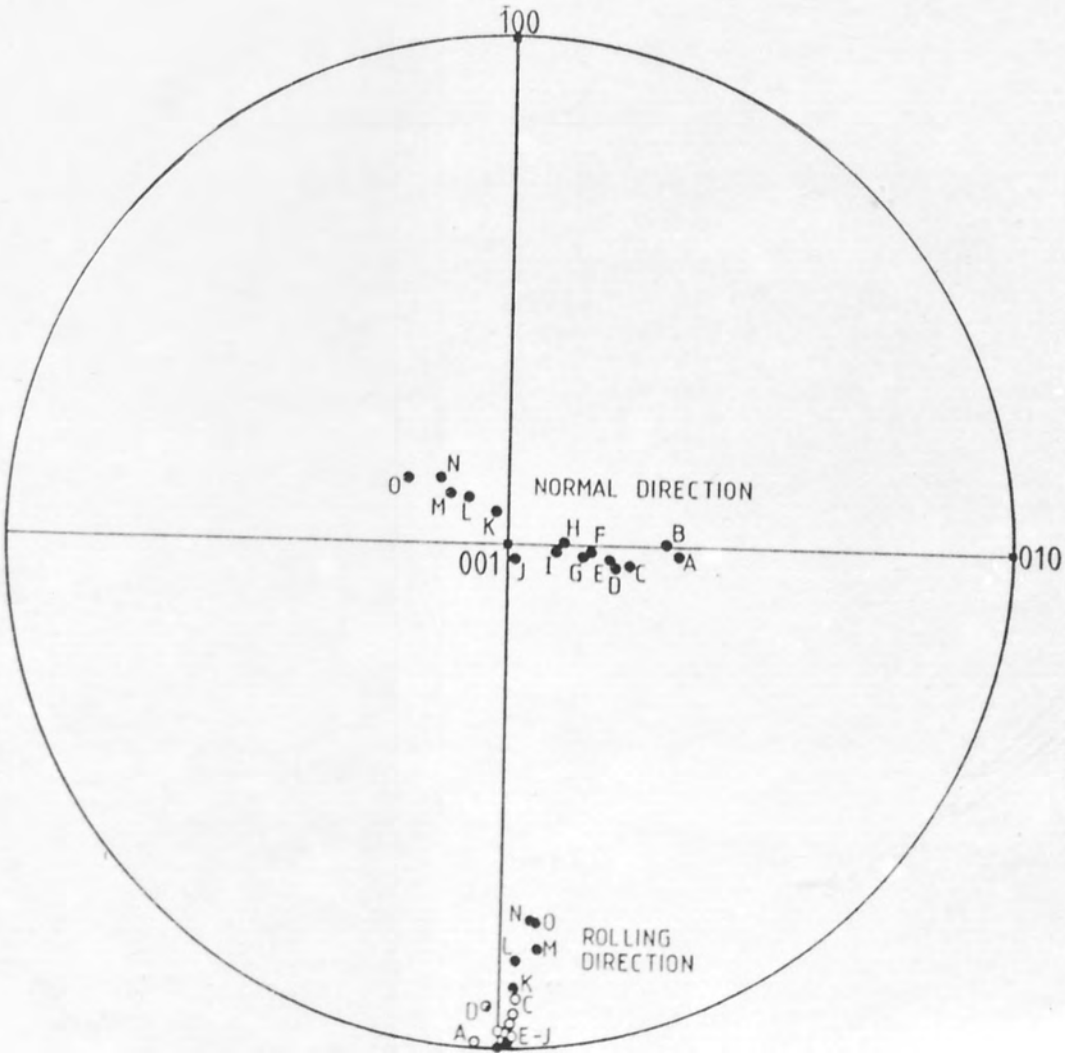
100
NORMAL DIRECTION
001
010
ROLLING
DIRECTION

Fig.(60) - (a) Micrograph of a region containing the cube orientation in copper A cold rolled 90 %. Locations of selected area Kikuchi patterns are indicated.
(b) Orientations of the cells shown in (a).

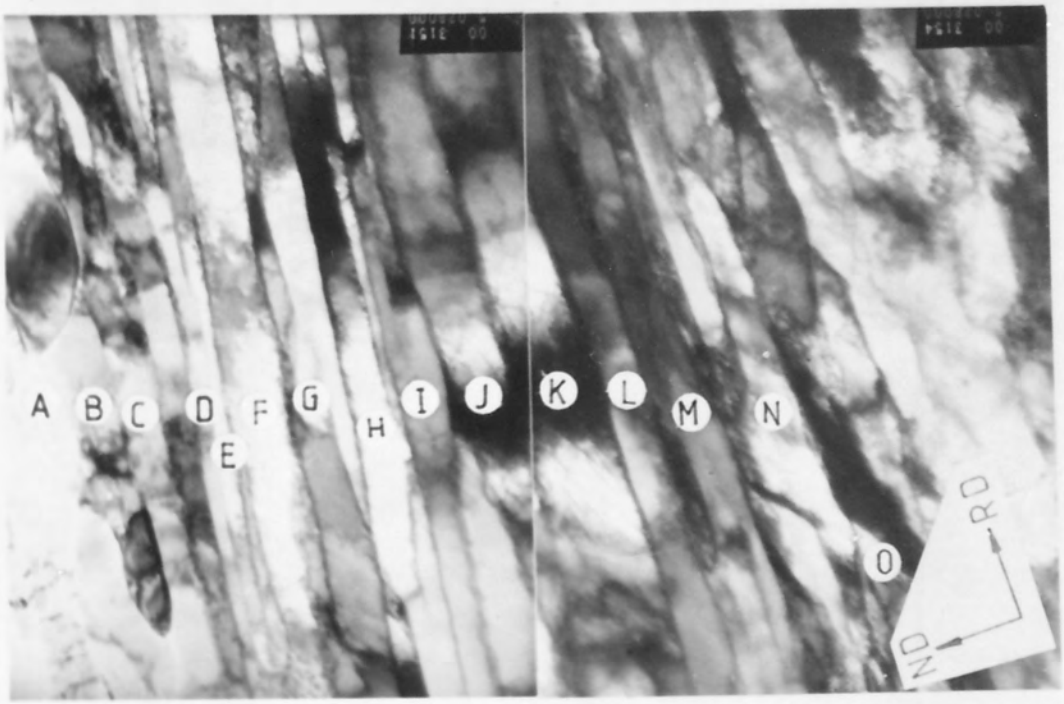
A
B
C
D
E
F
G
H
I
J
K
L
M
N
O
RD
ND

1 μ

-a-

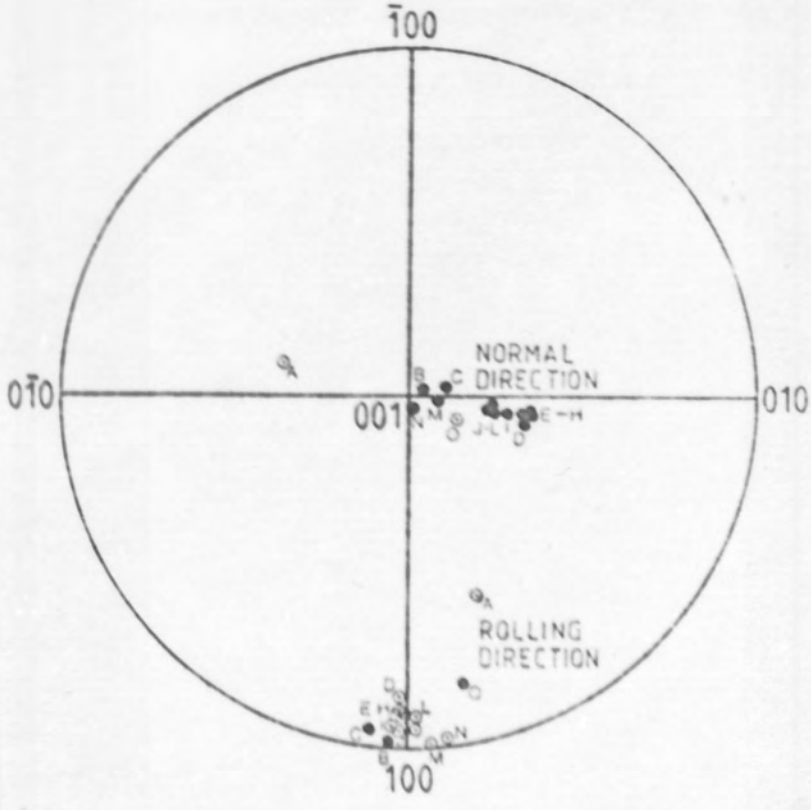
$\bar{1}00$
$0\bar{1}0$
001
010
100
NORMAL
DIRECTION
ROLLING
DIRECTION

-b-

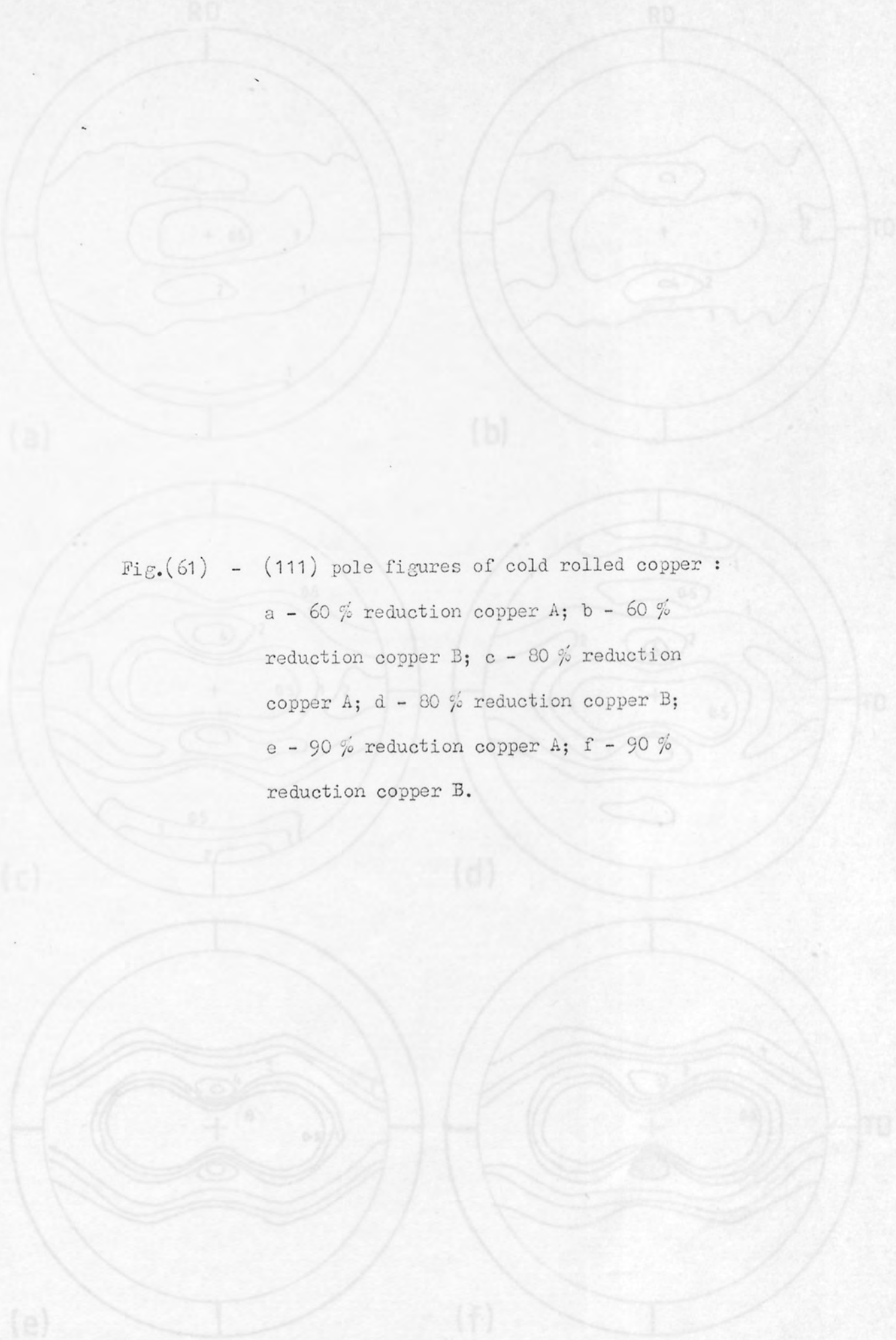

Fig.(61) - (111) pole figures of cold rolled copper : a - 60 % reduction copper A; b - 60 % reduction copper B; c - 80 % reduction copper A; d - 80 % reduction copper B; e - 90 % reduction copper A; f - 90 % reduction copper B.

Fig.(62) - (111) pole figure :

a - Copper A rolled 90 % at -100 C;

b - Coarse grain copper A rolled 90 %

at room temperature.

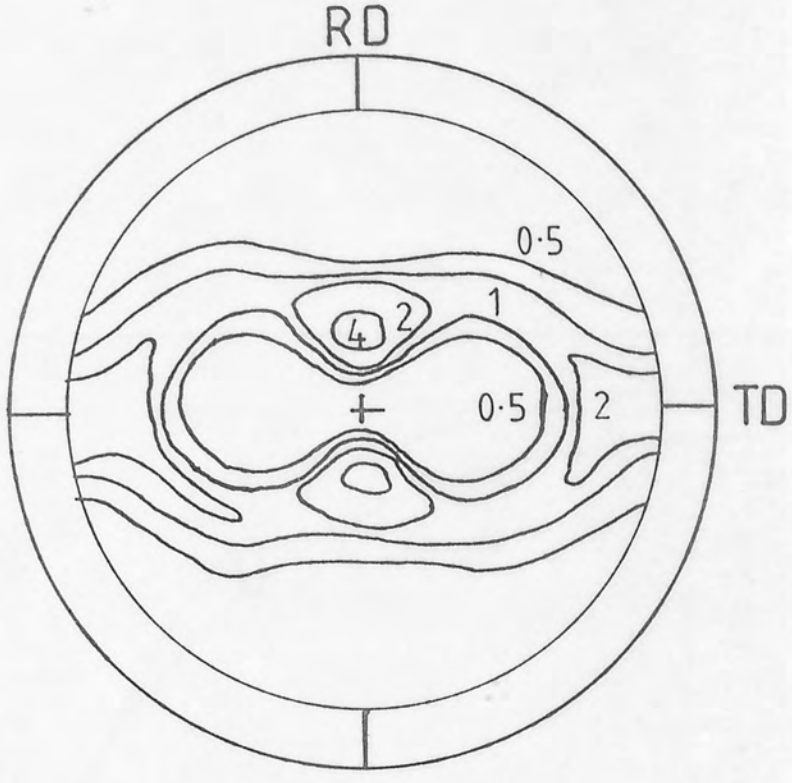

(a)

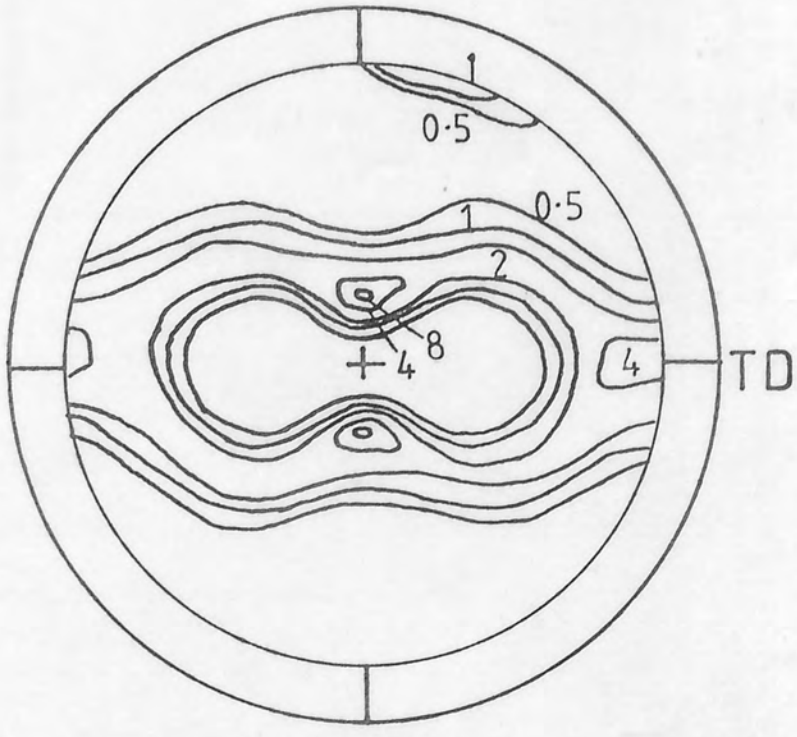

(b)

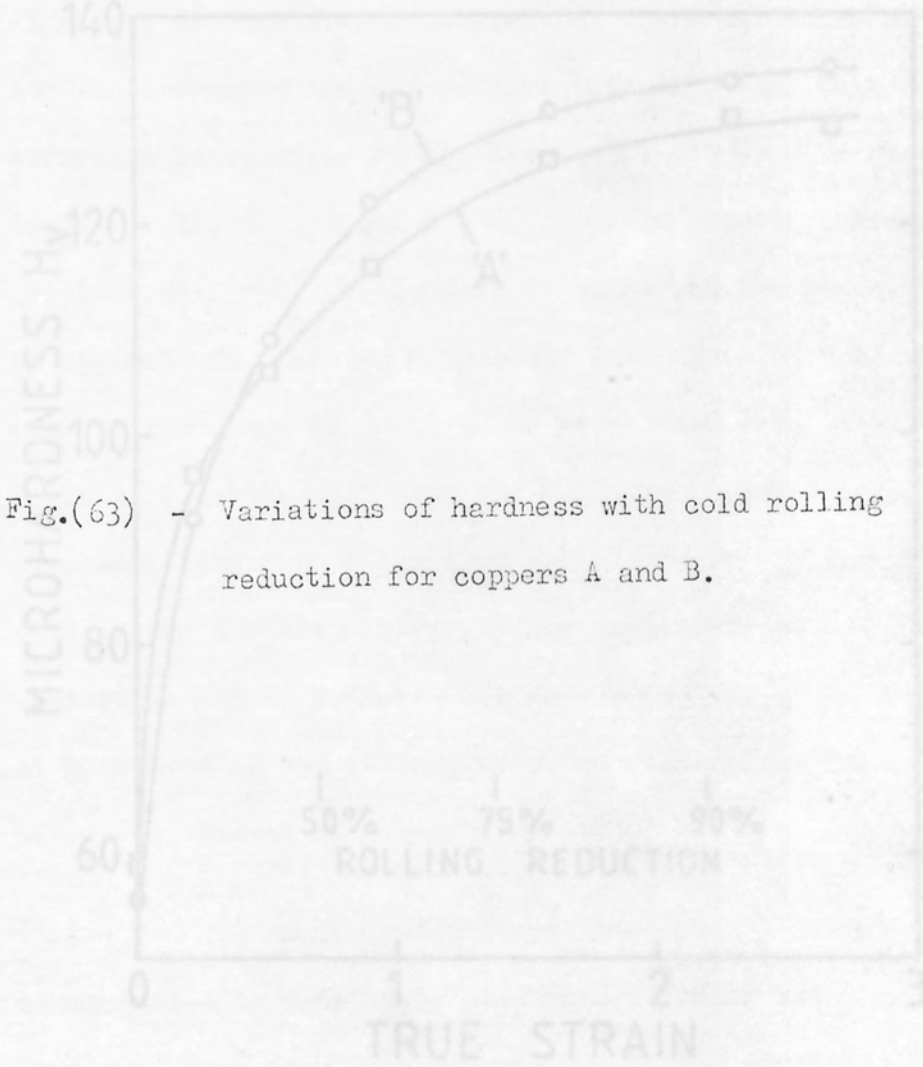

Fig.(63) - Variations of hardness with cold rolling reduction for coppers A and B.

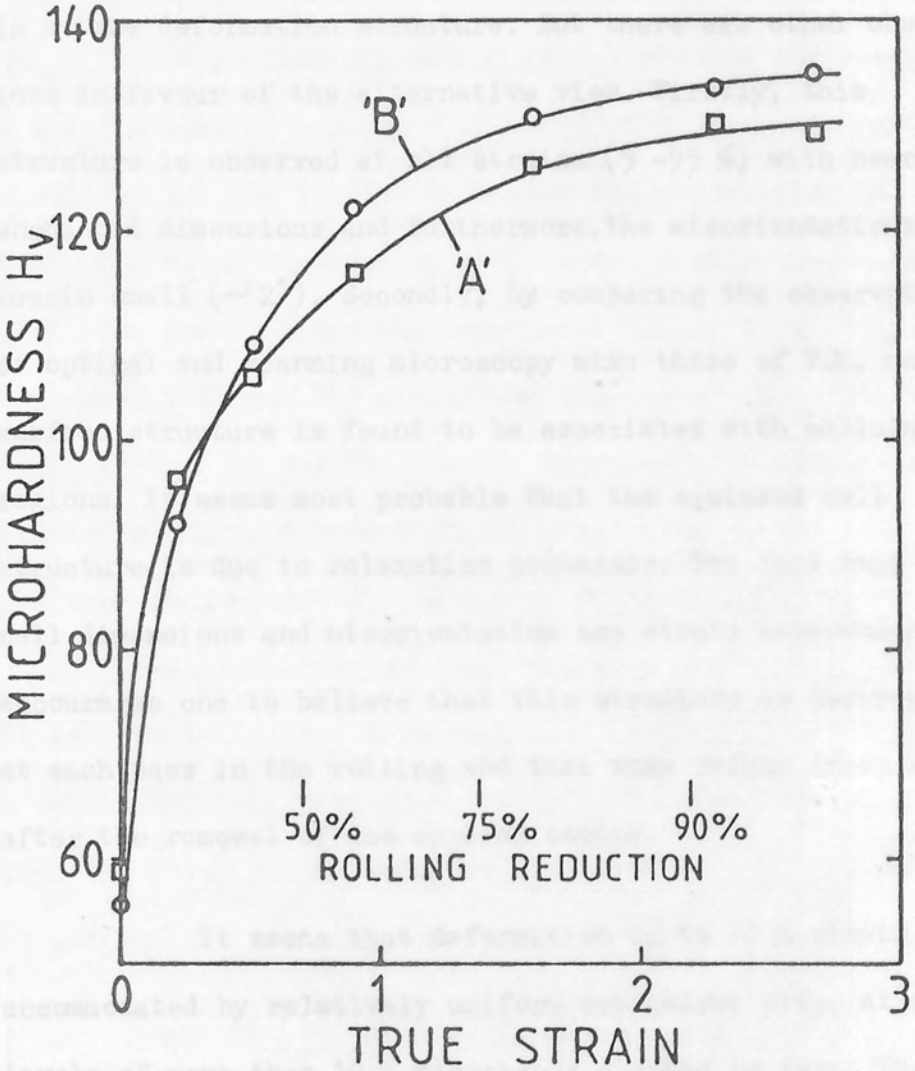
140
120
100
80
60
MICROHARDNESS Hv
'B'
'A'
50%
75%
90%
ROLLING REDUCTION
0
1
2
3
TRUE STRAIN

Now the question which should be answered is whether the equiaxed cells are a deformation structure or whether they form due to relaxation after the passes. It has been reported by many workers (e.g.28) that this structure developed gradually as the deformation increased, first with boundaries parallel to the slip plane suggesting that the cell structure is a true deformation structure. But there are other observations in favour of the alternative view. Firstly, this structure is observed at all strains (5 -95 %) with nearly unchanged dimensions and furthermore, the misorientations remain small ($\sim 2^{\circ}$). Secondly, by comparing the observations of optical and scanning microscopy with those of TEM, no surface structure is found to be associated with cellular regions. It seems most probable that the equiaxed cell structure is due to relaxation processes. The fact that the cell dimensions and misorientation are strain independent, encourages one to believe that this structure is destroyed at each pass in the rolling and that they reform immediately after the removal of the applied stress.

It seems that deformation up to 10 % strain is accommodated by relatively uniform octahedral slip. At strain levels of more than 10 % microbands started to form. The misorientations between microbands and the matrix are usually small and their rotation axes appear to be a combination of rotations around an axis perpendicular to TD and very small component of rotation around TD. The similarity in morphology, geometry, and strain level between the etch pit lines observed by optical microscopy, the banded region and slip lines in the

scanning electron microscope, the microbands, and type III indications reported by Samuels (9) Figs.(1b, 34b-c, 49) indicate that all these features are manifestations of the same phenomenon.

It has been reported by Horiuchi (44) and Malin (45) that microbands always form on {111} planes making angles of 35° with the rolling direction. In the present investigation a large number of specimens deformed 20 % were very carefully examined, and the results show that the majority of the microbands (70 %) do lie parallel to the {111} slip planes. However, 30 % were found to deviate very considerably from {111}. Malin (45) reported that the microbands started to form after only 5 % reduction by rolling. During the course of this work extensive searches were made for microbands in thin foils prepared from material rolled 5 %, but none has been found. Even if the microbands do form at a very low strain level (0.05) it is hard to believe that they can rotate sufficiently with a small additional strain to produce the observed deviations from the {111} plane. Furthermore the results of Horiuchi et al (44) are particularly surprising as they made their observations on copper drawn 80 %. Also, the diffraction patterns from which they defined the microband habit planes were far from symmetry and may be as far as 15° away from the true zone (180-181). Finally, their streographic projection analysis was based on the assumption that all microbands should have the same habit plane.

It is generally accepted that microbands are thin sheet-like volumes of shear, which cause marked displacements

at grain and annealing twin boundaries. Isolated microbands were first clearly described by Ahlborn et al (43) in drawn copper single crystals. It was assumed that they form from the equiaxed cells by elongation and amalgamation. Later Malin (45) postulated that the microbands formed by a co-operative process on a cluster of parallel {111} planes are so closely spaced as to be unresolved. The particular {111} plane concerned is always at approximately 35° to the rolling direction and parallel to the transverse direction. To account for such shear it was suggested that in each microband the slip occurs on consecutively operating slip planes, Fig.(64). The ideal orientation to satisfy this configuration is {110} ⟨001⟩. The statistical orientation determination for 43 grains containing microbands indicated clearly that there is no preferred orientation for these grains, Fig.(57). Furthermore, the angle between the microbands and the rolling direction measured at 20 % deformation shows that in general the microbands could form at any angle between 10° and 50° Fig.(35a) with the rolling direction. These results cast some doubt on Malin's mechanism for microbands formation. Observations based on optical and scanning microscopy, Figs.(34a-b, 36a) suggest that microbands with {111} habit planes are localised shears on slip planes with the maximum resolved shear stress.

High resolution dark field experiments show very clearly that the dislocations within the microbands differ from those in the matrix and the band boundaries. Furthermore, it was frequently observed in the transmission electron microscope that when a freshly formed microband sheared an

Aston University

Aston University

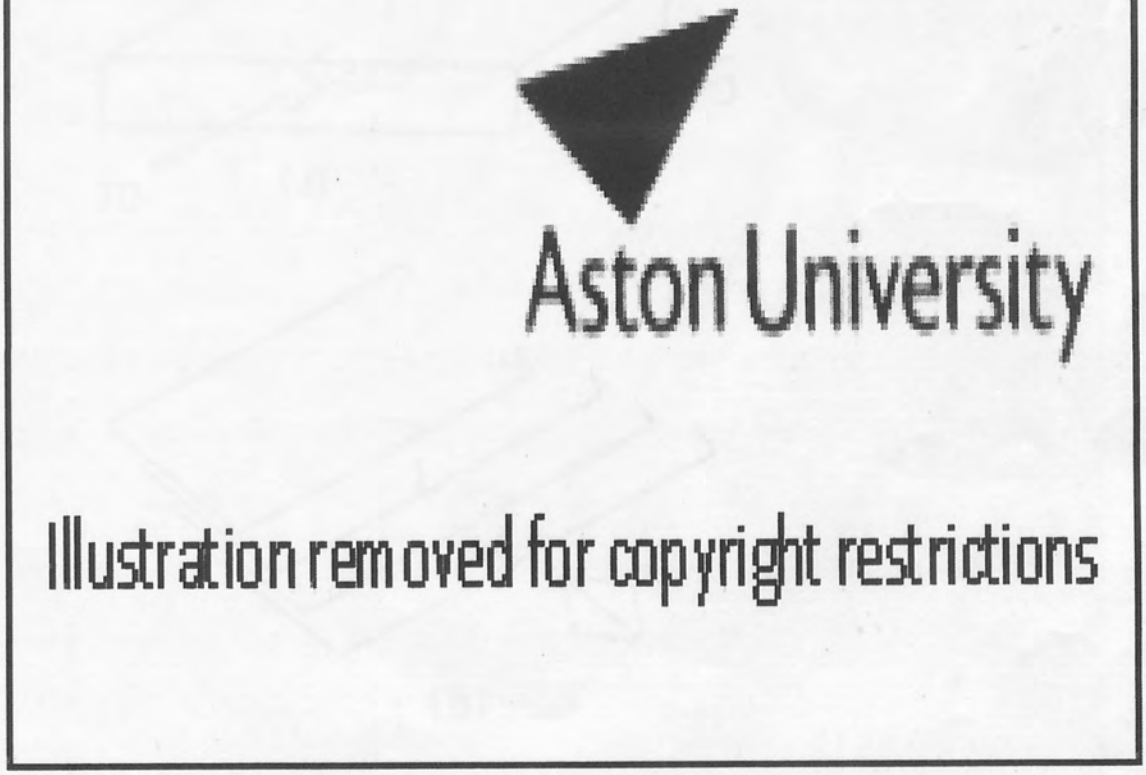

Ref.45.

old one, the sheared boundaries of the latter were eliminated in the new band. The last two observations indicate the following :-

a - Dislocations in the band boundaries are not the dislocations associated with the microband formation.

b - The stress field associated with the tip of a propagating microband is so high that it can sweep away all the matrix dislocations lying in its path, and the microband boundaries are built up of the displaced dislocations.

The misorientation between the fresh microbands and the matrix is usually small (1°-2.5°), with increasing strain the misorientation increases slightly, and by 90 % reduction it becomes about 4° with no simple rotation axis. On the basis that microbands are localised single slip, there should be no consistent misorientation between them and the matrix. The observed behaviour suggests that during microband formation the matrix may undergo some simultaneous homogeneous deformation.

After strains of $\sim$10 % microbands become the major deformation mode and usually one parallel set develops at this stage. With further deformation the lattice rotates, activating different slip system combinations which produces an alternative set of parallel bands. The incidence of microbands increases with strain and by 40 % many grains contain two sets, normally one of which shears the other and subdivides it into parallelogram shaped blocks, Fig.(49). At 60 % reduction the majority of the grains contain one set of bands with residual fragments of the other set, Fig.(50). This

has been confirmed by optical and scanning microscopy, Figs.(34d,39 c-d). As the deformation increases still further the microbands start to rotate towards the rolling plane and by 90 % reduction their alignment is almost perfect. This indicates that the elongated cells reported by many workers after heavy deformation (90 %) are in fact developed from the original microbands.

The sharpness of the elongated cell boundaries is believed to be due to dynamic recovery. As mentioned earlier, the cube oriented regions in as-deformed specimens are more dynamically recovered than any other regions. A possible explanation is as follows : In rolling deformation the operative slip systems in a cube oriented crystal are (111) $[\bar{1}01]$, $(1\bar{1}1)$ $[\bar{1}01]$, $(\bar{1}11)$ $[101]$ and $(\bar{1}\bar{1}1)$ $[101]$, because the other slip systems cannot contribute directly to the imposed strain. There are only two different Burgers vectors and these are perpendicular to each other, which implies that there can be no elastic interaction between them, because the force between perpendicular dislocations is zero. Also, they cannot reduce their energy by combining to form product dislocations. During recovery the positive and negative dislocations of a similar type will annihilate each other without interference. This unique characteristic makes the cube orientation rather susceptible to rapid dynamic and static recovery. This observation has been reported by other workers (105, 108), but no explanation has previously been given. Orientation analysis of the cube regions indicated that the change in orientation across the band is gradual and progressive (by steps of $\sim 4^{\circ}$ for each cell). These regions serve as transition

bands between two highly misoriented regions in the deformed structure, similar to those reported by Hu (42) and Walter et al (107). Dillamore et al (73) made a detailed study of transition band formation, and concluded that some orientations do not rotate (metastable) when subjected to specific strain, but small displacements in opposite senses from the initial orientation will cause the blocks of material to continue to rotate in opposite directions. The cube orientation is one such case. Thus if two different regions of the near (100) [001] orientation are displaced clockwise and anticlockwise respectively around the rolling direction, they will continue to rotate leading to the formation of highly misoriented regions linked by a transition band which passes through the cube orientation. Orientation analysis also showed that the spread of orientation across the transition band, Fig.(59) is similar to that predicted by Dillamore et al (173).

Evident differences occur between coppers A and B after heavy deformation, such as the degree of dynamic recovery, hardness, and substructure morphology. In copper B shear bands started to develop after 60 % reduction, and increased in frequency with further deformation such that by 90 % the structure contained a high density of shear bands. In copper A at this deformation level only very few shear bands were present. The reason why these occur so much more frequently in B than in A can be understood on the basis of the work hardening of the materials. Bands are not seen at low strain level where there is residual work hardening capacity, but only when this is almost exhausted so that strain localization

is not prevented by a concurrent hardening process. Recovery of the metal between passes will provide a stabilising effect which will resist localization of strain into shear bands. Hardness measurements and transmission electron microscopy observations support this. It appears that some trace of unknown impurity in material B has a strong inhibiting affect on dislocation movement causing rapid initial work hardening which saturates at high strain. Copper A on the other hand seems to recover during or between passes. Since recovery is a thermally activated process the following experiment was conducted to test this hypotheses. Copper A was rolled to 90 % at -100° C to reduce the rate of recovery in the material during deformation. Optical examination shows very dense shear banding, Fig.(38a), which supports strongly the work hardening hypothesis. Coarse grained (300μm) copper A also develops numerous shear bands after 90 % rolling at room temperature. It is believed that the reason in this case differs from that in the case of material B. It is known that shear band formation is strongly dependent on crystal orientation and texture. It is true that copper A of initial grain size (85μm) gives a sharp deformation texture, but the deformed structure at 90 % reduction consists of thin elongated regions of different orientation. Some of these regions which are suitable for shear band formation are not big enough for shear bands to be established. There seems to be a critical length necessary for the nucleation and growth of the bands.

Texture studies show that all materials developed similar rolling texture (copper type) after heavy deformation,

the only difference being the greater sharpness of texture in the material which did not develop shear bands. It is believed that this is due to shear band formation, because the shear process tends to rotate the aligned deformation structure between the bands, Fig.(40b) smearing out the sharp maxima. This is supported by the fact that the maximum peak intensity in material B deformed 60 % (4 random) is actually higher than that in material A (3 random), while after 90 % it is weaker than A (7 random and 10 random respectively).

CHAPTER 5.

Results and Discussion.

5. Recrystallization :

5.1. Optical metallography :-

The progress of recrystallization in both materials (A and B) was studied after 90 % reduction by annealing at 100°C for various periods of time using edge sections for each case. In copper A after one hour annealing, a few widely spread recrystallized grains were observed, the volume fraction recrystallized after 3 hours annealing was estimated to be less than 3 %. This increased steadily with annealing. After 10 hours recrystalized grains 5 - 10μm wide and 50 - 150μm long elongated along the rolling direction were developed, Fig.(65 a). The volume fraction recrystallized was about 20 % but the frequency of these thin and long recrystallized grains was small. With increasing annealing time the growth rate in the direction perpendicular to the length of the grain was usually faster than that along the grain length. After 30 hours annealing, about 90 % of the structure was recrystallized.

By contrast, material B developed very few and small equiaxed recrystallized grains after 7 hours annealing, the volume fraction of recrystallized grains at this stage was estimated to be less than 2 %. The first recrystallized grains were usually observed along the shear bands and occasionally elsewhere. As annealing continued these grains started to grow preferentially along the shear bands. Many recrystallized

grains were frequently observed within the same shear band. Fig. (65 b) shows a typical area in a sample annealed for 10 hours. At this stage, new grains were also observed in the elongated cell structure and the total volume occupied by recrystallized grains was about 5 %. In general the number of recrystallized grains in this material was much higher than that in material A. The recrystallized rate was not as high as in the case of copper A; after 100 hours annealing about 40 % of the deformed structure had been consumed. In Fig.(66) the volume percentage of recrystallized grains is plotted against annealing time. It is apparent that material A recrystallized approximately twenty times faster than that in B.

5.2. Scanning electron microscopy :-

This technique proved to be the most informative as it permitted unambiguous identification of the cold worked and recrystallized regions with good resolution over a wide field of view. The same sections were examined as for optical microscopy. The most interesting finding in material A annealed for 10 hours was the observation of very long thin ribbons, sometimes with straight faces, but often having a series of small bulges at various positions along their length. They were 50μm, or more, long and only 5μm, or less, in thickness, Fig.(67a). At this stage of their development the recrystallized grains normally contained a remnant substructure which can be seen as faint mottled diffraction contrast. As growth proceeded they became increasingly perfect. Orientations of six of these long thin nuclei were determined from selected area channelling patterns. The results show that these nuclei

have cube orientation (100) [001]. The orientation at various positions along their length were also determined and these results indicated that along a single nucleus the orientation was constant to within approximately 5°. With further annealing the rate of growth increased rapidly in a direction perpendicular to the length of these nuclei. Occasionally small and nearly equiaxed recrystallized grains were observed, but in general the number of recrystallized grains was small. After 30 hours annealing many grains 30μm wide and more than 50μm long were observed which frequently contained annealing twins making about 45° with traces of the rolling plane, indicating that their orientations were (100) [001]. By 100 hours annealing almost all the deformed structure was consumed by the recrystallized grains, the grain size was about 70μm and they were slightly elongated along the rolling direction.

In lightly annealed (10 hours) copper B the same type of long thin nuclei were also found, but here they were much less common. Recrystallization dominated within the shear bands and each band contained at least two different oriented grains together with their annealing twins. Fig.(67b). The annealing twins were comparable to the recrystallized grains in size and it was very difficult to distinguish which crystallite had grown from the original nucleus. Twins had evidently formed at an early stage of recrystallization. With further annealing the grains grow preferentially along the shear band and were normally restricted to the shear bands which they had nucleated. Colonies of grains in the elongated structure were also occasionally observed, with grains slightly

elongated along the rolling direction. Many unsuccessful experiments were conducted to determine the orientation of grains within shear bands, by selected area channelling patterns. These failures were attributed to the small size of the grains within a single shear band and the presence of residual internal substructure.

Scanning electron microscopy also showed very clearly that the recrystallization rate in material B was much smaller than that in A, and that the nucleation rate in the latter is much smaller than that in B.

5.3. Transmission electron microscopy :-

This technique was adopted to concentrate on the nucleation process in detail. Optical and scanning electron microscopy suggested that the most informative samples were copper A annealed for 10 hours and B annealed 10 and 30 hours. These samples were examined extensively in a large number of specimens. In A the long thin nuclei were often observed. Their thickness varied between 2 and 5μm, and they were usually more than 30μm long, with a series of mini bulges along their length. These bulges were often formed on only one side of the nuclei. A good example of one of these nuclei is shown in Fig. (68). In this long ($\sim$35μm)nucleus there were 5 bulges on one side, while the other side was almost straight. Some regions in this nucleus contain an internal dislocation structure. The deformed structure along the straight side of the nucleus (at the bottom of the montage) consists of very long and heavily recovered thin elongated cells. A detailed orientations

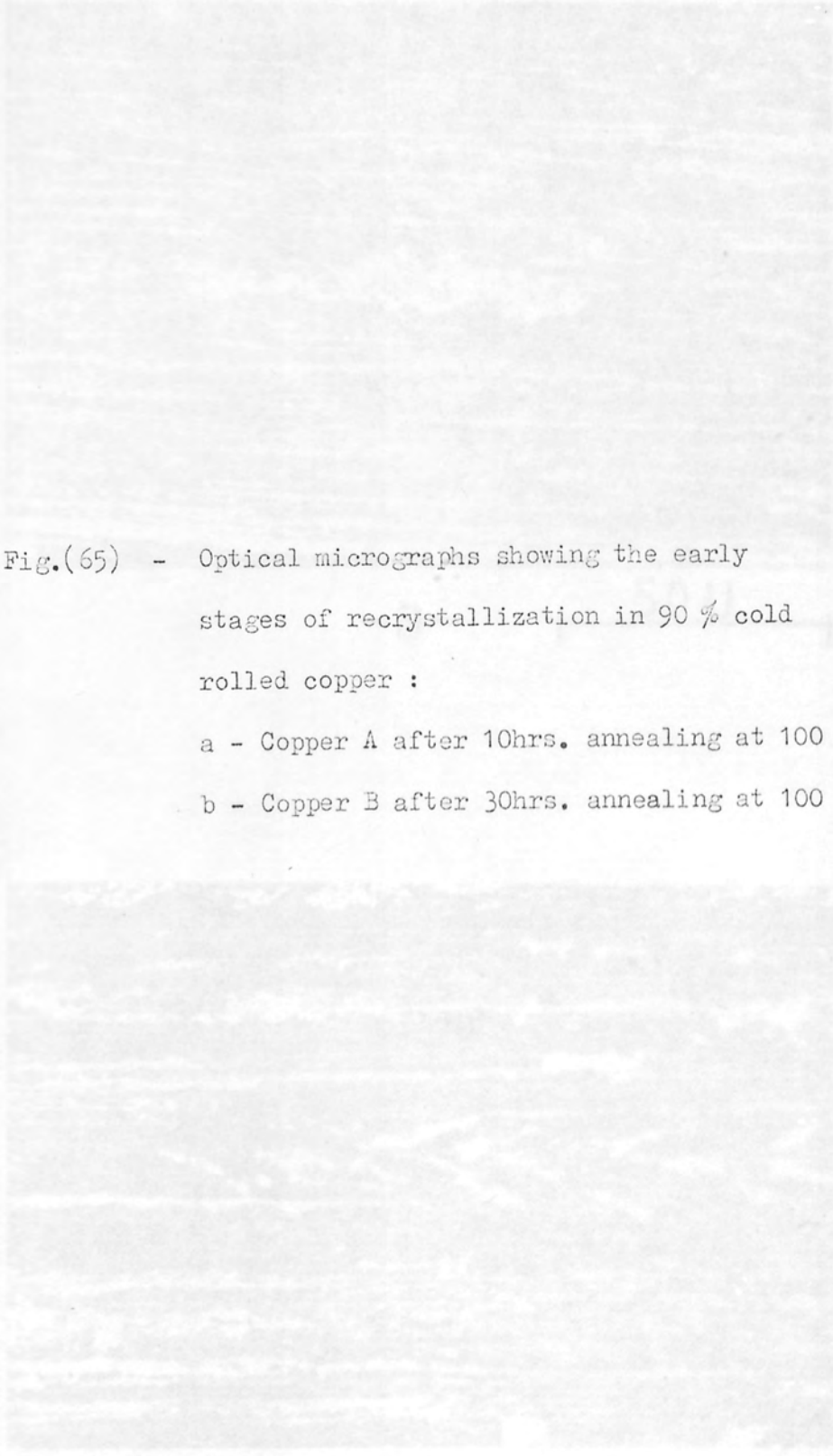

Fig.(65) - Optical micrographs showing the early stages of recrystallization in 90 % cold rolled copper :

a - Copper A after 10hrs. annealing at 100 C.

b - Copper B after 30hrs. annealing at 100 C.

-a- 50μ

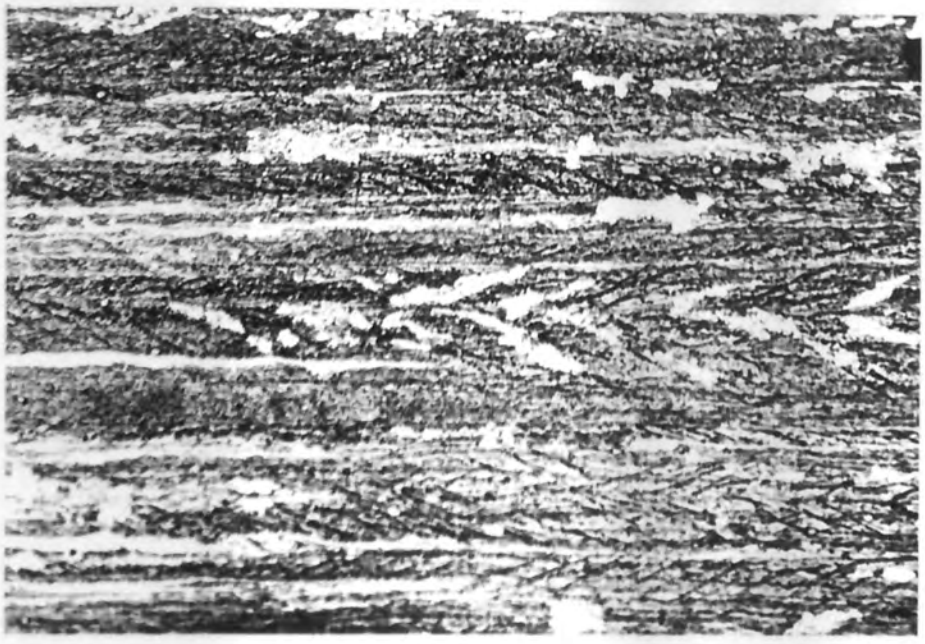

-b- 50μ

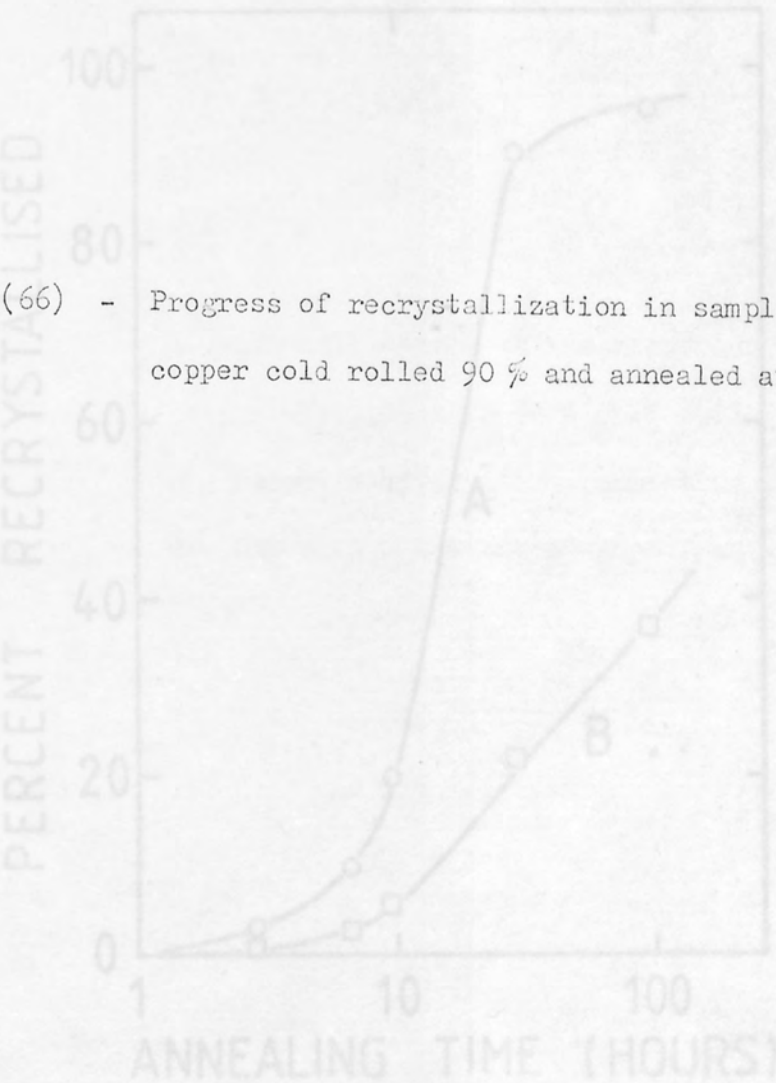

Fig.(66) - Progress of recrystallization in samples of copper cold rolled 90 % and annealed at 100 C.

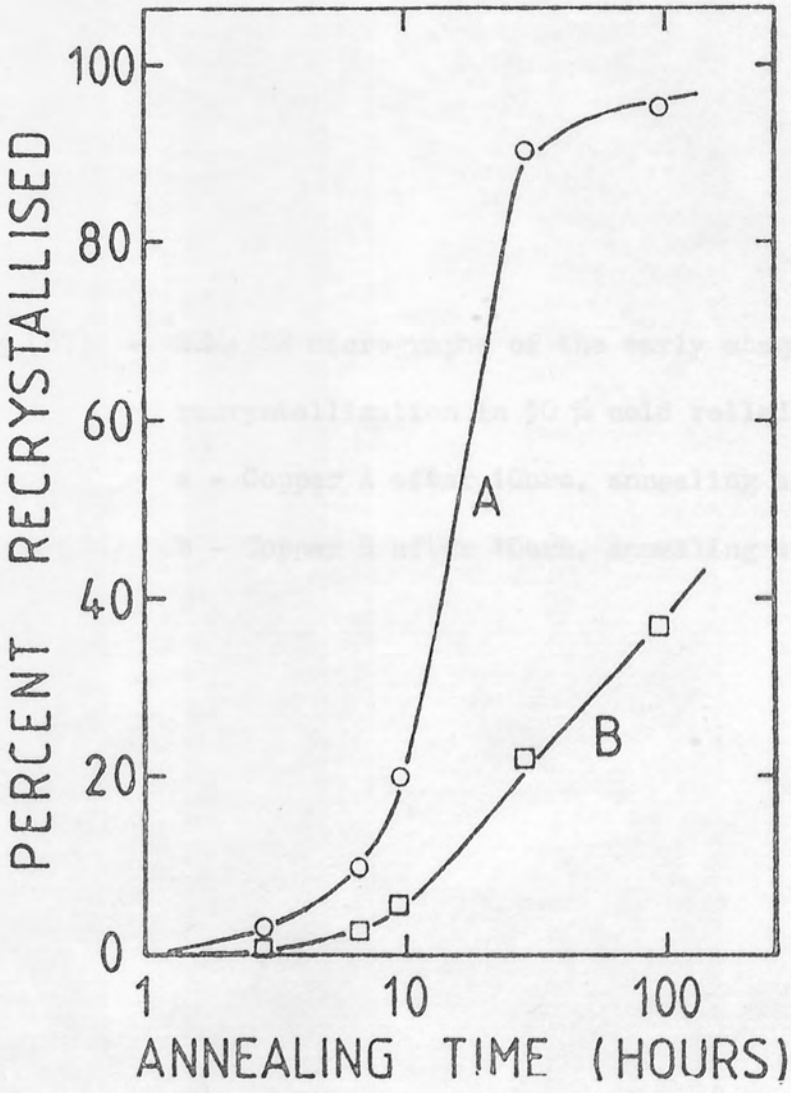
PERCENT RECRYSTALLISED
100
80
60
40
20
0
1
10
100
ANNEALING TIME (HOURS)
A
B

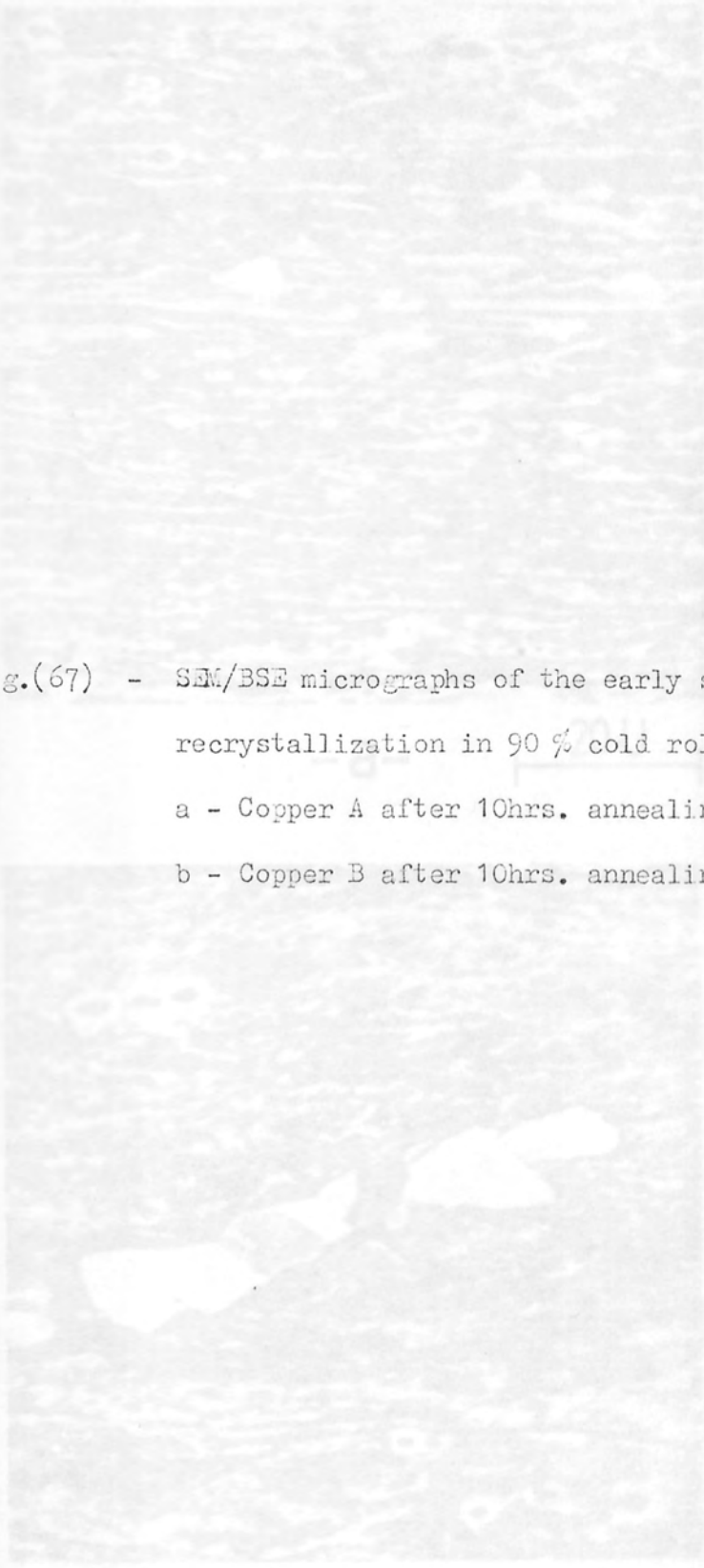

Fig.(67) - SEM/BSE micrographs of the early stages of recrystallization in 90 % cold rolled copper

a - Copper A after 10hrs. annealing at 100 C

b - Copper B after 10hrs. annealing at 100 C.

analysis by STEM microdiffraction was carried out across and along the nucleus, the deformed regions near the bulges, and along the straight side of the nucleus. Diffraction patterns corresponding to some of the different regions are shown in the same figure. The analysis shows that the orientations along the length of the nucleus were constant and were cube oriented within 2°. The orientations of the elongated cell structure near the straight edge of the nucleus were cube as well, whereas the misorientation between the cube regions in the bulges and the deformed structure near them were normally large. Fig.(69) shows another example of such an area where bulges form in both sides of the cubic nucleus. In this, positions 2 and 3 were found to deviate from the cube $(\bar{1}00)\,[010]$ by only 2°, and the misorientation between them were very small ($\sim$0.8°). They contain some dislocation internal structure and the boundaries between the two regions started to disappear in many places. The orientations of the deformed structure near the bulges (positions 1 and 4) were $\sim(1\bar{3}\bar{2})\,[\bar{1}\bar{1}1]$ and $\sim(0\bar{1}1)\,[\bar{4}11]$ respectively, which indicated a high misorientation between these regions and the cubic oriented bulges.

A few unrecrystallized cubic oriented regions were observed in samples prepared from material A annealed for 10 hours. These regions were in the form of bands of heavily recovered elongated cells. They were similar to the regions described in Chapter 4, the only difference being that most of the boundaries between the individual elongated cells were very faint, and in some cases almost disappeared (see the arrows in Fig.70). Occasionally the outer elongated cells of

the cubic oriented bands form small bulges (see the left top side in Fig.70).

Examinations of material B annealed for 10 and 30 hours revealed that some of the long thin nuclei were present but here they were much less common. New grains in the partially recrystallized sample were mostly of typical equiaxed shape, isolated, or in small groups. Frequently, these could be seen to be located at shear bands where they were sometimes elongated along the direction of the band. It seems that there was a tendency for recrystallization to commence at the edges of the shear bands. As this process the developed nuclei within the shear bands grew to consume all the deformed structure of the band. These grains normally contained a high frequency of annealing twins. Fig.(71) shows a montage representing a typical region in a partially recrystallized specimen. In this, the deformed structure is recovered to a smaller extent than in copper A annealed to the same level. There are two nuclei, one at the edge and the other in the interior of the shear band.

The orientations of recrystallized grains within the shear bands were determined in lightly annealed (10 hours) specimens of copper B. Microbeam Kikuchi diffraction patterns were obtained. A practical difficulty was that these grains were twinned and it was seldom possible to distinguish the original nucleus and the subsequent twin. However, the orientations of thirty-five grains were determined and the results were plotted in two unit triangles, one for the rolling plane orientation, and the other for the rolling direction,

Fig.(72). The grain orientations were widely spread, and no single cubic oriented grain was found.

5.4. Texture studies :-

(111) pole figures were determined for both materials (A and B) after 90 % cold rolling and annealing for 1 hour at 310°C. Copper A showed only very sharp cube texture {100} <100> (25 random) accompanied with its twin components {212} <122> see Fig.(73a). By contrast B shows very weak cube texture (3 random) with a diffuse spread of orientations, Fig. (73b). As mentioned earlier, the only difference between these two materials was that the frequency of shear bands in copper B was much higher than that in A after heavy deformation. To examine further the effect of shear banding on recrystallization textures, copper A rolled to 90 % at -100°C and copper A of initial grain size 300μm rolled 90 % at room temperature (both with a high frequency of shear bands) were annealed for 1 hour at 310°C. (111) pole figures of both are shown in Fig. (74). It is apparent that the recrystallization textures have very weak cube components (< 2 random after rolling at -100°C and 2 random in the other case) and a wide spread of other orientations.

5.5. Discussion :-

In Chapter (4) the examinations indicated that material B deformed 90 % is harder, its deformed structure is more fragmented, and contains more shear bands than material A. Despite this the recrystallization kinetics determined by

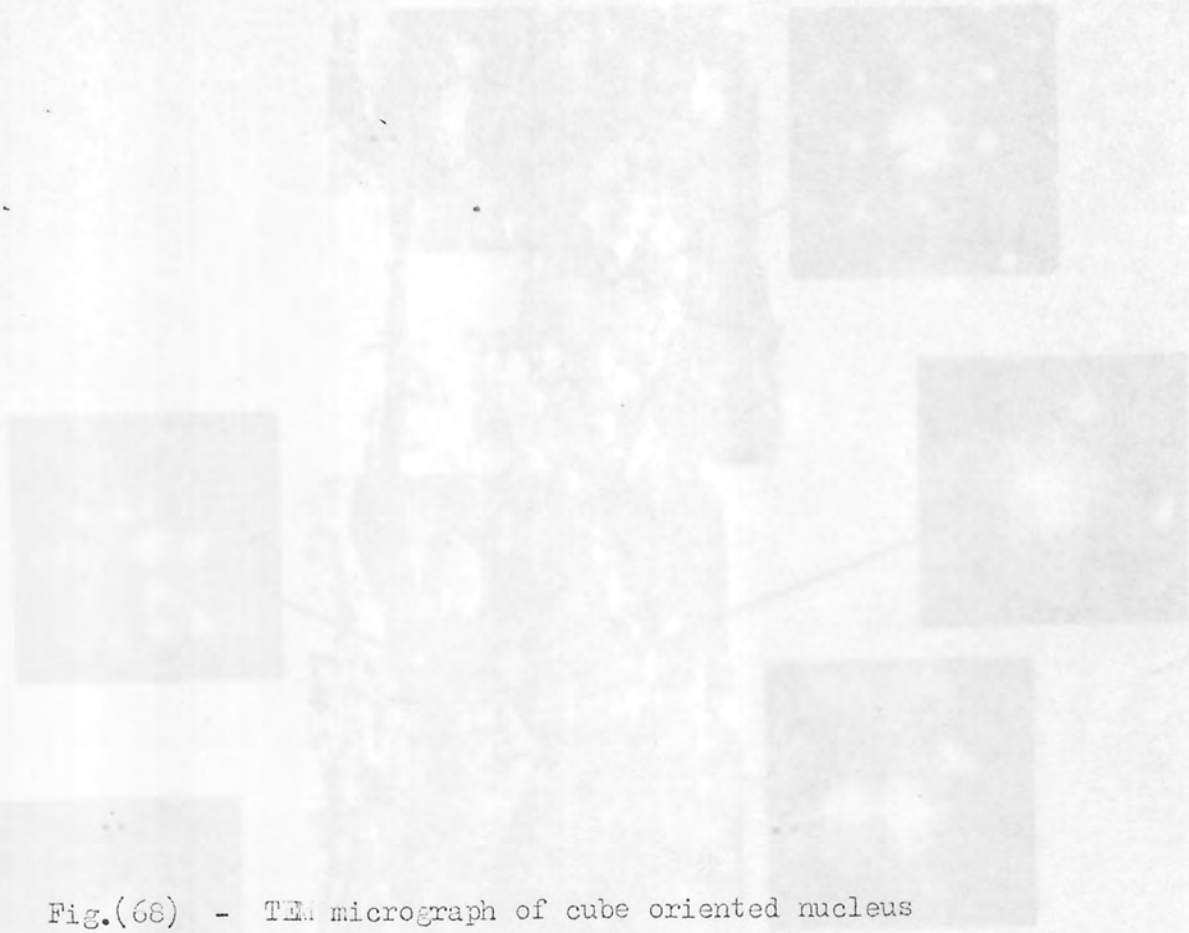

Fig.(68) - TEM micrograph of cube oriented nucleus bulging into the surrounding substructure. STEM diffraction patterns correspond to the indicated regions.

ND
RD

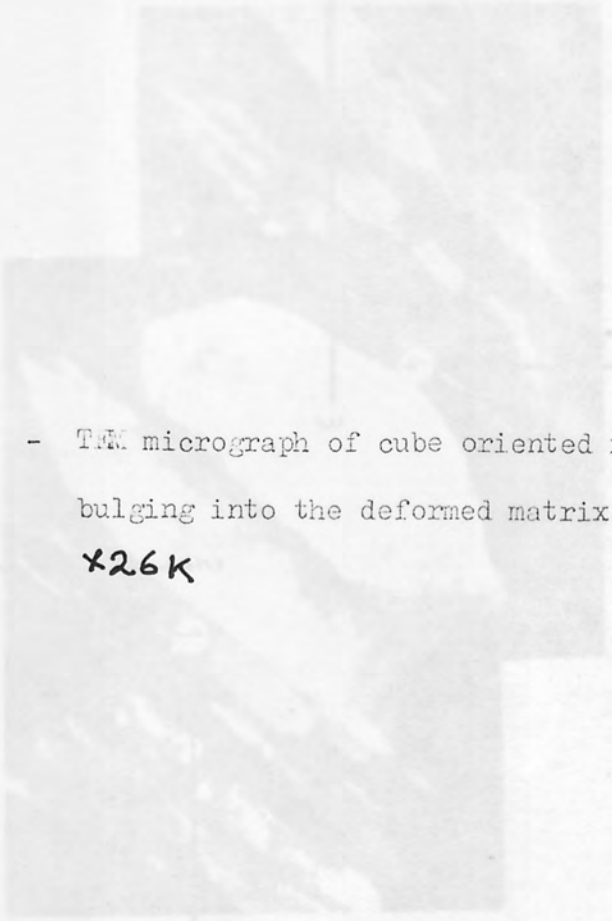

Fig.(69) - TEM micrograph of cube oriented nucleus bulging into the deformed matrix.
×26K

~(13̄2̄)[1̄1̄1]
[010](00l̄)
~(01̄1)[4̄11]
1
2
3
4

Fig.(70) - TEM micrograph of heavily recovered cube oriented region in copper A cold rolled 90 % and annealed at 100 C for 10hrs.
Some of the boundaries between the elongated cells (arrows) have started to disappear.

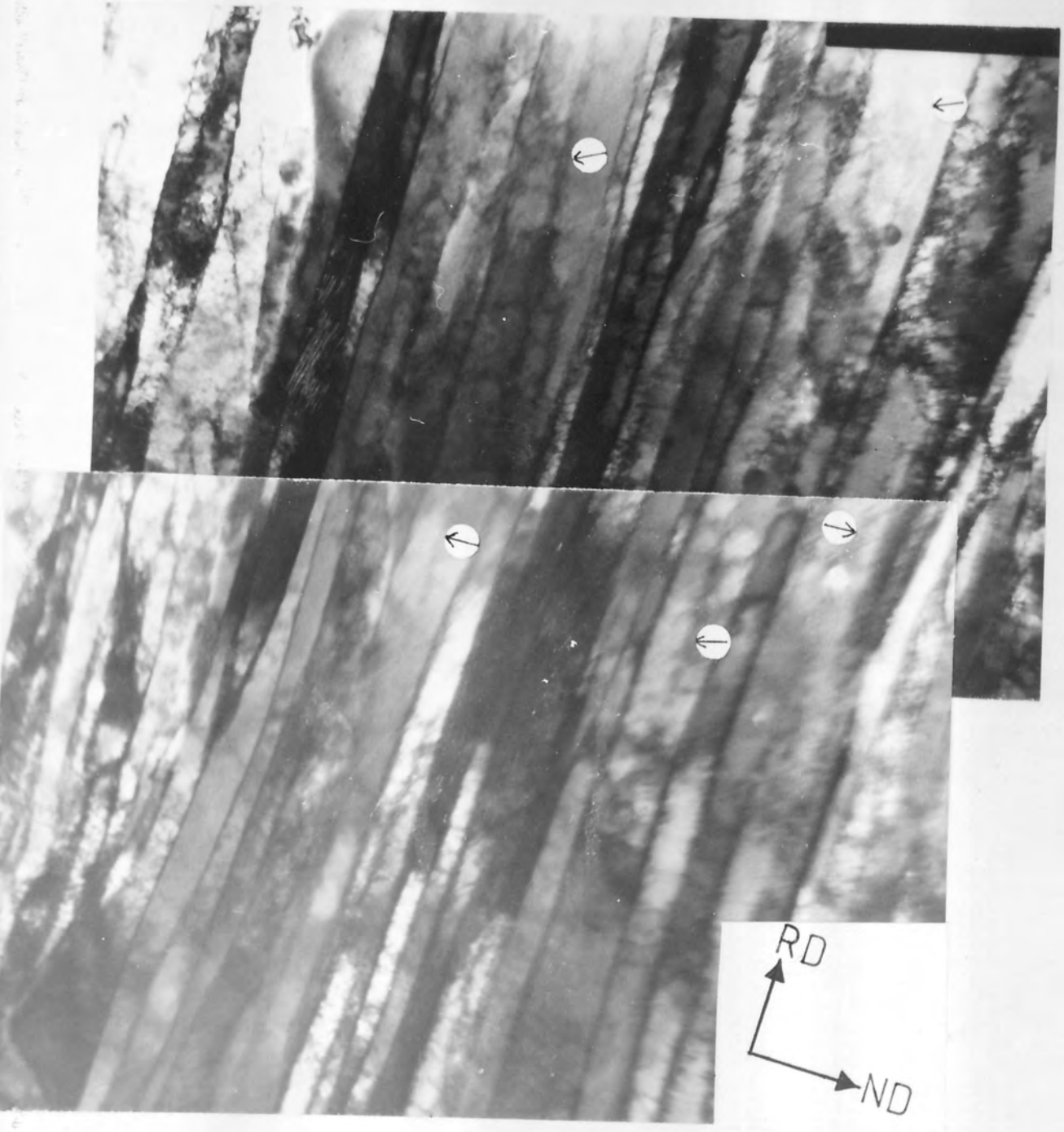
RD
ND
1 μ

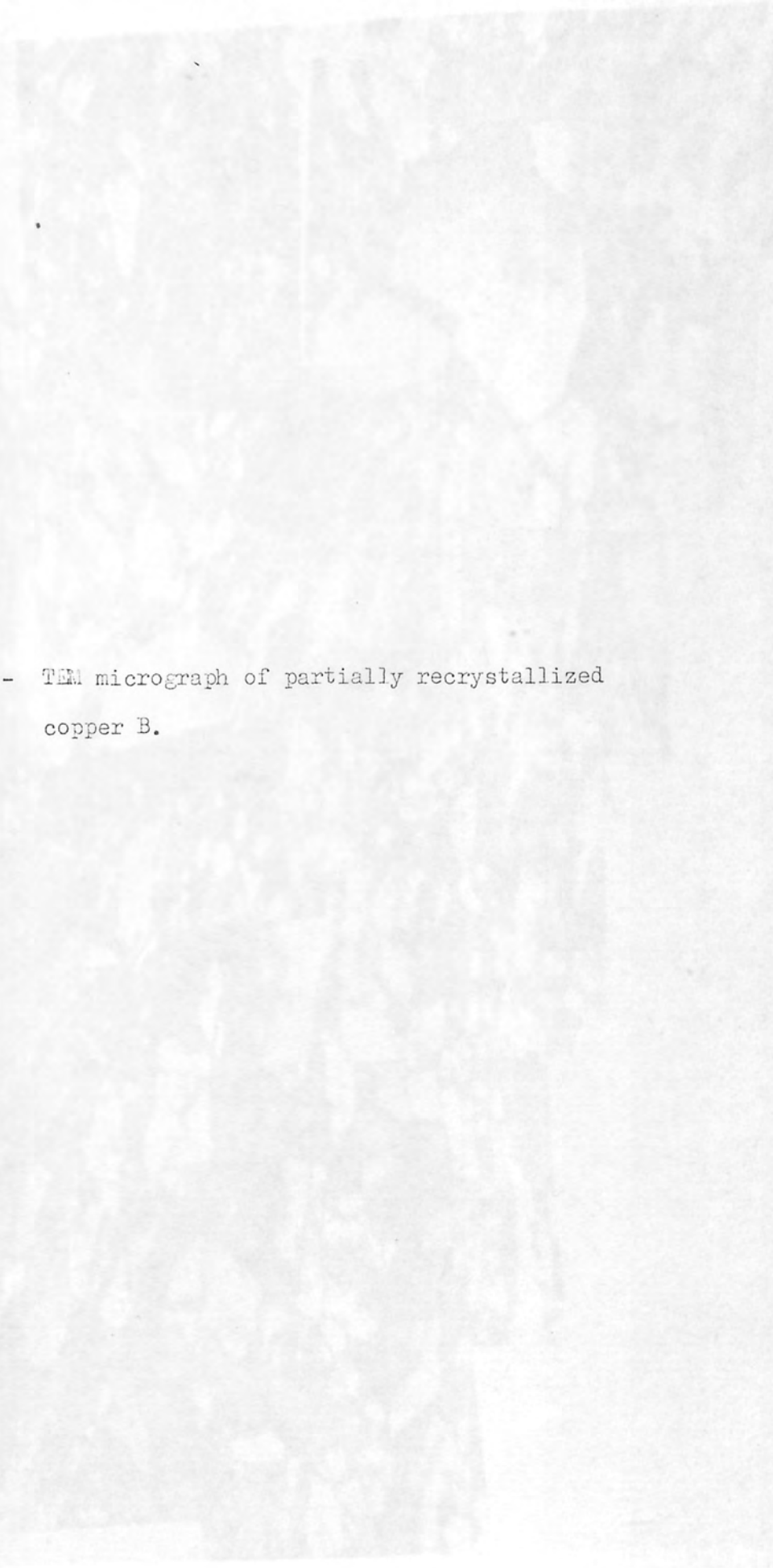

Fig.(71) - TEM micrograph of partially recrystallized copper B.

RD
ND
1 μ

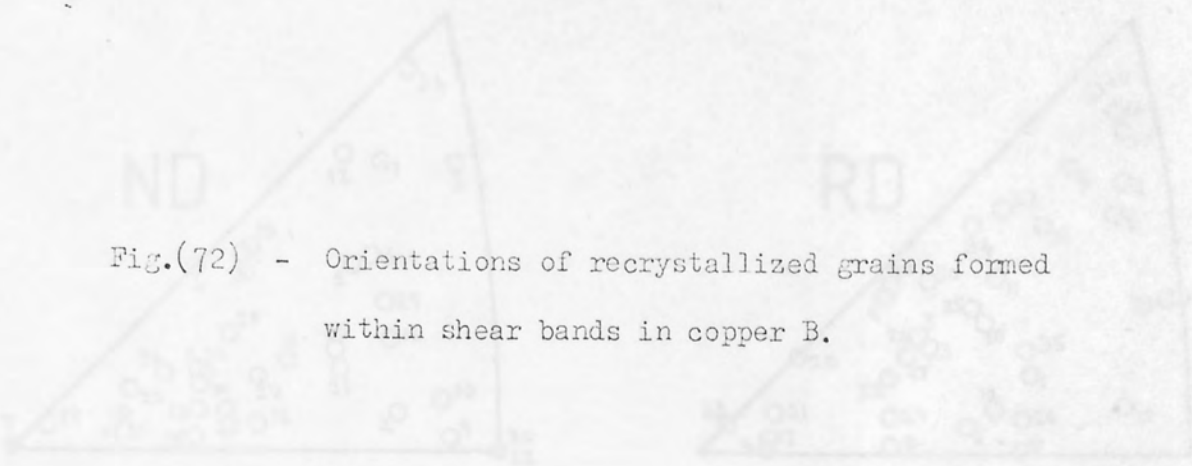

Fig.(72) - Orientations of recrystallized grains formed within shear bands in copper B.

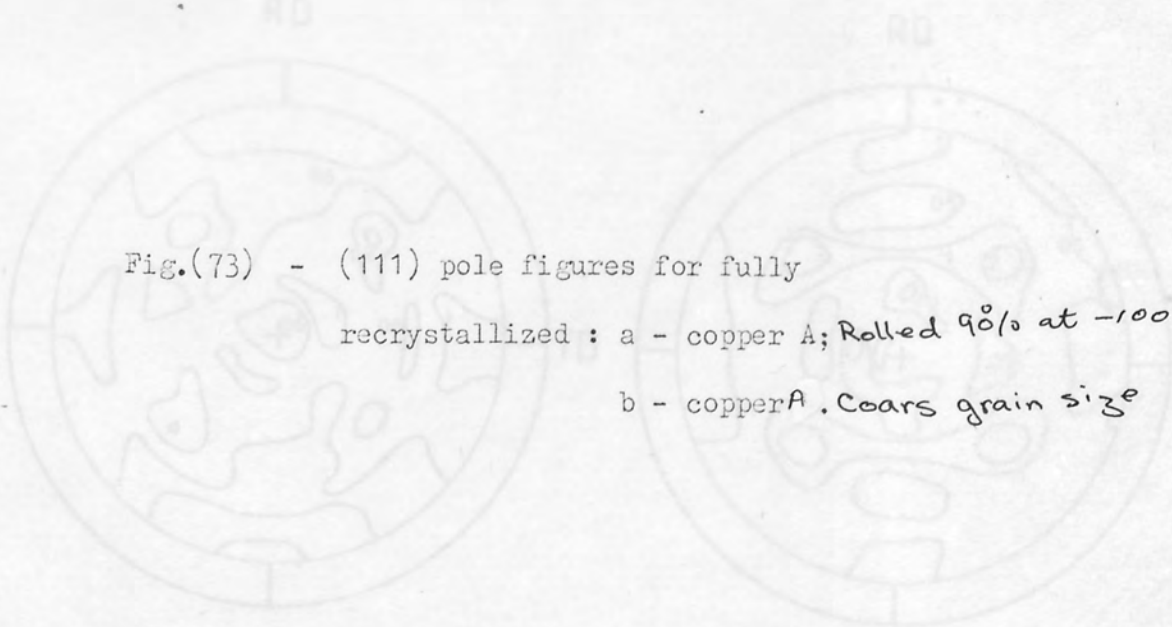

Fig.(73) - (111) pole figures for fully recrystallized : a - copper A; Rolled 90% at -100°C.
b - copper A. Coars grain size

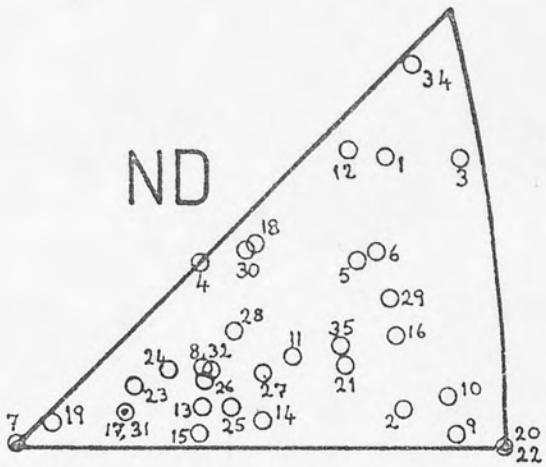
ND
34
12
1
3
18
30
4
5
6
29
28
35
16
11
24
8,32
21
23
26
27
10
13
25
14
2
7
19
17,31
15
9
20
22

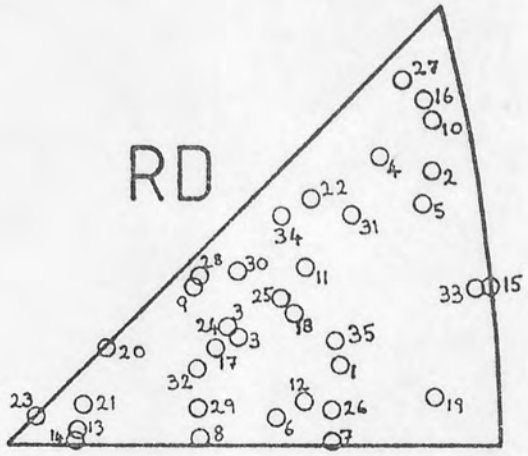
RD
27
16
10
4
2
22
5
31
34
28
30
11
33
15
25
9
24
3
18
35
20
17
1
32
12
23
21
29
26
19
14
13
6
8
7

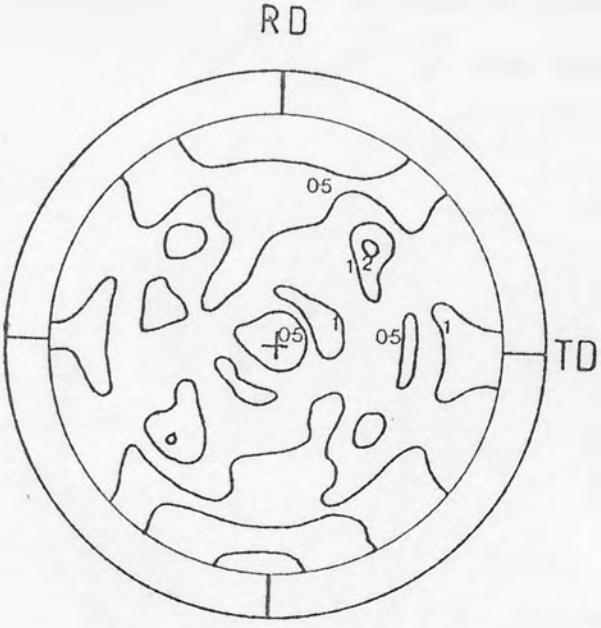
RD
05
1
2
05
1
05
1
TD

-a-

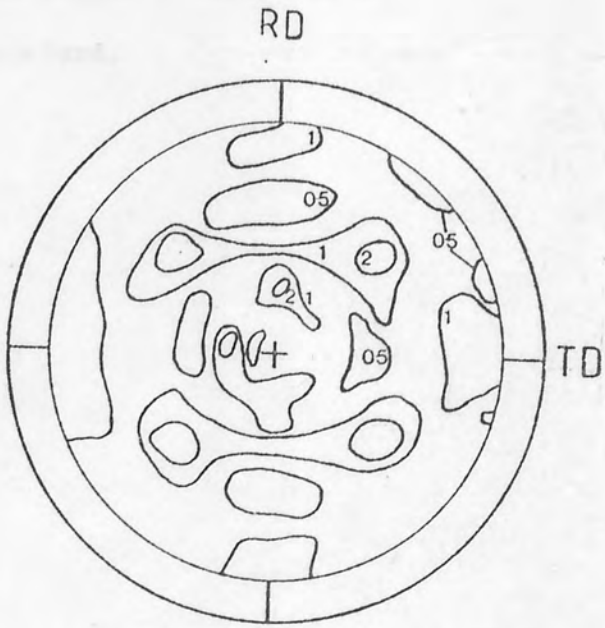
RD
1
05
1
2
05
2
1
05
1
TD

-b-

Fig.(74) - (111) pole figures for fully recrystallized :

a - copper A rolled 90 %.

b - coarse grained copper B rolled 90 % at room temperature.

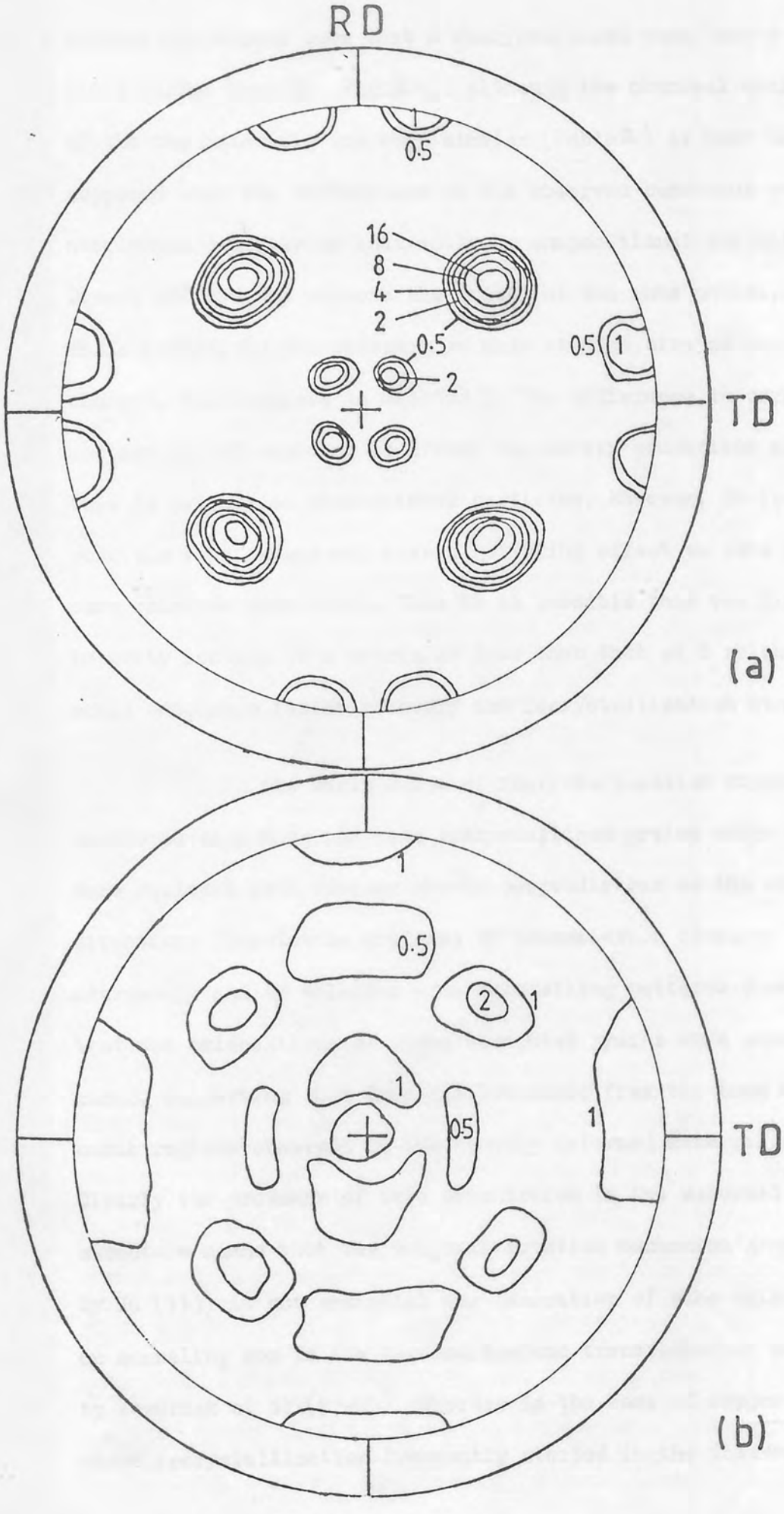
RD
1
0.5
16
8
4
2
0.5
2
0.5
1
TD
(a)
1
0.5
2
1
1
05
1
TD
(b)

optical microscopy show that A recrystallized some twenty times faster than B, Fig.(66). Although the chemical analysis of the two materials are very similar (Table 2) it must be supposed that the differences in the observed behaviour are attributed directly or indirectly to compositional variations. Direct effects may supress the growth of the cube nuclei, while indirectly the deformation mode at high strains is changed, as discussed in Chapter 4. The difference in oxygen content is not expected to affect the matrix properties since this is present as precipitated particles. However, it is possible that oxygen may have a gettering effect on some of the more reactive impurities. Thus it is possible that the dissolved impurity content in A matrix is less than that of B which would encourage faster recovery and recrystallization kinetics.

In the early stage of recrystallization copper A developed very long and thin recrystallized grains which became more equiaxed with further growth perpendicular to the rolling direction. Orientation analyses by transmission electron microscopy and by selected area channelling patterns showed that the orientations of these elongated grains were constantly cubic, suggesting that they had developed from the long thin cubic regions observed in the heavily deformed material. Clearly the presence of this orientation in the deformed structure means that the subgrain rotation mechanism proposed by Hu (113) is not essential for generation of cube orientation on annealing nor is the inverse Rowland transformation proposed by Verbraak et al (97-98). Whereas in the case of copper B where recrystallization frequently started in the intersection

areas of the shear bands with the elongated structure, the grains were normally very small and nearly equiaxed. With further annealing, growth first occurred preferentially within the shear bands. This behaviour may be expected because of the sharp lattice curvature produced by the shear process (50, 126), and the high dislocation density (stored energy) associated with them. Similar observations have been reported in cupro-nickel (25), copper 0.6 wt % Cr (50), and in 70 : 30 brass (126).

Irrespective of the nucleation site, it is generally accepted that any potential nucleus should have a size advantage over its neighbours and environmental advantages (i.e. the misorientation between the nucleus and the adjacent deformed regions must be sufficient to provide a high boundary mobility for the growth process) over the other embryos. All the examinations showed clearly that the cube oriented nuclei were exceptionally long and so could increase in volume by increasing their thickness while experiencing almost no resistance from their own surface tension.

The question now to be answered is how these cubic nuclei developed the high angle boundaries to ease their migration. It was shown in Chapter (4) that the cube oriented cells are contained within transition bands which accommodate large misorientations between two regions in the deformed structure. Many workers (42, 107) reported that transition bands provide the most favourable conditions for both nucleation and for continued growth. Dillamore et al (73) proposed a mechanism for nucleation and growth in transition bands, which involves cell boundary migration at the expense

of neighbouring elongated cells. A brief description of this mechanism was given in section (2.3-2). The experimental results of the present study show that in lightly annealed samples the cubic regions were heavily recovered and the boundaries between slightly misoriented ($\sim 1^{\circ}$) elongated cells started to disappear, Fig.(70). The very small initial misorientation across these boundaries suggests that they are mainly composed of statistically stored dislocations. As was discussed above, the residual dislocations in the cube oriented regions cannot interact with one another because of their orthogonal Burgers vector and so rapid recovery may be expected. The evidence did not suggest that recrystallized grains were created by a series of coalescences in the manner proposed by Hu. A nucleus with a mobile boundary would require as many as five successive coalescences of neighbouring elongated cells and this was never observed. It is believed that the elongated cell boundary migration mechanism suggested by Dillamore et al (73) plays the major role by which the cubic oriented nuclei in transition bands achieve high angle boundaries. As this happens the nucleus will grow by bulging into the deformed structure. Orientation analysis shows that the bulges are usually associated with high angle boundaries.

In the initial stages of recrystallization copper A developed a small number of cubic elongated grains which grew very rapidly with subsequent annealing. Some small equiaxed grains were also occasionally observed, but by this time the cubic grains were so large that they could consume smaller grains during grain growth and so produce an almost

perfect cube recrystallization texture. Material B, on the other hand, developed a very weak recrystallization texture. To understand this behaviour one should go back to the early stages of the annealing process. Initially, the material developed a large number of small nearly equiaxed grains, some clustered in groups, but mainly aligned along the shear bands. Orientation analysis indicated clearly that these grains were randomly oriented, Fig.(72). As the annealing time increased these grains started to grow, and there was no selectivity of the type reported by Lücke et al (170) in commercial purity aluminium. The annealing texture is the result of random growth of randomly oriented nuclei. In fact the pole figure studies are in good agreement with the orientation analysis by microbeam diffraction patterns as both give a fairly random orientation, the only difference being that the pole figures show an additional weak cube component. This could be explained on the basis that in the latter only the orientation of the grains within the shear bands were determined, and any elongated cube nuclei were ignored. Similar observations have been reported by Duggan et al (126) in 70 : 30 brass.

As mentioned earlier it is believed that the differences in the recrystallization textures were due to some unknown impurity which suppressed the cube texture in material B. Extensive transmission electron microscopy did not show any type of impurity precipitation on grain or cell boundaries in either material, which might be expected to suppress the growth of the cube oriented nuclei. The only differences the examinations showed were that the heavily deformed structure

in A was more recovered than that in B, and there was a high frequency of shear bands in the latter. This led to the conclusion that the impurity in this particular case affects indirectly the recrystallization texture by modifying the deformation mode at high strains. This explanation is supported strongly by the results of the copper A rolled at low temperature and with coarse initial grain size. In both cases the materials developed a high frequency of shear bands. The results in Fig.(74) show that the sharp cube texture is suppressed and recrystallization textures are generated which are more or less similar to that in material B. There are two ways in which occurrence of shear bands can weaken the cube texture.

a - Shear bands cut the long cubic regions making them smaller and subsequently less competitive on annealing.

b - They provide randomly oriented competitive nuclei.

The cube oriented regions in heavily deformed copper have the minimum possible M value for rolling deformation and they are relatively more dynamically recovered than other regions. Both of these factors makes them resistant to shear banding. Only powerfully driven shear bands are capable of cutting through them, however, such shear bands were observed in copper B. When this happens the cube regions will be subdivided into smaller lengths, and on annealing these small cubic regions may recrystallize, but their growth rate will be slower than that in copper A because they have lost their special length advantage (73). As already seen, on annealing the shear bands provide a randomly oriented

competitive nuclei , which also tends to randomise the recrystallization texture. The facts that the cube nuclei grew much faster in copper A than in copper B and that the coarse grained copper A recrystallized more slowly than the finer grained, suggest that destruction of the cube regions by shear bands is more significant in controlling the final cube texture than is the provision of randomly oriented competitive nuclei.

Merlini et al (176) reported in cross-rolled copper that the deformed structure contained about twice as much cube oriented volume as in straight-rolled copper, but after annealing it did not develop cube texture. This result has been used as evidence against an oriented nucleation theory (162) explanation for the origin of the cube texture. The present work demonstrated that it is the special characteristics of the cube cells in the deformed structure which make them such highly favoured nuclei. It is most probable that with cross-rolling deformation the geometry of the cube orientation will differ from that in straight rolling which will make them less competitive. The special combination of orthogonal Burgers vector will certainly not be present.

The results of the present work support strongly the oriented nucleation mechanism for the following reasons :

a - In the early stages of recrystallization the nucleation process in copper A was dominated by cubic nuclei, and the recrystallization texture comprised a very sharp cube texture.

b - In copper B the nucleation was random and no selective growth has been observed, as suggested by oriented growth theory (163).

c - According to oriented growth theory the recrystallization texture should be related to the deformation texture by 30° to 40° rotations around common <111> poles. The present work shows that similar deformation textures developed different recrystallization textures after annealing. These observations are incompatible with the oriented growth mechanism of the formation of annealing texture.

CHAPTER SIX.

CONCLUSIONS.

1. At low strain levels (< 10 % reduction) deformation normally takes place by homogeneous octahedral slip, and the observed equiaxed cell structures are due to the relaxation process taking place after each pass.

2. Between 10 % and 60 % reduction much of the slip is concentrated in localised microbands. These are sheets 0.1 to 0.25μm thick, slightly misoriented ($\sim 2^{\circ}$) from the matrix, and almost parallel to the transverse direction, making angles from 10° to 50° with the rolling direction. They are entirely contained within grains and are found in grains of almost all orientations. They seem to be a localised single slip process and are commonly, but not always, aligned parallel to $\{111\}$ planes.

3. Clusters of parallel microbands occur and these rotate after 60 % reduction, becoming approximately parallel to the rolling plane by 90 % reduction. The elongated cell structure typical of high strain deformation is created by these processes.

4. At high strains (> 60 %) coarse shear bands may operate. Their occurrence is favoured by large initial grain size, low rolling temperature and unknown conditions of chemical purity.

5. Shear banding is associated with exhaustion of

work hardening capacity, and is also orientation-sensitive. Dynamic recovery restores work hardening capacity and prevents the occurrence of shear banding.

6. Cube-oriented regions are present in heavily cold rolled copper. They exist as unusually long bands ($> 30\mu m$) of highly elongated thin cells. The number of cells across each band varies, but usually they form a long range lattice curvature. This transition band structure is in good agreement with the predictions of Dillamore and Katoh.

7. Cells in the cube orientation are relatively dislocation-free and they continue to recover rapidly on annealing. This behaviour is probably due to the lack of interaction between dislocations present after deformation as a result of the orthogonality of their Burgers vectors. This particular condition can only be achieved in the cube orientation.

8. On annealing, nuclei grow rapidly in the cube oriented regions of the deformed structure as a result of the favourable geometry and rapid recovery. Their growth mechanism involves a series of small bulges into the deformed structure at various positions along the band of cube cells. The initial rate of growth of cubic nuclei is much higher than that of other nuclei because of their exceptional length.

9. Shear bands are very favoured sites for nucleation of recrystallization but the resulting grains have little or no preferred orientation.

10. The existence of shear bands in the deformed structure weakens the resulting cube recrystallization texture in two ways. Firstly, they cut up the long cube oriented bands in the deformation structure which makes the cube nuclei less favoured on subsequent annealing. Secondly, they provide alternative nuclei of widely scattered orientations.

ACKNOWLEDGEMENTS.

This work was carried out under the supervision of Dr.W.B.Hutchinson to whom I am deeply indebted for his excellent guidance, encouragement and help. Thanks are due to Professor I.L.Dillamore for his useful discussions and provision of laboratory facilities, and to Dr.I.Jones for his help with the scanning transmission electron microscope.

The author also thanks the technicians of the department and the workshop staff for their help, and to the University of Technology (Iraq) for their financial support throughout this work.

I wish to express grateful thanks to my wife for her support and assistance.

Finally, thanks are due to Mrs.Howell for typing this thesis.

REFERENCES.

1. A.J.Ewing and W.Rosenhain, Phil. Trans. Roy. Soc., A193, 353, (1900)
2. L.E.Samuels and M.Hatherly, J. Inst. Met., 84, 84, (1955-56).
3. H.Wilsdorf and D.Kuhlman - Wilsdorf, Z.Angew. Phys., 4, 418, (1952)
4. D.Kuhlman-Wilsdorf and H.Wilsdorf, Acta Met., 1, 394, (1953)
5. C.H.Mathewson and A.Phillips, Trans. A.I.M.E., 54, 608, (1916)
6. R.M.Brick, Trans. A.I.M.E., 137, 193, (1940).
7. R.M.Brick and M.A.Williamson, Trans. A.I.M.E., 143, 84, (1941)
8. J.E.Burke and C.S.Barrett, Trans. A.I.M.E., 175, 106, (1948).
9. L.E.Samuels, J. Inst. Met., 83, 359, (1954-55)
10. M.Hatherly and L.E.Samuels, J. Inst. Met., 85, 437, (1956-57).
11. L.E.Samuels and M.Hatherly, J. Inst. Met., 86, 442, (1957-58).
12. M.Hatherly, J. Inst. Met., 88, 60, (1960-61).
13. C.H.Samans, J. Inst. Met., 55, 209, (1934).
14. C.H.Mathewson, Trans. A.S.M., 32, 38, (1944).
15. C.S.Barrett, "Imperfection in Nearly Perfect Crystals", John Wiley and Sons, New York, (1952), P.97.
16. B.E.Warren and R.P.Warekois, Acta Met., 3, 473, (1955).
17. C.W.J.Wagner, Acta Met., 5, 427, (1957)
18. P.T.Wakefield, A.S.Malin and M.Hatherly "1976 I.I.W. and Metals Technology Conference, Vol. B", Sydney, (1976), P.14-3-1.
19. K.Morii, M.Mera and Y.Nakayama, Trans. Jap. Inst. Met., 18, 7, (1977).
20. P.T.Wakefield, A.S.Malin and M.Hatherly, J. Aust. Inst. Met., 22, 143, (1977).
21. B.J.Duggan, M.Hatherly, W.B.Hutchinson and P.T.Wakefield,

Met. Sci., 12 ,343, (1978).

22. M.Hatherly and A.S.Malin, Met. Tech., 308. (1979).

23. W.B.Hutchinson, B.J.Duggan and M.Hatherly, Met. Tech., 398, (1979)

24. A.S.Malin and M.Hatherly, Met. Sci., 13 ,463, (1979).

25. F.Adcock, J. Inst. Met., 27, 73, (1922).

26. J.D.Embury, A.S.Keh and R.M.Fisher, 236, 1252, (1966).

27. H.Hu, "Textures in Research and Practice", Ed. J.Grewen and G.Wassermann, Springer, Berlin, (1969), P.200.

28. P.R.Swann, "Electron Microscopy and Strength of Crystals", Ed. G.Thomas and J.Washburn, Interscience, (1963), P.131.

29. S.J.Basinski and Z.S.Basinski, "Recrystallization Grain Growth and Textures", A.S.M., Ohio, (1966), P.1.

30. P.B.Hirsch and T.E.Mitchell, "Work Hardening", A.I.M.E., 46, Gordon and Breach, New York, (1968), P.65.

31. R.D.Heidenreich, J. App. Phys., 20, 993, (1949).

32. P.Gay, P.B.Hirsch and A.Kelly, Acta. Met., 1, 315, (1953).

33. P.Gay, P.B.Hirsch and A.Kelly, Acta Cryst., 7, 41, (1954).

34. A.Wingrove, J. Inst. Met., 100, 313, (1972).

35. S.Weissman, T.Imura and N.Hosokawa, "Recovery and Recrystallization of Metals", Ed. L.Himmel, Interscience, New York, (1963), P.241.

36. A.Seeger, "Dislocations and Mechanical Properties of Crystals", John Wiley, New York, (1956), P.243.

37. M.J.Whelan, Proc. Roy. Soc. London, A249, 114, (1958).

38. P.B.Hirsch, "Internal Stresses and Fatigue in Metals", Ed. G.M.Rassweiler and G.L.Grube, Elsevier, Amsterdam, (1958), P.139.

39. P.RSwann and J.Nutting, J. Inst. Met., 90, 133, (1961-62).

40. P.T.Wakefield, Ph.D. Thesis, University of N.S.W., (1980), Australia.

41. V.Essmann, Phys. Stat. Sol., 12, 723, (1965).

42. H.Hu, "Recovery and Recystallization of Metals", Ed. L.Himmel, Interscience Publishers, New York, (1963), P.311.

43. H.Ahlborn and D.Sauer, Z.Mettallk, 59, 658, (1968).

44. S.Horiuchi, K.Asakura, G.Wassermann and J.Grewen, Texture, 2, 17, (1975).

45. A.S.Malin, Ph.D. Thesis, University of N.S.W. (1978), Australia.

46. J.Grewen, J.Huber and M.Hatherly, Met. Forum, Vol.1, No.3, 115, (1978).

47. J.H.Cairns, J.Clough, M.A.P.Dewey and J.Nutting, J. Inst. Met. 99, 93, (1971).

48. J.Nutting, "Proc. 8th International Congress on Electron Microscopy" Eds. J.V.Sanders and D.J.Goodchild, Vol.1, 580, (1974), Canberra, Australian Academy of Science.

49. A.S.Malin and M.Hatherly, ibid, P.582.

50. J.Grewen, T.Noda and D.Sauer, Z.Metallk., 68, 260, (1977).

51. K.Brown, J. Inst. Met., 100, 341, (1972).

52. P.Karduck, J.M.Goux and G.Gottstein, KSMA5, Vol.1, 107, (1979).

53. J.W.H.G.Slakhorst and M.J.ten Bouwhuijs, Scripta Met., 11, 947, (1977).

54. H.Hu, R.S.Cline and S.R.Goodman, "Recrystallization, Grain Growth and Texture", A.S.M., Ohio,(1966) P.295.

55. K.Sekine and T.Kamijo, Trans Jap. Ins. Met., 17, 11, (1976).

56. W.Ratuszek and J.Karp, Met. Sci., 10, 214, (1976).

57. W.Ratuszek, P.Korgul and S.Gorczyca, Metalurgial Odle Wnictwo-Tom 5-Zeszyt 2. P.309, (1979).

58. T.Leffers and A.Grum-Jensen, Trans. A.I.M.E., 242, 314, (1968)

59. D.M.Turley, J. Inst. Met., 97, 237, (1969).

60. A.J.Baker and B.F.Peters, "Internation Conference on Strength of Materials and Alloys" Jap. Inst. Met., Tokyo, P.919 (1967).

61. Y.C.Liu and G.A.Alers, Met. Trans., 4, 1491, (1973).

62. M.Blicharki and S.Gorezca, Met. Sci., 12, 303, (1978).

63. R.N.Caron and S.Shapiro, Metall. Trans., 8A, 111, (1977).

64. I.L.Dillamore, J.G.Roberts and A.C.Bush, Met.Sci., 13, 73, (1979).

65. O.Johari and G.Thomas, Acta Met., 12, 679, (1964).

66. A.S.Appleton and J.S.Waddington, Acta Met., 12, 965, (1964).

67. R.L.Nodler and G.Thomas, Acta Met., 11, 994, (1963).

68. R.L.Nodler and G.Thomas, Acta Met., 12, 227, (1964).

69. W.N.Roberts, Trans. A.I.M.E., 227, 422, (1963).

70. A.S.Keh and S.Weissmann, "Electron Microscopy and Strength of Crystals" Ed. G.Thomas and J.Washburn, Interscience (1962) P.231.

71. T.Mori and H.Fujita, Trans. Jap. Inst. Met., 18, 17, (1977).

72. I.L.Dillamore, C.J.E.Smith and T.W.Watson, Met.Sci.J., 1, 49, (1967).

73. I.L.Dillamore, P.L.Morris, C.J.E.Smith and W.B.Hutchinson, Pro. Roy. Soc., 329A, 405, (1972)

74. G.Longford and M.Cohen, Trans. A.M.S., 62, 623, (1969).

75. J.Nuttall and J.Nutting, Met. Sci., 12, 430, (1978).

76. R.L.Aghan and J.Nutting, Met. Seci, 14, 233, (1980).

77. B.L.Averbach, M.B.Bever, M.F.Comerford, and J.L.Leach, Acta Met., 4, 477, (1956).

78. D.Michell, Phil. Mag., 1, 584, (1956).

79. D.Michell and F.D.Haig, Phil. Mag., 2, 15, (1957).

80. F.Haessner, "Recrystallization of Metalic Materials" Ed. F.Haessner, Dr.Reider-Verlag, GMBH, Stuttgart, P.1, (1978)

81. K.Bohnenkamp, K.Lüke, and G.Masing., Z. Metall., 46, 765, (1955).

82. P.Greenfield and B.Bever, Acta Met., 4, 125, (1957).

83. L.M.Clarebrough, M.E.Hargreaves and M.H.Lorretto, "Recovery and Recrystallization of Metals", Ed. L.Himmel, Inter Science, New York, P.63, (1963).

84. L.M.Clarebrough, M.E.Hargreaves, D.Michell and G.W.West, Proc. Roy. Soc. A215, 507, (1952).

85. L.M.Clarebrough, M.E.Hragreaves and G.W.West, Proc. Roy. Soc. A232, 252, (1955).

86. B.L.Averbach, M.B.Bever, M.F.Comberford and J.L.Leach, Acta Met., 4, 477, (1956).

87. J.G.Byrne, "Recovery, Recrystallization and Grain Growth", The Macmillan Co., New York, P.37, (1965).

88. R.Drouard, J.Washburn and E.R.Parker, Trans. A.I.M.E., 197, 1226, (1953).

89. A.S.Keh, "Direct Observation of Imperfection in Crystal", New York, Interscience, (1962).

90. R.W.Cahn, "Recrystallization, Grain Growth and Textures", Ed. H.Margolin, ASM Metal Park, Ohio, P.99 (1966).

91. R.W.Cahn "Recrystallization of Metalic Materials", Ed. F.Haessner, Dr.Rieder-Verlag, GMBH, Stuttgart, P.43, (1970).

92. R.D.Doherty and R.W.Cahn, J. Less--Common Metals, 22, 279, (1972).

93. R.D.Doherty, Met. Sci. J., 8, 132, (1974).

94. P.A.Beck, Adva in Phys., 3, 245, (1954).

95. R.D.Doherty, "Recrystallization of Metalic Materials", Ed. F.Haessner, Dr.Riederer-Verlag, GMBH, Stuttgart, P.23 (1978).

96. J.E.Burke and D.Turnbull, "Progress in Met. Phy.", 3, 220, (1952).

97. C.A.Verbraak and W.G.Burger, Acta Met., 5, 765, (1957).

98. C.A.Verbraak, Acta Met. 6, 580, (1958).

99. R.W.Chan, Pro. Phys. Soc., 60A, 323, (1950).

100. P.A.Beck, J. Appl. Phys., 20, 633, (1949).

101. A.H.Cottrell, "Prog. in Metal. Phys.", 4, 255, (1953).

102. P.A.Beck and P.R.Sperry, J. Appl. Phys., 21, 150, (1950).

103. R.K.Ray, W.B.Hutchinson, F.M.G.Besag and R.Smallman, J. Micro., 97, 217, (1973).

104. R.K.Ray, W.B.Hutchinson and B.J.Duggan, Acta. Met., 23, 831, (1975).

105. R.K.Ray, Ph.D. Thesis, Birmingham University, (1973).

106. H.Hu and A.Szirmae, Tras. A.I.M.E., 221, 839, (1961).

107. J.L.Walter and E.F.Koch, Acta Met., 11, 923, (1963).

108. T.Noda and J.Huber, Z. Metall. Kunde, 69, 570, (1978).

109. A.Kreisler and R.Doherty, Met. Sci. 12, 551, (1978).

110. Y.Inokuti and R.Doherty, Metallurgica, 26, 61, (1978).

111. P.Faivre and R.Doherty, J. Mat. Sci., 14, 897 (1979).

112. C.J.E.Smith and I.L. Dillamore, Met. Sci. J. 4, 161, (1970).

113. H.Hu, "Electron Microscopy and Strength of Crystals", London and New York, Interscience, P.564 (1963).

114. H.Hu, Trans. A.I.M.E., 224, 75, (1962).

115. J.L.Walter and E.F.Koch, Acta Met., 11, 999, (1963).

116. J.C.M.Li, J. Appl. Phy., 33, 2958, (1962).

117. M.Fujita, J.Phys. Soc. (Japan), 16, 397, (1961).

118. R.C.Koo and G.Sell, "Recrystallization , Grain Growth and Texture" Ed. Margolin, ASM, Metal Park, Ohio, P.99 (1965).

119. H.Hu, Acta Met., 11, 1000, (1963).

120. L.C.Michels and B.G.Ricketts. Trans. A.I.M.E., 239, 1841, (1967)

121. P.K.Marsden, J. Matr. Sci., 6, 1038, (1971)

122. J.Grewen and J.Huber, "Texture and Properties if Materials", 4th International conf. on Texture, The Met. Soc., Cambridge, (1975) P. 138.

123. J.E.Bailey, Phill. Mag., 5, 833, (1960).

124. J.E.Bailey, P.B.Hirsch, Proc. Roy. Soc., A267, 11, (1962).

125. S.P.Bellier and R.D.Doherty, Acta Met., 25, 521, (1977).

126. B.J.Duggan, W.B.Hutchinson and M.Hatherly, Scripta Metall., 12, 293, (1978).

127. M.Blicharski, Metalurgial Odle Wnictwo-Tom 5 - Zeszyt 2, 235, (1979).

128. I.L.Dillamore and W.T.Roberts, Met. Rev., 10, 271, (1965).

129. A.Merlini and P.A.Beck, Trans. A.I.M.E., 203, 385, (1955).

130. R.E.Smallman, J. Inst. Met., 84, 10, (1955-56).

131. R.H.Richman and Y.C.Liu, Trans. A.I.M.E., 221, 720, (1961).

132. Y.C.Liu and R.H.Richman, Trans. A.I.M.E., 218, 688, (1960).

133. U.Schmidt, K.Lücke and J.Pospiech, "Texture and Properties of Material", 4th International Conference on Texture, The Met. Soc., Cambridge, P.147, (1975).

134. H.Hu and R.S.Cline, J.Appl. Phys., 32, 760, (1961).

135. H.Hu, R.S.Cline and S.R.Goodman, J.Appl. Phys., 32, 1392, (1961).

136. H.Hu and S.R.Goodman, Trans. A.I.M.E., 227, 627, (1963).

137. S.R.Goodman and H.Hu, Trans. A.I.M.E., 230, 1413, (1964).

138. T.L.Richards, J.Inst. Met., 84, 503, (1955).

139. T.L.Richards and S.F.Pugh, J.Inst Met., 88, 399, (1959).

140. F.Haessner, Z.Metalk., 54, 98, (1963).

141. I.L.Dillamore and W.T.Roberts, Acta Met., 12, 281, (1964).

142. R.E.Smallman and D.Green, Acta Met., 12, 145, (1964).

143. Y.C.Liu, Trans. A.I.M.E., 230, 656, (1964).

144. J.F.W.Bishop, J.Mech. Phys. Sol., 3, 130, (1954).

145. E.A.Calnan, Acta Met., 2, 865, (1954).

146. R.F.Braybrook and E.A.Calnan, J. Inst. Met., 85, 11, (1956-57)

147. G.Wassermann, Z. Metalk., 54, 61, (1963).

148. J.S.Kallend and G.T.Davies, Tex., 1, 51, (1972).

149. K.Morii, M.Mera and Y.Nakayama, Trans. Jap. Inst. Met., 18, 7, (1977).

150. H.Hu and P.A.Beck, J. Metals, 2, 1214, (1950).

151. E.Schmid and H.Thomas, Z. Physik, 130, 293, (1951).

152. C.A.Verbraak, Z. Metal., 51, 646, (1960).

153. P.A.Beck and H.Hu, J. Metals, 4, 83, (1952).

154. W.B.Hutchinson and R.K.Ray, Met. Sci., 13, 125, (1979).

155. R.H.Richman and Y.C.Liu, Trans. A.I.M.E., 224, 720, (1962).

156. M.Meixner, H.D.Mengelberg and K.Lücke, Acta Met., 13, 855, (1965).

157. T.Richards and S.F.Pugh, J. Inst. Met., 88, 399, (1959-60).

158. K.Lücke, Z. Metal., 19, 664, (1965).

159. P.A.Beck and H.Hu, Trans. A.I.M.E., 194, 83, (1952).

160. J.Grewen, Z. Metal., 19, 664, (1965).

161. J.Grewen, "Recrystallization of Metallic Materials", Ed. F.Heassner, Dr. Riederer - Verlag, GMBH, Stuttgart, P.135, (1970).

162. W.G.Burgers and P.C.Louwerse, Z. Physik, 67, 605, (1931).

163. C.S.Barrett, Trans. A.I.M.E. , 137, 128, (1940).

164. P.A.Beck and H.Hu, Trans. A.I.M.E., 185, 627, (1949).

165. N.K.Chen and C.H.Mathewson, Trans. A.I.M.E., 194, 501, (1952).

166. Y.CLiu and W.R.Hibbard, J. Trans. A.I.M.E., 197, 673, (1953).

167. R.Maddin, C.H.Mathewson and W.R.Hibbard, J. Trans. A.I.M.E., 185, 655, (1949).

168. S.Kohars, M.N.Parthasarathi and P.A.Beck, Trans. A.I.M.E., 212, 875, (1958).

169. M.N.Parthasarathi and P.A.Beck, Trans. A.I.M.E., 212, 831, (1961).

170. B.Licbmann, K.Lücke and G.Masing, Z.Metal., 47, 57, (1956).

171. W.G.Burgers, Y.Liu and T.J.Tiedema, Pro.Kon. Ned. Acadvwet, 54, 459, (1951).

172. B.F.Decker and D.Harker, J. Appl. Phys., 22, 900, (1951).

173. I.L.Dillamore and H.Katoh, Met. Sci., 8, 73, (1974).

174. F.Heassner, U.Jakubowski and M.Wikens, Phys. Stat. Sol., 7, 701, (1964).

175. K.Lücke, H.Perlwitz and W.Pitsch, Phys. Stat. Sol., 7, 733, (1964).

176. A.Merlini and P.A.Beck, Acta Met., 1, 598, (1953).

177. H.Heller, J.Slakhorst and T.Verbraak, Z. Metal., 68, 31, (1977).

178. W.B.Hutchinson, Met. Sci. J., 8, 185, (1974).

179. M.Hatherly and W.B.Hutchinson "An Introduction to Texture in Metals", The Institution of Metallurgists, Monograph No. 5., (1979).

180. C.Laird, E.Eichen and W.R.Bitler, J. Appl. Phys., 37, 2225, (1966).

181. B.J.Duggan and I.P.Jones, Tex. of Cryst. Sol., 2, 205, (1977).